UNIVERSITEIT GENT

UNIVERSIDAD AUTONOMA DE MADRID

Development of photosensitiser conjugates for furan-oxidation based interstrand crosslinking to nucleic acids.

Eva Marina Llamas Garcinuño

Supervisors:

Prof. Dr. Annemieke Madder

And

Prof. Dr. Tomás Torres

2017

"Development of photosensitiser conjugates for furan-oxidation based interstrand crosslinking to nucleic acids"

Eva Marina Llamas Garcinuño

Muchos esfuerzos se han dedicado durante las últimas décadas a desvelar el intrincado puzle que conforman todos los papeles que juegan los ácidos nucleicos en los seres vivos. Los ácidos nucleicos no solo definen la constitución genética de un organismo sino que también participan en procesos enzimáticos y regulan la expresión genética. Por todo ello, existe un gran interés en el desarrollo de nuevas herramientas que puedan ser útiles en aplicaciones para diagnósticos o terapia basadas en estos procesos.

Previamente, se ha sido establecido en el grupo OBCR (Organic and Biomimetic Chemistry) que la introducción de un grupo furano en un oligonucleótido puede logarse de forma sencilla utilizando síntesis automática. Como resultado se obtiene una sonda equipada con un grupo funcional altamente reactivo que ha sido enmascarado y es capaz, una vez que el grupo furano ha sido oxidado, de producir un entrecruzamiento entre cadenas de forma selectiva con la secuencia complementaria. La oxidación del grupo furano se puede lograr o bien usando NBS o bien, de una forma más biocompatible, usando oxígeno singlete. Para la formación de este último, los compuestos azul de metileno y rosa de bengala han sido estudiados en detalle.

El objetivo de este estudio es expandir esta metodología al uso de fotosensibilizadores porfirínicos para la generación de oxígeno singlete con el objetivo final de desarrollar un método que se pueda aplicar en un contexto celular.

Para ello, se seleccionaron tres fotosensibilizadores distintos: la clorina e6 (comercial), una porfirínica tripiridínica (TriPyCOOH) y una ftalocianina de zinc decorada con grupos *tert*-butilo. (TT1).

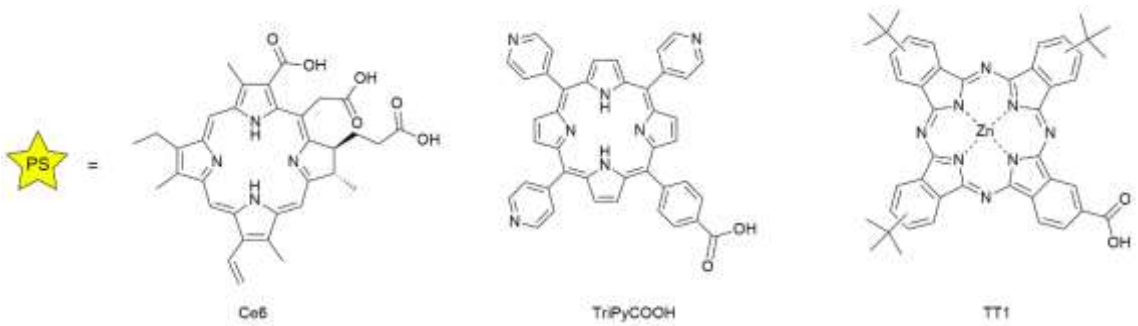

Primero, se evaluó la habilidad de cada fotosensibilizador para producir el entrecruzamiento entre cadenas cuando se añaden en solución. Para ello, un oligonucleótido modificado con un

grupo furano fue hibridado con la cadena complementaia en presencia del respectivo fotosensibilizador para evaluar la generación del entrecruzamiento una vez se produce la irradiacción necesaria. Una cuidados optimización de varios factores se llevó a cabo, incluyendo el tiempo de reacción, la concentración de los fotosensibilizadores, el ratio entre el dúplex y el fotosensibilizador y el tipo de luz utilizada. Fue hallado que de los tres fotosensibilizadores, el uso de Ce6 produce los rendimientos de entrecruzamiento más altos (conversión del 52%) cuando las condiciones son óptimas. TT1 fue capaz de producir el entrecruzamiento solo a bajos rendimientos, debido a su insolubidad en condiciones acuosas que son necesarias para esta reacción.

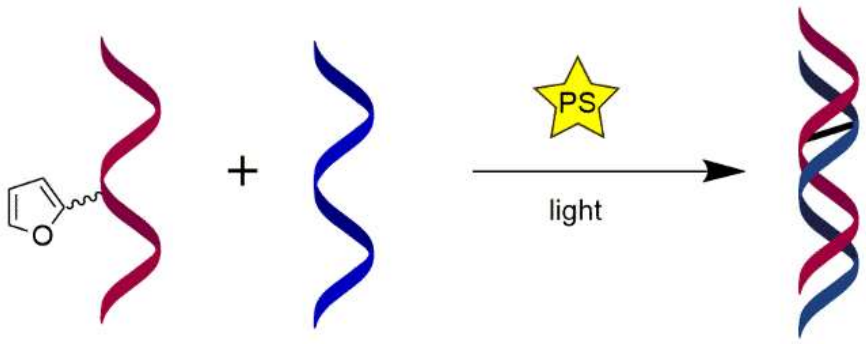

En el siguiente paso, se planteó la hipótesis de que al conjugar los fotosensibilizadores a la cadena complementaria al oligonucleótido que contiene el grupo furano resultaría en dos mejoras importantes: la generación de oxígeno singlete se produciría cerca del grupo furano y la solubilidad en agua de los fotosensibilizadores sería mayor.

Para conjugar cada fotosensibilizador se usó una estrategia de conjugación distinta, todas ellas basadas en la activación del ácido carboxílico en los fotosensibilizadores seguida por la adicción de un oligonucleótido que contiene un grupo amino. La conjugación de la TT1 fue particularmente problemática y esta reacción tuvo que llevarse a cabo con el oligonucleótido todavía en el soporte sólido donde se había sintetizado, para evitar el uso de condiciones acuosas y los problemas de solubilidad asociados.

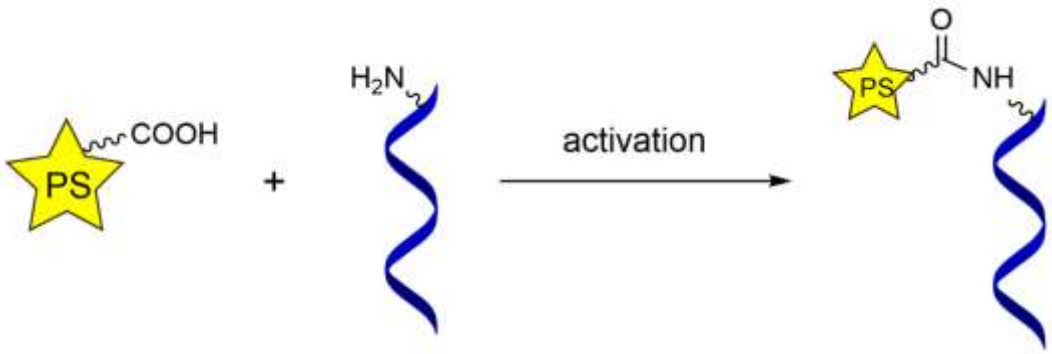

Una vez que los tres conjugados fueron sintetizados, se hibridaron al oligonucleótido que contiene el grupo furano y se evaluó la generación del entrecruzamiento. De nuevo, el entrecruzamiento que dio lugar a los rendimientos más altos fue en el que se usó el conjugado con Ce6, gracias una generación suficiente de oxígeno singlete y a una estabilización del dúplex que ocurre como consecuencia de introducir Ce6 en el oligonucleótido. Sorprendentemente, el uso del conjugado con TriPyCOOH no fue capaz de producir el entrecruzamiento, presuntamente debido la gran desestabilización que tiene lugar al introducir este fotosensibilizador y la pobre generación de oxígeno singlete. El conjugado con la TT1 mostró una alta generación de oxígeno singlete y fue capaz de producir el entrecruzamiento entre cadenas pero con rendimientos menores debido a una desestabilización del dúplex debido a la presencia del fotosensibilizador.

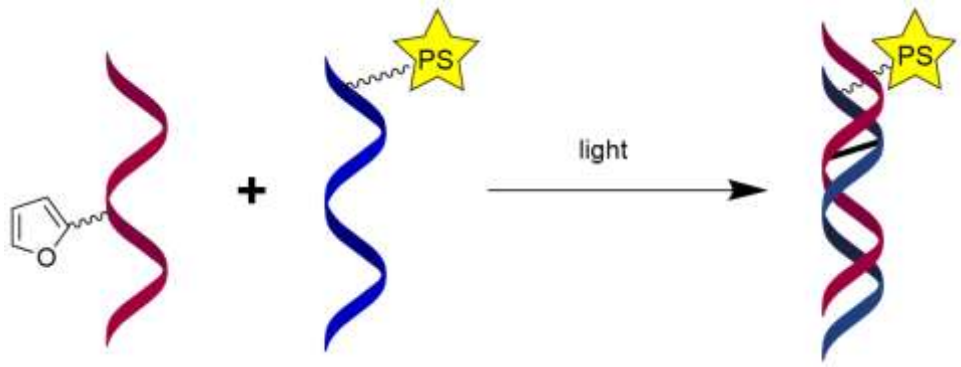

Con la idea de permitir el entrecruzamiento con una secuencia no modificada, se sintetizaron y evaluaron sondas doblemente modificadas con un grupo furano y un fotosensibilizador. Sin embargo, la síntesis y el manejo de estas sondas auto-activables fue problemática, probablemente debido a la generación prematura de oxígeno singlete y la consiguiente desactivación de las sondas, y cuando la reacción de entrecruzamiento se intentó llevar a cabo no tuvo éxito en ningún caso.

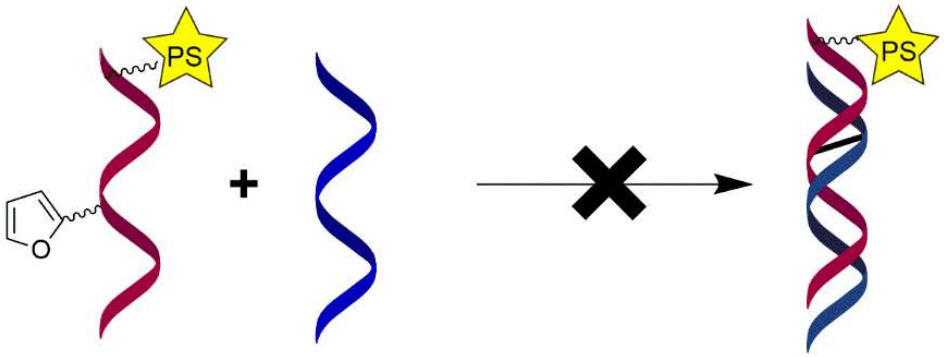

Como alternativa, se probó el uso de un sistema plantilla en el que el furano y el fotosensibilizador fueron introducidos en oligonucleótidos distintos y posteriormente

hibridados a un oligonucleótido más largo sin modificaciones, que los mantiene próximos el uno al otro. Mientras que este enfoque tuvo éxito en un estudio anterior en el que se usaron sondas que contenían azul de metileno y rosa de bengala, en nuestro caso no pudimos demostrar la generación del entrecruzamiento. Debido a falta de tiempo, este enfoque no fue estudiado en más detalle ya que una tercera estrategia fue puesta en práctica (*vide infra*).

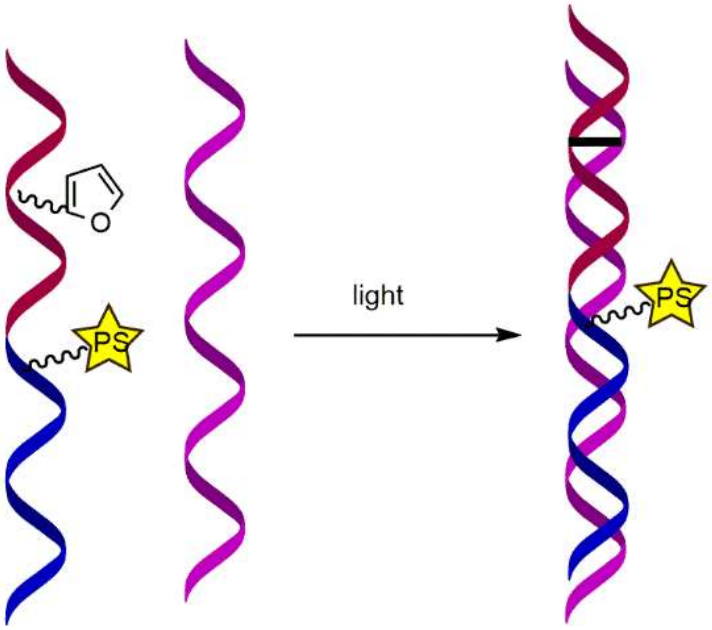

En esta nueva estrategia se estudió el uso de un péptido de penetración celular como transportador. Los ácido nucleicos no son capaces de ganar acceso a las células y se ha descrito el uso de estos péptidos para terapias basadas en el uso de ácidos nucleicos ya que son capaces de asistir en la internalización de los ácidos nucleicos. En concreto, algunos de estos péptidos son capaces de formar complejos supramoleculares entre los péptidos cargados positivamente y los oligonucleótidos cargados negativamente, lo que resulta en la formación de nanopartículas.

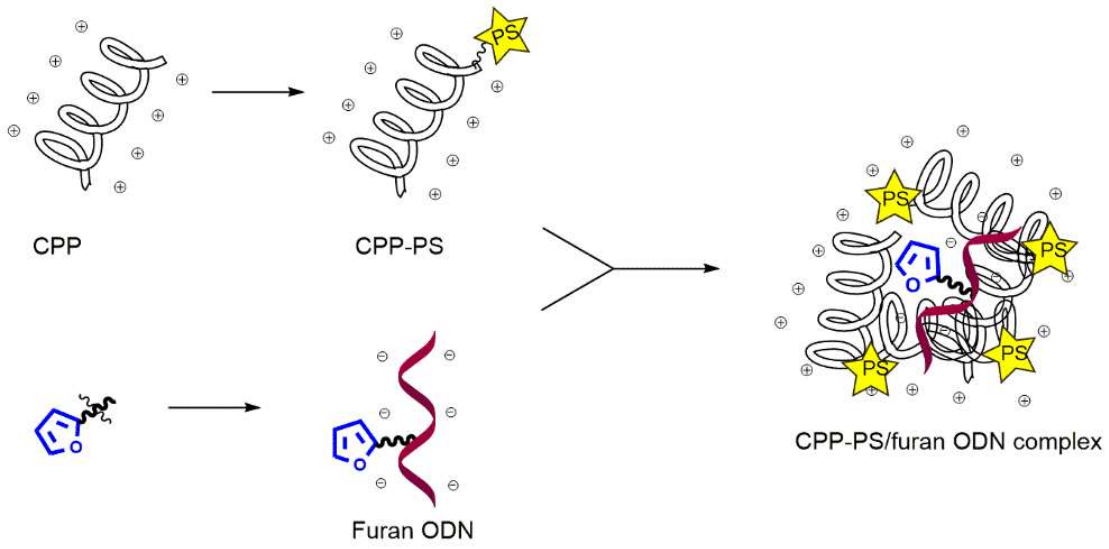

En este caso, el uso del péptido conocido como MPG-8, que contiene 21 aminoácidos, se eligió para la formación de complejos con el oligonucleótido que contienen el furano. Al añadir la cadena complementaria y una concentración suficiente de Ce6 como fotosensibilizador, se observó la formación del entrecruzamiento, usando heparina para facilitar la liberación del oligonucleótido cuando es necesario. Posteriormente, MPG-8 fue conjugado a Ce6 y la formación del correspondiente complejo con el oligonucleótido que contiene el furano resultó en la formación de nanopartículas auto-activables que fueron capaces de producir el entrecruzamiento con un oligonucleótido no modificado.

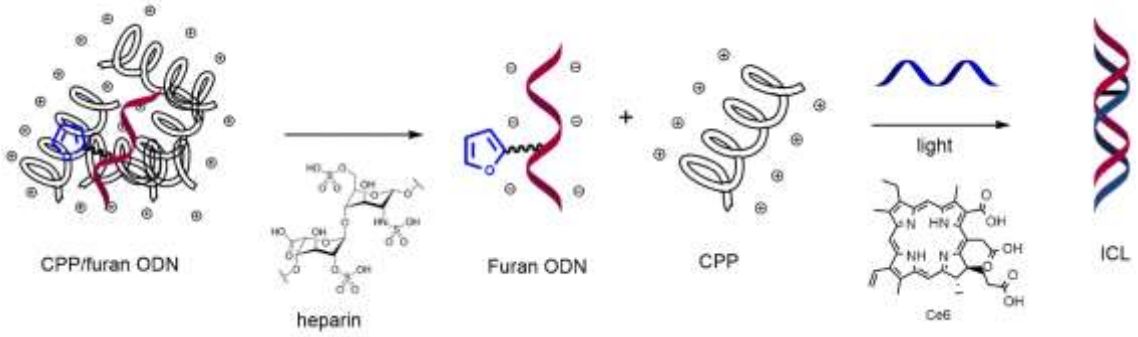

Acknowledgements

I would like to thank all the people on the OBCR group for the great environment during my PhD. I have learnt a lot during these last years and met so many great people.

A special thank you goes to my two supervisors, Prof. Annemieke Madder and Prof. Tomás Torres, for all the useful advice.

And last but not least, to my family and friends who have been a constant source of support.

The research leading to these results has received funding from the European Union's Seventh Framework Program (FP7/ 2007-2013)/Marie Curie ITN Grant Agreement No. 316975.

Abbreviations table

ABDA: 9,10-anthracenediyl-bis(methylene)dimalonic acid

ACN: acetonitrile

CPG: controlled pore glass

DCC: *N,N'*-Dicyclohexylcarbodiimide

DCM: dichloromethane

DIPEA: (*N,N*-diisopropylethylamine

DLS: dynamic light scattering

DMF: dimethylformamide

DMSO: dimethyl sulfoxide

DMS(O)MT: dimethoxymethylsulfonyltrityl

DMT: dimethoxytrityl

EDT: 1,2-ethanedithiol

Et_2O: diethyl ether

HBTU: 2-(1*H*-benzotriazol-1-yl)-1,1,3,3-tetramethyluronium hexafluorophosphate

LC-MS: liquid chromatography–mass spectrometry

MALDI-TOF: matrix-assisted laser desorption/ionization

mRNA: messenger RNA

MTBE: methyl tert-butyl ether

NHS: *N*-hydroxysuccinamide

NBS: N-bromosuccinamide

NP: nanoparticle

ODN: oligonucleotide

PAGE: polyacrylamide gel electrophoresis

PNA: peptide nucleic acid

PS: photosensitiser

RP HPLC: reverse phase high-performance liquid chromatography

SNP: single nucleotide polymorphism

TBE: Tris/Borate/EDTA

TCA: trichloroacetic acid

TEAA: triethylammonium acetate

TFA: trifluoroacetic acid

TIS: triisopropylsilane

Chapter I.
Nucleic acids structure and relevance.
Nucleic acid based diagnostics and therapeutics.

I.1. DNA structure

DNA contains the genetic information necessary for all the processes that take place during an organism's metabolism and this information can be transmitted to the next generation. DNA consists of a four letter 'code' where these four units, called nucleobases, are supported by a phosphate-sugar backbone. Two of these nucleobases are pyrimidine bases, cytosine (C) and thymine (T), whereas the other two are purine bases, adenine (A) and guanine (G). One molecule of DNA consists of two antiparallel strands where the nucleobases on one strand recognises the base on the opposite strand by hydrogen bonding: G pairs with C, A pairs with T, following Chargaff's rules. The nucleobases also interact with each other by nonspecific π–π stacking due to their aromatic character, and the combination of those two forces holds the duplex together.

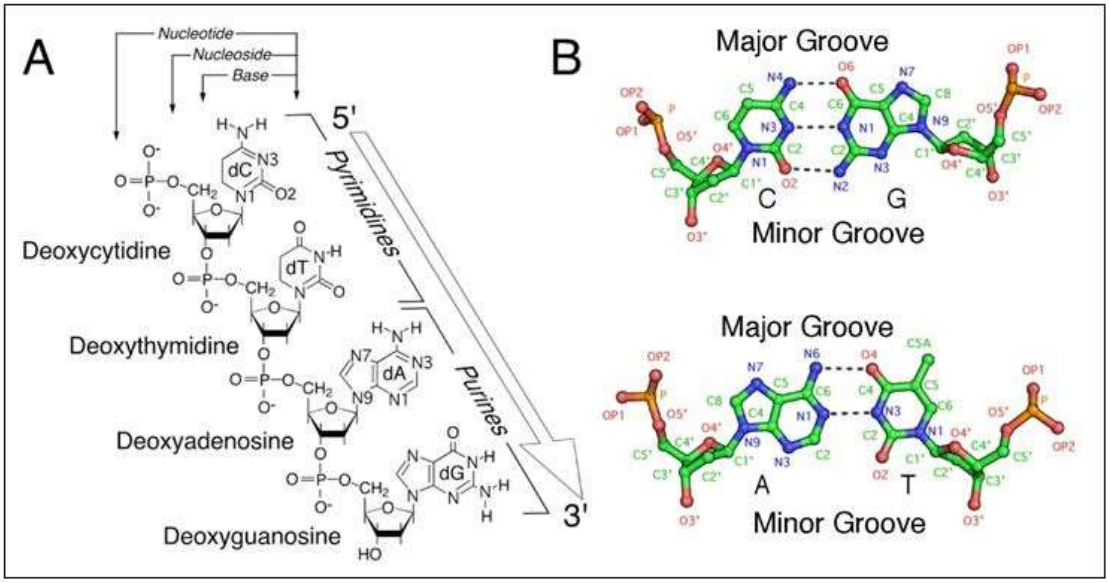

Figure I-1. DNA structure. Reproduced with permission from (1)

DNA duplexes have been observed in three different conformations: A, B and Z. The B-form is the most stable under physiological conditions, the A-form is found at low humidity conditions and the Z-form is the only characterised left-handed form of duplex and occurs only under particular conditions such as high salt concentrations.

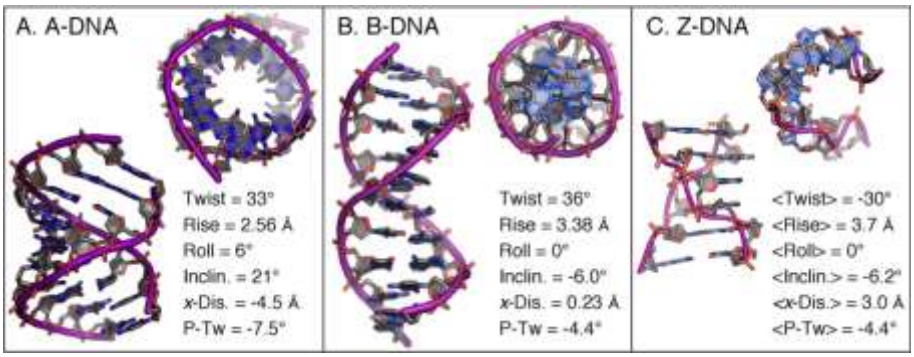

Figure I-2. Different structures of double helical DNA. Incl. = inclination, x-Disp. = x-displacment, P-Tw = propeller twist. For Z-DNA, the helical parameters are given as averages of the alternating dinucleotide steps. Reproduced with permission from (1)

I.2. History of the discovery of DNA

DNA was first isolated by F. Miescher in 1868 but it was not until the 1940s that the experiment performed by O.T. Avery, C. MacLeod and M. McCarty showed evidence that the genetic information encoding biomolecules it was DNA-based, and no protein-based. In this experiment, a non-virulent strain of *Streptococcus pneumoniae* was transformed into a virulent one by injection of DNA from a virulent strain of the same bacterium, showing that the genetic information for virulence was encoded in DNA. In the same decade, E. Chargaff observed that the nucleobase composition varies from one species to another, but is constant within the same organism, indifferent to external factors like age or changing environment and, importantly, that the amount of A is equal to T, and G is equal to C.

Another important clue that led to the discovery of the DNA structure was unraveled by R. Franklin and M. Wilkins in the early 1950s, using X-ray diffraction. From the pattern obtained it was inferred that DNA possessed a helical structure.

Based on all this information J. Watson and F. Crick proposed their DNA model that was published in *Nature* in 1953 (2) and they were awarded the Nobel prize in Medicine or Physiology in 1962, together with M. Wilkins.

I.3. DNA metabolism

The central dogma of molecular biology describes the flow of genetic information and it states, in a simplified manner, that the genetic information encoded in DNA is transcribed into messenger RNA (mRNA) which is then translated into proteins.

The whole picture, however, is much more complex. For example, mRNA is just one of several types of RNA that occur in cells: ribosomal RNAs are components of ribosomes and transfer RNAs participate in the translational machinery recognising the mRNA and adding amino acids to a growing peptide. More recently, the relevance of non-coding RNAs has only started to become apparent. Non-coding RNAs correspond to sequences that do not codify for any known protein but they have regulatory functions. They are classified according to their size: 18-25 nucleotides for microRNAs and small interfering RNA, 20-300 nucleotides for small RNAs and between 300-10000 (or more) nucleotides that for medium and long non-coding RNAs.

For example, the role of microRNA (miRNAs) in gene regulation has only been known since the early 1990s. (3) These noncoding RNA sequences, of around 22 nucleotides, play an important role in the regulation of mRNA, by repressing their translation or triggering cleavage. (4,5)

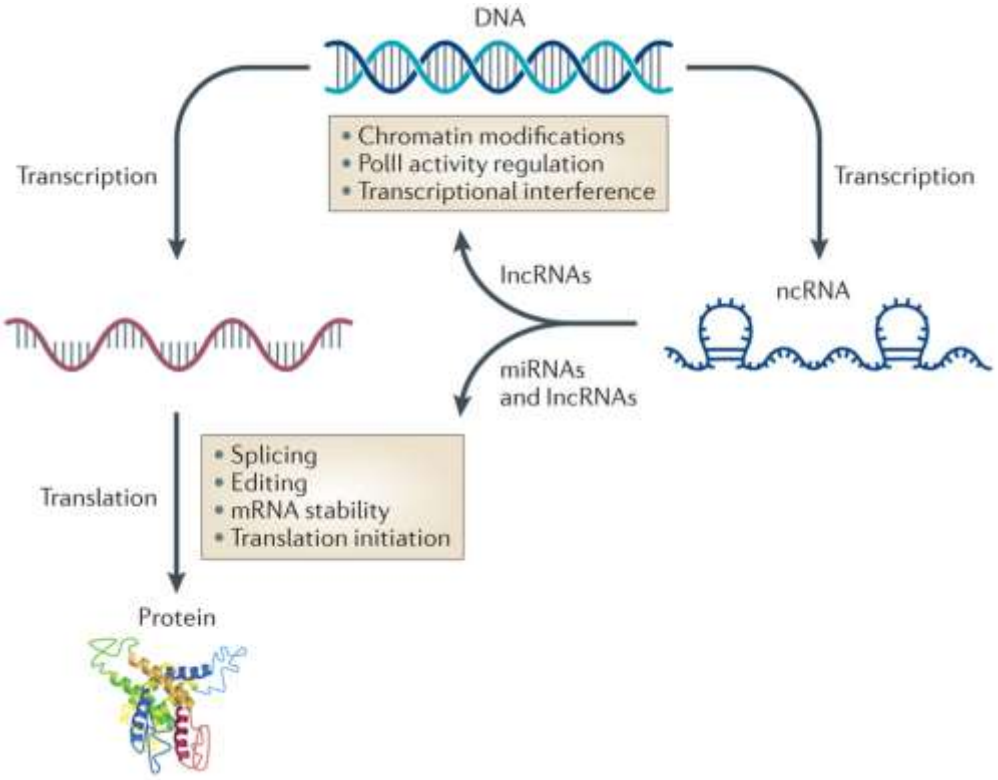

Figure I-3. DNA metabolism including regulation processes by non-coding RNAs. Reproduces with permission from (6).

The higher stability of DNA compared to RNA seems to be one of the reasons why DNA is the genetic 'library' in most organisms. However, DNA damage does occur, and it has been estimated that between 10^3 and 10^6 molecular lesions happen per cell per day. Cells have repair mechanisms to minimise the effects of these lesions as will be discussed in the following section.

I.4. Repair mechanisms

DNA damage has various origins such as the cell metabolism, due to reactive oxygen species produced (endogenous), environmental agents such as UV radiation (exogenous) or even errors during replication. In order to maintain the integrity of the genetic information, cells possess complex mechanisms that are able to minimise damage accumulation in their DNA. Understanding these repair mechanisms provides vital knowledge about living cells processes that can help in the development of for example new cancer treatments. In 2015, T. Lindahl, P. Modrich and A. Sancar were awarded the Nobel Prize in Chemistry for their works mapping different repair systems *i.e* base excision repair, nucleotide excision repair and mismatch repair.

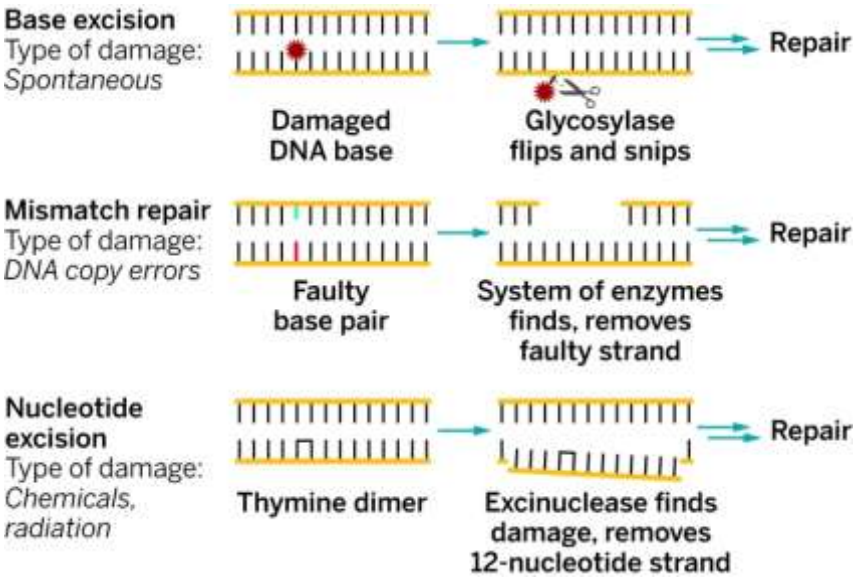

Figure I-4. Types of DNA repair.

However, most repair mechanisms rely on the integrity of one of the strands of the DNA duplex since it is used as template to synthesise the new, error free strand section, after nicking the damaged fragment.

However, there is a particular type of DNA lesions where both strands are involved by covalent linkage of two nucleobases on opposite strands, called interstrand crosslinks (ICLs). ICLs occur in the presence of exogenous agents and also by the formation of abasic sites(7), and there have been many efforts dedicated to the study of their repair processes as well as to the generation of site-specific and high yielding ICLs that allow their study.

I.5. Genotyping and discrimination of single point mutations.

The genome of a given organism contains all information about their structure and metabolism and complete access to this information is key for understanding the origin of many diseases.

However, even within the same species there are genetic differences among individuals that account for the different characteristics that they display. The determination of those genotype differences, known as genotyping, finds application in many fields including biomedicine (8–10), molecular epidemiology (11,12) and forensics (13) among others.

Several methods have been developed for genotyping including PCR and DNA sequencing. However, these methods are labour intensive and only a limited number of sequences can be investigated at a time. In recent years, the development of high throughput methods has attracted a lot of attention. For example, DNA arrays have been developed as a powerful tool that allows screening of a high number of DNA sequences (14,15), even an organism whole genome. As they rely on DNA hybridisation, they are inherently limited by the specificity of hybridisation and interrogation of complex samples is cumbersome, particularly when differences are as small as one nucleotide, as in single nucleotide polymorphisms (SNPs).(13,16–18)

Single stranded DNA (ssDNA) detection typically relies on different detection methods, (19) including fluorescence, (20–22) electrochemistry (23,24) and more recently nanoparticle-based detection, particularly Au NPs. (25–29)

Some of these methods allow detection at femtomolar concentrations, however the aim is to detect at the single biomolecule level avoiding the use of PCR for amplification (30,31)

Recently, some examples of crosslinking-assisted point mutation detection have been reported, showing the potential of crosslinking methodologies not only for repair mechanisms study but also for sequencing and diagnosis applications. Greenberg at al. described the use of bifunctional ODNs that induce crosslink formation under mild oxidation conditions towards a 16-nt long sites on plasmid DNA with a point mutation. Fluorescence based detection allowed probing of the target sequence at nanomolar concentrations. (32)

Moreover, the group of Fujimoto showed the potential of the use of photocrosslinking molecular beacons for detecting SNPs in a dsDNA context. The crosslinking formation stabilised the complex formed between the molecular beacon and the target, allowing strand displacement or invasion of the duplex. (33)

I.6. DNA based therapeutics

Nucleic acids and derivatives thereof have been used for therapeutic applications to target different biomolecules:

- In the antigene strategy, the aim is to modulate gene expression and the use of triplex forming oligonucleotides (TFOs) has been described. (34) Such TFOs are sequence specific, binding the target duplex through the formation of Hoogsteen bonds. The successful *in vitro* and *in vivo* use of this method has been reported (34) but their clinical application is hampered by the rare occurrence of the polypurine or polypyrimidine sequences that are required for the formation of the triplex.
- Another approach consists in the targeting of transcription factors which are responsible for transcription of DNA into mRNA. The use of a decoy duplex DNA competes with the targeted promoter thus influencing the transcription levels. (35) The use of polyamides has been described as an alternative to the use of dsDNA since polyamides are able to easily diffuse into the nucleus. (36–38)
- On the other hand, targeting mRNA instead of DNA shows the advantage that access to the nucleus is not necessary. Also in this case, the use of decoy oligoribonucleotides has been reported, which compete for the proteins involved in the translation. (39,40)
- Also targeting mRNA, the use of the so-called antisense strategy relies on the delivery of a complementary sequence that results in the formation of different complexes with the mRNA and at last inhibits translation. (41,42) Several approaches have been explored, including interference with the splicing of RNA into mature mRNA, (43,44) recruitment of RNaseH (45,46), ribozymes (47,48) or DNA enzymes (49,50), which results in the cleavage of the mRNA, or the steric blockage of the mRNA preventing translation. (51,52)

However, the reversible nature of the duplex hybridisation between the targeted nucleic acid and the therapeutic nucleic acid is disadvantageous and the formation of a covalent bond between the two strands has been recently shown to enhance the antisense effect. (53–56)

I.7. ICL generation methodologies

The damage that ICLs inflict to DNA forms the basis of the use of many chemotherapeutic drugs and also chemical weapons. However, in the case of the therapeutic use, the lack of selectivity of chemotherapeutic drugs such as mitomycin C, nitrogen mustard and cisplatin is the reason for their detrimental secondary effects.

Chemistry provides a valuable tool for the generation of more selective ICLs as it allows the introduction of unnatural moieties into synthetic oligonucleotides for a site-specific and controlled generation of ICL. Among all the ICL approaches, most crosslinking probes rely either

on alkylation, [2+2] cycloadditions or the use of masked carbonyl functionalities for the ICL formation.

I.7.1. Alkylation based ICL formation

- Alkyl halides

  Although alkylation based ICL formation has been carried out using highly reactive moieties such as unprotected alkyl halides, (57–59) the inherent reactivity of these functionalities (figure I-5a and b) may result in off-target reactions and are unsuitable for biological applications. Attempts to achieve a more biocompatible methodology have been made by the group of Luedtke, which reported the use of a O^6-(2-chloroethyl)guanine residue containing a photolabile ortho-nitrobenzyloxycarbonyl (NBOC) group at the N^2 position (Figure I-5c). NBOC acts as an electron-withdrawing group stabilising the chloroethyl moiety until is deprotected by irradiation at 365nm. An intramolecular reaction results in a highly reactive cyclic cation that can alkylate a cytosine base on the opposite strand. The crosslinked adduct possess an analogous structure as the crosslinking formed using the chemotherapeutic agent BCNU. (60)

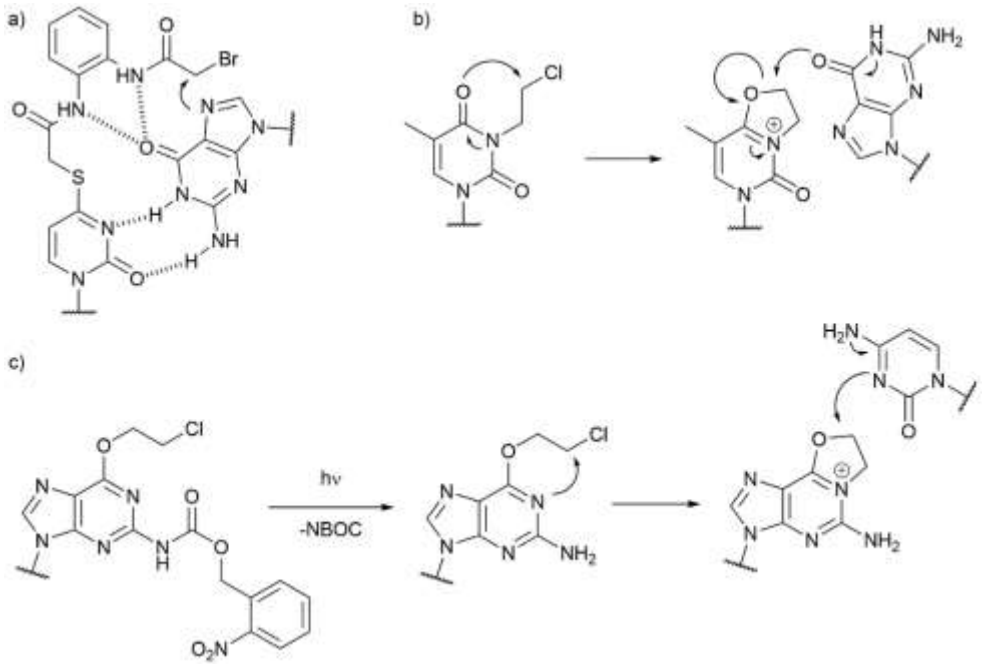

Figure I-5. Examples of alkyl halides for ICL formation.

- Strained systems

  One of the first approaches for ICL formation was the use of nucleosides containing conformationally strained rings (figure I-6a) or heterocycles such as aziridine (figure I-6b) (61,62) or a cyclopropapyrroloindole. (63) Recently, the group of Kobori reported

the synthesis of a 2'-O-diazirine-conjugated adenosine that undergoes ICL formation towards DNA upon UV irradiation (figure I-6c). (64)

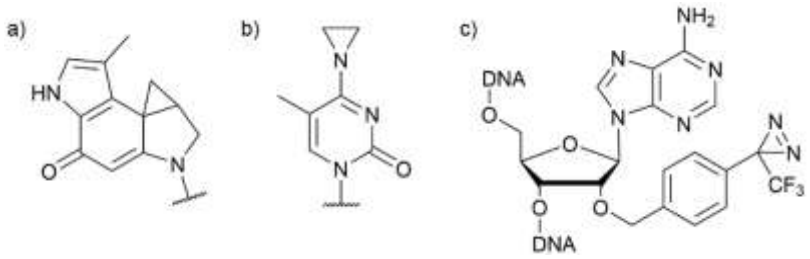

Figure I-6. Synthetic nucleosides containing strained rings.

- Vinyl-modified nucleotides

Sasaki et al. have described the synthesis of vinyl containing nucleosides that allow selective target of different nucleobases situated on the opposite strand. The use of a 2-amino-6-vinylpurine nucleoside allowed to produce selective ICL formation towards cytidine that was triggered by hybridisation. They showed the beneficious effect of masking the double bond as a phenyl sulfoxide, which resulted in higher crosslinking yields compared to the unmasked vinyl group. (65)

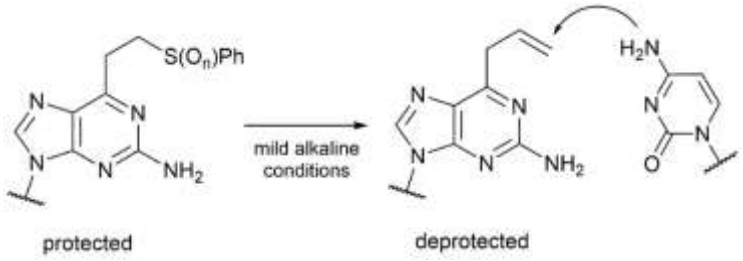

Figure I-7. ICL formation between a 2-amino-6-vinylpurine and cytosine.

On the other hand, when a 4-vinylpirimidine-2-one nucleoside was used in the context of RNA or duplex DNA crosslinking, selectivity was towards adenine or uracil, depending on the target sequence and the reaction conditions. (66) This methodology was also applied in biological systems by enhancing antisense effects. (66–68)

Moreover, the group of Greenberg described the use of selenide derivatives that upon oxidation, via $NaIO_4$ or singlet oxygen (69), result in alkylating agents via a [2,3]-sigmatropic rearrangement and were applied for SNP detection. (32,70)

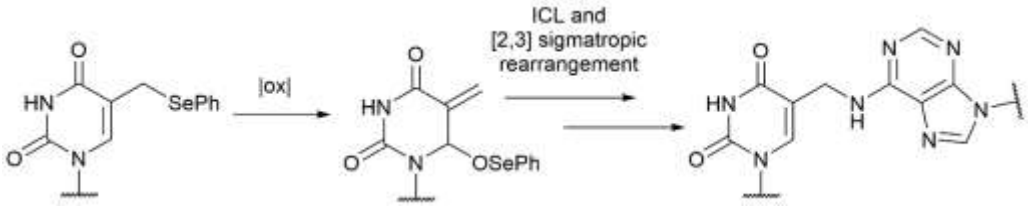

Figure I-8. Generation of ICL precursor via oxidation and crosslinking towards adenine.

- Radical precursor nucleotides

  Greenberg *et al.* described the first radical-based method for ICL formation by using aryl selenide or sulphide derivatives as radical precursors that can be activated using photochemical activation, thermal activation. (71) The exact mechanism of radical generation and ICL formation was elucidated.(72)

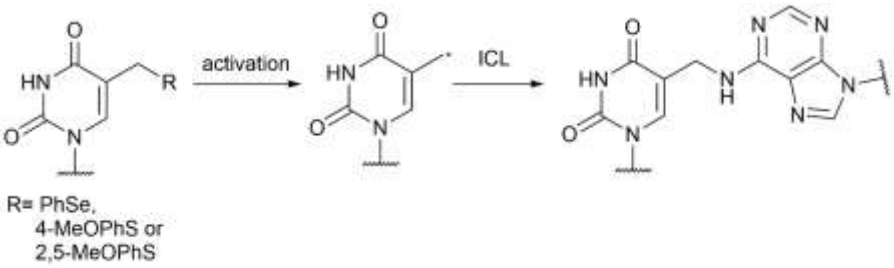

Figure I-9. ICL formation via a radical intermediate.

I.7.2. [2+2] cycloaddition

One of the damaging processes that DNA undergoes consists in a [2+2] cycloaddition between two adjacent thymidines when exposed to UV light. The 5,6-double bond of pyrimidine nucleobases is susceptible of a [2+2] cycloaddition not only by another nucleobase but also by exogenous agents. Introduction of such compounds into oligonucleotides results in light triggerable crosslinking probes, and three main type of compounds have been used with this purpose:

- Coumarins

  The group of Peng reported for the first time the synthesis of a coumarin containing ODNs that undergo reversible ICL formation (350/254nm irradiation) with an opposite dT or dC (73). Real time ICL monitoring by fluorescence was achieved after optimisation of the position and type of linker used to introduce the coumarin in the ODN. (74)

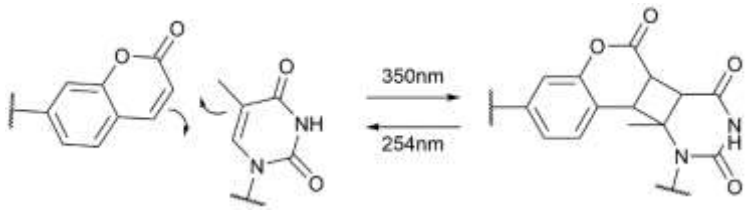

Figure I-10. General mechanism for coumarin based ICL.

- Psoralen

  Psoralens are closely related to coumarins, consisting of a furan ring that is fused to the bicyclic coumarin skeleton, and can also undergo [2+2] cycloadditions upon UV irradiation. The group of Murakami showed that introduction of a psoralen derivative at the 5' end of a ODN methylphosphonate results in ICL formation with the base on the complementary strand when irradiated at 365nm, and it was highly dependent upon the fidelity of base pairing (75) and was later on shown to be able to inhibit translation of mRNA in a cell-free medium. (53)

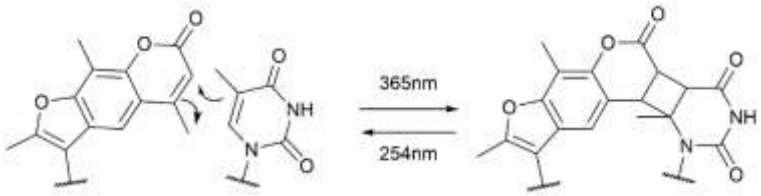

Figure I-11. General mechanism for psoralen based ICL.

The use of phosphorothioate derivatives was explored and applied to inhibit the proliferation of human cervical carcinoma cells (76) and also as a decoy for restriction endonucleases(77) or estrogen receptors. (78) Also, the use of a hairpin conformation allowed a better sequence specificity when used for RNA crosslinking. (79)

To broaden the targeted sequences repertoire, a dA nucleoside decorated with the psoralen moiety at the 2' position was synthesised and resulted in an enhanced sequence specificity compared to the 5' modified ODN. (80,81) These ICL probes were effective for antisense strategy by inhibit K-ras-immortalized cell proliferation (82) and for RNA-induce silencing complex regulation by targeting microRNA. (54)

- Cyanovinylcarbazole

  The group of Fujimoto developed a crosslinking strategy based on a 3-cyanovinylcarbazole nucleoside that allows an ultrafast reversible ICL formation with pyrimidine bases upon UV irradiation (366/312nm) and the crosslinking formation was explored in the context of DNA/DNA and DNA/RNA duplexes. (83,84) This methodology has been applied to antisense strategy, (55,85) detection of SNPs (33) and stabilisation of nanostructures. (86–88)

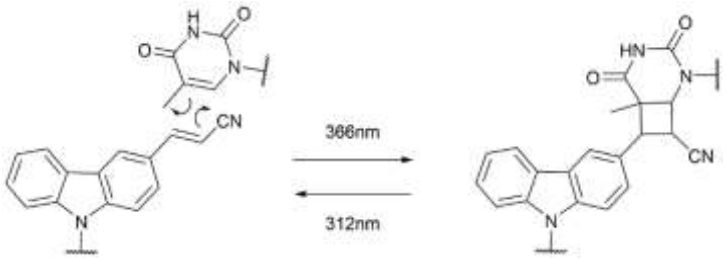

Figure I-12. Reversible ICL formation using a 3-cyanovinylcarbazole nucleoside.

1.1. Masked carbonyls

The susceptibility of carbonyl groups towards nucleophilic attack can be exploited for ICL formation. However, introduction of a carbonyl functionality into synthetic ODNs is troublesome and different strategies for masking the carbonyl groups have been used. Kobori *et al.* developed ODNs containing caged α-chloro- and α-bromoaldehyde moieties at the 5' end that are activated by UV irradiation and induce ICL formation (Figure I-13a) (89,90). Introduction of the caged carbonyl at different positions in the ODN was later achieved and applied for crosslinking formation with RNA having a point mutation (Figure I-13b). (91)

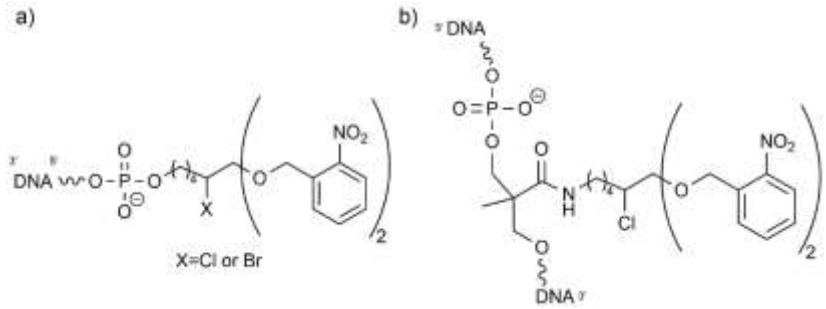

Figure I-13. Protected carbonyl groups introduced into ODNs.

An analogous protecting group was used for the introduction of a 4-oxo-enal functionality into an ODN that selectively formed an ICL towards T and G. (92)

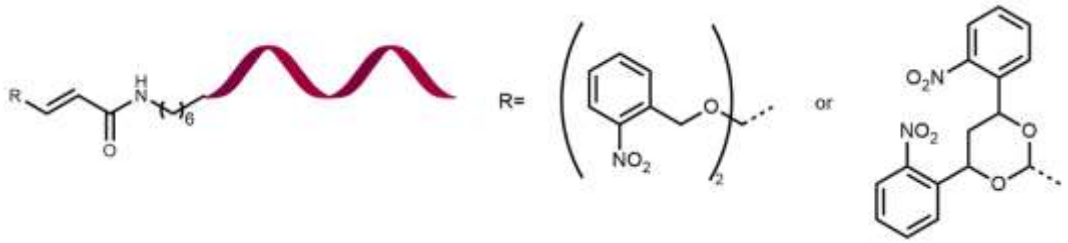

Figure I-14. Introduction of a 4-oxo-enal functionality using two different protecting gorups.

The furan methodology developed by our group falls into this category of masked carbonyls as furan can be seen as a stable precursor of a 4-oxo-enal which is unmasked upon oxidation.

It is worth noticing that many of these methodologies rely on the use of UV light for activation as this allows spatiotemporal control of the ICL formation. However, UV irradiation can promote the formation of thymidine dimers in DNA and is not the most suitable for therapeutic applications as it can damage surrounding tissues. For this reason the use of longer wavelength light for irradiation is desirable.

I.8. Furan as a masked functionality for ICL formation

Our group developed a strategy for ICL formation that took inspiration from furan toxicity. Upon metabolism in the liver by cytochrome P450 furans are transformed into reactive intermediates that can react with nucleophiles or further rearrange to form a cis-enedione, which is also susceptible to nucleophilic attack by different biomolecules. This is the reason for furan toxicity, especially kidney and liver toxicity, and therefore, furan is classified as a carcinogen by the IARC. (93,94)

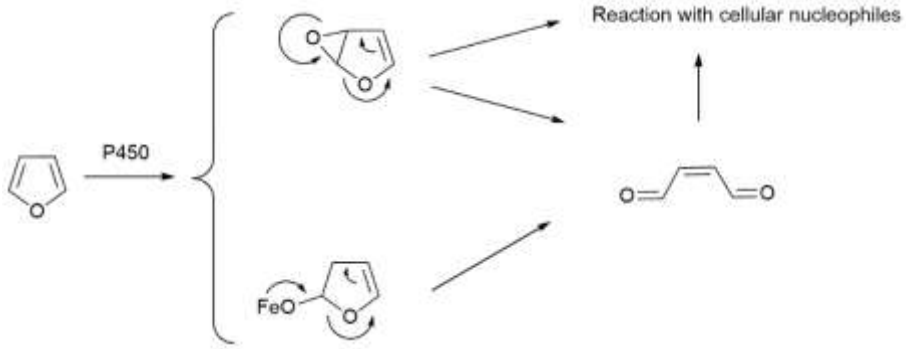

Figure I-15. Furan metabolism by cytochrome P450.

This susceptibility towards nucleophiles makes furan an ideal candidate for ICL as nucleobases contain nucleophilic groups that can react with the oxidised furan. Therefore, several furan

containing building blocks were developed by our group during the last years and they all can be easily incorporated during standard solid phase synthesis of oligonucleotides. (95–100)

The scope of the furan methodology has been explored in the context of crosslink formation in duplex DNA (98,100,101), duplex RNA (102), triplex forming ODNs (103), furan-PNA towards single and double stranded DNA (104). The versatility of this strategy allows it to be even applied for DNA-peptide crosslinking (105) and peptide labelling. (106)

The building blocks used for ICL formation in DNA or RNA showed selectivity towards (d)A or (d)C by reacting with their exocyclic amines. Although (d)G contains an exocyclic amine it is not oriented towards the major group hampering the formation of ICL formation. Last, dT or U do not have any exocyclic amine that can react with the oxidised furan and ICL formation with this nucleobases was never observed.

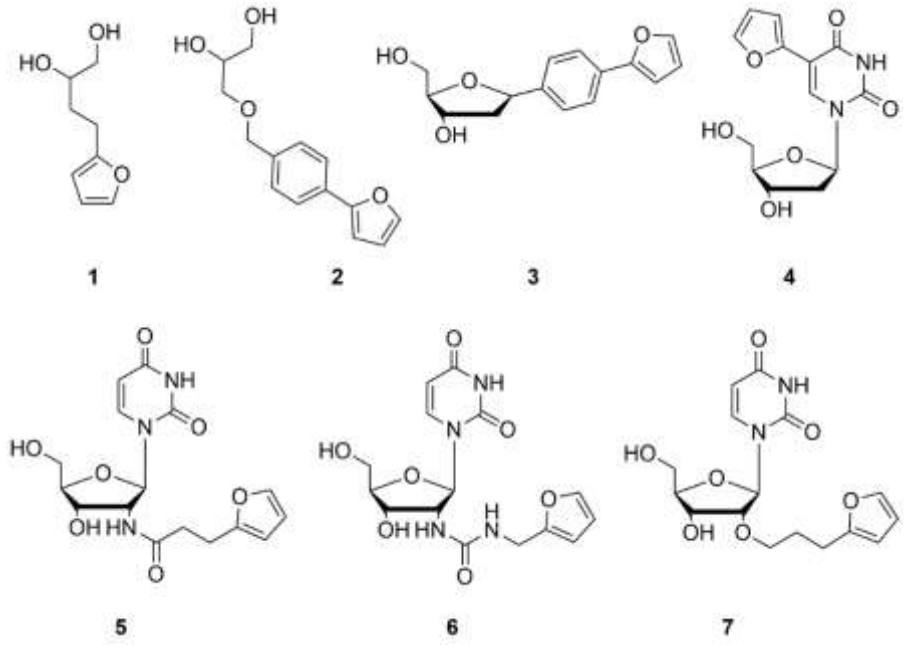

Figure I-16. Building blocks containing a furan moiety.

The crosslinking mechanism consists in the attack of the exocyclic amine to the aldehyde yielding a hemiaminal that undergoes cyclisation upon attack of the endocyclic nitrogen to the Michael acceptor that resulted after furan oxidation. The crosslinking reaction, depicted here (Figure I-17) for ICL towards dC, may stop at this point or proceed to form an aromatic adduct after losing a molecule of H_2O, depending on the furan building block of choice. During this study, building blocks **2** and **5** were used. Upon use of **5**, the reaction stops before aromatisation, whereas when using **2**, the aromatic adduct is obtained. It is worth noticing that when the ICL formation stops before aromatisation, the presence of two stereocentra results in the formation of

diasteromeric adducts that can be observed as two distinct signals by RP HPLC, as will be shown in the next chapters.

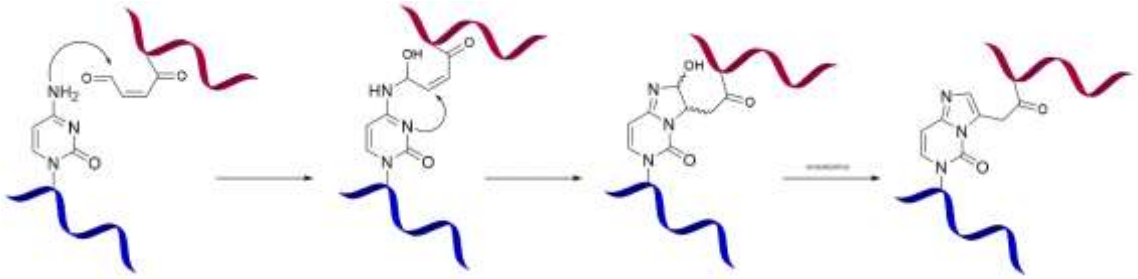

Figure I-17. Crosslinking mechanism between the oxidised furan and a cytosine on the complementary strand.

Two different triggers have been reported for furan ICL formation. First, the use of NBS results in the addition of a bromide to the 2 position of furan, followed by attack of a molecule of H_2O (figure I-18a). The ring opening leads to the formation of the 4-oxo-enal. Although effective, this activation method prevents the use of the furan methodology for biological applications and in some cases presents a side product resulting for the bromination of furan, which decreases the overall yield. Therefore, the use of a more biocompatible oxidant was envisioned and photosensitised singlet oxygen was the chosen agent.

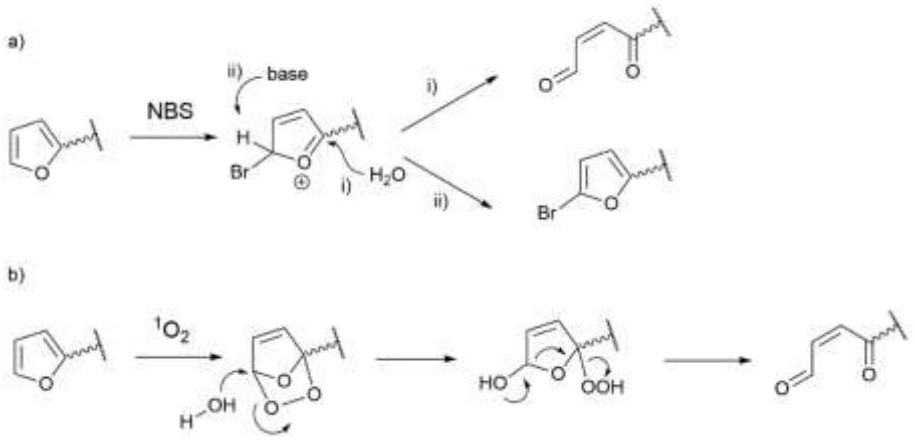

Figure I-18. Mechanism of furan oxidation by NBS and singlet oxygen.

Singlet oxygen-mediated oxidation of furan follows a different mechanism to NBS and consists of a [4+2] cycloaddition between the furan and the oxygen molecules. Addition of a H_2O molecule and rearrangement leads to the open 4-oxo-enal (figure I-18b). (107,108)

I.9. Properties and generation of singlet oxygen

Ground state oxygen is a paramagnetic molecule where two electrons with parallels spins occupy two different π^* orbitals. Since most organic molecules are diamagnetic, there is a spin restriction for reactions where oxygen accepts more than one electron at a time.

Excitation of molecular triplet oxygen ($^3O_2$) results in the formation of a more reactive oxygen species, the so-called singlet oxygen ($^1O_2$), where the two electrons possess opposite spins. Since the spin restriction is removed, $^1O_2$ is more oxidising than $^3O_2$ (1V) and reacts with molecules such as unsaturated C-C bonds, neutral nucleophiles and anions, which makes it a versatile synthetic reagent. (109)

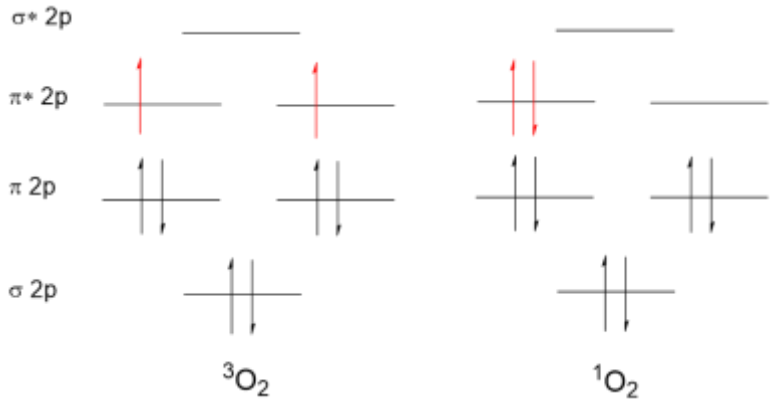

Figure I-19. Molecular orbitals diagrams for $^3O_1$ and $^1O_2$

1.2. <u>Singlet oxygen generation</u>

In 1926, Moureau and Dufraisse discovered that the aromatic compound rubrene (Figure I-20a) is able to covalently bind oxygen, and that this process is reversible, producing $^1O_2$ and $^3O_2$ when it decomposes. Since then many aromatic compounds have been described to undergo a reversible [4+2] cycloaddition with O_2. (110) MNP and the corresponding endoperoxide $MNPO_2$ are the only ones that require a mild activation such as (Figure I-20b). (111) These compounds are poorly water soluble (10^{-2} M at pH 7.5) but this problem was overcome by introducing a second sodium propylcarboxylate group in $NDPO_2$ and NDP, (111) and these compounds are widely used in biological environments to generate controlled amounts of $^1O_2$.

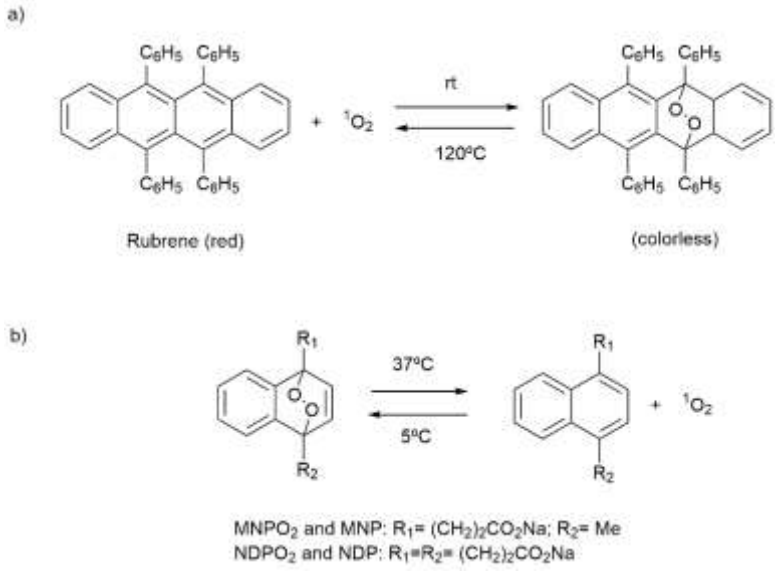

Figure I-20. Singlet oxygen reversible reaction with aromatic compounds.

However, the most common mechanism for $^1O_2$ generation is by means of a photosensitiser (PS). PSs are compounds that are able to harvest light and transfer the energy to another molecule, in this case to $^3O_2$. As depicted in figure I-21 upon light irradiation the PS goes to the excited singlet state where it can deactivate via a radiative (fluorescence) or non-radiative process or, by intersystem crossing, lead to the triplet state PS. This ^{3}PS is able to interact with $^3O_2$, generating $^1O_2$ in what is known as Type II mechanism, whereas deactivation via Type I mechanism involves electron and/or proton transfer and leads to the generation of other reactive oxygen species (ROS) such as hydroxyl radical ($^{\cdot}$OH), superoxide anion ($O_2^{\cdot-}$) and hydrogen peroxide (H_2O_2).

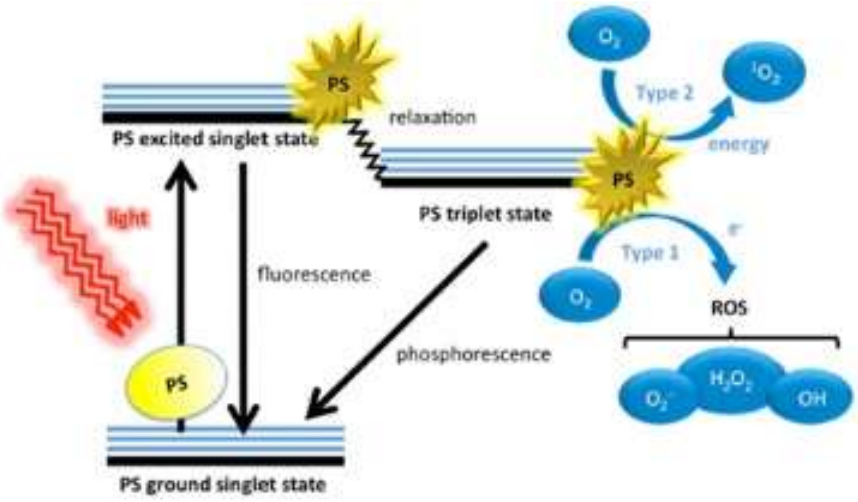

Figure I-21. Jablonski diagram for ROS generation. Reproduced with permission from (109)

1.3. *Singlet oxygen applications*

- As reagent in organic synthesis

  The electrophilic character of $^1O_2$ determines the type of reactions that it can undergo and those can be divided in three classes: a) ene reactions, b) [4+2] and [2+2] cycloadditions and c) reactions with heteroatom centres.

  a) Ene reactions consist in the addition of a molecule of $^1O_2$ to a sp^2 carbon of an alkene substrate and abstraction of hydrogen from a distal allylic carbon, resulting in an allylic hydroperoxide.

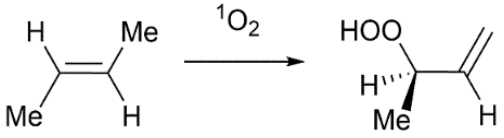

Figure I-22. Ene reaction.

  b) [4+2] and [2+2] cycloadditions

  The [4+2] cycloaddition (figure I-23a) between a rich cis-diene and $^1O_2$ is analogous to the Diels-Alder reaction where an endoperoxide is formed, in a stereospecific manner. Different types of dienes can be used such as acylic, cyclic, polyaromatic, or hetero- atomatic

  In [2+2] cycloaddtions (figure I-23b), dioxoetanes are formed by addition of $^1O_2$ to an electron rich alkene. However, the formation of the [4+2] and ene reaction products as contaminants is common.

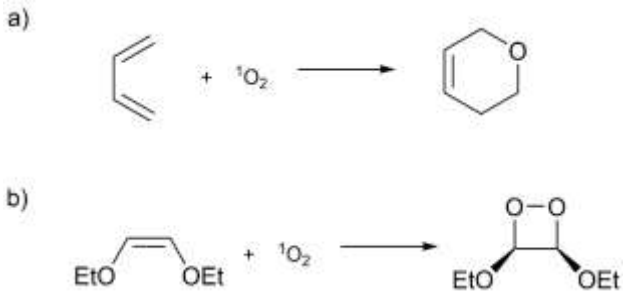

Figure I-23. Singlet oxygen cycloadditions

c) Reactions with heteroatom centres

Reaction between $^1O_2$ and heteroatoms have been studied with a variety of heteroatom containing organic molecules including: organosulfur compounds, phosphines, nitrogen compounds and some organometallic complexes. However, the efficiency of the reaction is low, since the physical deactivation of the intermediates competes to result in $^3O_2$ and the original substrate (figure I-24)

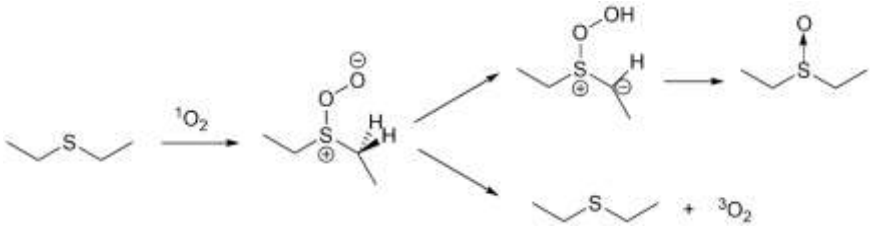

Figure I-24. Example of a reaction between $^1O_2$ and an organosulfur compound and the competing deactivation

- Photodynamic therapy.

  Photodynamic therapy (PDT) is the use of a combination of light, oxygen and a photosensitiser for producing a therapeutic effect and it relies on the generation of ROS, especially $^1O_2$. Those three elements do not individually exert a therapeutic effect but in combination, result in a versatile technique for treating various diseases such as cancer, psoriasis, dermatitis, etc. (112) Closely related, ROS can be used for elimination of microorganisms in the so called antimicrobial PDT (aPDT). (113,114)

Figure I-25. Oxygen, light and photosensitiser are the components needed for PDT.

One of the main drawbacks of PDT comes from the need of light irradiation which limits the widespread clinical use of PDT (115) and several strategies have been followed

recently to overcome this issue. For example, the design and synthesis of photosensitisers that absorb in the near infrared region (NIR) allows to expand the possibilities for treatment of malignancies situated deeper in the organisms. Two photon absorbance PDT has been very promising and self-irradiating compounds have been designed as well. (116,117)

Many types of PSs have been used for $^1O_2$ generation and they can be classified into porphyrin and non-porphyrin based. As dark toxicity can be a problem, porphyrin based molecules, which are devoid of that problem, have come into play. Porphyrins are aromatic macrocyclic compounds that strongly absorb in the visible part of the electromagnetic spectrum. They can exist as the free base, where no metal is coordinated by the four nitrogen atoms in the central cavity, or metallated with a variety of metal atoms. Closely related to porphyrins, chlorins possess the same aromatic core but one of the double bonds is reduced. If two of the double bonds have been reduced they receive the name of bacteriochlorins. Phthalocyanines possess extra nitrogens in the meso positions and benzene rings to the pyrroles.

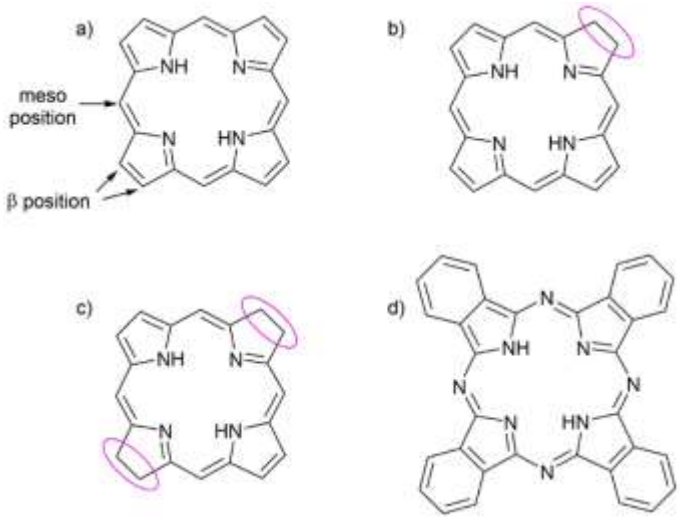

Figure I-26. General structure of a) porphyrins b) chlorins c) bacteriochlorins and d) phthalocyanines.

For PDT applications, many different PSs have been reported and studied, trying to improve their properties such as absorption, $^1O_2$ quantum yield, biocompatibility, solubility, etc. The first PS approved for clinical use was a synthetic polymer derived from haemotoporphyrin (Hp), commercialised under the name of Photofrin™. However, this compound is actually a complex mixture of monomers and oligomers and its absorption in the therapeutic window is low (1170 M^{-1} cm^{-1} at 630 nm) requiring higher doses of the drug to induce an effect. For this reason, a second generation of PSs was developed where the absorbance in the red region of the electromagnetic spectrum, more interesting for clinical application, was improved. Chlorins, phthalocyanines, texaphyrins, etc are among these compounds. Development of the

third generation PSs focusses on improving the specific targeting of the PS, for example by conjugation to antibodies, ODNs, etc. (118)

I.10. References

1. Shing P, Carter M. DNA Structure: Alphabet Soup for the Cellular Soul. In: DNA Replication-Current Advances. InTech; 2011. p. 1–27.

2. Watson JD, Crick FHC. Molecular structure of nucleic aids: A structure for deoxyribose nucleic acid. Nature. 1953 Apr 25;171(4356):737–8.

3. Lee RC, Feinbaum RL, Ambros V. The C. elegans heterochronic gene lin-4 encodes small RNAs with antisense complementarity to lin-14. Cell. 1993 Dec;75(5):843–54.

4. Bartel DP. MicroRNAs: Target Recognition and Regulatory Functions. Cell. 2009 Jan;136(2):215–33.

5. Zeng Y. Principles of micro-RNA production and maturation. Oncogene. 2006 Oct 9;25(46):6156–62.

6. Wahlestedt C. Targeting long non-coding RNA to therapeutically upregulate gene expression. Nat Rev Drug Discov. Nature Publishing Group, a division of Macmillan Publishers Limited. All Rights Reserved.; 2013 Jun;12(6):433–46.

7. Greenberg MM. Abasic and oxidized abasic site reactivity in DNA: Enzyme inhibition, cross-linking, and nucleosome catalyzed reactions. Acc Chem Res. 2014;47(2):646–55.

8. Greenman C, Stephens PR, Bignell G, Birney E, Stratton MR, Smith RM, et al. Patterns of somatic mutation in human cancer genomes. Nature. 2007;446(7132):153–8.

9. Costabile M, Quach A, Ferrante A. Molecular approaches in the diagnosis of primary immunodeficiency diseases. Hum Mutat. 2006 Dec;27(12):1163–73.

10. Li Y. Detection of Paternally Inherited Fetal Point Mutations for β-Thalassemia Using Size-Fractionated Cell-Free DNA in Maternal Plasma. JAMA. 2005 Feb 16;293(7):843.

11. Leinberger DM, Grimm V, Rubtsova M, Weile J, Schröppel K, Wichelhaus TA, et al. Integrated detection of extended-spectrum-beta-lactam resistance by DNA microarray-based genotyping of TEM, SHV, and CTX-M genes. J Clin Microbiol. 2010;48(2):460–71.

12. Pulido MR, García-Quintanilla M, Martín-Peña R, Cisneros JM, McConnell MJ. Progress on the development of rapid methods for antimicrobial susceptibility testing. J

Antimicrob Chemother. 2013;68(12):2710–7.

13. Homer N, Szelinger S, Redman M, Duggan D, Tembe W, Muehling J, et al. Resolving Individuals Contributing Trace Amounts of DNA to Highly Complex Mixtures Using High-Density SNP Genotyping Microarrays. Visscher PM, editor. PLoS Genet. 2008 Aug 29;4(8).

14. Chee M, Yang R, Hubbell E, Berno A, Huang XC, Stern D, et al. Accessing Genetic Information with High-Density DNA Arrays. Science. 1996;274(5287):610–4.

15. Bashir R. BioMEMS: State-of-the-art in detection, opportunities and prospects. Adv Drug Deliv Rev. 2004;56(11):1565–86.

16. Syvänen A-C. Accessing genetic variation: genotyping single nucleotide polymorphisms. Nat Rev Genet. 2001 Dec;2(12):930–42.

17. McGuigan FE a, Ralston SH. Single nucleotide polymorphism detection: allelic discrimination using TaqMan. Psychiatr Genet. 2002;12(3):133–6.

18. Gunderson KL, Steemers FJ, Ren H, Ng P, Zhou L, Tsan C, et al. Whole-Genome Genotyping. Methods Enzymol. 2006;410(2003):359–76.

19. Kumar Khanna V. Existing and emerging detection technologies for DNA (Deoxyribonucleic Acid) finger printing, sequencing, bio- and analytical chips: A multidisciplinary development unifying molecular biology, chemical and electronics engineering. Biotechnol Adv. 2007;25(1):85–98.

20. Li YB, Zhang H, Zhu HY, Ling LS. A sensitive fluorescence method for sequence-specific recognition of single-stranded DNA by using glucose oxidase. Anal Methods. Royal Society of Chemistry; 2015;7(13):5436–40.

21. Wang F, Elbaz J, Orbach R, Magen N, Willner I. Amplified analysis of DNA by the autonomous assembly of polymers consisting of DNAzyme wires. J Am Chem Soc. 2011;133(43):17149–51.

22. Liu B, Bazan GC. Methods for strand-specific DNA detection with cationic conjugated polymers suitable for incorporation into DNA chips and microarrays. Proc Natl Acad Sci. 2005 Jan 18;102(3):589–93.

23. Xiao Y, Lubin AA, Baker BR, Plaxco KW, Heeger AJ. Single-step electronic detection of femtomolar DNA by target-induced strand displacement in an electrode-bound duplex.

Proc Natl Acad Sci. 2006;103(45):16677–80.

24. Zhang J, Wu X, Chen P, Lin N, Chen J, Chen G, et al. Electrochemical genotyping and detection of single-nucleotide polymorphisms based on junction-probe containing 2'-deoxyinosine. Chem Commun (Camb). 2010;46(37):6986–8.

25. Taton TA, Mirkin CA, Letsinger RL. Scanometric DNA array detection with nanoparticle probes. Science. 2000 Sep 8;289(5485):1757–60.

26. Storhoff JJ, Lucas AD, Garimella V, Bao YP, Müller UR. Homogeneous detection of unamplified genomic DNA sequences based on colorimetric scatter of gold nanoparticle probes. Nat Biotechnol. 2004;22(7):883–7.

27. Xue X, Xu W, Wang F, Liu X. Multiplex single-nucleotide polymorphism typing by nanoparticle-coupled DNA-templated reactions. J Am Chem Soc. 2009;131(33):11668–9.

28. Reynolds RA, Mirkin CA, Letsinger RL. Homogeneous, Nanoparticle-Based Quantitative Colorimetric Detection of Oligonucleotides. J Am Chem Soc. 2000 Apr;122(15):3795–6.

29. Dubertret B, Calame M, Libchaber a J. Single-mismatch detection using gold-quenched fluorescent oligonucleotides. Nat Biotechnol. 2001;19(4):365–70.

30. Kwon SJ, Bard AJ. DNA analysis by application of Pt nanoparticle electrochemical amplification with single label response. J Am Chem Soc. 2012;134(26):10777–9.

31. Knemeyer JP, Marme N, Sauer M. Probes for detection of specific DNA sequences at the single-molecule level. Anal Chem. 2000;72(16):3717–24.

32. Peng X, Greenberg MM. Facile SNP detection using bifunctional, cross-linking oligonucleotide probes. Nucleic Acids Res. 2008 Jan 10;36(5):e31–e31.

33. Fujimoto K, Yamada A, Yoshimura Y, Tsukaguchi T, Sakamoto T. Details of the Ultrafast DNA Photo-Cross-Linking Reaction of 3-Cyanovinylcarbazole Nucleoside: Cis–Trans Isomeric Effect and the Application for SNP-Based Genotyping. J Am Chem Soc. 2013 Oct 30;135(43):16161–7.

34. Helene C. Control of oncogene expression by antisense nucleic acids. Eur J Cancer. Elsevier; 1994;30(11):1721–6.

35. Sharma HW, Perez JR, Higgins-Sochaski K, Hsiao R, Narayanan R. Transcription factor decoy approach to decipher the role of NF-kappa B in oncogenesis. Anticancer Res.

1995;16(1):61–9.

36. Kielkopf CL, White S, Szewczyk JW, Turner JM, Baird EE, Dervan PB, et al. A structural basis for recognition of A· T and T· A base pairs in the minor groove of B-DNA. Science (80-). American Association for the Advancement of Science; 1998;282(5386):111–5.

37. Kielkopf CL, Baird EE, Dervan PB, Rees DC. Structural basis for G• C recognition in the DNA minor groove. Nat Struct Mol Biol. Nature Publishing Group; 1998;5(2):104–9.

38. Kielkopf CL, Bremer RE, White S, Szewczyk JW, Turner JM, Baird EE, et al. Structural effects of DNA sequence on T· A recognition by hydroxypyrrole/pyrrole pairs in the minor groove. J Mol Biol. Elsevier; 2000;295(3):557–67.

39. Beelman CA, Parker R. Degradation of mRNA in eukaryotes. Cell. Elsevier; 1995;81(2):179–83.

40. Liebhaber SA. mRNA stability and the control of gene expression. In: Nucleic acids symposium series. 1996. p. 29–32.

41. Scanlon KJ, Ohta Y, Ishida H, Kijima H, Ohkawa T, Kaminski A, et al. Oligonucleotide-mediated modulation of mammalian gene expression. FASEB J. FASEB; 1995;9(13):1288–96.

42. Stein CA. How to design an antisense oligodeoxynucleotide experiment: a consensus approach. Antisense Nucleic Acid Drug Dev. 1998;8(2):129–32.

43. Kole R, Sazani P. Antisense effects in the cell nucleus: modification of splicing. Curr Opin Mol Ther. 2001;3(3):229–34.

44. Dominski Z, Kole R. Identification and characterization by antisense oligonucleotides of exon and intron sequences required for splicing. Mol Cell Biol. Am Soc Microbiol; 1994;14(11):7445–54.

45. Zamaratski E, Pradeepkumar PI, Chattopadhyaya J. A critical survey of the structure-function of the antisense oligo/RNA heteroduplex as substrate for RNase H. J Biochem Biophys Methods. Elsevier; 2001;48(3):189–208.

46. CROOKE ST. Molecular mechanisms of antisense drugs: RNase H. Antisense Nucleic Acid Drug Dev. 1998;8(2):133–4.

47. Castanotto D, Scherr M, Rossi JJ. Intracellular expression and function of antisense catalytic RNAs. Methods Enzymol. Elsevier; 2000;313:401–20.

48. Rossi JJ. Ribozymes, genomics and therapeutics. Chem Biol. Elsevier; 1999;6(2):R33–7.

49. Santoro SW, Joyce GF. A general purpose RNA-cleaving DNA enzyme. Proc Natl Acad Sci. National Acad Sciences; 1997;94(9):4262–6.

50. Wu Y, Yu L, McMahon R, Rossi JJ, Forman SJ, Snyder DS. Inhibition of bcr-abl oncogene expression by novel deoxyribozymes (DNAzymes). Hum Gene Ther. Mary Ann Liebert, Inc.; 1999;10(17):2847–57.

51. SUMMERTON J, WELLER D. Morpholino Antisense Oligomers: Design, Preparation, and Properties. Antisense Nucleic Acid Drug Dev. 1997 Jun;7(3):187–95.

52. Iversen PL. Phosphorodiamidate morpholino oligomers: favorable properties for sequence-specific gene inactivation. Curr Opin Mol Ther. 2001;3(3):235.

53. Kean JM, Murakami A, Blake KR, Cushman CD, Miller PS. Photochemical cross-linking of psoralen-derivatized oligonucleoside methylphosphonates to rabbit globin messenger RNA. Biochemistry. 1988 Dec;27(26):9113–21.

54. Matsuyama Y, Yamayoshi A, Kobori A, Murakami A. Functional regulation of RNA-induced silencing complex by photoreactive oligonucleotides. Bioorg Med Chem. Elsevier Ltd; 2014 Feb 1;22(3):1003–7.

55. Sakamoto T, Shigeno A, Ohtaki Y, Fujimoto K, Miller PS, Braiterman LT, et al. Photo-regulation of constitutive gene expression in living cells by using ultrafast photo-cross-linking oligonucleotides. Biomater Sci. Royal Society of Chemistry; 2014 Jun 26;2(9):1154.

56. Ali MM, Oishi M, Nagatsugi F, Mori K, Nagasaki Y, Kataoka K, et al. Intracellular inducible alkylation system that exhibits antisense effects with greater potency and selectivity than the natural oligonucleotide. Angew Chem Int Ed Engl. 2006;45(19):3136–40.

57. Coleman RS, Kesicki E a. Template-Directed Crosslinking of Oligonucleotides: Site-Specific Covalent Modification of dG-N7 within Duplex DNA. J Org Chem. 1995 Oct;60(20):6252–3.

58. Coleman RS, Pires RM. Covalent cross-linking of duplex DNA using 4-thio-2'-deoxyuridine as a readily modifiable platform for introduction of reactive functionality into oligonucleotides. Nucleic Acids Res. 1997 Dec 1;25(23):4771–7.

59. Alzeer J, Schärer OD. A modified thymine for the synthesis of site-specific thymine-guanine DNA interstrand crosslinks. Nucleic Acids Res. 2006 Sep;34(16):4458–66.

60. Hentschel S, Alzeer J, Angelov T, Schärer OD, Luedtke NW. Synthesis of DNA Interstrand Cross-Links Using a Photocaged Nucleobase. Angew Chemie Int Ed. 2012 Apr 2;51(14):3466–9.

61. Webb TR, Matteucci MD. Hybridization triggered cross-linking of deoxyoligonucleotides. Nucleic Acids Res. 1986;14(19):7661–74.

62. Webb TR, Matteucci MD. Sequence-specific cross-linking of deoxyoligonucleotides via hybridization-triggered alkylation. J Am Chem Soc. 1986 May;108(10):2764–5.

63. Lukhtanov EA, Podyminogin MA, Kutyavin I V., Meyer RB, Gamper HB. Rapid and Efficient Hybridization-Triggered Crosslinking Within a DNA Duplex by an Oligodeoxyribonucleotide Bearing a Conjugated Cyclopropapyrroloindole. Nucleic Acids Res. 1996 Feb 1;24(4):683–7.

64. Sugihara Y, Tatsumi S, Kobori A. Development of Novel Photoresponsive Oligodeoxyribonucleotides with a 2'- O -Diazirine-conjugated Adenosine for DNA Interstrand Crosslinking. Chem Lett. 2017 Feb 5;46(2):236–9.

65. Nagatsugi F, Kawasaki T, Usui D, Maeda M, Sasaki S. Highly Efficient and Selective Cross-Linking to Cytidine Based on a New Strategy for Auto-Activation within a Duplex. J Am Chem Soc. 1999 Jul;121(28):6753–4.

66. Nishimoto A, Jitsuzaki D, Onizuka K, Taniguchi Y, Nagatsugi F, Sasaki S. 4-vinyl-substituted pyrimidine nucleosides exhibit the efficient and selective formation of interstrand cross-links with RNA and duplex DNA. Nucleic Acids Res. 2013;41(13):6774–81.

67. Imoto S, Hori T, Hagihara S, Taniguchi Y, Sasaki S, Nagatsugi F. Alteration of cross-linking selectivity with the 2'-OMe analogue of 2-amino-6-vinylpurine and evaluation of antisense effects. Bioorganic Med Chem Lett. Elsevier Ltd; 2010;20(20):6121–4.

68. Hagihara S, Kusano S, Lin WC, Chao XG, Hori T, Imoto S, et al. Production of truncated protein by the crosslink formation of mRNA with 2'-OMe oligoribonucleotide containing 2-amino-6-vinylpurine. Bioorganic Med Chem Lett. Elsevier Ltd; 2012;22(12):3870–2.

69. Hong IS, Greenberg MM. DNA Interstrand Cross-Link Formation Initiated by Reaction between Singlet Oxygen and a Modified Nucleotide. J Am Chem Soc. 2005

Aug;127(30):10510–1.

70. Peng X, In SH, Li H, Seidman MM, Greenberg MM. Interstrand cross-link formation in duplex and triplex DNA by modified pyrimidines. J Am Chem Soc. 2008;130(31):10299–306.

71. Hong IS, Greenberg MM. Efficient DNA Interstrand Cross-Link Formation from a Nucleotide Radical. J Am Chem Soc. 2005 Mar;127(11):3692–3.

72. Hong IS, Ding H, Greenberg MM. Oxygen independent DNA interstrand cross-link formation by a nucleotide radical. J Am Chem Soc. 2006;128(2):485–91.

73. Haque MM, Sun H, Liu S, Wang Y, Peng X. Photoswitchable Formation of a DNA Interstrand Cross-Link by a Coumarin-Modified Nucleotide. Angew Chemie Int Ed. 2014 Jul 1;53(27):7001–5.

74. Sun H, Fan H, Peng X. Quantitative DNA interstrand cross-link formation by coumarin and thymine: Structure determination, sequence effect, and fluorescence detection. J Org Chem. 2014;79(23):11359–69.

75. Lee BL, Murakami A, Blake KR, Lin S Bin, Miller PS. Interaction of psoralen-derivatized oligodeoxyribonucleoside methylphosphonates with single-stranded DNA. Biochemistry. 1988 May;27(9):3197–203.

76. Murakami A, Yamayoshi A, Iwase R, Nishida J, Yamaoka T, Wake N. Photodynamic antisense regulation of human cervical carcinoma cell growth using psoralen-conjugated oligo(nucleoside phosphorothioate). Eur J Pharm Sci. 2001 Apr;13(1):25–34.

77. Murakami A, Yamamoto Y, Namba M, Iwase R, Yamaoka T. Photo-Cross-Linked Oligonucleotide Duplex as a Decoy-DNA for Inhibition of Restriction Endonuclease Activity. Bioorg Chem. 2001 Aug;29(4):223–33.

78. Yamayoshi A, Shimazu N, Higuchi M, Kobori A, Murakami A. Gene regulation by decoy approach (II): Development of photo-cross-linked oligonucleotides duplex as a decoy DNA for estrogen receptor. Nucleic Acids Symp Ser (Oxf). 2007;(51):91–2.

79. Yamayoshi A, Iwase R, Yamaoka T, Murakami A. Psoralen-conjugated oligonucleotide with hairpin structure as a novel photo-sensitive antisense molecule. Chem Commun (Camb). 2003;1370–1.

80. Higuchi M, Yamayoshi A, Yamaguchi T, Iwase R, Yamaoka T, Kobori A, et al. Selective

Photo-Cross-Linking of 2'- O -Psoralen-Conjugated Oligonucleotide with Rnas Having Point Mutations. Nucleosides, Nucleotides and Nucleic Acids. 2007 Apr 9;26(3):277–90.

81. Higuchi M, Kobori A, Yamayoshi A, Murakami A. Synthesis of antisense oligonucleotides containing 2'-O-psoralenylmethoxyalkyl adenosine for photodynamic regulation of point mutations in RNA. Bioorg Med Chem. Elsevier Ltd; 2009 Jan;17(2):475–83.

82. Higuchi M, Yamayoshi A, Kato K, Kobori A, Wake N, Murakami A. Specific Regulation of Point-Mutated K- ras -Immortalized Cell Proliferation by a Photodynamic Antisense Strategy. Oligonucleotides. 2010 Feb;20(1):37–44.

83. Yoshimura Y, Fujimoto K. Ultrafast reversible photo-cross-linking reaction: Toward in situ DNA manipulation. Org Lett. 2008;10(15):3227–30.

84. Yoshimura Y, Ohtake T, Okada H, Fujimoto K. A New Approach for Reversible RNA Photocrosslinking Reaction: Application to Sequence-Specific RNA Selection. ChemBioChem. 2009 Jun 15;10(9):1473–6.

85. Shigeno A, Sakamoto T, Yoshimura Y, Fujimoto K. Quick regulation of mRNA functions by a few seconds of photoirradiation. Org Biomol Chem. 2012;10(38):7820.

86. Tagawa M, Shohda K, Fujimoto K, Suyama A. Stabilization of DNA nanostructures by photo-cross-linking. Soft Matter. 2011;7(22):10931.

87. Nakamura S, Fujimoto K. Creation of DNA array structure equipped with heat resistance by ultrafast photocrosslinking. J Chem Technol Biotechnol. 2014;89(7):1086–90.

88. Gerrard SR, Hardiman C, Shelbourne M, Nandhakumar I, Nordén B, Brown T. A new modular approach to nanoassembly: Stable and addressable DNA nanoconstructs via orthogonal click chemistries. ACS Nano. 2012;6(10):9221–8.

89. Kobori A, Nagae Y, Sugihara Y, Yamayoshi A, Murakami A. Rate-adjusted cross-linking reaction by photoresponsive α-bromoaldehyde (PBA)-conjugated ODN. Bioorg Med Chem Lett. Elsevier Ltd; 2013 Nov;23(21):5825–8.

90. Kobori A, Yamauchi T, Nagae Y, Yamayoshi A, Murakami A. Novel photoresponsive cross-linking oligodeoxyribonucleotides having a caged α-chloroaldehyde. Bioorg Med Chem. Elsevier Ltd; 2012 Sep;20(17):5071–6.

91. Sugihara Y, Nakata Y, Yamayoshi A, Murakami A, Kobori A. Cross-linking antisense oligodeoxyribonucleotides with a photoresponsive α-chloroaldehyde moiety for RNA

point mutations. J Org Chem. 2016;81(3):981–6.

92. Sun J, Tang X. Photouncaged Sequence-specific Interstrand DNA Cross-Linking with Photolabile 4-oxo-enal-modified Oligonucleotides. Sci Rep. Nature Publishing Group; 2015 Sep 28;5(1):10473.

93. IARC Working Group on the Evaluation of Carcinogenic Risks to Humans. IARC monographs on the evaluation of carcinogenic risks to humans. Ingested nitrate and nitrite, and cyanobacterial peptide toxins. In: Iarc Monographs on the Evaluation of Carcinogenic Risks to Humans. IARC, Distributed for the International Agency for Research on Cancer by the Secretariat of the World Health Organization; 2010. p. v-412.

94. Bakhiya N, Appel KE. Toxicity and carcinogenicity of furan in human diet. Arch Toxicol. 2010 Jul 17;84(7):563–78.

95. Halila S, Velasco T, Clercq P De, Madder A. Fine-tuning furan toxicity: fast and quantitative DNA interchain cross-link formation upon selective oxidation of a furan containing oligonucleotide. Chem Commun (Camb). 2005 Feb 21;(7):936–8.

96. Stevens K, Madder A. Synthesis and Incorporation of a Simple Acyclic Furan Containing Phosphoramidite. Nucleosides, Nucleotides and Nucleic Acids. 2007 Nov 26;26(10–12):1359–62.

97. Jawalekar AM, Op de Beeck M, van Delft FL, Madder A. Synthesis and incorporation of a furan-modified adenosine building block for DNA interstrand crosslinking. Chem Commun (Camb). 2011 Mar 14;47(10):2796–8.

98. Stevens K, Madder A. Furan-modified oligonucleotides for fast, high-yielding and site-selective DNA inter-strand cross-linking with non-modified complements. Nucleic Acids Res. 2009 Apr;37(5):1555–65.

99. Stevens K, Claeys DD, Catak S, Figaroli S, Hocek M, Tromp JM, et al. Furan-oxidation-triggered inducible DNA cross-linking: acyclic versus cyclic furan-containing building blocks--on the benefit of restoring the cyclic sugar backbone. Chemistry. 2011 Jun 14;17(25):6940–53.

100. Op de Beeck M, Madder A. Unprecedented C-selective interstrand cross-linking through in situ oxidation of furan-modified oligodeoxynucleotides. J Am Chem Soc. 2011 Feb 2;133(4):796–807.

101. De Laet N, Madder A. Synthesis and evaluation of methylene blue oligonucleotide

conjugates for DNA interstrand cross-linking. J Photochem Photobiol A Chem. Elsevier B.V.; 2016;318:64–70.

102. Carrette LLG, Gyssels E, Loncke J, Madder a. A mildly inducible and selective cross-link methodology for RNA duplexes. Org Biomol Chem. 2014;12:931–5.

103. Gyssels E, Carrette Dr LLG, Vercruysse E, Stevens Dr K, Madder A. Triplex crosslinking through furan oxidation requires perturbation of the structured triple-helix. ChemBioChem. 2015;16(4):651–8.

104. Manicardi A, Gyssels E, Corradini R, Madder A. Furan-PNA: a mildly inducible irreversible interstrand crosslinking system targeting single and double stranded DNA. Chem Commun. Royal Society of Chemistry; 2016;52:6930–3.

105. Carrette LLG, Morii T, Madder A. Toxicity inspired cross-linking for probing DNA-peptide interactions. Bioconjug Chem. 2013;24(12):2008–14.

106. Antonatou E, Hoogewijs K, Kalaitzakis D, Baudot A, Vassilikogiannakis G, Madder A. Singlet Oxygen-Induced Furan Oxidation for Site-Specific and Chemoselective Peptide Ligation. Chem - A Eur J. 2016 Jun 13;22(25):8457–61.

107. Chen LJ, Hecht SS, Peterson LA. Identification of cis-2-butene-1,4-dial as a microsomal metabolite of furan. Chem Res Toxicol. 1995;8(7):903–6.

108. Montagnon T, Noutsias D, Alexopoulou I, Tofi M, Vassilikogiannakis G. Green oxidations of furans—initiated by molecular oxygen—that give key natural product motifs. Org Biomol Chem. 2011;9(7):2031.

109. Zamadar M, Greer A. Singlet oxygen as a reagent in organic synthesis. Handb Synth Photochem. Wiley Online Library; 2010;353–86.

110. Aubry JM, Pierlot C, Rigaudy J, Schmidt R. Reversible binding of oxygen to aromatic compounds. Acc Chem Res. 2003;36(9):668–75.

111. Saito I, Matsuura T, Inoue K. Formation of superoxide ion from singlet oxygen. Use of a water-soluble singlet oxygen source. J Am Chem Soc. American Chemical Society; 1981 Jan 1;103(1):188–90.

112. Dolmans DEJGJ, Fukumura D, Jain RK. Photodynamic therapy for cancer. Nat Rev Cancer. 2003 May;3(5):380–7.

113. Maisch T, Baier J, Franz B, Maier M, Landthaler M, Szeimies R-M, et al. The role of

singlet oxygen and oxygen concentration in photodynamic inactivation of bacteria. Proc Natl Acad Sci. 2007 Apr 24;104(17):7223–8.

114. Jiang L, Gan CRR, Gao J, Loh XJ. A Perspective on the Trends and Challenges Facing Porphyrin-Based Anti-Microbial Materials. Small. 2016 Jul;12(27):3609–44.

115. Fan W, Huang P, Chen X. Overcoming the Achilles' heel of photodynamic therapy. Chem Soc Rev. Royal Society of Chemistry; 2016;45(23):6488–519.

116. Ogawa K, Kobuke Y. Recent Advances in Two-Photon Photodynamic Therapy. Anticancer Agents Med Chem. 2008 Apr 1;8(3):269–79.

117. Hsu C-Y, Chen C-W, Yu H-P, Lin Y-F, Lai P-S. Bioluminescence resonance energy transfer using luciferase-immobilized quantum dots for self-illuminated photodynamic therapy. Biomaterials. Elsevier Ltd; 2013 Jan;34(4):1204–12.

118. DeRosa MC, Crutchley RJ. Photosensitized singlet oxygen and its applications. Coord Chem Rev. 2002 Nov 1;233–234:351–71.

Chapter II.

Aims and objectives

Nucleic acids have been exploited as versatile compounds in diverse fields for diagnosis, therapy and nanomaterial applications. Introduction of an interstrand crosslink has proven to offer great potential for enhancing the properties of nucleic acids or providing them with new characteristics, and a variety of crosslinking techniques have been developed, as described in the previous chapter. However, in some of those applications the use of a mild, spatiotemporally controlled activation of the crosslinking is desirable. In this context, the use of the furan methodology coupled with the triggering of the reaction *via* singlet oxygen allows efficient crosslinking under biocompatible conditions, as has been previously stablished using methylene blue and rose bengal.

In this study the generation of singlet oxygen is achieved using three porphyrin-based photosensitisers. Chlorin e6 (Ce6), a tripyridyl porphyrin (TriPyCOOH) and a zinc phthalocyanine decorated with tert-butyl groups in the periphery (TT1) have been evaluated for singlet oxygen generation to induce interstrand crosslink formation.

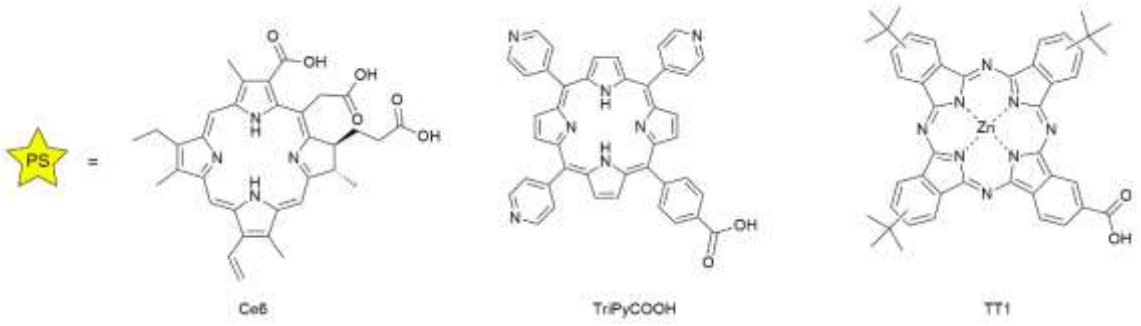

It was previously established that the use of singlet oxygen in a nucleic acid context requires fine tuning of the reaction conditions to maximise the crosslink formation without undesired degradation of the duplex. For this reason, the first step during this work was to study the crosslink reaction with the photosensitisers added in solution in the presence of the duplex, where one of the strands contains the furan moiety. Variation of the concentration, reaction time, light type, etc will be explored and optimised to maximise the crosslink formation while minimising degradation.

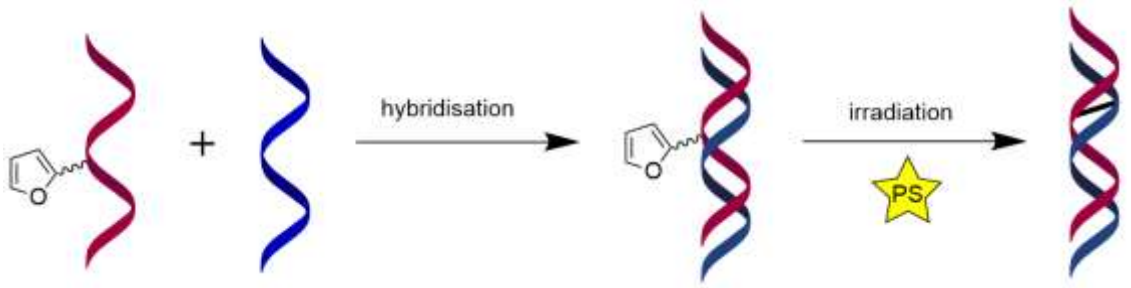

Once these conditions will be established, we hypothesise that conjugation of the photosensitisers to an oligonucleotide can have two important advantages: the solubility in aqueous conditions of the photosensitisers is improved and singlet oxygen is generated in close proximity to the furan moiety, minimising off-target reactions. Therefore, each dye will be conjugated to the furan oligonucleotide complementary strand, and the crosslink formation will be evaluated using these compounds.

However, this system does not allow targeting of natural unmodified sequences, preventing the use of the furan methodology for potential therapeutic applications. For this reason, a self-activating probe, where the photosensitiser and the furan moiety are introduced in the same oligonucleotide is envisioned. The synthesis and handling of such double modified probes might be problematic, and therefore as an alternative, the use of a templated system where a furan and a photosensitiser oligonucleotide together target a longer, unmodified sequence will be explored. Indeed, this kind of system showed promising results when the photosensitiser of choice was methylene blue or rose Bengal.

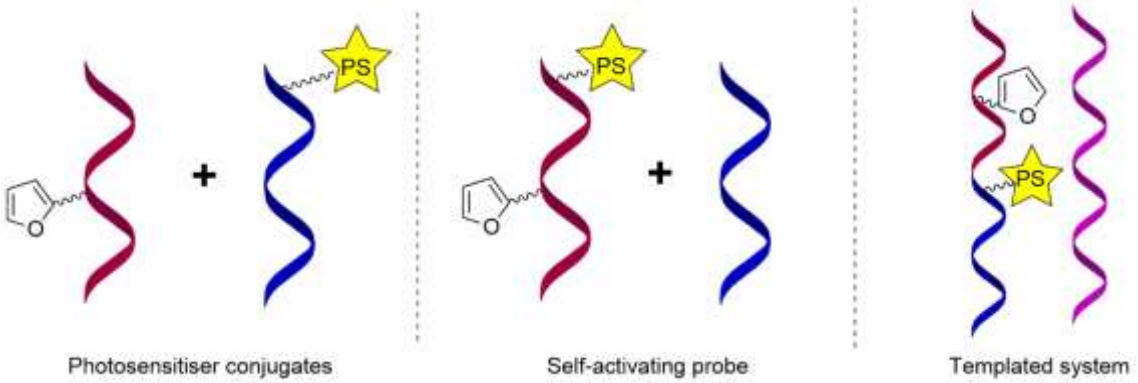

Finally, the use of a cell penetrating peptide as carrier for the furan modified oligonucleotide is envisioned. These compounds are able to complex nucleic acids by electrostatic interactions between the positively charged peptide and the negatively charged oligonucleotides, resulting in the formation of nanoparticles that can gain access inside cells while protecting the integrity of the nucleic acid. Moreover, conjugation of a photosensitiser to the peptide should result in

the formation of a self-activating nanoparticle that allows the targeting of unmodified nucleic acid sequences and the photosensitiser delivery at the same time as the furan oligonucleotide.

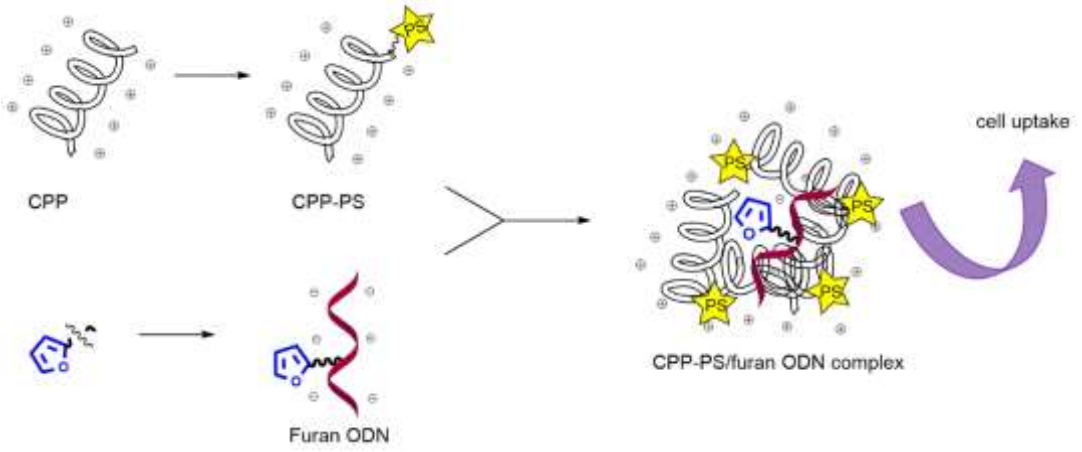

To summarize, several aims were set for the study of porphyrin-based photosensitisers for interstrand crosslink formation:

- Optimisation of the conditions for the use of these compounds for interstrand crosslinking in solution.
- Conjugation of the photosensitisers to oligonucleotides and evaluation of their potential to induce crosslinking formation with a complementary furan strand.
- Construction of a self-activating system that allows targeting of unmodified sequences.

Chapter III.

Crosslinking experiments using porphyrin-based photosensitisers in solution

---

Part of this work was published in:

Porphyrin-based photosensitizers and their DNA conjugates for singlet oxygen induced nucleic acid interstrand crosslinking, Org. Biomol. Chem., 2017

In this chapter three different porphyrin based photosensitisers are selected and evaluated in solution for their capacity to induce DNA interstrand crosslink formation. A chlorin, a porphyrin and a phthalocyanine are evaluated under different conditions changing parameters such as the photosensitiser/ODN ratio, type of light, reaction times and furan building block. It was clear from this study that an optimisation of the reaction conditions is necessary for each different system to obtain optimal ICL formation.

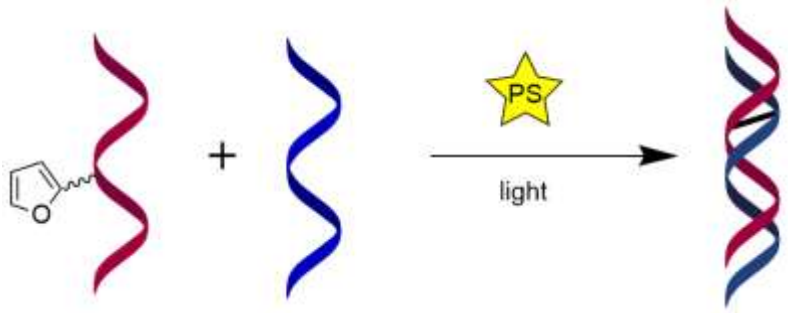

III.1. Synthesis of furan modified ODNs

In this study, building blocks **1** and **2** (figure III-1) were evaluated. Building block **1** was reported to induce a higher crosslinking yield upon oxidation with NBS rather than $^1O_2$. (1) However, during this previous study the irradiation conditions were not optimised for this building block, which could explain the lower yields obtained. Building block **2** was shown to produce crosslinking yields up to 57%, determined by RP HPLC analysis, when the conditions where optimised for the use of MB for $^1O_2$ generation. We here aimed at the full optimisation and comparison for both building blocks.

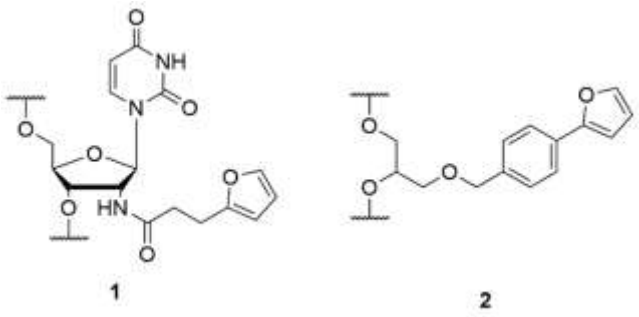

Figure III-1. Furan building blocks evaluated during this study.

Synthesis of the furan modified ODNs was carried out by automated solid phase synthesis using phosphoramidite chemistry, apart from the incorporation of the furan building block which was achieved by manual coupling. During the solid phase synthesis, one nucleotide is added per synthesis cycle to a growing chain that is linked to a controlled-pore glass (CPG) solid support via the 3' terminus (figure III-2). The high yields obtained when using this technique results from the use of several protecting groups that prevent side reactions: the 5'-OH of the nucleotides are protected using a dimethoxyltrityl (DMT) group, the exocyclic amino groups of the nucleobases are protected using benzoyl (dA and dC) or isobutyryl (dG) groups and the phosphate groups are protected as 2-cyanoethyl phosphotriesters.

At the start of the synthesis, removal of the DMT group of the first nucleotide, which is usually already attached to the CPG, is achieved using trichloroacetic acid (TCA) in DCM. Throughout the synthesis, the detritylation step results in the formation of the brightly orange trityl cation, which can be used to monitor the coupling of the nucleosides. Subsequently, the next nucleoside phosphoramidite is mixed with tetrazole, which activates it towards the nucleophilic attack by the 5'-OH of the previous nucleoside.

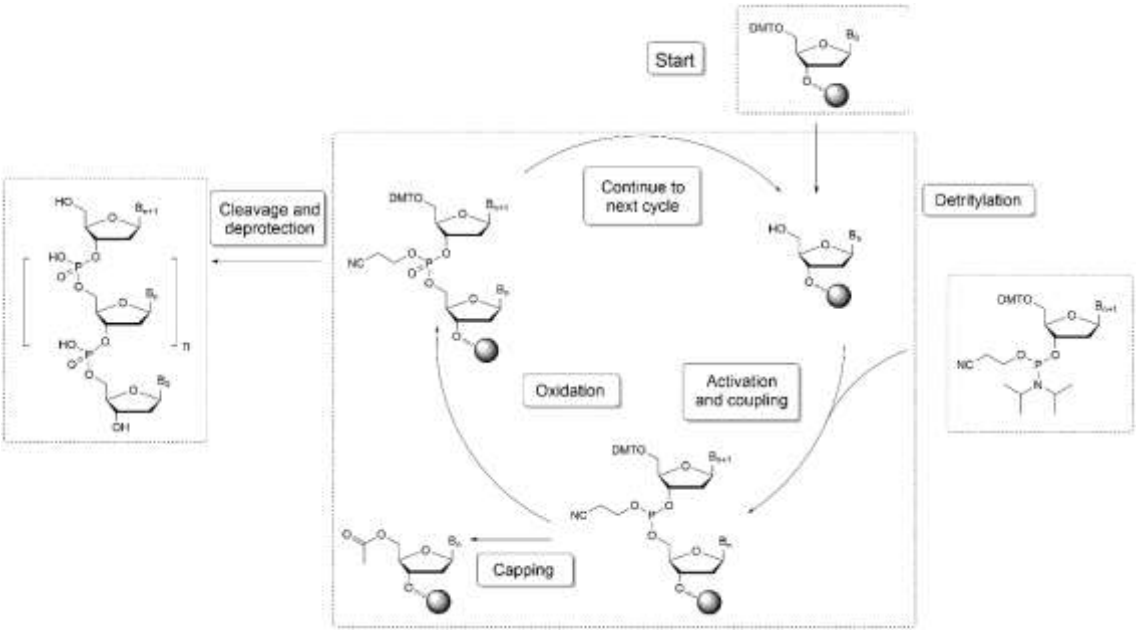

Figure III-2. Schematic representation of the automated solid phase synthesis of ODNs.

In spite of the high yields of the coupling reaction (up to 99.5%), any unreacted chains would be available in the next cycle for incorporating the next nucleoside, leading to deletion sequences. To prevent the formation of a complex mixture of different deletion sequences, a capping step is included after the coupling that blocks the unreacted 5'-OH. During the capping, a mixture of acetic anhydride and *N*-methylimidazole (NMI), containing pyridine to maintain the basic pH to avoid detritylation, is used to acetylate the unreacted 5'-OHs.

Finally, oxidation of the phosphitetriester using iodine in the presence of water and pyridine leads to the formation of the phosphotriester bond and the cycle starts again with the detritylation of the 5'-OH of the last incorporated nucleoside.

For the introduction of the furan building block, the corresponding phosphoramidite was synthesised from the DMT-protected precursor 24 h before the ODN synthesis was carried out, to minimise hydrolysis of the sensitive phosphoramidite moiety (figure III-3). During the automated synthesis, the synthesiser is interrupted just before the coupling step. Then, a solution containing the furan-modified phosphoramidite and a dicyanoimidazole (DCI) solution are alternately applied. DCI is used instead of tetrazole to maximise the coupling of the furan building block, in view of its higher reactivity compared to tetrazole. After applying a capping step, the automated synthesis is resumed.

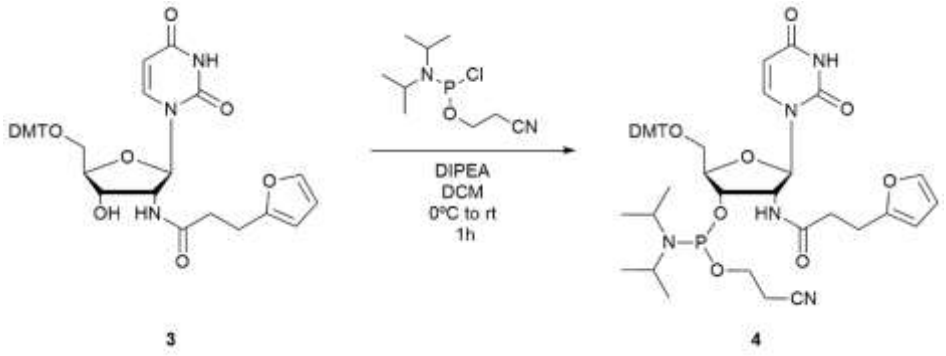

*Figure III-3. Example of the phosphoramidite synthesis previous to the automated synthesis using building block **1**.*

At the end of the synthesis, the last trityl group of the synthesised ODN can be kept (DMT on) to be used as a handle during reverse phase purification: the increased hydrophobicity that the DMT confers allows a better separation between the desired strand and the deletion sequences that do not contain the DMT group.

When the synthesis is completed, the obtained ODN is deprotected and cleaved from the CPG by treatment with NH_4OH at 55ºC. Subsequent purification can be carried out by different methods. Our purification method of choice consists in the use of reverse phase cartridges where, upon loading of the reaction mixture after deprotection, the DMT-ODNs are retained in the cartridge, whereas the deletion sequences and protection groups are eluted. Treatment with trifluoroacetic acid (TFA) results in the cleavage of the DMT group allowing elution of the desire ODN.

Two different furan containing ODNs were synthesised using the two different furan building blocks (table III-1) and their crosslink generation abilities will be evaluated and compared in this chapter.

Table III-1. Furan containing ODNs used during this study.

Name	Sequence (5'-3')	Modification
FON1	CTG ACG G**X**G TGC	X= **1**
FON2	CTG ACG G**X**G TGC	X= **2**

III.2. Crosslink formation with a PS in solution

Three PSs have been evaluated: chlorin e6 (Ce6), TriPyCOOH porphyrin and TT1 phthalocyanine (figure III-4). These porphyrin-based PSs have very different spectroscopic properties as can be observed in figure III-5. Porphyrins present an intense absorption band around 400 nm, the so called Soret band, and some less intense bands around 500-700 nm, known as Q bands; chlorins also present an intense Soret band but have an improved absorption around 650 nm compared to porphyrins; on the other hand, the main absorption of phthalocyanines appears at 600-800 nm.

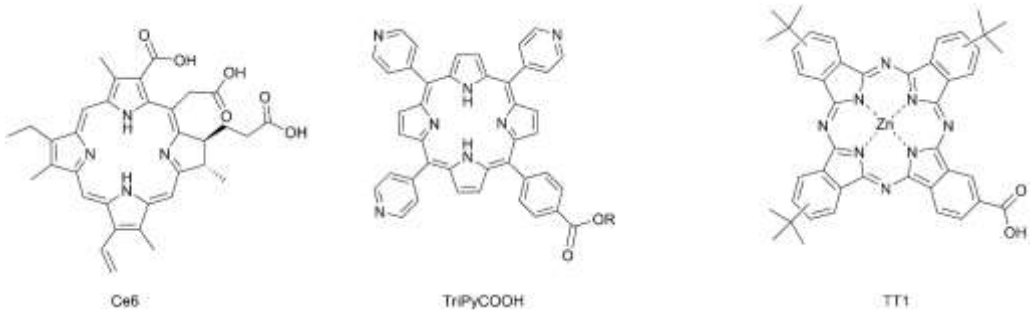

Figure III-4. PSs evaluated during this study: chlorin e6, TriPyCOOH porphyrin and TT1 phthalocyanine.

Apart from the different spectroscopic properties, differences in the core decoration results in a different hydrophilic/hydrophobic character of the PS. Moreover, the phthalocyanine extended aromatic system makes these compounds very prone to aggregation. Keeping these factors in mind we carried out an evaluation of these PSs in an ICL context under conditions as biocompatible as possible *e.g.* minimising the presence of organic solvents and prioritising the use of red light and the optimised conditions for each PS are reported.

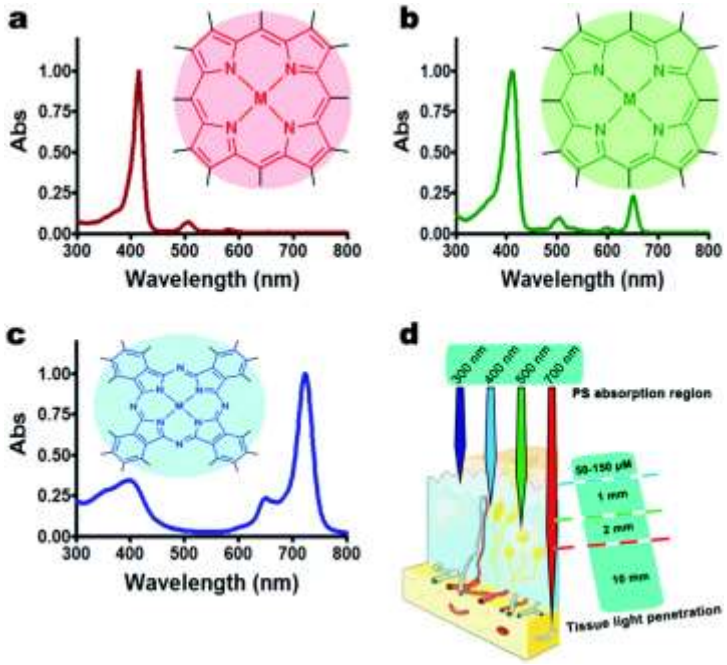

Figure III-5. Depiction of generic spectroscopic features of a) porphyrins, b) chlorins and c) phthalocyanines, and the tissue penetration of different types of light. Reproduced with permission from (2)

During the optimisation process to find optimal conditions for ICL formation for each PS, the duplex **FON1**-**ON1** was used (table III-2). Previously, it was established that this furan building block is able to induce ICL formation towards dA and dC, particularly the latter, in spite of this combination resulting in a mismatch. Therefore, the complementary sequence **ON1** contains a dC opposite to the furan building block.

*Table III-2. Furan modified strand (**FON1**) and its complementary sequence (**ON1**) used during the following crosslinking experiments.*

Name	Sequence
FON1	5’ - CTG ACG G**1**G TGC - 3’
ON1	3’ - GAC TGC CCC ACG – 5’

The use of this duplex results in the generation of a diastereomeric mixture since the reaction does not proceed to aromatisation (figure III-6), and the crosslinked adducts are observed as two different signals by RP HPLC.

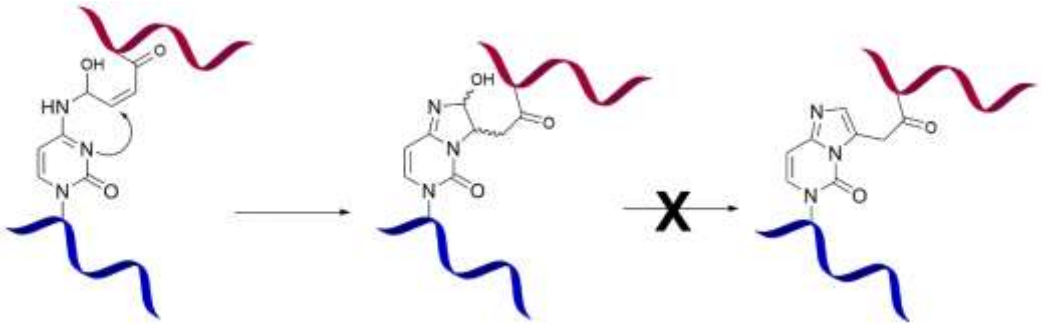

Figure III-6. Generation of a crosslinked adduct towards dC that consists of a diastereomeric mixture.

III.2.1. Chlorin e6 as a photosensitiser

First, chlorin e6 (Ce6) was evaluated. Ce6 is a commercially available, second generation PS that can be harvested from green algae species (*Chlorella ellipsoidea*) (3) and has been widely used for photodynamic therapy (PDT), (4–6) including conjugated to aptamers for targeted PDT (7–9) and derivatised with an aspartyl moiety. Mono-L-aspartyl Ce6, also known as Talaporfin or NPe6, is approved in Japan for lung cancer treatment. (10,11)

Chlorins present a rather strong absorption around 650 nm (667 nm in ethanol for Ce6) that ensures a sufficient light absorbance if red light is used for irradiation and therefore this will be the light type of choice. The dye was dissolved in DMSO and added to the reaction mixture (1% final DMSO content) just before irradiation to the duplex in phosphate buffer solution. Samples were taken at different irradiation times for subsequent analysis by RP HPLC and PAGE. The crosslink reaction was carried out at a concentration of 2 or 20 μM of the duplex. By also evaluating the ICL formation at lower duplex concentration, we attempted to use more biologically relevant concentrations and to establish a comparison point for the later use of the PS conjugated ODN (chapter IV). At this concentration, a 1:1 duplex/PS ratio was used. When a 20μM concentration of the duplex was used, the PS was added at 5 and 10μM. The ICL formation was fast and already after 5 min the crosslinking yield reached a plateau or started to decrease (figure III-7a). The used of an equimolar duplex/PS ratio resulted in the highest yields (52%, figure III-7b) as determined by integration of the peak areas of the two signals at 14.5 min in the HPLC chromatogram, corrected by the corresponding extinction coefficient of each ODN and duplex, which have been previously identified as the crosslinked adduct when the aromatisation does not proceed. (12) The crosslink formation was confirmed by PAGE, as a slower migrating band can be observed after irradiation, which indicates the presence of a higher molecular weight species, which under denaturing conditions is believed to correspond to a crosslinked adduct. The appearance of this species

is concurrent with the consumption of the ON1 and FON1 signals and was previously characterized by MS analysis during earlier work..

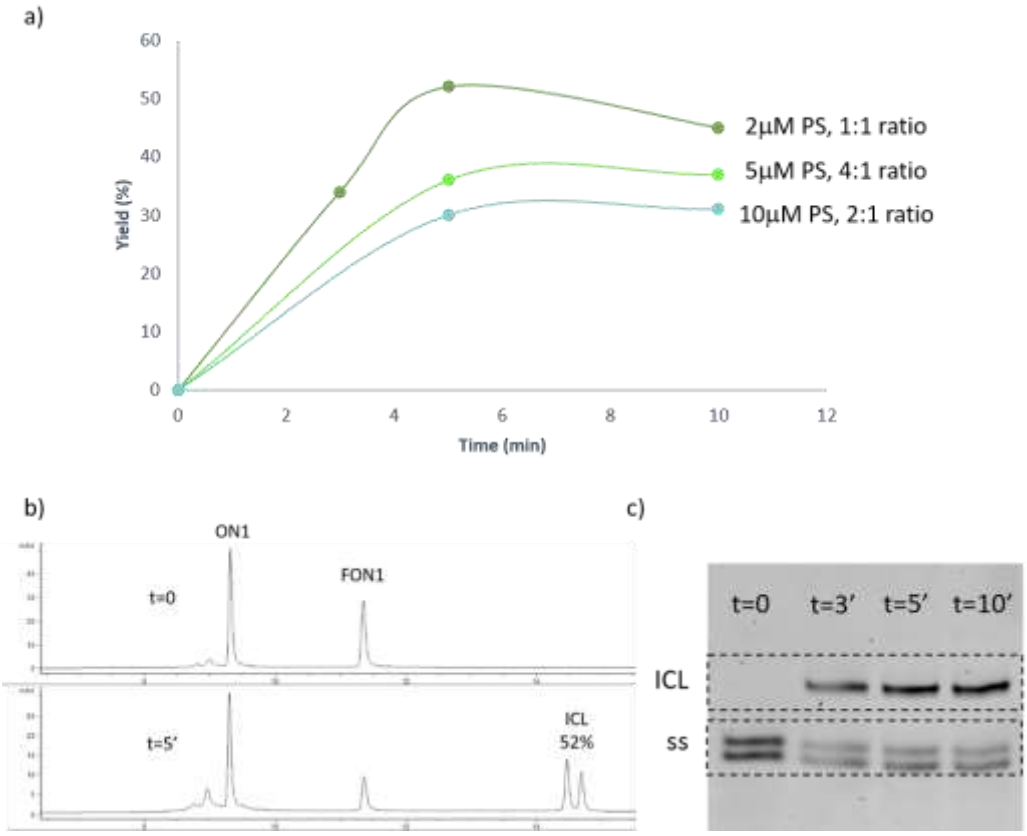

Figure III-7. ICL formation using Ce6 as PS. a) Summary of the crosslinking yields at 3 different ratios. b) RP HPLC analysis of the ICL experiment where [duplex]=[Ce6]=2 µM (XBridge column, linear gradient of 0-20% ACN in 30 min); c) PAGE analysis of the same experiment (20% polyacrylamide, 1x TBE buffer, GelRed™ used for staining).

Moreover, to assess the versatility of this PS, ICL formation was evaluated using no DMSO or a higher amount (20%), but either case does not have a large influence in the ICL generation as it can be observed in figure III-8. Increasing the amount of DMSO under otherwise optimised conditions for ICL formation using Ce6 only seemed to slightly slow down the crosslinking formation, but similar yields were obtained. When no DMSO was used at a lower duplex/Ce6 ratio, the crosslink was formed at the same extent as when 1% DMSO was added, indicating no significant quenching in the $^1O_2$ generation.

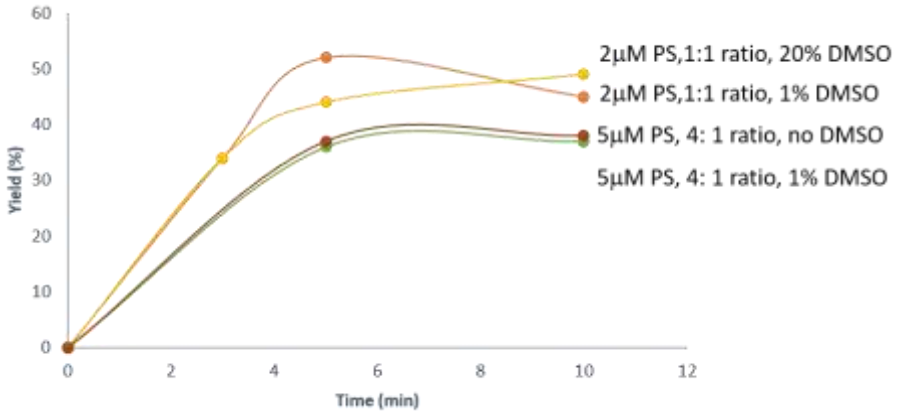

Figure III-8. Evaluation of the ICL formation using Ce6 and different DMSO concentrations.

III.2.2. TriPyCOOH as a photosensitiser

TriPyCOOH porphyrin was kindly provided by Dr. Tomé (Universidade de Lisboa), in the context of a collaboration established within the SO_2S ITN. This porphyrin has been successfully used against Gram-positive bacteria in wastewater treatment, (13) against herpes simplex virus type 1 (HSV-1) (14) and for PDT. (15) The presence of only one carboxylic acid functionality should allow for a selective and directed attachment of the molecule to an ODN. Since porphyrin absorbance in the red region is rather low, we first set out to evaluate whether red or white light was the most suitable for crosslinking generation (figure III-9). Solutions of the duplex were prepared at 20 μM and the porphyrin was added just before irradiation at 5 or 10 μM, that is, keeping a 4:1 or 2:1 duplex/porphyrin ratio respectively. HPLC analysis of the samples showed that, surprisingly, the use of red light led to higher crosslinking yields, since the use of white light resulted in a lower yield of the crosslinked adduct that also started to decay after 30-60 min irradiation. On the other hand, when red light was used, ICL formation proceeded until 3-4 hours before a decrease in yield was observed.

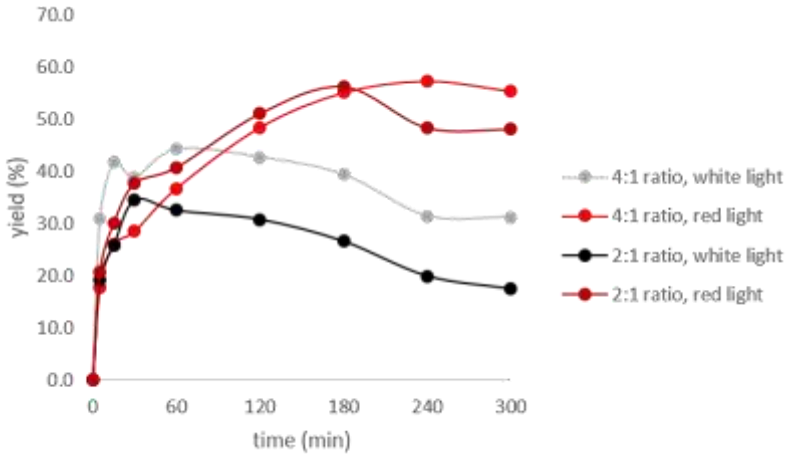

Figure III-9. Evaluation of red and white light irradiation using TriPyCOOH as PS. Experiments at 4:1 duplex/TriPyCOOH ratio contain 20 μM concentration of the duplex and 5 μM concentration of TriPyCOOH; 2:1 duplex/TriPyCOOH ratio contain 20 μM concentration of the duplex and 10 μM concentration of TriPyCOOH. Yields were calculated by dividing the peak area of the cross-linked product in the chromatogram by the peak area of the limiting single stranded oligonucleotide in the initial HPLC chromatogram, both corrected for their extinction factor

Subsequently, the crosslink generation using TriPyCOOH and red light was evaluated. As when using Ce6, the duplex was used at 2 or 20 μM concentration and TriPyCOOH was used at either 2 μM concentration, in the case of 2 μM of the duplex, or 5 or 10 μM when 20 μM of the duplex was used. RP HPLC and PAGE analysis will be shown here for the experiment showing the highest crosslinking yield.

Only small differences were found among the three systems and after 3 hours the same yield was obtained. Further irradiation of the solution where 10 μM was used resulted in a slow decrease of the crosslinking yield and the highest yield was obtained when using 5 μM after 4 hours (47%) and PAGE analysis confirmed the formation of the crosslink as a slower migrating band can be observed (figure III-10b and c).

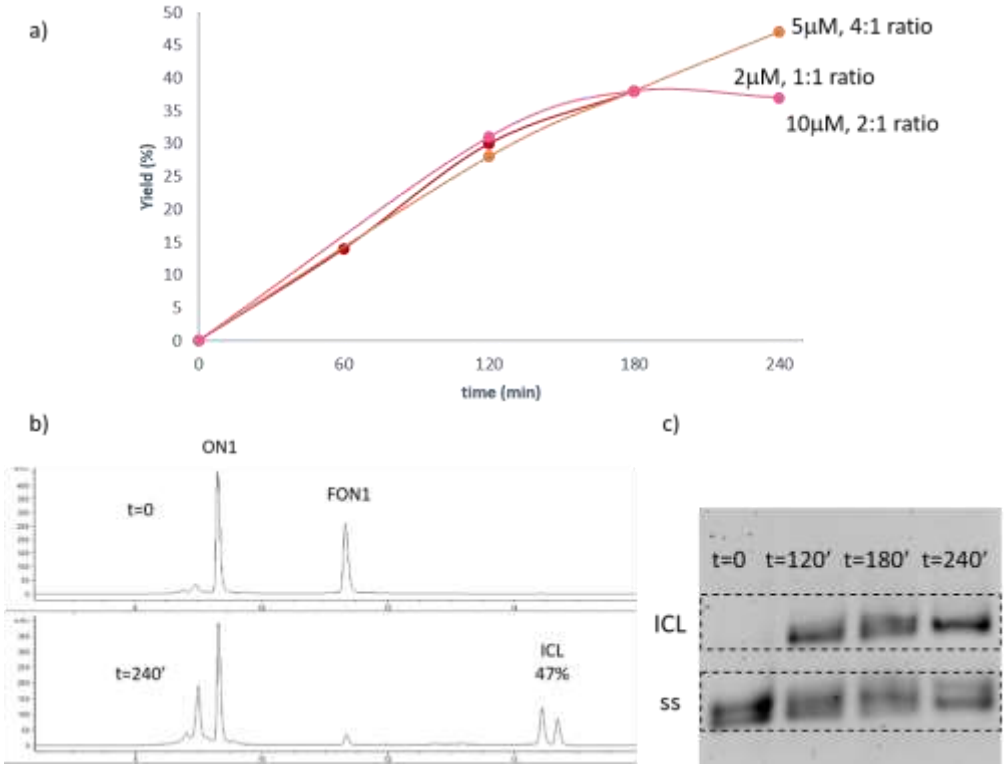

Figure III-10. ICL formation using TriPyCOOH as PS. a) Summary of the crosslinking yields at 3 different ratios. b) RP HPLC analysis of the ICL experiment where [duplex]=20 μM and [TriPyCOOH]=5 μM (XBridge column, linear gradient of 0-20% ACN in 30 min); c) PAGE analysis of the same experiment (20% polyacrylamide, 1x TBE buffer, GelRed™ used for staining).

III.2.3. TT1 as a photosensitiser

The third PS evaluated was TT1 phthalocyanine which was kindly provided by Prof. Torres (Universidad Autónoma de Madrid), also as part of a collaboration within the SO_2S ITN. TT1 was originally designed as a photosensitizer for Dye-Sensitized Solar Cells as its bulky, hydrophobic substituents result in an improved solubility in organic solvents and allow to avoid aggregation which is so common among phthalocyanines due to their extended aromatic system. (16) Since aggregation of this hydrophobic compounds would especially occur in aqueous conditions, during the evaluation of TT1 in solution higher amounts of DMSO were used, up to 20%. However, even the addition of DMSO did not seem to prevent aggregation as the crosslink formation was rather inefficient. Phthalocyanine aggregation results in quenching of the excited states of the PS which interferes with $^1O_2$ generation, even though light absorption in the red region is particularly strong for these compounds.

Again, TT1 was evaluated at different duplex/PS ratios. When the duplex concentration was 20 μM, TT1 was added at 5, 10 and 20 μM, at a final DMSO concentration of 5, 10 and 20% respectively. When the duplex concentration was 2 μM, TT1 was added in a 1:1 ratio and at 20% DMSO concentration. A summary of the crosslinking yields can be found in figure III-11. In this case, there is a direct correlation between the PS concentration and the ICL formation, probably due to the fact that most of the phthalocyanine is quenched leading to an inefficient $^1O_2$ generation and addition of more PS has a beneficial effect on the ICL formation.

However, it is worth noting that the use of higher amounts of DMSO may have an influence on the duplex stability. For this reason, the melting temperatures (Tm) of the duplexes in the presence of 5, 10 and 20% DMSO were evaluated. As can be observed in table III-3, there was almost no influence up to 10% DMSO. Only when the concentration was increased up to 20% some destabilisation was observed but even in this case, most of the duplex was formed at the temperature at which the crosslinking experiments are performed (25ºC).

*Table III-3. Tm of the **FON1**-**ON1** duplex in the presence of different DMSO concentrations. Measurements were carried out at 1 μM duplex concentration in a 100 mM NaCl and 10 mM phosphate buffer following the absorption at λ = 260 nm..*

DMSO (%)	Tm (ºC)	ΔTm with 0% DMSO
0	36.7	0
5	35.8	-0.9
10	37.0	0.3
20	32.2	-4.5

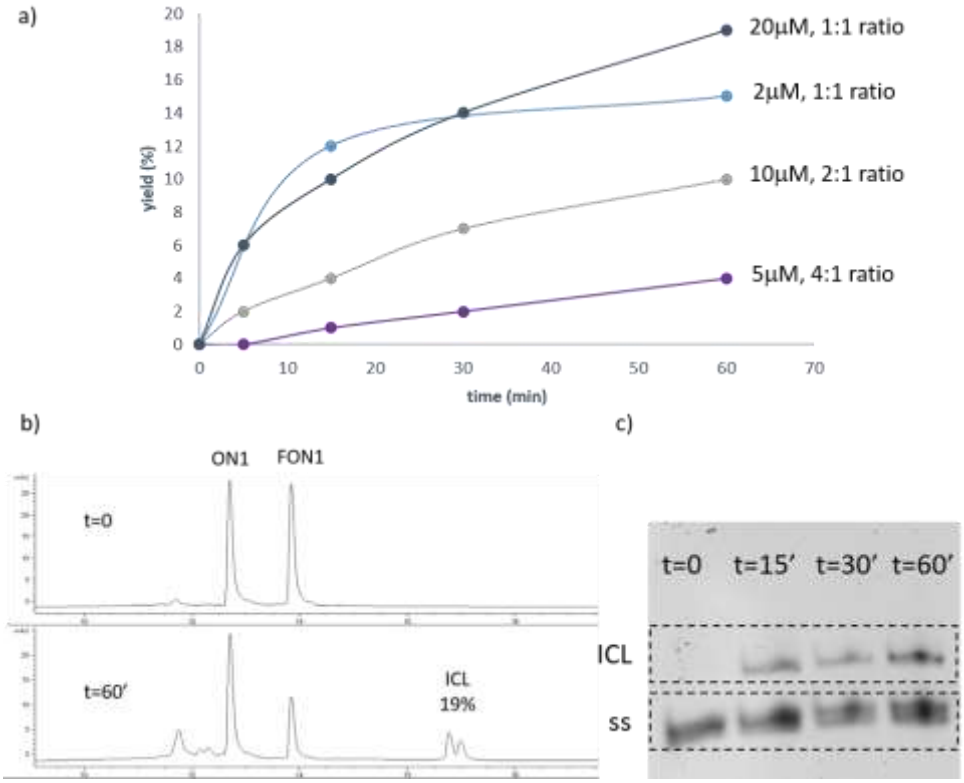

Figure III-11. ICL formation using TT1 as PS. a) Summary of the crosslinking yields at 3 different ratios and concentrations. b) RP HPLC analysis of the ICL experiment where [duplex] = [TT1]= 20 µM and (Aeris column, linear gradient of 0-20% ACN in 30 min); c) PAGE analysis of the same experiment (20% polyacrylamide, 1x TBE buffer, GelRed™ used for staining).

III.3. Evaluation of a non-nucleobase furan building block.

Once the optimised conditions for ICL generation for each PS were established using the **FON1/ON1** duplex, we decided to evaluated the second furan containing ODN, **FON2**, hybridised to its complementary strand ON1 (table III-4). This building block showed a high yielding ICL formation when using MB for $^1O_2$ generation (1,17). It is important to note that the use of this furan building block spontaneously proceeds to the aromatised adduct (figure III-12) and it is observed as a single signal by RP HPLC, contrary to the previous furan building block evaluated.

Table III-4. Furan modified strand (FON2) and its complementray sequence (ON1) used during the following crosslinking experiements.

Name	Sequence
FON2	5' - CTG ACG G**2**G TGC - 3'
ON1	3' - GAC TGC CCC ACG – 5'

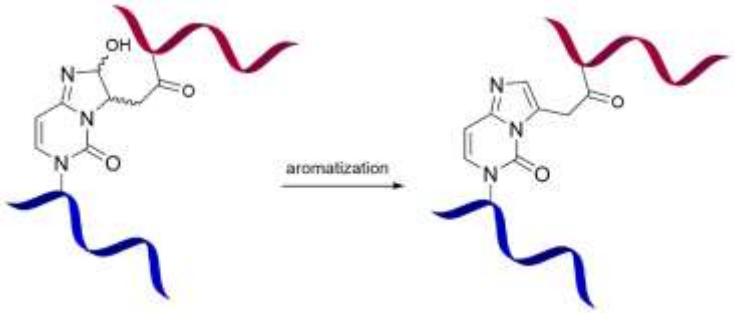

Figure III-12. Formation of the aromatic crosslinked adduct that results when FON2 is used for ICL with the complementary strand ON1.

As in the previous experiments, the two ODNs were mixed together and allowed to hybridise in a phosphate buffer solution. Then, the PS of choice was added just before irradiation and samples were taken at different times and analysed by RP HPLC and PAGE.

When Ce6 was used as a PS, the duplex and the dye were added at 2 μM concentration as it was shown before to induce the highest ICL formation. However, under these conditions the crosslink yield was much lower, only up to 19%, compared to the 52% obtained before (figure II-13b).

In the case of TriPyCOOH, the used of this PS under the previously optimised conditions (20 μM concentration of the duplex, 5 μM concentration of TriPyCOOH) did not produce a crosslink that can be easily observed in the HPLC chromatogram (figure III-14a). However, the formation of the crosslink is confirmed by PAGE (figure III-14b) but crosslinking yields could not be estimated. The use of a higher (10 μM) concentration and white light were also attempted, but under none of these conditions the formation of the crosslinked adduct was observed by RP HPLC (the original chromatograms are included in chapter X)

Finally, the use of TT1 at 1:1 duplex/PS ratio (2μM) in the presence of 20% DMSO, resulted in crosslink formation at slightly lower yields compared to when **FON1** was used (Figure III-15b). A comparison between the crosslink yields using the two building blocks is shown in table III-5.

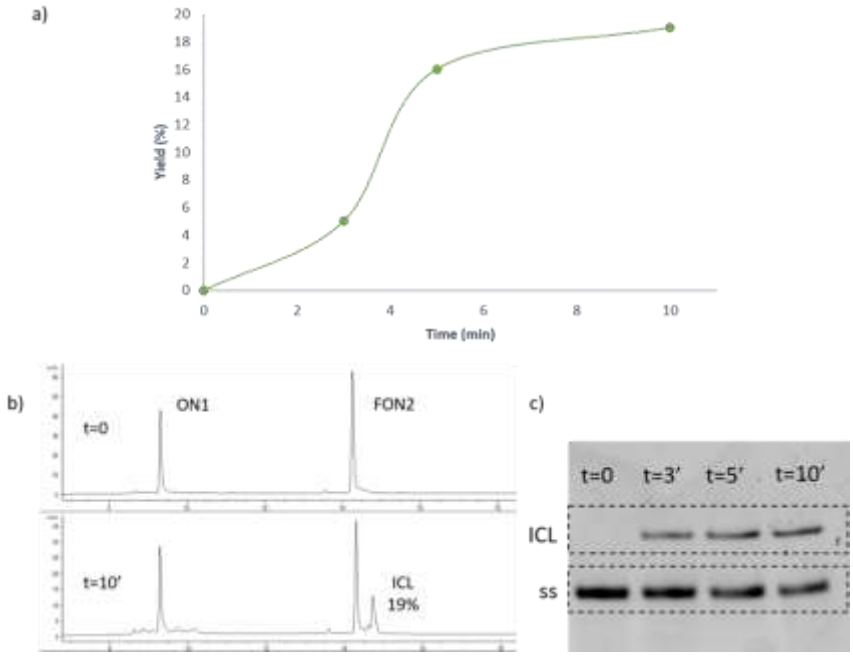

*Figure III-13. ICL formation using Ce6 as PS and **FON2/ON1** as duplex where [duplex]=[Ce6]=2 μM. a) Evolution of the crosslinking yield over time. b) RP HPLC analysis of the ICL experiment (XBridge column, linear gradient of 0-20% ACN in 30 min); c) PAGE analysis of the same experiment (20% polyacrylamide, 1x TBE buffer, GelRed™ used for staining).*

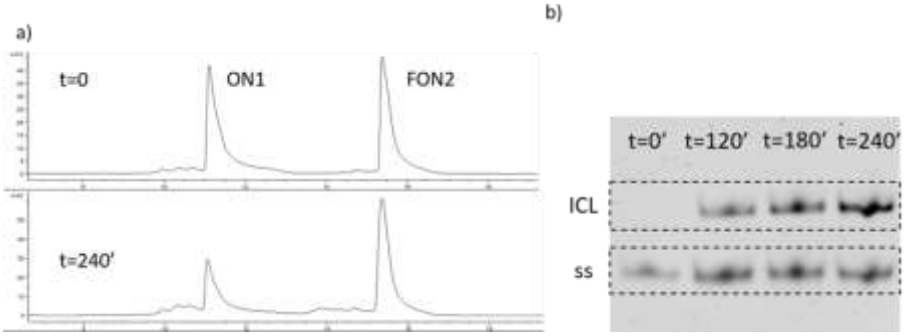

*Figure III-14. ICL formation using TriPyCOOH as PS and **FON2/ON1** as duplex where [duplex]=20 μM and [TriPyCOOH]=5 μM. a) RP HPLC analysis of the ICL experiment (XBridge column, linear gradient of 0-20% ACN in 30 min); b) PAGE analysis of the same experiment (20% polyacrylamide, 1x TBE buffer, GelRed™ used for staining).*

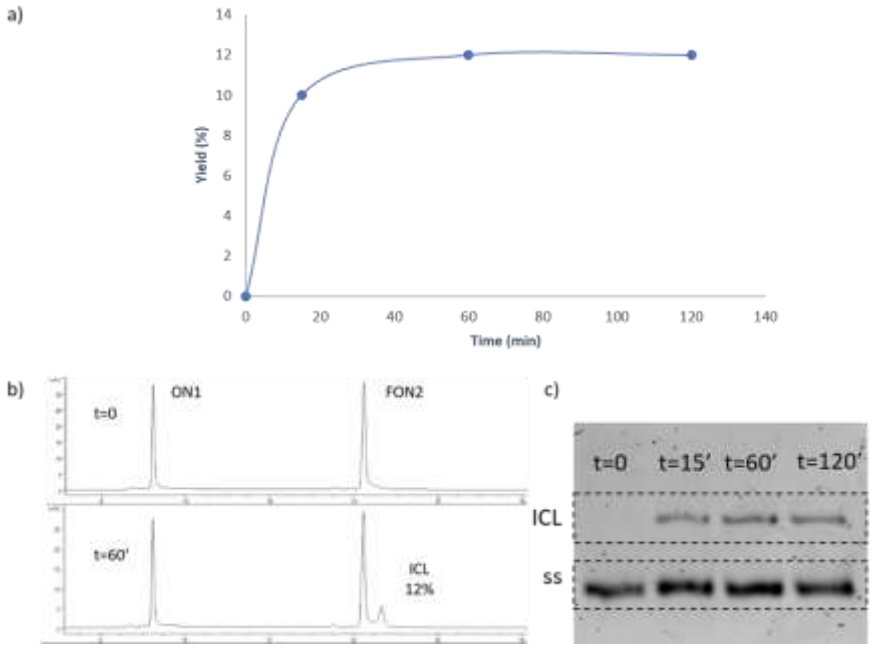

*Figure III-15. ICL formation using TT1 as PS and **FON2/ON1** as duplex where [duplex] = [TT1]= 2 μM. a) Evolution of the crosslinking yield over time. b) RP HPLC analysis of the ICL experiment and (Aeris column, linear gradient of 0-20% ACN in 30 min); c) PAGE analysis of the same experiment (20% polyacrylamide, 1x TBE buffer, GelRed™ used for staining).*

Table III-5. Comparison between the ICL yields using the two furan ODNs.

PS	ICL yield using FON2 (%)	ICL yield using FON1 (%)
Ce6	19	52
TriPyCOOH	-	47
TT1	12	17

III.4. Crosslinking using porphyrin containing nanoparticles.

These NPs were available to us through a collaboration with the University of Aveiro in the context of the European ITN SO_2S. The attachment of porphyrins to magnetic silica NPs has been used for wastewater treatment since the presence of the Fe_3O_4 core allows the recovery of the NPs after the water treatment allowing the recycling of these compounds. (18) In the present study, glucose-decorated porphyrin conjugated NPs (figure III-16), synthesised by Lucía Fernández, were used for crosslinking generation.

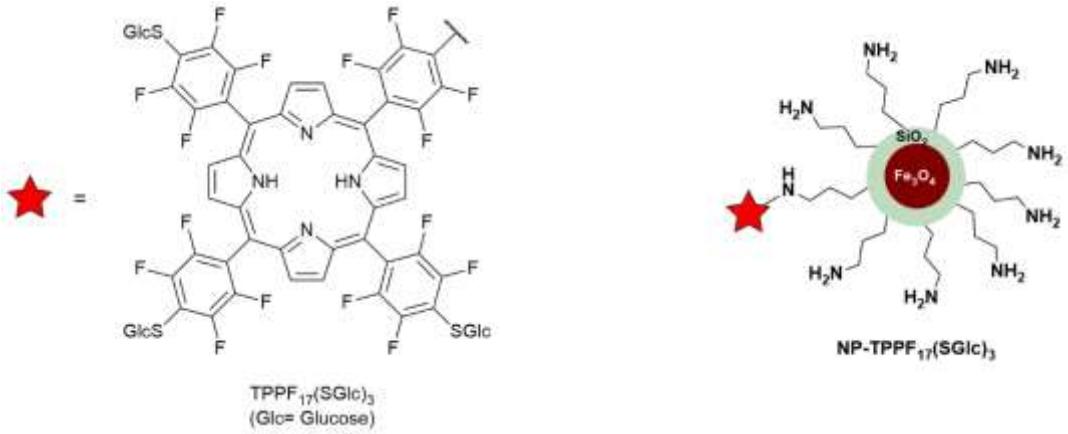

Figure III-16. Structure of NPs used for ICL generation. They consist of a magnetic core coated with a silica shell that is functionalised with the porphyrins.

Since porphyrins are the only active element in the NP, the concentration in this case refers to the porphyrin content. An estimation of the porphyrin content was calculated by the difference between the amount of porphyrin used during the synthesis of the functionalised NPs and the remaining dye at the end of the reaction, determined by UV-Vis absorbance. The crosslink experiments were carried out using the **FON1-ON1** duplex at a 20 μM concentration and the NPs were added at 10 μM concentration just before irradiation. Under these conditions, red and white light irradiation was evaluated (figure III-17a), and samples were taken at different times and subsequently analysed by RP HPLC and PAGE.

The use of white light resulted in this case in better crosslinking yields when compared to the red light irradiation, up to 28% as determined by RP HPLC (figure III-17b), and the formation of the ICL could be confirmed by PAGE analysis (figure III-17c).

It can be concluded from these experiments that PS-equipped NPs are suitable $^1O_2$ generators for inducing ICL formation.

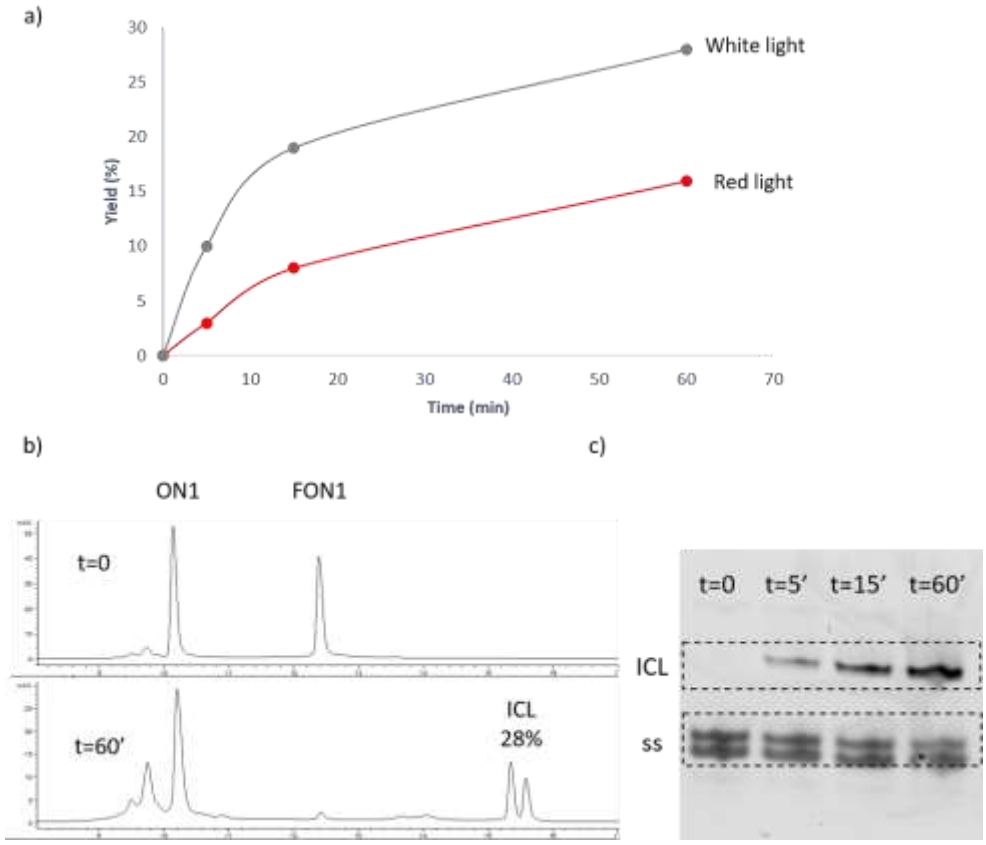

Figure III-17. ICL formation using PS-equipped magnetic silica NPs. a) Overview of the crosslinking yields in function of time of irradiation using 2 different light types, red and white. b) RP HPLC analysis of the ICL experiment where [duplex]=20 μM and [NPs]= 10 μM and white light (XBridge column, linear gradient of 0-20% ACN in 30 min); c) PAGE analysis of the same experiment (20% polyacrylamide, 1x TBE buffer, GelRed™ used for staining).

III.5. Conclusions

During this chapter, an extensive study of the three PSs of choice was carried out under a variety of reaction conditions and for each system a set of optimal parameters was defined.

Among the PSs tested, Ce6 performed the best for inducing ICL, closely followed by TriPyCOOH. On the other hand, TT1 phthalocyanine seemed to suffer from its low solubility in aqueous conditions that would induce aggregation among the dyes.

Moreover, an alternative furan building block was used for comparison, showing lower crosslinking yields than the uridine based building block

Finally, an alternative $^1O_2$ generation system was evaluated consisting of magnetic silica NPs decorated with porphyrins. The NPs were tested in a crosslinking context and they were able to successfully induce ICL formation. These NPs seem to be promising candidates for ICL generation compared under white light irradiation since they showed a crosslink formation up to 28%

already after one hour, whilst in the case of the free porphyrins only yields up to 15% were observed after this irradiation time. Further investigation of this system is worthy but was not undertaken here due to lack of time.

III.6. References

1. Op de Beeck M, Madder A. Sequence specific DNA cross-linking triggered by visible light. J Am Chem Soc. 2012 Jul 4;134(26):10737–40.

2. Pereira PMR, Korsak B, Sarmento B, Schneider RJ, Fernandes R, Tomé JPC. Antibodies armed with photosensitizers: from chemical synthesis to photobiological applications. Org Biomol Chem. Royal Society of Chemistry; 2015;13(9):2518–29.

3. Moon YH, Kwon SM, Kim HJ, Jung KY, Park JH, Kim SA, et al. Efficient preparation of highly pure chlorin e6 and its photodynamic anti-cancer activity in a rat tumor model. Oncol Rep. 2009 Sep 16;22(5):1085–91.

4. Lee S, Koo H, Na JH, Han SJ, Min HS, Lee SJ, et al. Chemical tumor-targeting of nanoparticles based on metabolic glycoengineering and click chemistry. ACS Nano. 2014 Mar 25;8(3):2048–63.

5. Saravanakumar G, Lee J, Kim J, Kim WJ. Visible light-induced singlet oxygen-mediated intracellular disassembly of polymeric micelles co-loaded with a photosensitizer and an anticancer drug for enhanced photodynamic therapy. Chem Commun. 2015;51(49):9995–8.

6. Li Y, Yu Y, Kang L, Lu Y. Effects of chlorin e6-mediated photodynamic therapy on human colon cancer SW480 cells. Int J Clin Exp Med. 2014;7(12):4867–76.

7. Yuan A, Laing B, Hu Y, Ming X. Direct oligonucleotide–photosensitizer conjugates for photochemical delivery of antisense oligonucleotides. Chem Commun. Royal Society of Chemistry; 2015;51(30):6678–80.

8. Mallikaratchy P, Tang Z, Tan W. Cell specific aptamer-photosensitizer conjugates as a molecular tool in photodynamic therapy. ChemMedChem. 2008;3(3):425–8.

9. Wang J, Zhu G, You M, Song E, Shukoor MI, Zhang K, et al. Assembly of aptamer switch probes and photosensitizer on gold nanorods for targeted photothermal and photodynamic cancer therapy. ACS Nano. 2012;6(6):5070–7.

10. Hargus JA, Fronczek FR, Vicente MGH, Smith KM. Mono-(l)-aspartylchlorin-e 6. Photochem Photobiol. 2007 Sep;83(5):1006–15.

11. Yoon I, Li JZ, Shim YK. Advance in photosensitizers and light delivery for photodynamic therapy. Clin Endosc. 2013;46(1):7–23.

12. Halila S, Velasco T, Clercq P De, Madder A. Fine-tuning furan toxicity: fast and quantitative DNA interchain cross-link formation upon selective oxidation of a furan containing oligonucleotide. Chem Commun (Camb). 2005 Feb 21;(7):936–8.

13. Carvalho CMB, Gomes ATPC, Fernandes SCD, Prata ACB, Almeida M a., Cunha M a., et al. Photoinactivation of bacteria in wastewater by porphyrins: Bacterial β-galactosidase activity and leucine-uptake as methods to monitor the process. J Photochem Photobiol B Biol. 2007;88(2–3):112–8.

14. Tomé JPC, Silva EMP, Pereira AMVM, Alonso CM a., Faustino M a. F, Neves MGPMS, et al. Synthesis of neutral and cationic tripyridylporphyrin-d-galactose conjugates and the photoinactivation of HSV-1. Bioorg Med Chem. 2007;15(14):4705–13.

15. Habdas J, Boduszek B. Synthesis of 5-(4'-carboxyphenyl)-10,15,20-tris-(4 pyridyl)-porphyrin and its peptidyl phosphonate derivatives. J Pept Sci. 2009;15(4):305–11.

16. Cid J-J, Yum J-H, Jang S-R, Nazeeruddin MK, Martínez-Ferrero E, Palomares E, et al. Molecular Cosensitization for Efficient Panchromatic Dye-Sensitized Solar Cells. Angew Chemie. 2007 Nov 12;119(44):8510–4.

17. De Laet N, Madder A. Synthesis and evaluation of methylene blue oligonucleotide conjugates for DNA interstrand cross-linking. J Photochem Photobiol A Chem. Elsevier B.V.; 2016;318:64–70.

18. Fernández L, Esteves VI, Cunha Â, Schneider RJ, Tomé JPC. Photodegradation of organic pollutants in water by immobilized porphyrins and phthalocyanines. J Porphyr Phthalocyanines. 2016;20(01n04):150–66.

Chapter IV.

Photosensitiser conjugated oligonucleotides.

Synthesis, $^1O_2$ generation and crosslinking evaluation.

The main part of this work was published in:

Porphyrin-based photosensitizers and their DNA conjugates for singlet oxygen induced nucleic acid interstrand crosslinking, Org. Biomol. Chem., 2017

In this chapter, the PSs evaluated in Chapter 3 are conjugated to the ODN sequences complementary to the furan containing ODNs. Conjugation of the PSs to the ODNs results in the local generation of $^1O_2$, minimising off-target reactions and avoiding the need to add organic solvents for solubility. Then, the $^1O_2$ generation of these conjugates is evaluated and a comparative study of the different probes for crosslink formation is carried out.

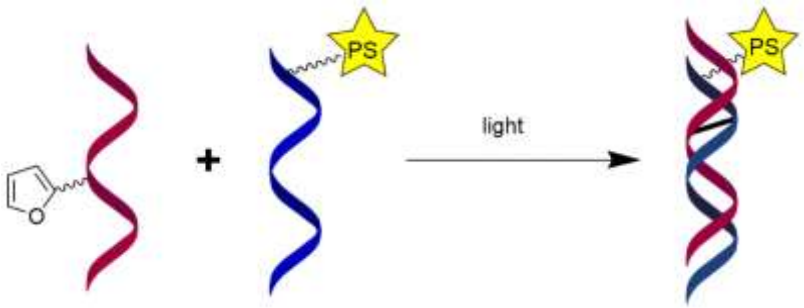

IV.1. Photosensitiser conjugated nucleic acids

Conjugation of photosensitisers to nucleic acids has been studied in various contexts, ranging from therapeutic applications to structural studies. Ce6 has been used in conjugation with aptamers for directed PDT and with antisense oligonucleotides to achieve a combined PDT (1,2) and splicing switching effect for cancer treatment. (3) In a different therapeutic approach, PS-induced cleavage has been reported using cationic porphyrins (4) or napthoquinones (5) or more recently the use of photosensitiser conjugated peptide nucleic acids (PNA) derivatised with rose bengal or 5-carboxytetramethylrhodamine (TAMRA). (6,7)

The study of the structure and dynamics of nucleic acids using porphyrin conjugated oligonucleotides has been reported in detail by the group of Berova (8–11) and Stulz. (12–14)

Introduction of the photosensitisers has been carried out through various approaches but the introduction of amino groups is the most widely used due to the availability of commercially available modifiers that allow in terminal or in internal modification and also the feasibility of the conjugation reaction. (1,3,4,7) However, other approaches have been explored *e.g.* previous conjugation of the PS to a nucleoside for later introduction into the growing chain, (8,15,16) terminal modification via the H-phosphonate approach (17) or via postsynthetic cycloaddition reaction using a furan containing oligonucleotide, directly inspired by the methodology developed in the OBCR group. (18)

IV.2. Synthesis of amino modified ODNs.

Different amino modified ODNs were synthesised to study the behaviour of the PSs of interest when conjugated to an ODN. First, 5'-amino modified ODNs complementary to the furan containing sequences used in the previous chapter (**FON1** and **FON2**) were either purchased or synthesised and kept on the CPG for conjugations on solid support. Two different 5'-amino modifiers were used, differing in the linker length between the amino group (three or six carbon atoms) and the phosphate group of the last nucleobase (figure IV-1). The different sequences are presented in table IV-1.

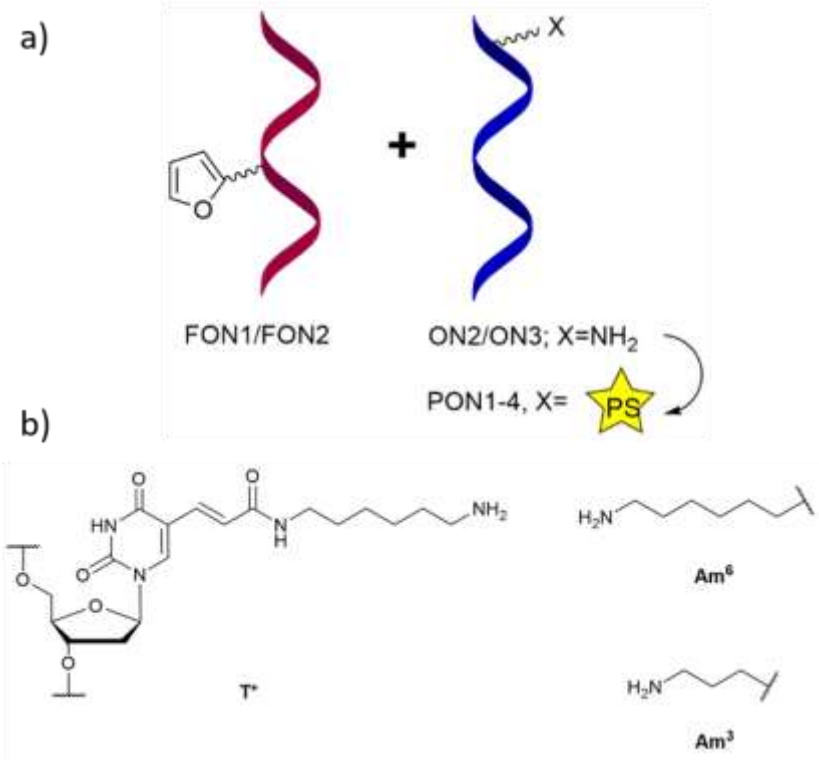

Figure IV-1. a) Schematic representation of the furan ODN/amino or PS-ODN duplexes; b) Amino modifiers and furan building block used for the ODN synthesis.

Table IV-1. Summary of the amino and furan modified sequences. All sequences were in home synthesised except ON3. ON2 was purchased as the free ODN but synthesised for on solid support conjugations.

Name	Sequence (5'-3')	Modification
ON2	**X**-GCA CCC CGT CAG	**X= Am^6**
ON3	**X**-GCA CCC CGT CAG	**X= Am^3**
FON1	CTG ACG G**1**G TGC	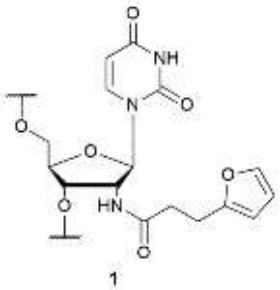 1
FON2	CTG ACG G**2**G TGC	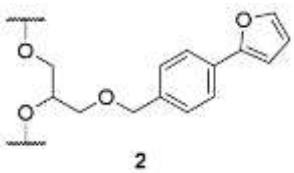 2

IV.3. Synthesis of PS conjugated ODNs.

Conjugation between the different PSs and the ODNs was achieved via amide bond formation between the amine functionality of the ODNs and the carboxylic acid of the dyes. First, the ODN of choice was ON2, functionalised with the C6 linker at the 5' end. For each PS a different activation method of the carboxylic acid needed to be used, as described below.

IV.3.1 Ce6 conjugated ODN

For Ce6, DCC/NHS activation was used. First, the chlorin was dissolved in DMF and DCC and NHS were added and this mixture was stirred in the darkness at 0ºC for 1 hour under Ar atmosphere. Then, **ON2** was added dissolved in $NaHCO_3$ buffer solution (pH 8.3, to minimise the hydrolysis of the NHS ester). The reaction mixture was stirred overnight in the darkness, to prevent undesired $^1O_2$ generation at this point. Subsequently, part of the unreactive Ce6 was removed by precipitation before RP HPLC purification. Conjugate **PON1** was obtained in 30% yield.

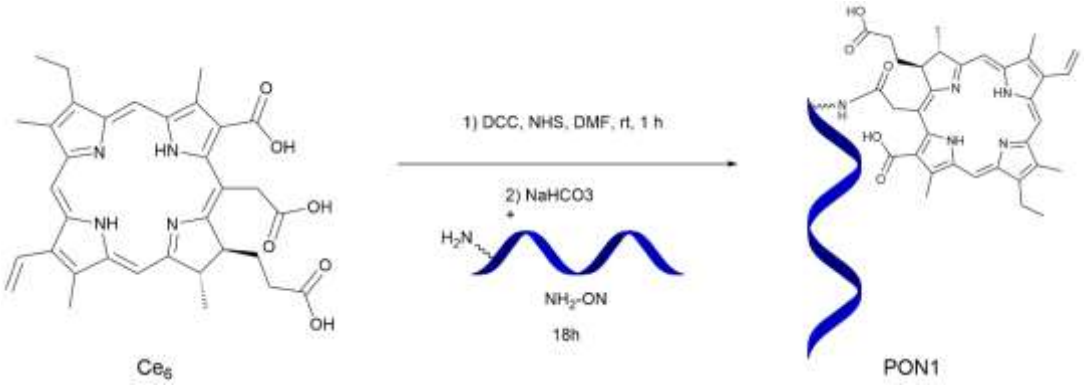

Figure IV-2. Synthesis of the Ce6 conjugated ODN, PON1.

During RP HPLC purification, the conjugate was identified by its characteristic UV-Vis absorbance, featuring maximums at 260 nm, 400 nm and 650 nm (figure IV-3 and IV-4) and by mass analysis using MALDI-TOF. After purification, the absorption coefficients characteristic of the Ce6 moiety were calculated based on the absorption at 400 nm and the concentration of the conjugate as determined by the absorption at 260 nm, as presented in table IV-2.

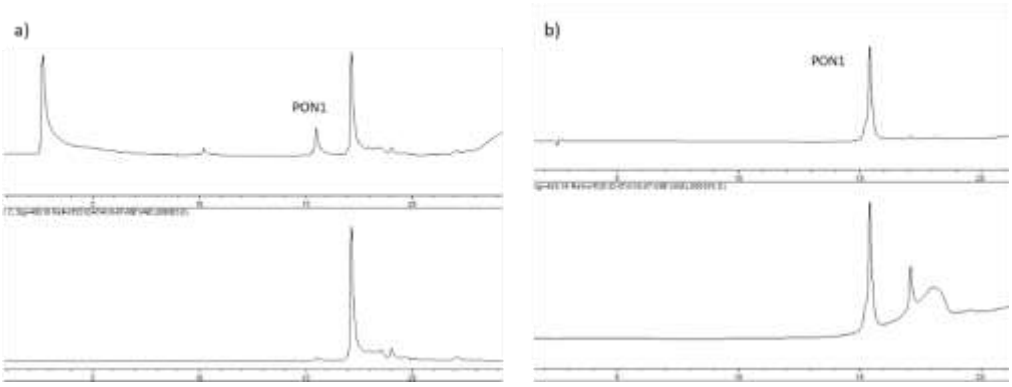

*Figure IV-3. RP HPLC chromatogram of **PON1** a) before purification b) after purification (0-50% ACN in 15 min, Discovery BIO Wide Pore C5 column, top: 260 nm and bottom: 400 nm).*

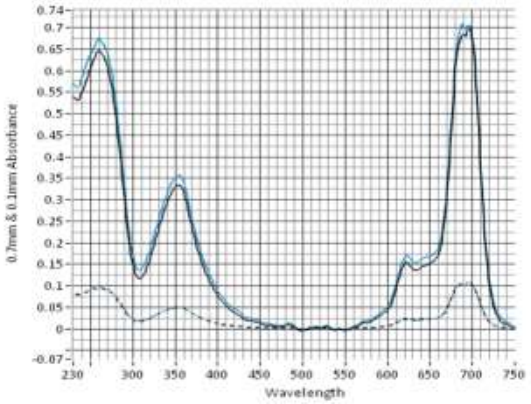

*Figure IV-4. UV-Vis spectrum of **PON1**.*

*Table IV-2. **PON1** absorption coefficients.*

	PON1	
Wavelength (nm)	410	645
ε ($L \cdot mol^{-1} \cdot cm^{-1}$)	$1.66 \cdot 10^5$	$2.2 \cdot 10^4$

IV.3.2 TriPyCOOH conjugated ODN

In the case of the porphyrin, the NHS activated ester was also provided by the group of Dr. Tomé. The conjugation was carried out by dissolving the porphyrin in DMSO and adding **ON2** in $NaHCO_3$ and allowing the reaction mixture to stir overnight in the darkness under Ar atmosphere. The unreacted TryPyCOONHS was removed by precipitation before RP HPLC purification (figure IV-6). The obtained **PON2** conjugate (17% yield) was analysed by MALDI-TOF and UV-Vis (figure IV-7). The absorption coefficients were calculated and are presented in table IV-3.

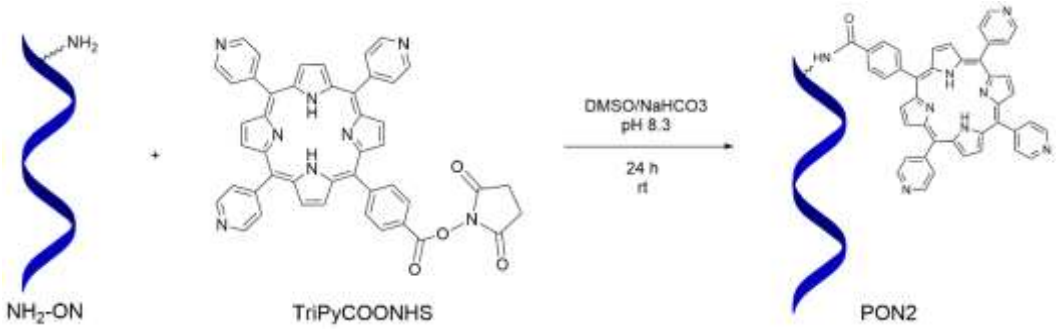

*Figure IV-5. Synthesis of the TriPyCOOH conjugate, **PON2**.*

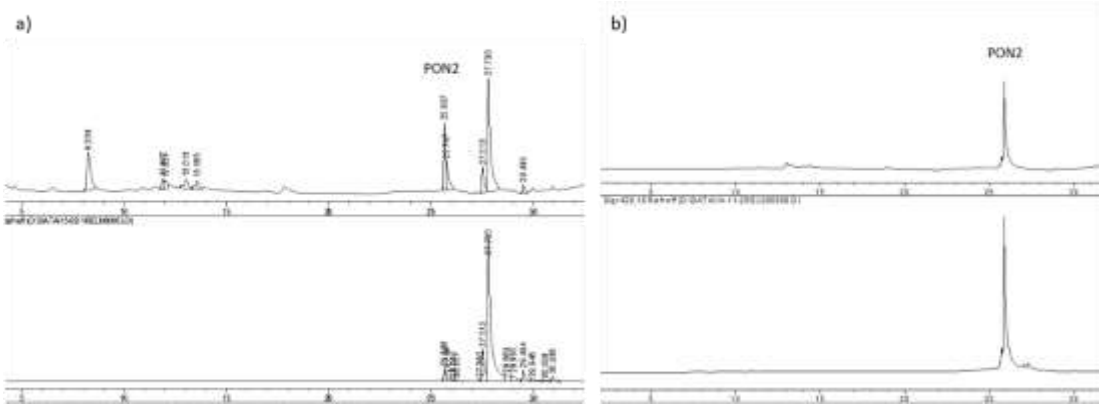

*Figure IV-6. RP HPLC chromatogram of **PON2** a) before purification b) after purification (0-50% ACN in 15 min, Discovery BIO Wide Pore C5 column top: 260 nm and bottom: 420 nm).*

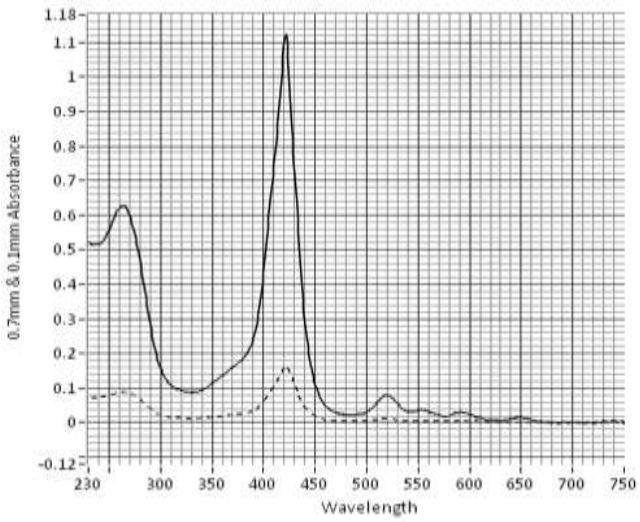

*Figure IV-7. UV-Vis spectrum of **PON2**.*

Table IV-3. PON2 absorption coefficients.

	PON2				
Wavelength (nm)	425	520	555	590	650
ε ($L \cdot mol^{-1} \cdot cm^{-1}$)	$1.82 \cdot 10^5$	$1.5 \cdot 10^4$	$7 \cdot 10^3$	$6 \cdot 10^3$	$3 \cdot 10^3$

IV.3.3 TT1 conjugated ODN

Conjugation between TT1 phthalocyanine and **ON2** was troublesome, probably due to the high insolubility of this dye in the aqueous conditions required to solubilise the ODN. The NHS activated ester of TT1 was synthesised and several attempts were carried out in solvent mixtures of DMSO or DMF with $NaHCO_3$, NH_4HCO_3 or Tris, at different ratios, but the conjugation was unsuccessful in all cases.

*Table IV-4.Summary of conditions screened for the TT1 conjugation to **ON2**.*

Organic solvent (org)	DMF	DMF	DMSO	DMSO	DMF	DMSO
Buffer (buf)	NH_4HCO_3	Tris	NH_4HCO_3	Tris	NH_4HCO_3	$NaHCO_3$
Ratio org/buf	20:80	20:80	20:80	20:80	80:20	80:20

We rationalised that the use of a water-free solvent system would favour a conjugation where one of the partners is highly insoluble in aqueous conditions. For this, a new ODN needed to be synthesised and, in this case, kept attached to the solid support selectively deprotecting the 5'-amino group. After the conjugation using HBTU/DIPEA activation of TT1, following a previously reported modified procedure, (19) the ODN was deprotected and cleaved from the solid support by NH_4OH treatment at 55ºC overnight and the obtained conjugate **PON3** was purified by RP HPLC (figure IV-9) and characterised by UV-Vis (figure IV-10 and table IV-5) and MALDI-TOF.

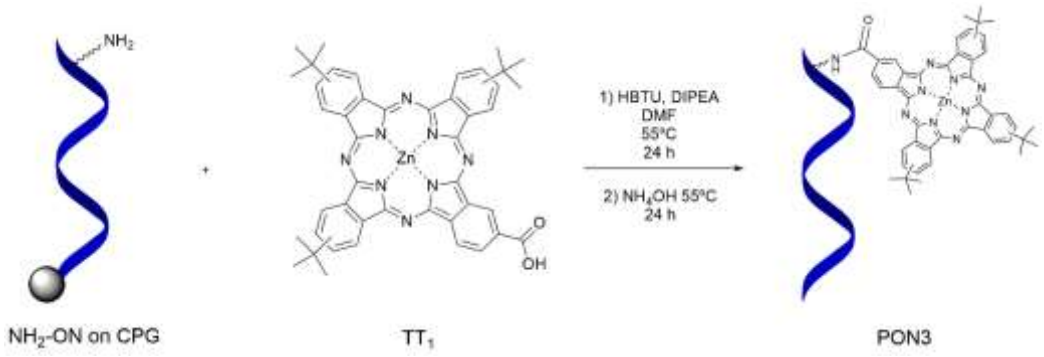

Figure IV-8. Synthesis of the TT1 conjugate, PON3.

It is important to note that this conjugation on solid support does not allow monitoring of the reaction, and reaction times had to be estimated. Moreover, even under these conditions low yields were obtained so we carried out an additional optimisation of the reaction. For this purpose, another batch of **ON2** was synthesised, this time on a CPG with bigger pores (1000 Å rather than 500 Å) to facilitate the reaction on the solid support.

Besides, TT1 was premixed with HBTU and DIPEA in DMF and added portion wise over 2 hours. Following this procedure, yields up to 20% were obtained after RP HPLC purification. As can be observed in figure IV-9, **PON3** appears as two different signals in the HPLC chromatogram. This is explained by the fact that TT1 is actually a regioisomeric mixture and upon conjugation to **ON2** results in a mixture of different species of the PS conjugated ODN. The two main signals were separately isolated and characterized and were found to have the same mass and spectroscopic properties. Therefore, the mixture of conjugates was further used as if one single compound for the crosslinking experiments.

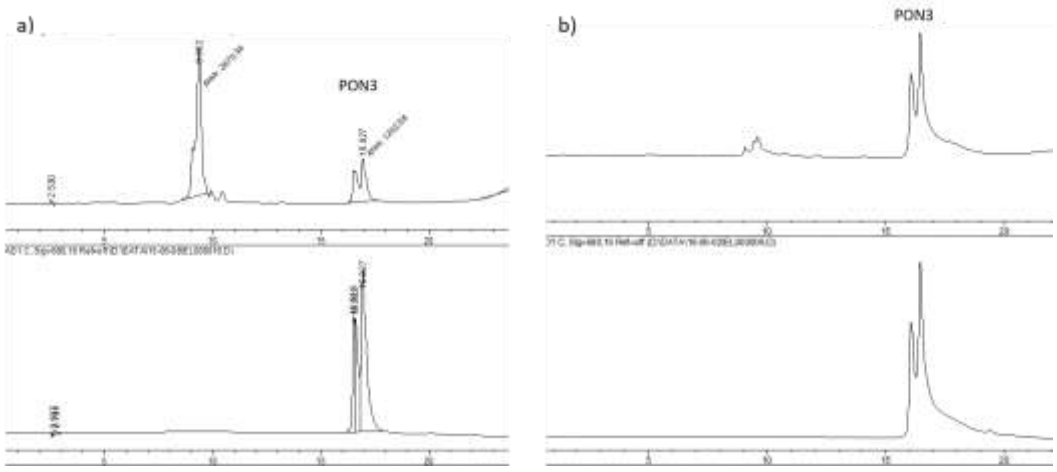

*Figure IV-9. RP HPLC chromatogram of **PON3** a) before purification and b) after purification (0-80% ACN in 15 min, Discovery BIO Wide Pore C5 column, top: 260 nm and bottom: 680 nm).*

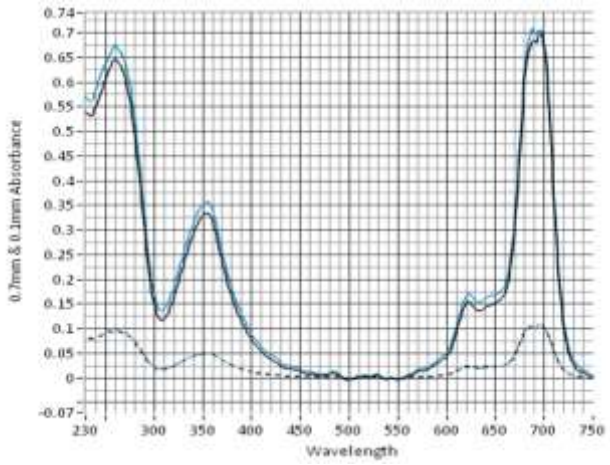

*Figure IV-10. UV-Vis spectrum of **PON3**.*

*Table IV-5. **PON3** absorption coefficients.*

	PON3		
Wavelength (nm)	350	685	695
ε ($L \cdot mol^{-1} \cdot cm^{-1}$)	$5.9 \cdot 10^4$	$1.17 \cdot 10^5$	$1.20 \cdot 10^5$

IV.4. Singlet oxygen generation of the PS conjugated ODN.

Since the synthesised PS conjugated ODNs will be evaluated for ICL formation using $^1O_2$ as oxidant, it is important to determine their $^1O_2$ generation capacities under the conditions that will be used during the crosslinking experiments.

Determination of $^1O_2$ generation can be done *via* several methods, *e.g.* by detecting its phosphorescence at 1270 nm or using a chemical trap that reacts with $^1O_2$, producing a structural change that can be easily measured, for example, a decrease in the reporter absorption. Here, we use the chemical trap method for its simplicity and the possibility of using very small amounts of the PS-ODN conjugates.

As a reporter, 9,10-anthracenediyl-bis(methylene)dimalonic acid (ABDA) was used. ABDA is soluble in PBS buffer and, by following the decrease of its absorbance at 350-415 nm (over this range three absorption maxima can be observed, figure IV-12) upon irradiation in the presence of the PS conjugated ODNs, it is possible to compare the $^1O_2$ generation of the different conjugates.

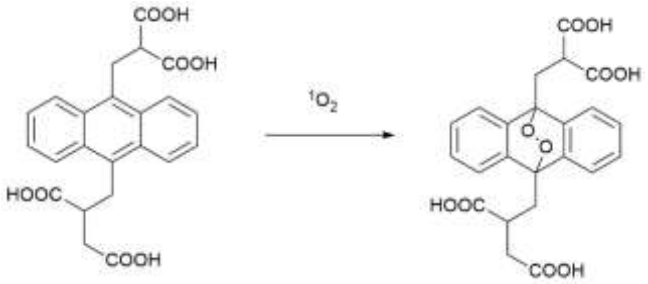

Figure IV-11. Reaction between ABDA and $^1O_2$ resulting in the quenching of the absorbance of ABDA at 350-415 nm.

Each conjugate was used at 2 μM concentration in the presence of 100 μM ABDA in a phosphate buffer solution. Upon irradiation with red light, samples were taken at different times and the UV-Vis absorption was determined (figure IV-12). For **PON1-3** the relative decrease in absorbance was determined at 380 nm and is presented in figure IV-12d.

The $^1O_2$ generation of the PS conjugated ODNs was **PON3** > **PON1** > **PON2**, in direct correlation with their light absorption in the red region. However, it is important to note that a higher $^1O_2$ generation does not necessarily means a higher crosslinking yield since we have observed that an excessive production of the oxidising agent leads to more degradation decreasing the overall ICL yield.

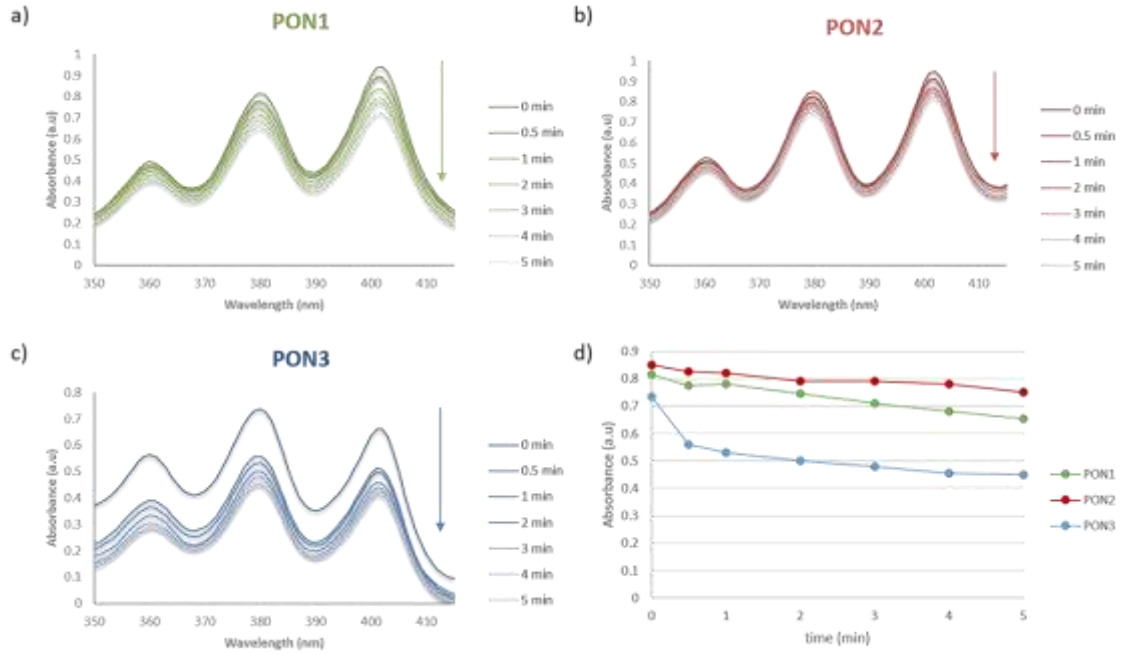

*Figure IV-12. Singlet oxygen generation of a) **PON1**, b) **PON2** , c) **PON3** and d) comparison of the conjugates by following the decrease in the absorption of ABDA at 380nm.*

IV.5. Crosslink evaluation using the PS conjugated ODNs.

With the PS conjugated ODNs in hands and having determined their abilities to produce $^1O_2$ in aqueous conditions under red light irradiation, we set out to evaluate the suitability of each conjugate for ICL formation with a furan modified complementary strand. During this first evaluation, FON1 was used in combination with **PON1-PON3** (table IV-6).

Table IV-6. Summary of modified sequences for ICL evaluation.

ODN	Sequence (5'-3')	Modification
FON1	CTG ACG G**1**G TGC	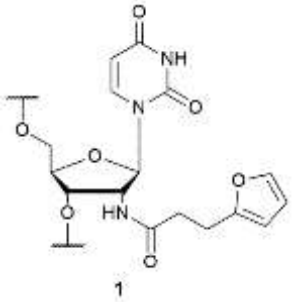 1
PON1	PS-**Am^6**- GCA CCC CGT CAG	PS = Ce6
PON2	PS-**Am^6**- GCA CCC CGT CAG	PS = TriPyCOOH
PON3	PS-**Am^6**- GCA CCC CGT CAG	P3 = TT1

The duplex was solubilised in phosphate buffer solution at 2 μM concentration, to minimise interaction between $^1O_2$ generated by one duplex and a neighbouring strand that would result from the use of higher concentrations. Irradiation times were optimised for each conjugate since too long irradiation results in a decrease of the crosslinking yield after a maximum is obtained. For all the conjugates, the time needed to achieve the highest ICL yields is much lower compared to the ICL experiments where the PSs were used in solution.

*IV.5.1 Ce6 conjugate (**PON1**)*

The **PON1** conjugate was added together with **FON1** in a buffer solution at a final concentration of 2 μM and the solution was irradiated using red light for 15 min, taking samples at different times. RP HPLC analysis showed that maximum ICL formation occurred after 3 min irradiation (34% yield), decreasing after this point (figure IV-13a and b). It is worth noting that in this case the two signals that were observed in previous crosslinking experiments using **FON1,** and which were assigned to be the crosslinked adduct, are not observed now. Instead, only one peak appears which suggests that either the two diastereomers are not formed or distinguished in this case, or that one of the signal overlaps with **PON3**, which would result in yield underestimation. PAGE analysis confirmed the formation of the crosslinked adduct that corresponds to the slower migrating band observed (figure IV-13c). In this case, GelGreen™ was used for staining since GelRed™ emits in the region of the electromagnetic spectrum where the chlorin absorbs, preventing a clear visualisation of the different bands.

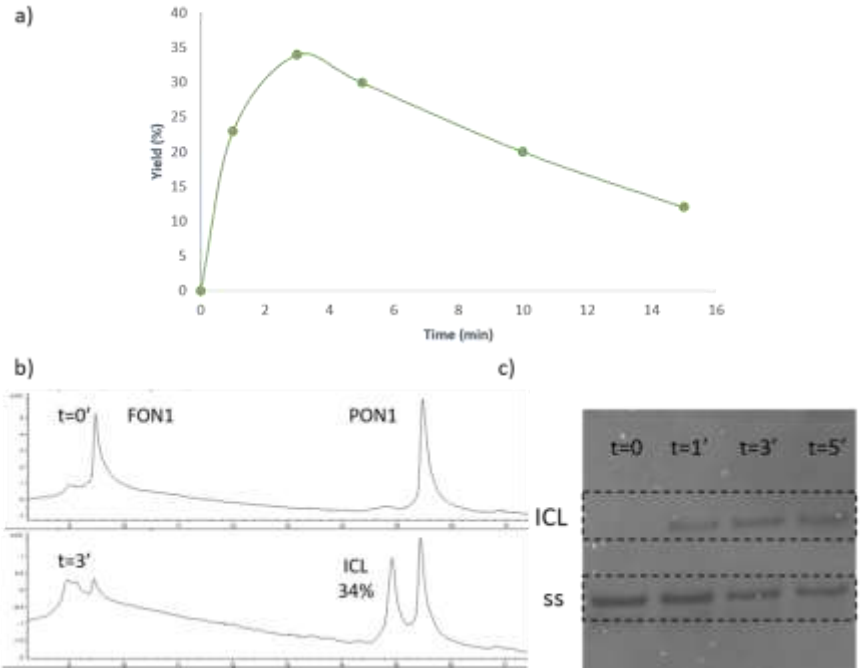

*Figure IV-13. ICL formation using the **PON1/FON1** duplex. a) Evolution of the ICL yields during irradiation. b) RP HPLC analysis of the ICL experiment (Discovery C5 column, linear gradient of 0-50% ACN in 15 min). c) PAGE analysis of the same experiment visualized using GelGreen™ (20% polyacrylamide, 1x TBE buffer).*

*IV.5.2 TriPyCOOH conjugate (**PON2**)*

As in the previous case, **PON2** was allowed to hybridise with **FON1** in phosphate buffer solution and the solution was irradiated using red light for 5 min. However, in this case no ICL formation was observed neither by RP HPLC or PAGE analysis. Rather, oxidation of **FON1** was followed by degradation thereof.

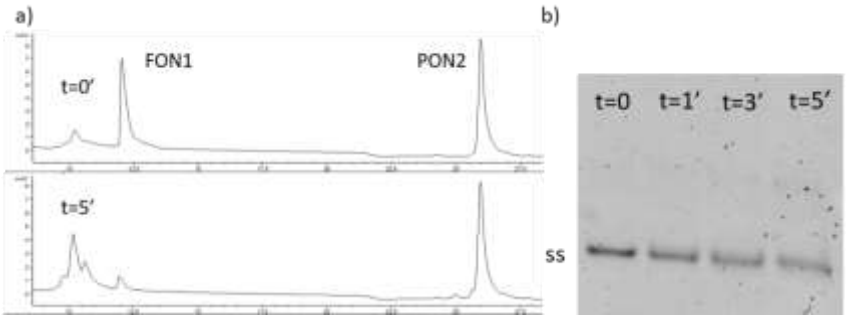

*Figure IV-14. No ICL formation occurred when using the **PON2/FON1** duplex. a) RP HPLC analysis of the ICL experiment (Discovery C5 column, linear gradient of 0-50% ACN in 15 min). b) PAGE analysis of the same experiment visualized using GelRed™ (20% polyacrylamide, 1x TBE buffer).*

One possible explanation for this could be the low $^1O_2$ generation as described in the previous section, due to the porphyrin low absorption of red light. For this reason, we

decided to evaluate other TriPyCOOH conjugated ODNs where the porphyrin will be in closer proximity to the furan on the opposite strand. If the lack of crosslink generation is related to an insufficient $^1O_2$ generation, placing the PS closer to the furan may help to ensure a higher local $^1O_2$ concentration at the reaction site. For this purpose, a 5'-amino modified ODN with a shorter (three carbon atoms instead of six) linker was used for conjugated to TriPyCOOH.

IV.5.2.1. Use of a shorter linker

For the synthesis of the porphyrin conjugate with a shorter linker, **ON3** was reacted with TriPyCOONHS in a DMSO/$NaHCO_3$ buffer solution following the same procedure as described in section IV-3.2. The obtained conjugate, **PON4**, was hybridised with **FON1** at 2 μM concentration and irradiated for 5 min using red light. The samples were analysed by RP HPLC and PAGE.

Table IV-7. Sequences used during the evaluation of TriPyCOOH as PS using shorter linker for conjugation to the ODN.

ODN	Sequence (5'-3')	Modification
FON1	CTG ACG G**1**G TGC	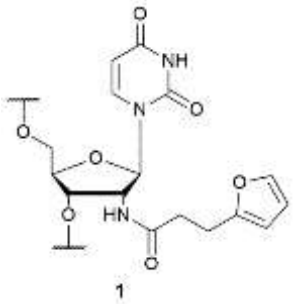 1
PON4	PS-**Am^3**- GCA CCC CGT CAG	PS = TriPyCOOH

Although RP HPLC analysis seemed to show the appearance of a new signal next to the signal corresponding to **PON4** and **FON1** was consumed after 5 min irradiation (figureIV-15a, bottom chromatogram) ICL formation could not be confirmed by PAGE (figure IV-15b).

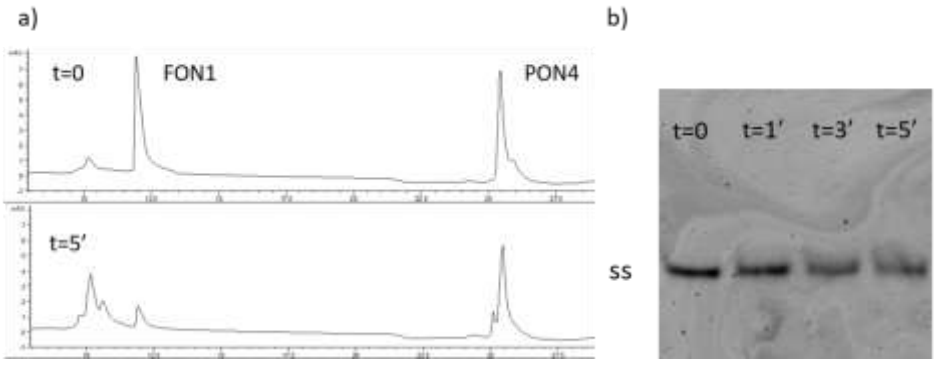

*Figure IV-15. No ICL formation occurred when using **PON4/FON1** duplex. a) RP HPLC analysis of the ICL experiment (Discovery C5 column, linear gradient of 0-50% ACN in 15 min). b) PAGE analysis of the same experiment visualized using GelRed™ (20% polyacrylamide, 1x TBE buffer).*

*IV.5.3 TT1 conjugate (**PON3**)*

Moving on to the last PS, the **PON3** conjugate was evaluated in combination with **FON1**. ICL formation was observed already after one minute irradiation, decreasing after this moment (figure IV-16a). HPLC analysis showed the appearance of two new signals next to that of PON3, reaching a maximum estimated yield of 12% (figure IV-16a and b). PAGE analysis confirmed the crosslink formation showing that several adducts were obtained, which is not surprising taking into account that PON3 was used as a mixture of different species resulting from the regioisomeric nature of TT1.

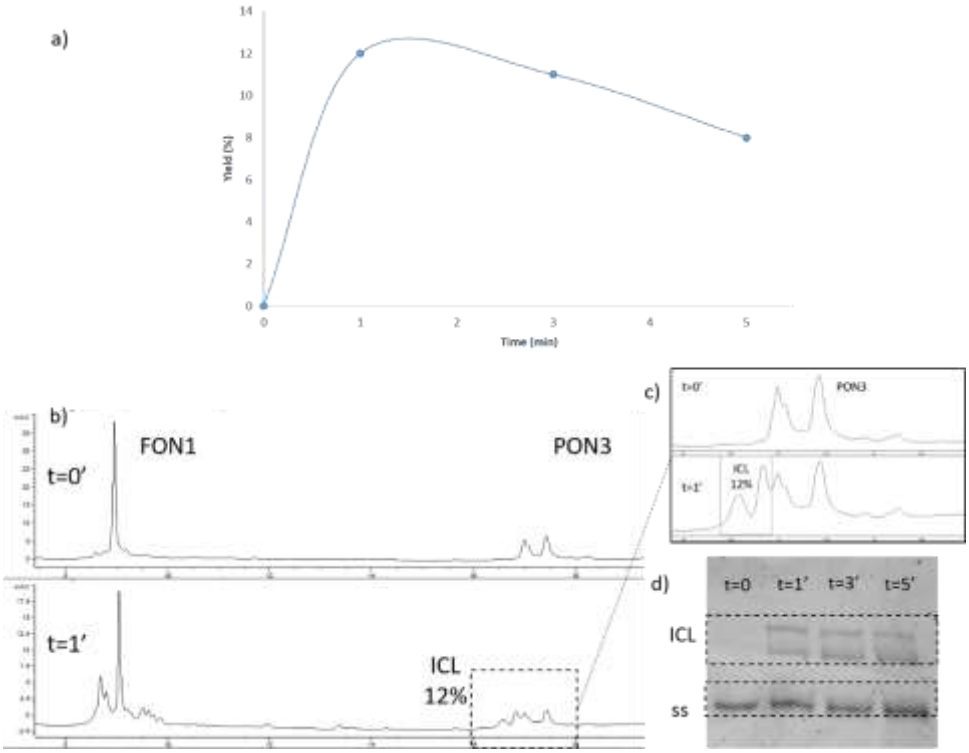

*Figure IV-16. ICL formation using the **PON3/FON1** duplex. a) Evolution of the ICL yields during irradiation. b) RP HPLC analysis of the ICL experiment (Discovery C5 column, linear gradient of 0-80% ACN in 15 min). c) Zoom-in of the chromatogram region where the formation of the ICL species takes place, overlapping the PON3 regioisomers d) PAGE analysis of the same experiment visualized using GelRed™ (20% polyacrylamide, 1x TBE buffer).*

IV.6. Melting temperature analysis of the duplexes.

The lack of crosslink formation when using the conjugates containing TriPyCOOH led us to study the duplex stability by determining the melting temperatures (Tm). Moreover, we expected to observe a correlation between the $^1O_2$ generation abilities of the PS-ODN conjugates and the ICL formation, which was not the case. **PON3**, which had a more efficient $^1O_2$ generation, only showed a 12% crosslinking yield in combination with **FON1**, compared to the 34% crosslinking yield obtained using **PON1**, which had a more mediocre $^1O_2$ generation. We expected that Tm determination would shed some light on this results.

The different 5' modified conjugates (**PON1-PON3**) were hybridised with **FON1** at 1 μM concentration in phosphate buffer solution and the Tm values were determined and compared to the duplex where no PS is conjugated, as presented in table IV-9.

*Table IV-8. Summary of the Tm values for 5' modified Ps conjugated ODNs and **FON1**.*

ODN 1	ODN 2	Tm (ºC)	ΔTm with the unmodified duplex
FON1	**ON1**	35.8	0
FON1	**PON1**	Tm = 38.3; Ta = 34.2	ΔTm= 2.5; ΔTa = -1.6
FON1	**PON2**	29.2	-6.6
FON1	**PON3**	33.5	-2.3

Ta: annealing temperature.

As can be inferred from these results, the duplex **PON2/FON1** is highly destabilised, which, in combination with the poor $^1O_2$ generation would explain the inability to induce a crosslink. Furthermore, the slight destabilisation of the **PON3/FON1** duplex could explain the rather low ICL formation in spite of the good $^1O_2$ generation of the PS-ODN conjugate. Finally, in the case of **PON1** the Ta and Tm values were rather different showing a stabilisation of the PON1/FON1 duplex once that is formed. This, together with a sufficient $^1O_2$ generation would account for this being the system that showed the highest ICL formation.

IV.7. ICL evaluation at lower temperature.

In view of the Tm results, we rationalised that lower temperatures may assist the ICL formation by performing the experiment in a context where the duplex is formed to a higher extent compared to 25ºC. We again used **PON1-PON3** conjugates in combination with FON1 at 2 μM concentration but the experiments were now carried out at 10ºC instead of 25ºC. However, even at lower temperature PON2 was not able to induce ICL formation and PON1 and PON3 performed in a similar manner, with slightly lower crosslinking yields (table IV-9).

*Table IV-9. Summary of the yields obtain at two different temperatures using **FON1** and **PON1-3**.*

PS-ODN conjugate	ICL yield at 10ºC	ICL yield at 25ºC
PON1	27%	34%
PON2	No ICL	No ICL
PON3	8%	12%

IV.8. Crosslinking using a non-nucleobase furan building block.

Conjugates **PON1**, **PON3** and **PON4** were also evaluated in combination with **FON2**, containing the phenyl-based furan building block, as presented in table IV-10.

*Table IV-10. Sequences used during the evaluation of **FON2** with the PS-ODN conjugates.*

ODN	Sequence (5'-3')	Modification
FON2	CTG ACG G**2**G TGC	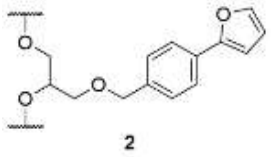 2
PON1	PS-**Am**^{6}- GCA CCC CGT CAG	PS = Ce6
PON4	PS-**Am**^{6}- GCA CCC CGT CAG	PS = TriPyCOOH
PON3	PS-**Am**^{3}- GCA CCC CGT CAG	PS = TT1

As in the previous experiments the duplexes were used at 2 μM concentration and irradiated using red light. Analysis by RP HPLC and PAGE showed similar results to the ones obtained when using the ODN containing the uridine-based furan building block **FON1**. The TriPyCOOH conjugated ODN, in this case with a shorter linker, **PON4**, did not showed any ICL formation (figure IV-18) whereas **PON1** and **PON3** reached somewhat lower crosslinking yields (**PON1**: 22% vs 34%, and **PON3** 9% vs 12%) but differences were not as striking as when the two building blocks were compared using the PSs in solution in the previous chapter.

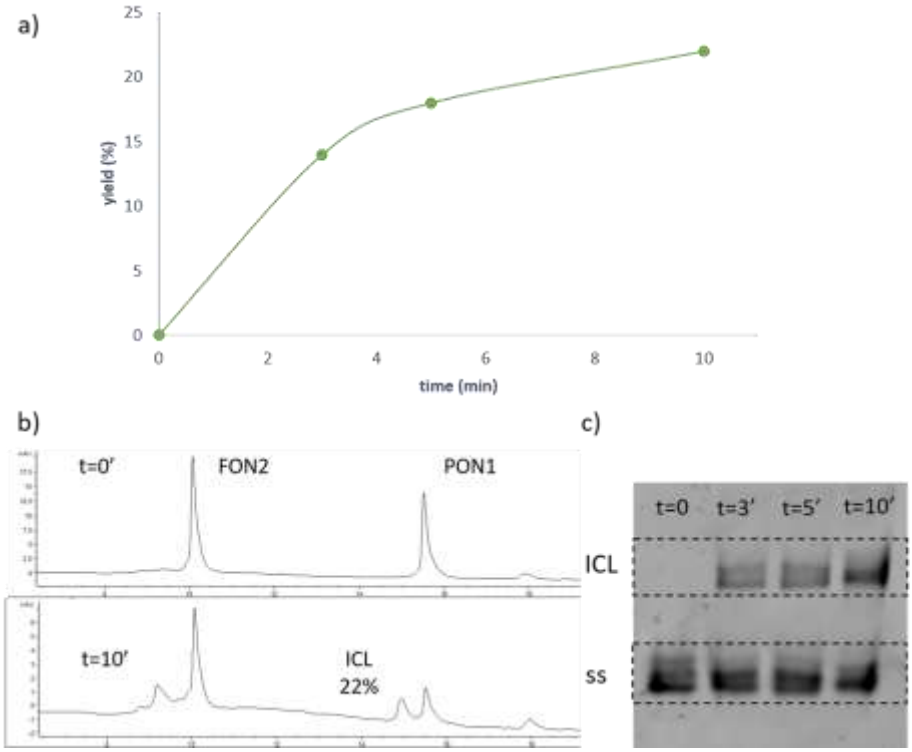

*Figure IV-17. ICL formation using **PON1/FON2** duplex. a) Evolution of the ICL yields during irradiation. b) RP HPLC analysis of the ICL experiment (Discovery C5 column, linear gradient of 0-50% ACN in 15 min). b) PAGE analysis of the same experiment visualized using GelGreen™ (20% polyacrylamide, 1x TBE buffer).*

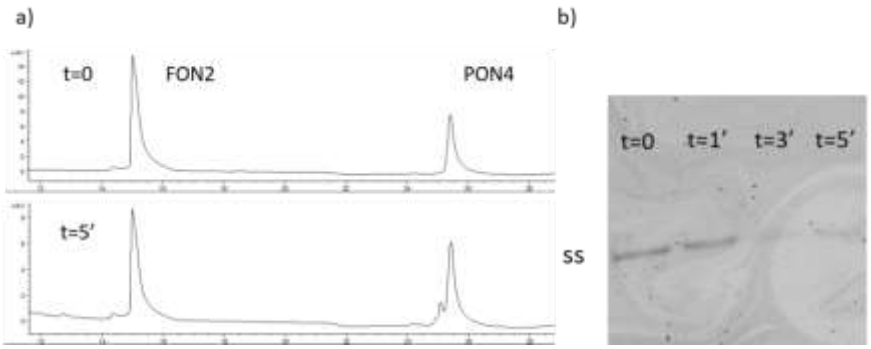

*Figure IV-18. No ICL formation occurred when using **PON4/FON2** duplex. a) RP HPLC analysis of the ICL experiment (Discovery C5 column, linear gradient of 0-50% ACN in 15 min). b) PAGE analysis of the same experiment visualized using GelRedTM (20% polyacrylamide, 1x TBE buffer).*

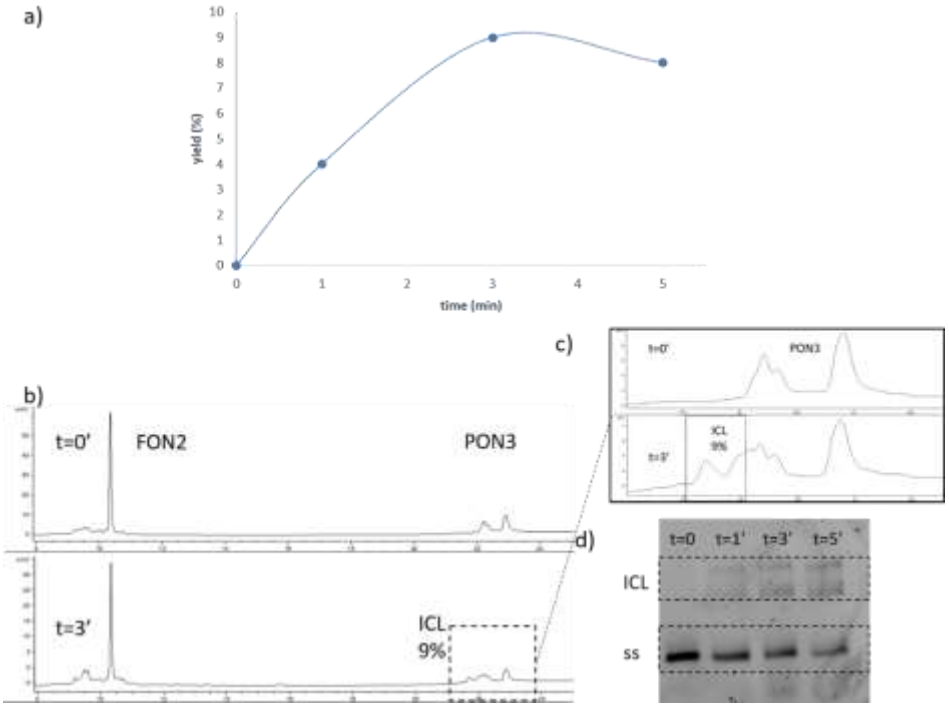

*Figure IV-19. ICL formation using **PON3/FON2** duplex. a) Evolution of the ICL yields during irradiation. b) RP HPLC analysis of the ICL experiment (Discovery C5 column, linear gradient of 0-80% ACN in 15 min). c) Zoom-in of the chromatogram region where the formation of the ICL species takes place, overlapping the PON3 regioisomers d) PAGE analysis of the same experiment visualized using GelRed™ (20% polyacrylamide, 1x TBE buffer).*

IV.9. Melting temperature analysis of the duplexes using FON2.

The duplexes formed by FON2 and the different PS conjugated ODN were also evaluated for their thermal stability as presented in table IV-11. A similar trend to the FON1 duplexes is observed: the biggest destabilisation is observed when using PON2 and PON3 duplex also shows some destabilisation. However, in this case, PON1 does not show any stabilisation.

Table IV-11. Summary of the Tm values for 5' modified Ps conjugated ODNs and FON2.

ODN 1	ODN 2	Tm (ºC)	ΔTm with the unmodified duplex
FON2	ON1	Tm = 52.2; Ta = 47.7	-
FON2	PON1	46.6	-3.4
FON2	PON2	Tm = 37.2; Ta = 34.5	ΔTm= -15 ; ΔTa =-13.2
FON2	PON3	45.4	-4.6

IV.10. Distance evaluation using a non-nucleobase building block

In view of the similar crosslinking yields when using FON2 and the PS conjugated ODNs, a further attempt was carried out to achieve ICL formation using the TriPyCOOH conjugates. For this

purpose, a new sequence was designed to containing several T nucleobases to introduce internal modifications and for each ODN, one modified T, **T***, was introduced at different positions. The amino modification is attached to the nucleobase via a six carbon linker and introduction was achieved via automated synthesis in an identical manner as with non-modified nucleobases, as described in chapter 3. For this sequences, the complementary furan sequence was synthesised, using the phenyl-based furan building block **2** due to availability. Duplex formation between **FON3** and **ON4**-**ON7** (table IV-12) results in four different systems that allow screening of the influence of the distance between the furan moiety and the PS, introduced through the amino modified nucleobase.

Table IV-12. Summary of the amino and furan modified sequences used for the distance evaluation.

Name	Sequence (5'-3')	Modification
ON4	GTA CCC TGT C**T***G	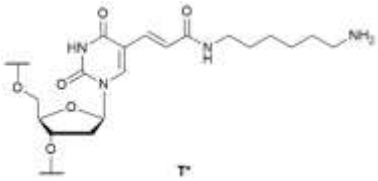
ON5	GTA CCC TG**T*** CTG	
ON6	GTA CCC **T***GT CTG	
ON7	G**T***A CCC TGT CTG	
FON3	CAG ACA G**2**G TAC	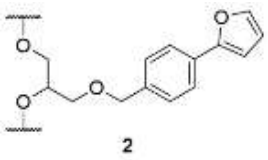

Four conjugates were synthesised using **ON4-ON7** and TriPyCOONHS (figure IV-20) following the same conjugation strategy as before (section IV-3.2) and purified by RP HPLC (figure IV-21).

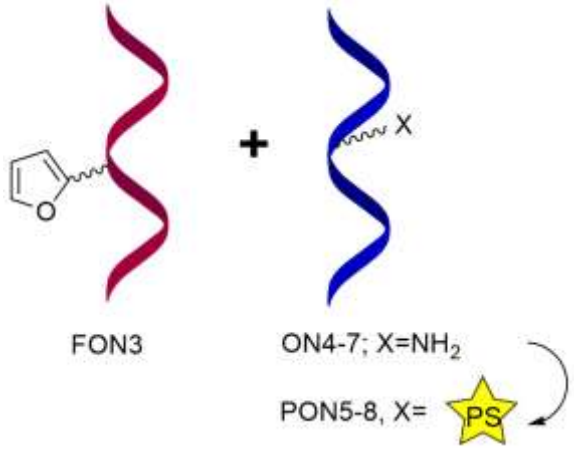

Figure IV-20. Schematic representation of the furan ODN/amino or PS duplexes (4 duplexes are formed in total).

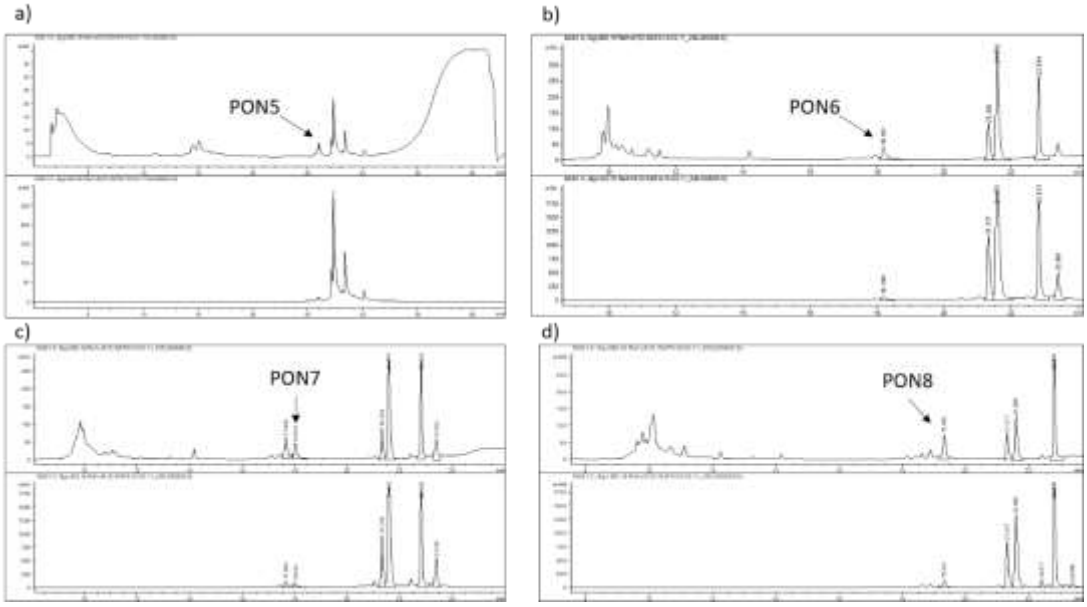

Figure IV-21. RP HPLC purification of PON5-PON8 conjugates (for each chromatogram, top: 260nm, bottom: 420nm). a) PON5 was purified using an Aeris Wide Pore column (0-10% ACN in 15 min then 10-100% ACN in 15 min; b), c) and d) PON6-PON8 were purified using a Discovery BIO Wide Pore C5 (linear gradient 0-50% ACN in 15 min).

Conjugates **PON5-PON7** were hybridised with the newly synthesised **FON3** (table IV-13), irradiated during 5 min using red light and samples were taken at different times that were subsequently analysed by RP HPLC and PAGE. Unfortunately, no ICL formation was observed for any of the duplexes (figure IV-23). Surprisingly, whereas for some of the experiments there was barely no consumption of the furan ODN (figure IV-23a and c), the closer the PS was introduced to the 5' end the faster reacted away **FON3** (figure IV-23e and g), suggesting that $^1O_2$ generation is facilitated. However, it cannot be concluded that $^1O_2$ generation is improved by placing the PS for closer to the strand termini, since **FON3** consumption when using **PON5** and **PON8** was clearly different (figure IV-23a and g) and in both cases TriPyCOOH was introduced one nucleobase away from the 3' and 5' end respectively. These results seem to indicate that position-dependant interactions between the PS and the duplex come into play and that the 5' end is a more suitable position for introducing the PS, in case $^1O_2$ is desired. However, the generated $^1O_2$ is in this case not leading to ICL formation but rather to degradation of the furan modified strand.

Table IV-13. Sequences used during the evaluation of TriPyCOOH introducing the PS as an internal modification.

Name	Sequence (5'-3')	Modification
PON5	GTA CCC TGT C**T**^{PS}G	PS= TriPyCOOH
PON6	GTA CCC TG**T**^{PS} CTG	
PON7	GTA CCC **T**^{PS}GT CTG	
PON8	G**T**^{PS}A CCC TGT CTG	
FON3	CAG ACA G**2**G TAC	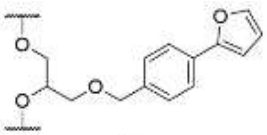 2

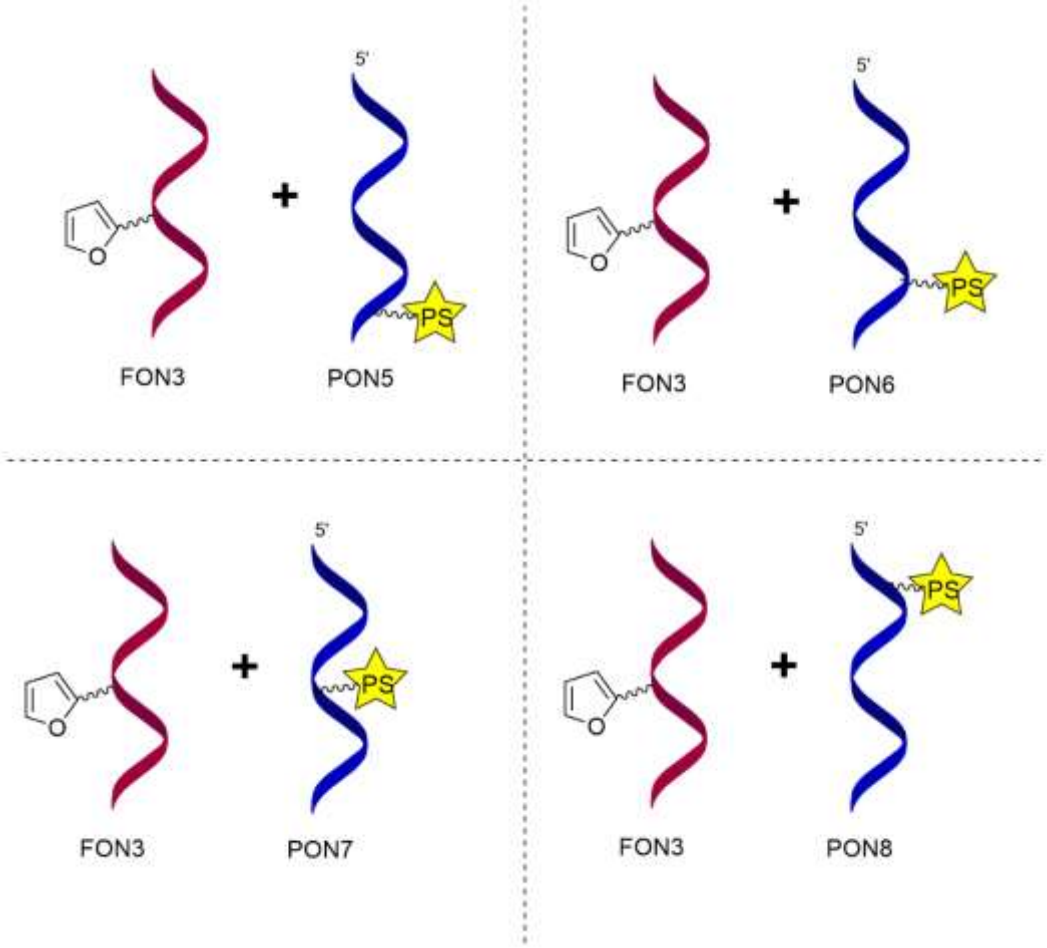

Figure IV-22. Schematic representation of the duplexes used for the distance evaluation.

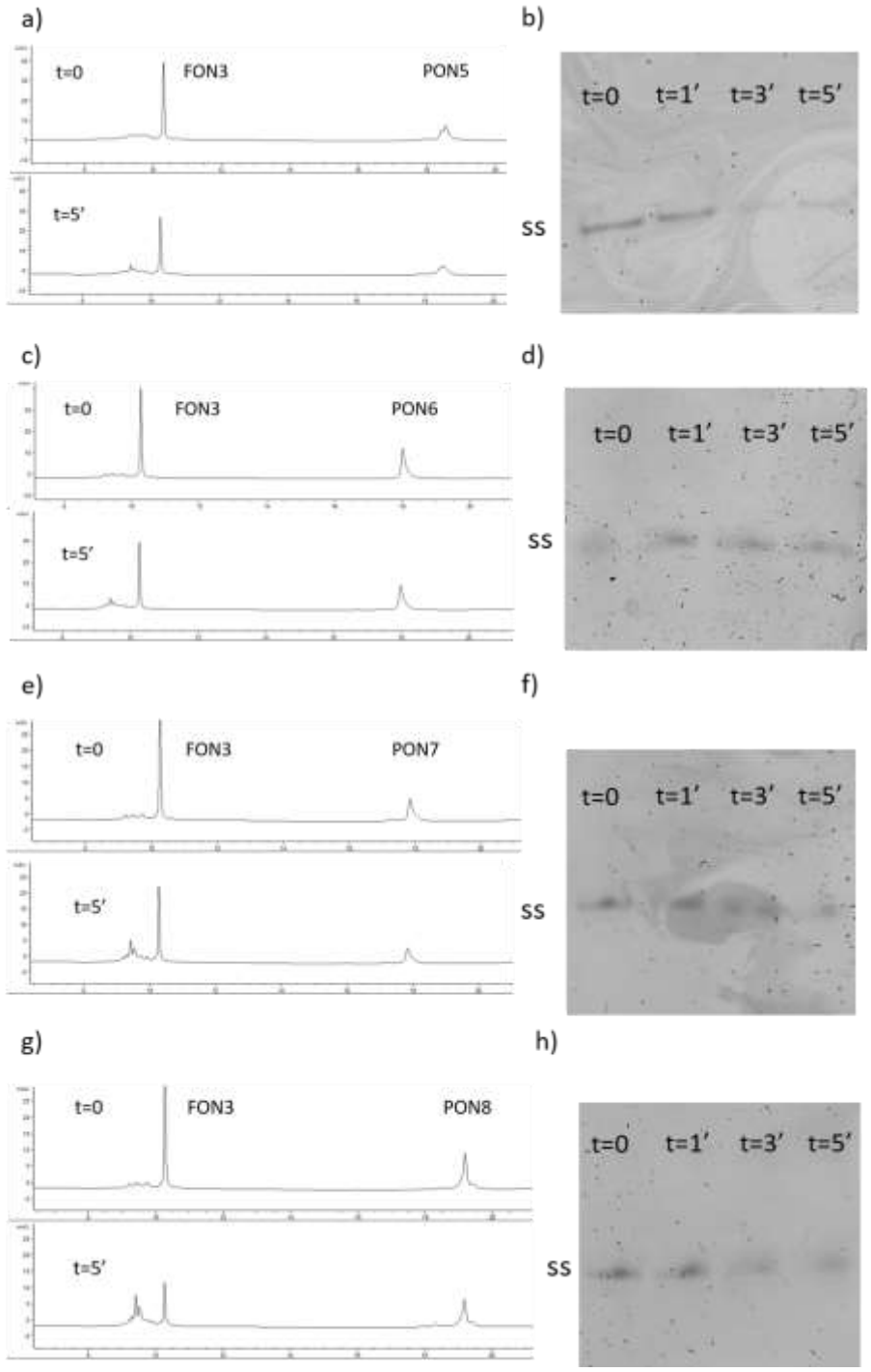

*Figure IV-23. No ICL formation occurred when using **PON5-8/FON1** duplexes. a), c), e) and g) RP HPLC analysis of the ICL experiments (Discovery C5 column, linear gradient of 0-50% ACN in 15 min). b), d), f) and h) PAGE analysis of the same experiment visualized using GelRed™ (20% polyacrylamide, 1x TBE buffer). a) and b) correspond to **PON5/FON3** duplex; c) and d) to **PON6/FON3** duplex; e) and f) to **PON7/FON3** duplex; g) and h) to **PON8/FON3** duplex.*

IV.11. Conclusions

During this chapter, several PS conjugated ODNs were synthesised and evaluated for ICL. The synthesis was straightforward in the case of TriPyCOOH porphyrin and chlorin e6 but became troublesome when the more hydrophobic TT1 phthalocyanine was used. This last synthesis was finally accomplished using on solid phase conjugation.

Evaluation of crosslink formation showed that the most effective PS-ODN conjugate was the ODN modified with Ce6, in agreement with the results reported in the previous chapter where the PSs were used in solution.

Unfortunately, no TriPyCOOH conjugate was able to induce ICL formation, even when the PS was placed closer to the furan moiety by the use of a shorter linker or internal modification. This PS seems to induce a large duplex destabilisation which in turn prevents crosslinking formation.

In the case of TT1, in spite of showing good $^1O_2$ generation when conjugated to the ODN, a lower ICL formation was observed, probably due to a slight destabilisation of the duplex.

Finally, the system versatility was tested changing parameters such as temperature and the furan building block of choice, but only a small influence on the ICL yield was observed.

IV.12. References

1. Mallikaratchy P, Tang Z, Tan W. Cell specific aptamer-photosensitizer conjugates as a molecular tool in photodynamic therapy. ChemMedChem. 2008;3(3):425–8.

2. Zhu Z, Tang Z, Phillips J a, Yang R, Wang H, Tan W. Regulation of Singlet Oxygen Generation Using Single-Walled Carbon Nanotubes. J Am Chem Soc. 2008 Aug;130(33):10856–7.

3. Yuan A, Laing B, Hu Y, Ming X. Direct oligonucleotide–photosensitizer conjugates for photochemical delivery of antisense oligonucleotides. Chem Commun. 2015;51(30):6678–80.

4. Mestre B, Jakobs a, Pratviel G, Meunier B. Structure/nuclease activity relationships of DNA cleavers based on cationic metalloporphyrin-oligonucleotide conjugates. Biochemistry. 1996;35(28):9140–9.

5. Yamada H, Tanabe K, Nishimoto S. Fluorometric Identification of 5-Methylcytosine

Modification in DNA: Combination of Photosensitized Oxidation and Invasive Cleavage. Bioconjug Chem. American Chemical Society; 2008 Jan 1;19(1):20–3.

6. Bøe SL, Longva AS, Hovig E. A novel photosensitizer for light-controlled gene silencing. Nucleic Acid Ther. Mary Ann Liebert, Inc. 140 Huguenot Street, 3rd Floor New Rochelle, NY 10801 USA; 2011;21(5):359–67.

7. Shemesh Y, Yavin E. PNA–Rose Bengal Conjugates as Efficient DNA Photomodulators. Bioconjug Chem. 2015;150818142506009.

8. Balaz M, Steinkruger JD, Ellestad GA, Berova N. 5'-porphyrin-oligonucleotide conjugates: Neutral porphyrin-DNA interactions. Org Lett. 2005 Dec;7(25):5613–6.

9. Balaz M, Li BC, Jockusch S, Ellestad G a., Berova N. Tetraarylporphyrin as a Selective Molecular Cap for Non-Watson–Crick Guanine–Adenine Base-Pair Sequences. Angew Chemie Int Ed. 2006;45(21):3530–3.

10. Mammana A, Pescitelli G, Asakawa T, Jockusch S, Petrovic AGG, Monaco RRR, et al. Role of environmental factors on the structure and spectroscopic response of 5'-DNA-porphyrin conjugates caused by changes in the porphyrin-porphyrin interactions. Chemistry. 2009 Nov 9;15(44):11853–66.

11. Mammana A, Asakawa T, Bitsch-Jensen K, Wolfe A, Chaturantabut S, Otani Y, et al. Synthesis and characterization of water-soluble free-base, zinc and copper porphyrin-oligonucleotide conjugates. Bioorg Med Chem. 2008 Jul 1;16(13):6544–51.

12. Nguyen T, Brewer A, Stulz E. Duplex Stabilization and Energy Transfer in Zipper Porphyrin-DNA. Angew Chemie Int Ed. 2009 Mar 2;48(11):1974–7.

13. Fendt L-AA, Bouamaied I, Thöni S, Amiot N, Stulz E. DNA as supramolecular scaffold for porphyrin arrays on the nanometer scale. J Am Chem Soc. 2007 Dec 12;129(49):15319–29.

14. Brewer A, Siligardi G, Neylon C, Stulz E. Introducing structural flexibility into porphyrin-DNA zipper arrays. Org Biomol Chem. 2011 Feb 7;9(3):777–82.

15. Morales-Rojas H, Kool ET. A Porphyrin C -Nucleoside Incorporated into DNA. Org Lett. 2002 Dec;4(25):4377–80.

16. Sitaula S, Reed SM. Porphyrin conjugated to DNA by a 2'-amido-2'-deoxyuridine linkage. Bioorg Med Chem Lett. 2008 Jan;18(2):850–5.

17. Li H, Fedorova OS, Trumble WR, Fletcher TR, Czuchajowski L. Site-Specific Photomodification of DNA by Porphyrin−Oligonucleotide Conjugates Synthesized via a Solid Phase H-Phosphonate Approach. Bioconjug Chem. 1997 Jan;8(1):49–56.

18. Wellner C, Wagenknecht H-A. Synthesis of DNA conjugates with metalated tetracationic porphyrins by postsynthetic cycloadditions. Org Lett. 2014 Mar 21;16(6):1692–5.

19. Kopecky K, Novakova V, Miletin M, Kučera R, Zimcik P. Solid-phase synthesis of azaphthalocyanine-oligonucleotide conjugates and their evaluation as new dark quenchers of fluorescence. Bioconjug Chem. 2010;21(10):1872–9.

Chapter V.

Dual modified photosensitiser/furan self-activating systems. Synthesis and evaluation of their crosslink behaviour.

In this chapter the different PSs will be introduced in a dual modified ODN, containing the furan moiety and an amino group for further conjugation. Construction of the so called self-activating probes would allow targeting unmodified sequences. However, this proved to be troublesome and an alternative design was envisioned, where two different ODNs, one containing the furan moiety and one containing the PS, target a longer complementary sequence. This longer ODN acts as a template to bring the two modified probes together.

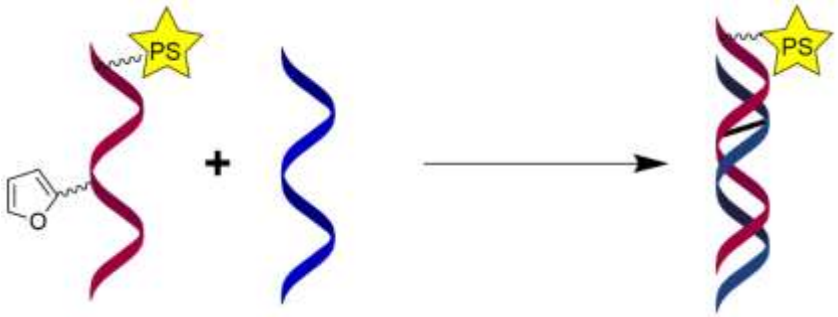

V.1. Synthesis of dual modified ODNs.

Design of the dual modified ODNs was carried out based on the results of the previous chapter. The amino modifier was situated at the 5' end since this allows easier synthetic access to PS-modified strands. The results in chapter 4 when using the internally modified TriPyCOOH conjugated ODNs (section IV-10) also showed that the $^1O_2$ generation seems to benefit from the PS being placed at the 5' terminus, at least in the case of the porphyrin. Since furan building blocks **1** and **2** (figure V-1) showed similar crosslinking abilities, they were both introduced in the double modified sequences.

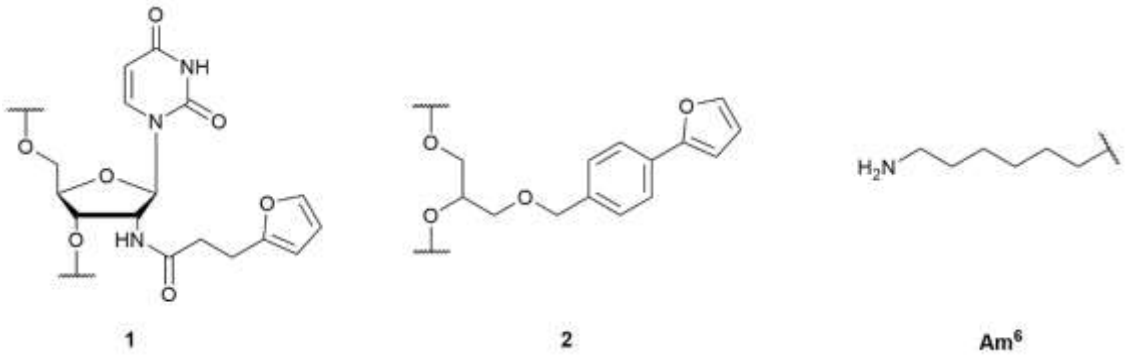

Figure V-1. Furan building blocks and amino modifier used for the self-activating probe synthesis.

Synthesis of the dual modified sequence was carried out by automated synthesis, including introduction of the amino modifier, as described in chapters 3 and 4. The furan phosphoramidites were introduced by manual coupling to maximise coupling efficiencies, as previously discussed.

After synthesis, the dual modified sequence containing building block **2**, **FON5** (table V-1), was divided into two batches (figure V-2). The first one was deprotected and cleaved from the CPG using NH_4OH, the amino group still protected, and purified using C18 cartridges. The second batch was kept on the solid support for conjugation of TT1 and the amino group was deprotected on column using TCA to allow the selective conjugation. In the case of **FON4**, the scarce availability of building block **1** only allowed for the synthesis of one sequence that was cleaved and deprotected and will only be used for conjugation with Ce6, since this PS showed the highest ICL formation between the Ce6 conjugated to an ODN and the furan modified ODN in the previous chapter.

Table V-1. Summary of the sequences used for the self-activating probe evaluation.

Name	Sequence (5'-3')
FON4	**Am^{6}**- CTG ACG G**1**G TGC
FON5	**Am^{6}**- CTG ACG G**2**G TGC
ON1	GCA CCC CGT CAG

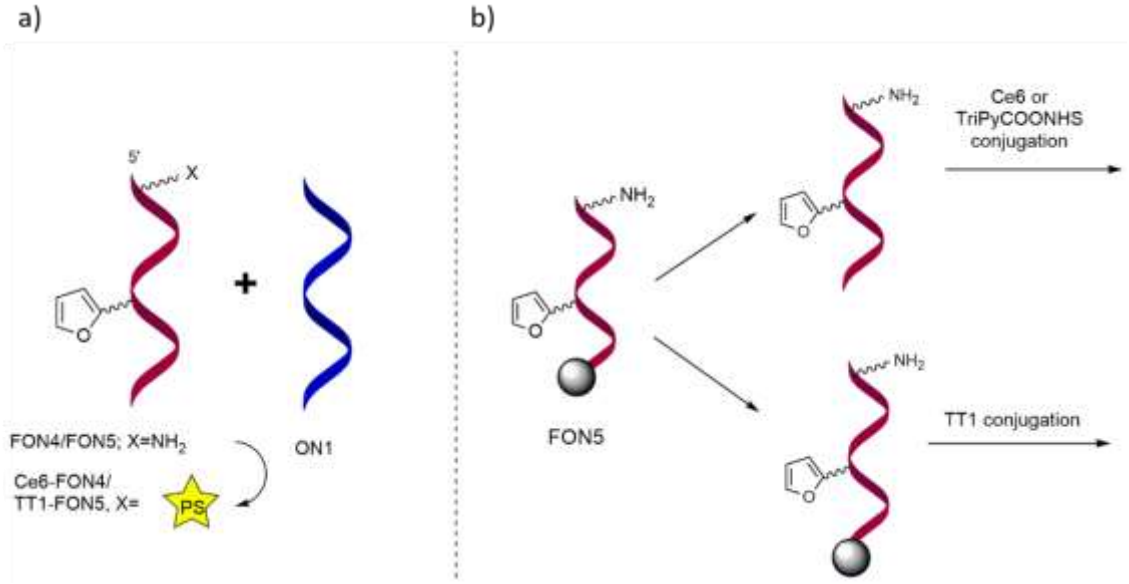

*Figure V-2. Schematic representation of a) the dual modified ODN/ON1 duplexes; b) Partitioning of **FON5** for the different synthetic approaches.*

V.2. Synthesis of self-activating furan probes.

V.2.1. Phenyl-based furan building block.

Due to the higher availability **FON5**, conjugation reactions were first attempted between this double modified ODN and the three PSs. However, the synthesis and characterisation of the different probes was troublesome in all cases.

V.2.1.1 Conjugation using Ce6

The strategy using DCC/NHS activation of Ce6, followed by addition of the dual probe in $NaHCO_3$ buffer solution, which was successfully used in chapter 4 (section IV.3.1) for the synthesis of the Ce6 conjugated ODN, was also attempted here (Figure V-3). However, in this case very low conversion was obtained, only enough to attempt characterisation and unfortunately, the correct mass could not be found by MALDI-TOF analysis.

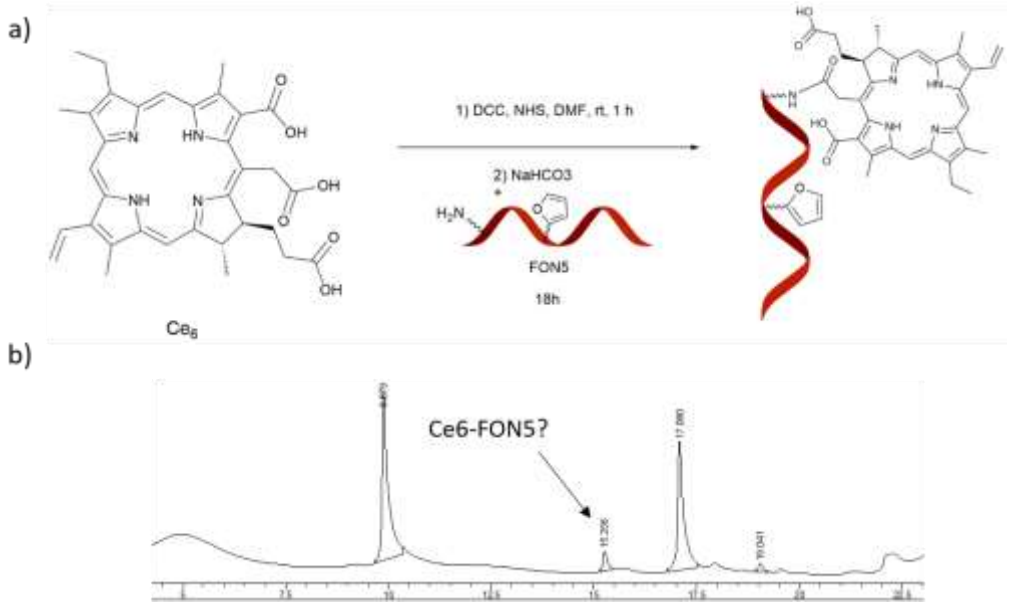

*Figure V-3. a) Synthesis of the self-activating probe using Ce6 and **FON5**; b) RP HPLC analysis of the reaction. The marked peak shows a UV-Vis spectrum with maxima at 260 and 400 nm that would correspond to the conjugate (0-50% ACN in 15 min, Discovery BIO Wide Pore C5 column).*

V.2.1.2 Conjugation using TriPyCOOH

As previously described in section IV.3.2 in chapter 4, the NHS ester of TriPyCOOH porphyrin was dissolved in DMSO and the dual modified **FON5** was added in $NaHCO_3$ buffer. In this case, the reaction seemed to proceed and the appearance of a new peak was observed by RP HPLC. After purification of this compound, the new species was analysed by MALDI-TOF but unfortunately the correct mass was not obtained.

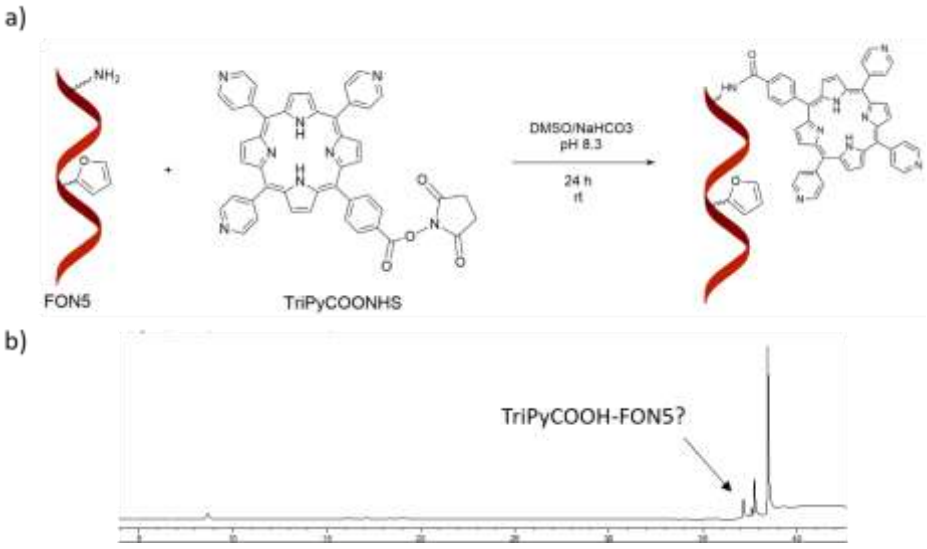

*Figure V-4. a) Synthesis of the self-activating probe using Ce6 and **FON5**; b) RP HPLC analysis of the reaction. The marked peak shows a UV-Vis spectrum with maxima at 260 and 420 nm that would correspond to the conjugate (0-20% ACN in 30 min, Clarity C18 column).*

V.2.1.3 Conjugation using TT1.

In this case, **FON5** was used while still attached to the CPG to allow conjugation without the use of buffer solutions, based on the optimised conditions in chapter 4 (section IV.3.3). The only change was to carry out the reaction at room temperature instead of at 55ºC since the higher temperature leads to a lower conversion in this case. After cleavage and deprotection using NH_4OH, the dual modified conjugate **TT1-FON5** was purified by RP HPLC and characterised by MALDI TOF. The expected mass was found among a complex set of signals that correspond, among others that could not be identified, to the species where the furan has been oxidised. However, since it cannot be ruled out that the oxidation of the furan happens due to $^1O_2$ generation upon laser irradiation during MALDI-TOF analysis, this compound was evaluated for ICL formation.

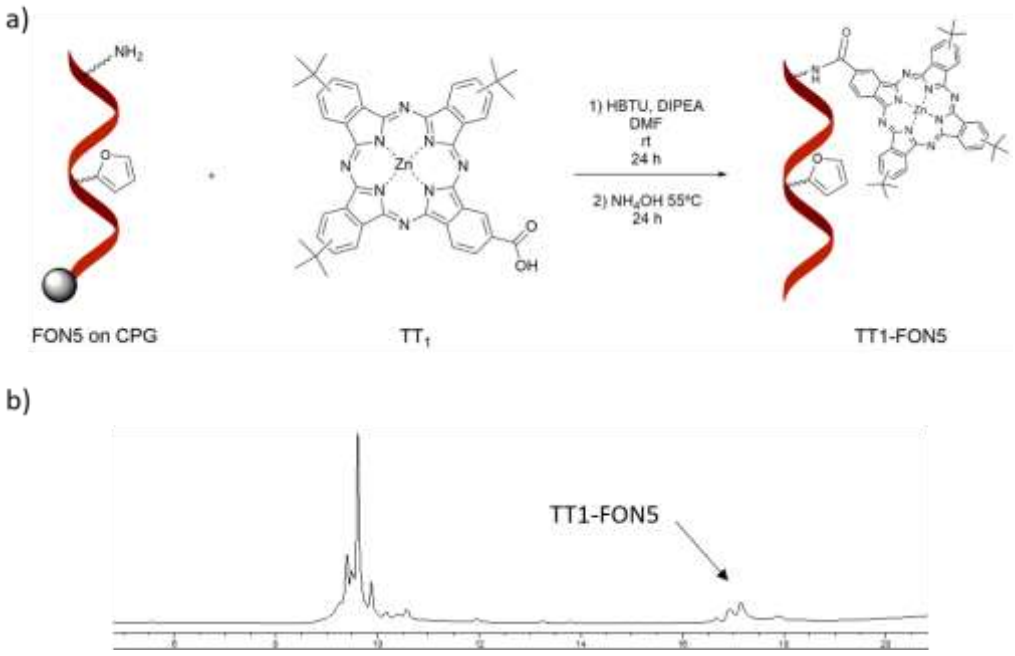

*Figure V-5. a) Synthesis of the self-activating probe using TT1 and **FON5**; b) RP HPLC analysis of the reaction. The marked peak shows a UV-Vis spectrum with maxima at 260 and 680 nm that would correspond to the conjugate (0-80% ACN in 15 min, Discovery BIO Wide Pore C5 column).*

V.2.2. Uridine-based furan building block

Since the highest crosslinking yields in chapter 4 were obtained using the Ce6 conjugated ODN, conjugation of this PS was attempted using **FON4** as an alternative dual modified ODN (**Ce6-FON4**). The same reaction conditions were used as when **FON5** was the ODN of choice

but in this case, the reaction proceeds and a new signal was observed by RP HPLC. Analysis by MALDI-TOF showed that the furan seems to be already oxidised but since there is the possibility that the oxidation happens as a result of the laser irradiation, this **Ce6-FON4** was tested for ICL formation.

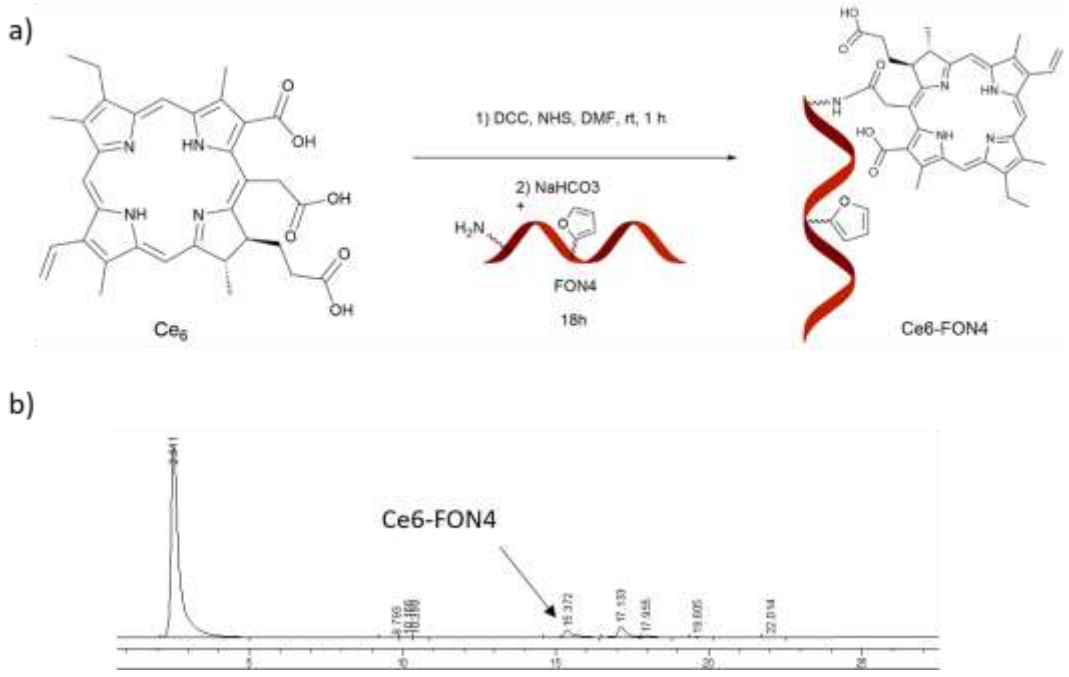

*Figure V-6. a) Synthesis of the self-probe using Ce6 and **FON4**; b) RP HPLC analysis of the reaction. The marked peak shows a UV-Vis spectrum with maxima at 260 and 400 nm that would correspond to the conjugate (0-50% ACN in 15 min, Discovery BIO Wide Pore C5 column).*

V.3. Crosslink evaluation using self-activating probes.

Self-activating probes **Ce6-FON4** and **TT1-FON5** were hybridised with the unmodified complementary sequence **ON1**, at 2 μM duplex concentration in phosphate buffer solution, and irradiated with red light for 5 minutes.

V.3.1. Ce6 modified self-activating probe.

In the case of self-activating probe **Ce6-FON4**, no ICL formation was observed. **Ce6-FON4** was partially consumed but **ON1** remained intact (figure V-8a) and PAGE analysis confirmed that no crosslinked adduct was formed (figure V-8b).

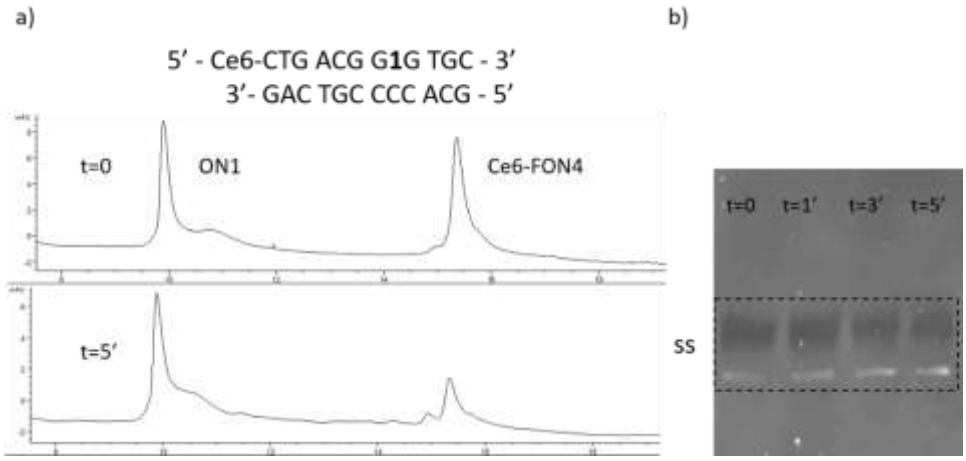

*Figure V-7. No ICL formation was observed using **Ce6-FON4**. a) RP HPLC analysis of the ICL experiment (Discovery C5 column, linear gradient of 0-50% ACN in 15 min). b) PAGE analysis of the same experiment visualized using GelGreen™ (20% polyacrylamide, 1x TBE buffer).*

V.3.2. TT1 modified self-activating probe.

Also when **TT-FON5** was used, no crosslink formation was observed either by RP HPLC or by PAGE (figure V-9), and as in the previous case, only the self-activating probe was consumed.

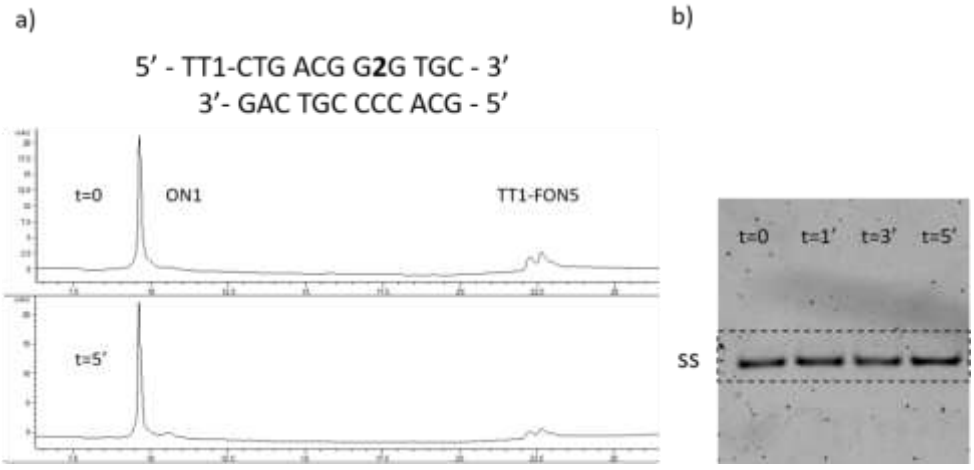

*Figure V-8. No ICL formation was observed using **TT1-FON5**. a) RP HPLC analysis of the ICL experiment (Discovery C5 column, linear gradient of 0-80% ACN in 15 min). b) PAGE analysis of the same experiment visualized using GelRed™ (20% polyacrylamide, 1x TBE buffer).*

V.4. Evaluation of a self-activating templated system.

Due to the problematic synthesis and characterisation of the dual modified self-activating probes, and their inability to induce ICL, a new strategy was designed in collaboration with Dr.

Nathalie De Laet. It was rationalised that the presence of the PS in the same strand as the furan moiety may easily lead to $^1O_2$ generation during the handling of the probes that would result in the premature oxidation of furan, rendering it unreactive for crosslink formation. Since ICL formation was proven successful during the evaluation of PS conjugated ODNs, where the PS and the furan moiety are situated in different strands (chapter IV), a system where also the two modifications are not placed in the same ODN but the self-activating principle is retained by targeting a longer complementary sequence, was designed (figure V-10).

Previously, this strategy was evaluated using methylene blue or rose bengal conjugated ODNs and they were found to be able to induce ICL formation at physiologically relevant concentrations (200 nM) towards a 24-mer unmodified ODN. In contrast, the use of such a low concentration of the externally added PS, abolished the crosslink formation.

In this case, sequences **FON3** and **PON1** (or the unmodified analogue **ON1**) were hybridised to **ON9** and evaluated for crosslink formation (table V-2).

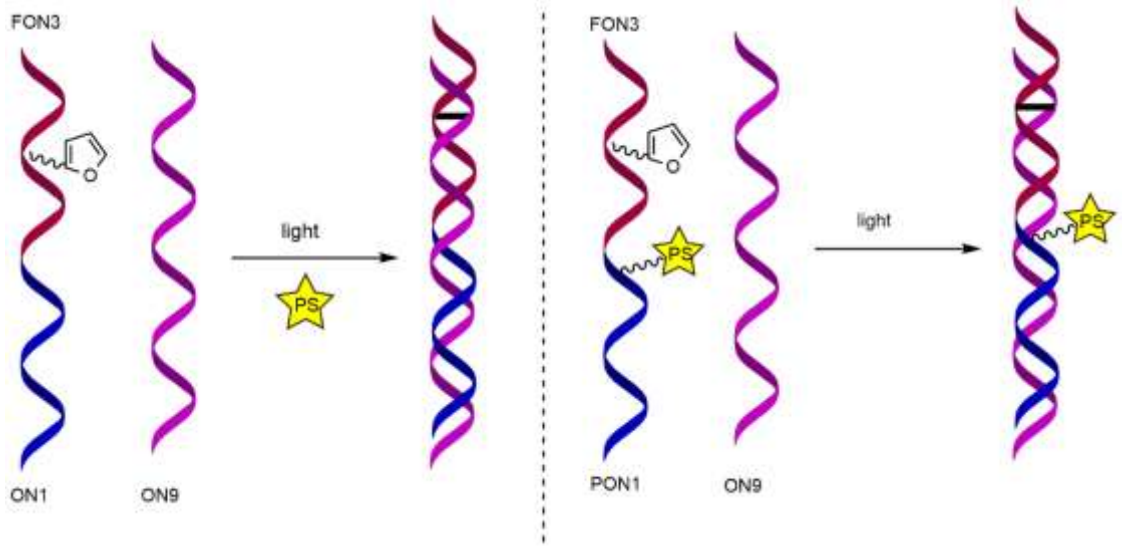

*Figure V-9. ICL formation using a templated system. a) Using Ce6 in solution and b) using a Ce6 modified ODN (**PON1**).*

Table V-2. Summary of the sequences that are used during the crosslinking experiments using the templated system.

ODN	Sequence	Modification
ON8	3' - GTC TGT CCC ATG - 5'	-
FON3	5' - CAG ACA G**2**G TAC - 3'	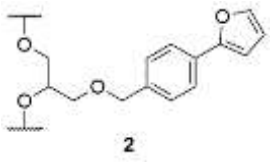
ON9	3' - GTC TGT CCC ATG CGT GGG GCA GTC - 5'	-
ON1	5' - GCA CCC CGT CAG - 3'	-
PON1	5' - PS-**Am**^{6} - GCA CCC CGT CAG - 3'	PS = Ce6
ON10	3' - CGT GGG GCA GTC - 5'	-

First, the melting temperatures of the different duplexes of this three-legged system were determined to ensure that the duplexes were not disturbed by the hanging single stranded region that exists when only one of the short strands has hybridised the longer target. As comparison, **FON3** and **PON1** were hybridised with their complementary sequences (**ON8** and **ON10** respectively), which correspond to half of **ON9**.

Table V-3. Melting temperature values of the duplexes used to evaluate the templated system.

ODN 1	ODN 2	Tm (ºC)	ΔTm with shorter duplex
ON8	**FON3**	37.1	-
ON9	**FON3**	65.7	+28.6
ON10	**PON1**	58.7	-
ON9	**PON1**	67.5	+8.8
ON9	**ON1**	66.5	-

The Tm values showed a surprisingly high value that may due to the formation of additional tertiary structures. We reasoned that upon hybridisation of **ON9** with both the furan-containing **FON3** as well as the PS containing strand **PON1** as illustrated in Figure V.10, the system would be stable enough to overcome potential tertiary structure formation. This is however difficult to ascertain by Tm measurements and we proceeded to evaluate these systems for their interstrand crosslinking behaviour.

The templated system was first evaluated adding Ce6 in solution (200 nM), hybridising **ON9** with **FON3** and the unmodified **ON1**. The use of lower concentrations allows to evaluate the crosslink

formation under conditions resembling a cellular context. Ce6 was added at 200 nM concentration to assess whether the crosslink formation is possible under highly dilute conditions and also 20 μM concentration was used for comparison purposes. Then, the self-activating system was assessed where the Ce6 modified ODN (**PON1**) was used instead of **ON1**.

V.4.1. *Crosslink formation using a templated system and Ce6 in solution.*

FON3, **ON9** and **ON1** were hybridised in phosphate buffer solution and Ce6 was added just before irradiation using red light. Samples were taken at different times and analysed by RP HPLC and PAGE.

When Ce6 was used at 20 μM concentration, ICL formation is observed, reaching a maximum of 12% yield after 10 minutes, even if **FON3** is almost completely consumed (figure V-11b). The formation of the crosslinked adduct was confirmed by PAGE, where a slower migrating band appears above the single stranded ODNs (figure V-11c).

As expected, lowering the Ce6 concentration to a 1:1 ratio with respect to the duplex concentration (200 nM) supressed the ICL formation (figure V-12). It is expected that the used of Ce6 conjugated ODN would facilitate the crosslink formation by generating $^1O_2$ in closer proximity to the furan moiety.

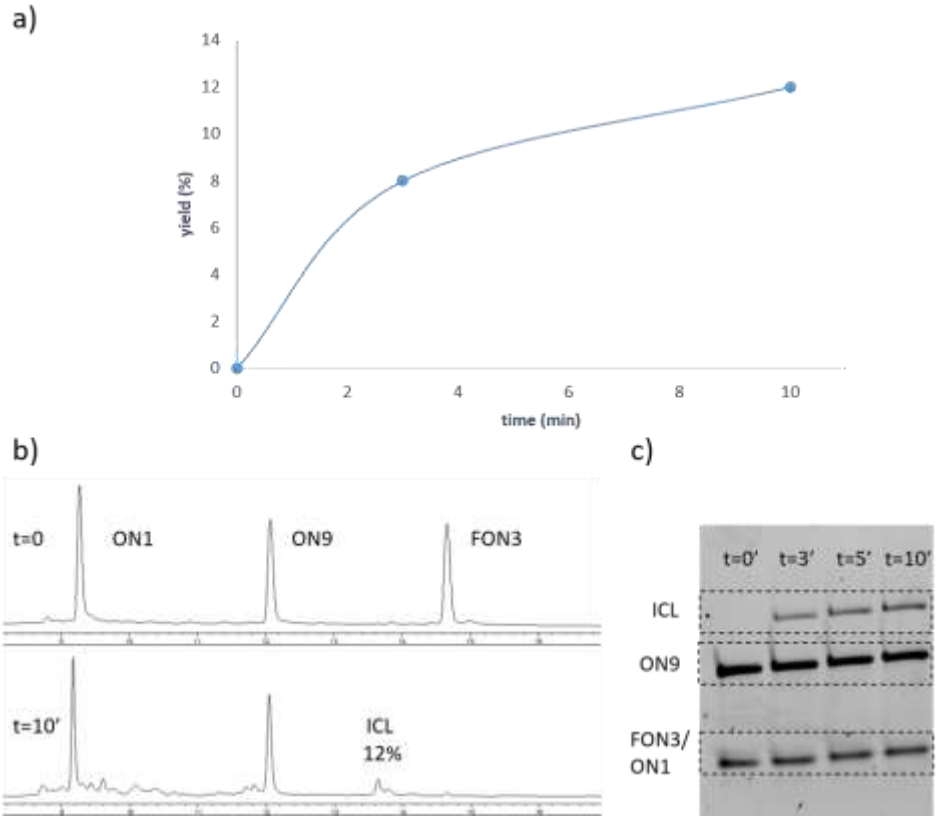

*Figure V-10. ICL formation using **ON1/ON9/FON3** templated system at 200 nM concentration and Ce6 at 20 μM concentration. a) Evolution of the ICL yield during irradiation. b) RP HPLC analysis of the ICL experiment (XBridge column, linear gradient of 0-20% ACN in 30 min). c) PAGE analysis of the same experiment visualized using GelRed™ (20% polyacrylamide, 1x TBE buffer).*

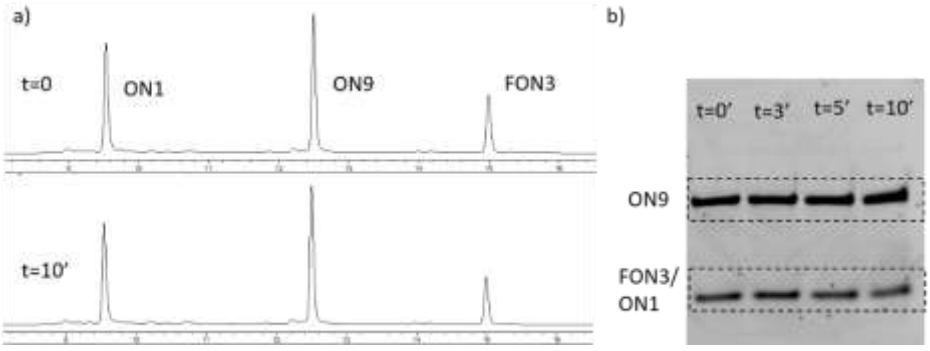

*Figure V-11. No ICL formation was observed when using **ON1/ON9/FON3** templated system at 200 nM concentration and Ce6 at 200 nM concentration. a) RP HPLC analysis of the ICL experiment (XBridge column, linear gradient of 0-20% ACN in 30 min). b) PAGE analysis of the same experiment visualized using GelRed™ (20% polyacrylamide, 1x TBE buffer).*

V.4.2. Self-activated templated system.

PON1 was used instead of **ON1** for hybridisation with **ON9** and **FON3** to evaluate whether a higher local $^1O_2$ generation assists crosslink formation under highly diluted conditions (200

nM). After hybridisation, the reaction mixture was irradiated using red light and samples were taken and analysed by RP HPLC and PAGE. Unfortunately, no crosslink formation was observed. The RP HPLC chromatogram shows no consumption of the furan containing **FON3** but **PON1** disappears. This suggests that $^1O_2$ generation in this system damages the Ce6 conjugated ODN, **PON1**, rather than traveling to the furan moiety to induce ICL. PAGE analysis was performed using the previous crosslink (**ON1**/**FON3**/**ON9** at 200 nM and Ce6 at 20 μM, section V.4.1) as reference.

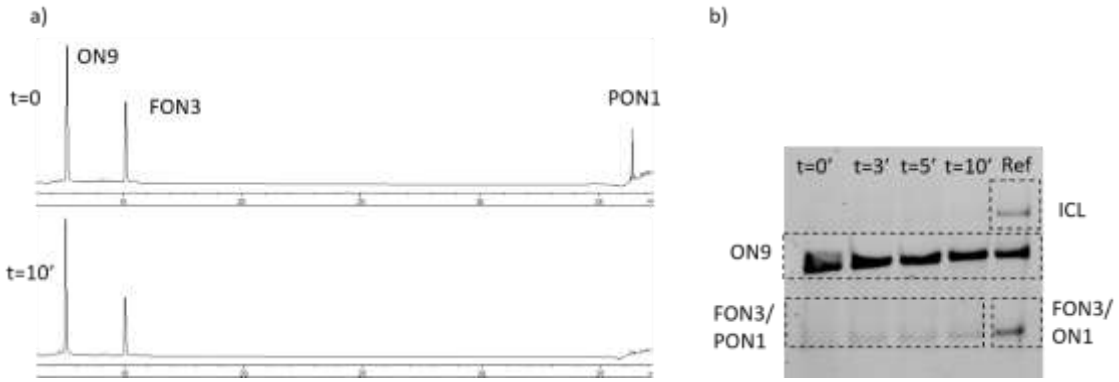

Figure V-12. No ICL formation was observed when using PON1/ON9/FON3 templated system at 200 nM concentration. a) RP HPLC analysis of the ICL experiment. The higher polarity of PON1 results in higher retention times under these analysis conditions (XBridge column, linear gradient of 0-20% ACN in 30 min). b) PAGE analysis of the same experiment visualized using GelRed™ (20% polyacrylamide, 1x TBE buffer).

The failure of the current approach was rather unexpected, given the earlier positive experiences with a very similar system featuring an identical setup but containing methylene blue or rose Bengal conjugates.(1)

However, upon closer inspection of the melting temperatures and consulting the literature, it seems that in the current case we had unfortunately chosen a sequence which is rather self-complementary and where **ON9:ON9** pairing is preferred over **ON9:FON3** or **ON9:PON1** pairing, and also over **ON9:PON1+FON3** pairing thus resulting in a melting temperature corresponding to the melting of the ON9:ON9 duplex, explaining the high values observed in Table V.2. This then also explains the absence of any interstrand crosslinking as the envisaged complementarity between furan-probe and the target as well as the proximity of the PS-probe is unexisting. In view of time constraints, we decided not restart the entire process and synthesize alternative, more suitable sequences but rather concentrate on an alternative approach as described in the next chapter.

Table V-4. Comparison between the sequences used in this work and a previous study using MB or RB.

Sequence used in this work	Previous sequence
5' - CAG ACA G**2**G TAC - 3'	5' - CAG ACA G**2**G TAC - 3'
3' - GTC TGT CCC ATG CGT GGG GCA GTC - 5'	3' - GTC TGT CCC ATG GAC CGT ACT AGT - 5'
5' - Ce6-**Am^{6}** - GCA CCC CGT CAG - 3'	5' - RB or MB - CTG GCA TGA TCA - 3'

V.5. Conclusions

During this chapter, several self-activating systems were developed with the aim of targeting an unmodified ODN. However, all these systems proved to be problematic regarding their synthesis, handling and characterisation and at last failed to induce ICL formation towards the unmodified target.

In the case of the self-activating probes, the presence of the PS in the same strand as the furan moiety is probably inducing premature oxidation of the latter, rendering it unreactive for crosslink formation.

As an alternative, the templated system was designed. Keeping the PS and the furan moiety in different strands should ensure the stability during synthesis and also ICL formation using PS conjugated ODN was already successfully assessed during chapter IV. Previously, this approach was found to be successful during the study carried out in collaboration with Dr. Nathalie De Laet using methylene blue and rose bengal. However in the current case, problems with unexpected self-complementarity of the chosen sequences interfered with the evaluation of the potential of this strategy. A new strategy had in the meantime been designed, aimed at tackling the self-activating principle at the same time as solving the problem of oligonucleotide delivery to a cell, an approach which is described in the next chapter.

V.6. References

1. N. De Laet, E. M. Llamas AM. Templated DNA cross-linking: towards a non-invasive triggering method. Chem Commun. 2017; Submitted and under revision.

Chapter VI.

Peptide based nanoparticles as activating delivery system for crosslinking oligonucleotides.

In this chapter, an alternative to the self-activating systems described in the previous chapter is developed. The problematic synthesis and handling of the doubly modified probes, where the presence of the PS in the same strand as the furan leads to a premature activation of the latter, inspired us to design a system where the activating and reacting moieties are distributed among two different molecules. Rather than using the complementary strand of the furan ODN, which prevents the possibility of targeting an unmodified strand, a nucleic acid carrier was used instead. Considering that the potential use of the furan strategy in a cellular environment would need assistance to gain access to the cell, we hypothesized that the use of a photosensitiser-modified cell penetrating peptide will be able to fulfil two tasks: providing a delivery system and activating the furan moiety upon irradiation, thus resulting in a self-activating complex.

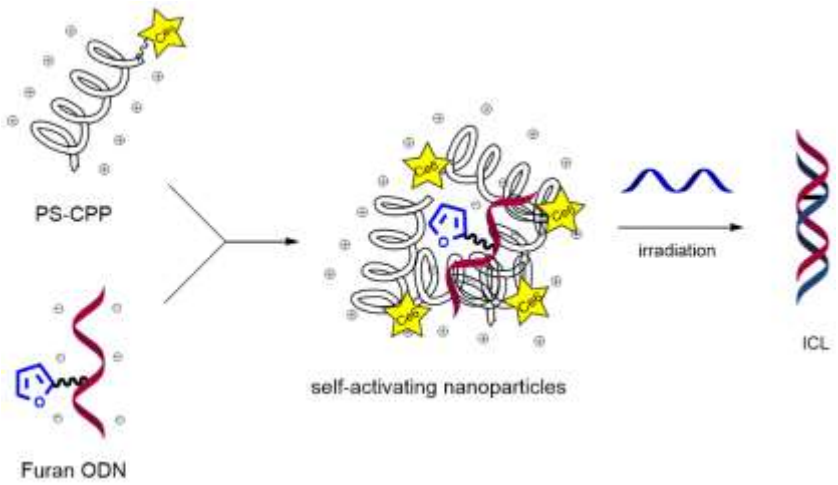

VI.1. Introduction

Nucleic acid based therapies have a great potential to treat an extensive variety of diseases. However, the main hurdle resides in the troublesome delivery of DNA and RNA based drugs, due to their size and highly anionic nature, (1) and therefore many efforts have been devoted to the development of carriers. (2–8) Moreover, nucleic acid drugs are readily degraded in the presence of enzymes and carriers that also protect them are desirable.

Many delivery systems have been explored to overcome this bottleneck. Two main strategies can be distinguished: covalent attachment of the carriers to the nucleic acids (9) or the formation of supramolecular complexes. (10) Covalently bound systems present the advantage to be discrete, fully characterised complexes. However, there is a risk to compromise the activity of the nucleic acid drug and the synthesis of such bioconjugates is time and money consuming and especially problematic when the cargo is charged *e.g* RNA or DNA. (11) On the other hand, the noncovalent strategy stands out for the facile complex synthesis and the lower doses required to elicit a biological response. (10)

The formation of noncovalent complexes between nucleic acids and carriers relies mainly on electrostatic interactions between the negatively charged nucleic acids and the positively charged carriers. Notably, the use of lipid based vectors to form lipoplexes has been widely studied (12–14), but they have not performed as expected in clinical trials, with low transfection efficiencies and high associated toxicity.

As an alternative, the use of cell penetrating peptides (CPPs) has also been explored. CPPs are 9-35mer cationic and/or amphipathic and are able to gain access into cells, taking their cargoes along. Most CPPs present positively charged residues that interact with the cell membrane before uptake and are also responsible for the electrostatic interactions with nucleic acids to form nanoparticles (NPs).

Several CPPs have been used for nucleic acid complexation and delivery, namely:

- MPG peptides: MPG was the first example reported of a CPP/DNA noncovalent complex that was able to induce vectorization of a cargo. MPG is a 27 residue amphipathic peptide that consist of a hydrophobic N-terminal domain derived from the fusion sequence of HIV gp41 and a hydrophilic C-terminal domain derived from the nuclear localization sequence (NLS) of SV40 T-antigen. (15) Several variants of this peptide have been reported to improve the transduction efficiency (16–18). Most of the MPG based

complexes were able to induce direct internalisation but the use of endocytic pathways was also observed. (18)

- Pep peptides: these are amphipathic peptides with a similar design to MPG peptides but they differ in the hydrophobic domain that was modified to allow delivery of other cargos such as PNA, peptides and proteins. (19–21)
- CADY peptides: these amphipathic CPPs were design for the more challenging delivery of plasmids. (22)
- Polyarginine peptides: stearic acid-modified octaarginine was reported to successfully transduce plasmid DNA with an efficiency in the same range as Lipofectamine™. (23) However, unmodified polyarginines are mostly unsuited for nanoparticle formation. (23–25) Moreover, polyarginine peptides are associated with a higher cytotoxicity, limiting their application. (26)
- Transportan and PepFects are chimeric CPPs that have been successfully used for ODN delivery (27), especially TP10. (28) PepFects consist of a series of chemically modified peptides (several of them using stearic acid) based on TP10 to render them more suited for supramolecular complex formation with nucleic acids. (24,29,30)

For this study, a CPP derived from MPG, MPG-8, was chosen for the formation of supramolecular complexes with a furan containing ODN, due to its improved transduction efficiency compared to the other MPG analogues, its simpler synthesis and the availability of the N-terminus for modification.

MPG-8 was designed by Divita et al. as a derivative of MPG shortened by 6 residues, resulting in a 21-mer peptide that was used for small interfering RNA (siRNA) delivery and was shown to compromise tumour growth using MPG-8/siRNA NPs to target cyclin B1. (17)

Complexation between MPG-8 and a furan modified ODN should allow to evaluate the feasibility of ICL generation in the presence of a carrier, aiming to exploit the antisense potential of the furan methodology in a cellular context. In one of its variants, the antisense effect relies on the steric blockage of a mRNA molecule by hybridisation to a complementary ODN. Formation of an interstrand crosslink between the antisense ODN and the target mRNA is expected to improve the antisense effect, as has previously been reported using other crosslinking methodology. (31)

For a successful ICL formation, recognition between the two complementary strands is required and entrapment of the furan ODN in the supramolecular complex may hinder the duplex formation. Highly negatively charged heparin has been widely used to induce nucleic acid

release from peptide based complexes by mimicking the interaction between the CPP and the heparansulfates proteoglycans that are present on the surface of most cells which seems to be a key process in the internalisation of several CPPs such as *e.g.* Tat and penetratin. (32–34)

Besides, furan activation *via* $^1O_2$ requires the presence of a PS and we rationalised that conjugation of the latter to MPG-8 will allow selective delivery of the dye, in close proximity to the furan ODN but avoiding the stability problems of the self-activating probe described in chapter 5. Ce6 was the PS of choice in view of the promising results obtained in previous chapters, and the Ce6 conjugated MPG-8 (**Ce6MPG-8**) was synthesised and evaluated for ODN complexation (figure VI-1). The resulting self-activating peptide-based NPs were studied for ICL formation with a complementary unmodified strand.

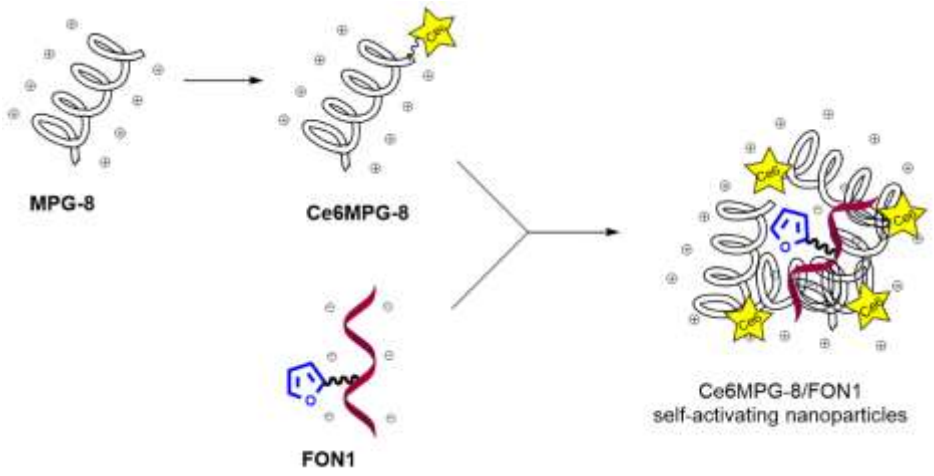

*Figure VI-1. Self-activating nanoparticle formation using **Ce6MPG-8** and **FON1**.*

PS conjugated CPPs have been object of intense study in the last decades to construct third generation PS, *i.e.*, PS attached to a targeting moiety. Applications include PDT, (35–38) antimicrobial PDT (39) and photochemical internalisation (40–43) showing that there is an inherent interest in the study of PS conjugated CPPs.

VI.2. Synthesis of MPG-8 and Ce6MPG-8 peptide conjugates

First, **MPG-8** peptide (tableVI-1) was synthesised following a modified version of the previously reported protocol (15–17). The synthesis was carried out on solid phase using Cysteamine 4-methoxytrityl resin, to introduce the cysteamide moiety in the C-terminus (figure VI-2), and the obtained peptide was divided into two batches, still on the solid support. The first batch was cleaved using a mixture 94:2.5:2.5:1 of TFA/H_2O/ EDT/TIS and purified by RP HPLC (figure VI-3).

The peptide was successfully identified by LC-MS analysis, showing also a small percentage of the oxidised **MPG-8** form (due to the Met residue).

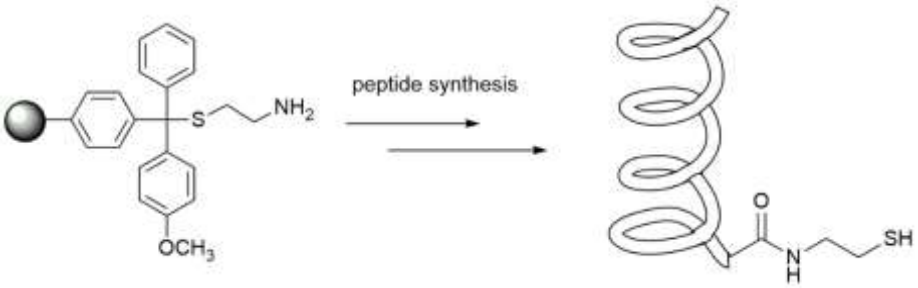

Figure VI-2. MPG-8 synthesis starting from the cysteamine 4-methoxitrityl resin.

Table VI-1. Sequence and modifications of the CPPs used in this chapter.

Name	Sequence	Modification
MPG-8	βAFLGWLGAWGTMGWSPKKKRK-Cya	Cya= cysteamide
Ce6MPG-8	Ce6–βAFLGWLGAWGTMGWSPKKKRK-Cya	Cya= cysteamide Ce6

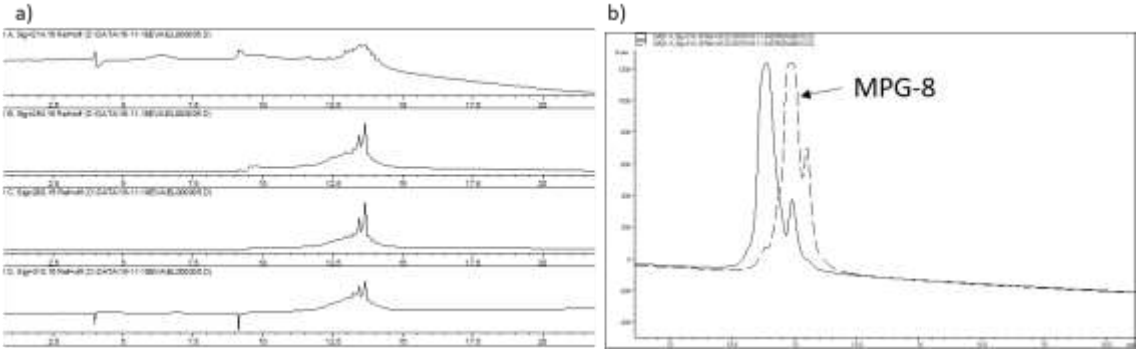

*Figure VI-3. HPLC traces of **MPG-8**, a) before purification, at different wavelengths and b) the two fractions collected after purification. Luna C18 linear gradient of 0-100% ACN in 15 minutes.*

The second batch was used for conjugation to Ce6 via the N-terminus (figure VI-4). First, Ce6 was activated with HBTU in the presence of DIPEA. Subsequent addition to the peptide, still attached to the solid support, was followed by cleavage under mild conditions using 0.1M HCl in HFIP instead of TFA (44) (mixture HCl in HFIP/EDT/TIS 96.5:2.5:1) to minimise degradation of the acid labile dye. Still, after reaction and cleavage a complex mixture of compounds was obtained. After RP HPLC purification, three fractions were separated corresponding to the three main peaks (figure VI-5) and they were analysed by MALDI-TOF. In all three cases the expected mass was found, which is easily explained by the three carboxylic acids functionalities on Ce6, each of them susceptible to activation and functionalisation. The higher reactivity of HBTU seems to interfere with the selective conjugation towards one single carboxylic acid

functionality, whereas in chapter IV activation using DCC/NHS led to the formation of only one of three possible regioisomers. Moreover, two of the fractions also presented a 16Da excess, probably due to the presence of a Met residue that can be readily oxidised. The first fraction was used for the next experiments.

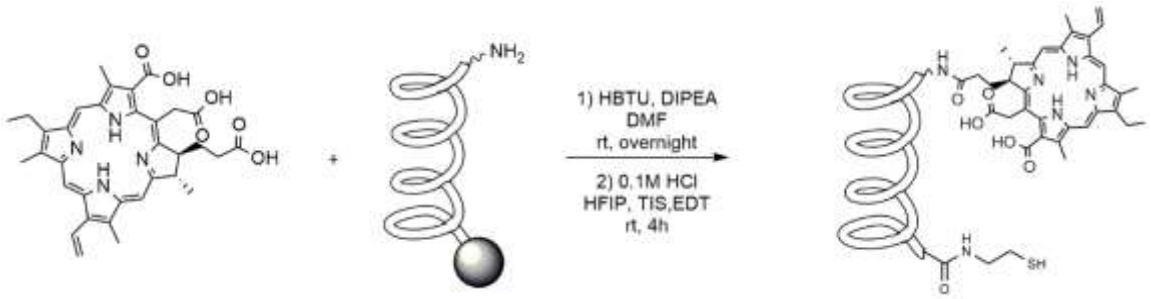

*Figure VI-4. Synthesis of **Ce6MPG-8**.*

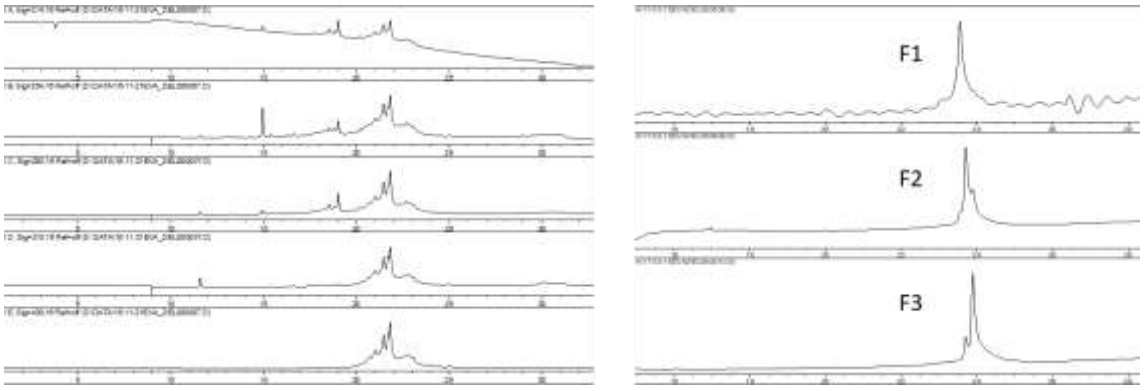

*Figure VI-5. HPLC traces of **Ce6MPG-8**, a) before purification, at different wavelengths and b) the three fractions obtained after purification. Jupiter C18 linear gradient of 0-100% ACN in 25 minutes*

VI.3. Nanoparticle formation using MPG-8 peptide

First, unmodified **MPG-8** was used for the CPP/ODN complex formation, relying on the electrostatic interactions between the cationic groups of the peptide and the anionic residues of the ODN (figure VI-6). Incubation of 1 µM **MPG-8** with 0.17 µM **FON1** at 37ºC for 30 minutes in phosphate buffer, which corresponds to a 2.4 N/P ratio (molar ratio between the positively charged groups on the peptide and the PO_4^- groups on the ODN), as it was previously reported to be the optimal value for nucleic acid complexation using **MPG-8** peptide (17), resulted in CPP/ODN nanoparticles. Since **MPG-8** possess five positive charges (four from Lys residues and one from an Arg residue), 1 µM **MPG-8** contains 5 µM positive charges. To keep the 2.4 ratio, the total concentration of negative charges should be 2.08 µM, which corresponds to 0.17 µM of **FON1**, since this ODN is a 12-mer containing 12 negative charges.

Formation of NPs was monitored by DLS showing an average size of 110 nm (figure VI-7). This NP size is in the same range as the complexes reported by Divita et al. showing the highest silencing efficiency. Formation of the NPs at higher concentrations or higher charge ratios lead to bigger size NPs, which tend to accumulate primarily in the liver, the spleen and the bone marrow. (45)

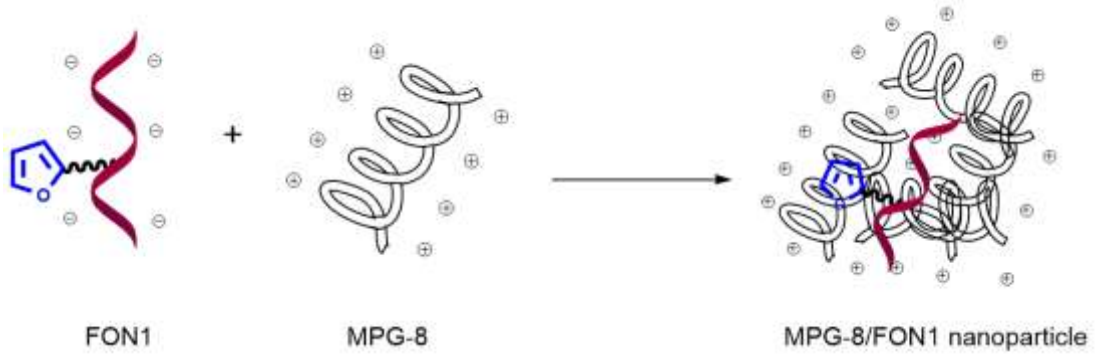

Figure VI-6. Formation of NPs by electrostatic interaction between MPG-8 and FON1.

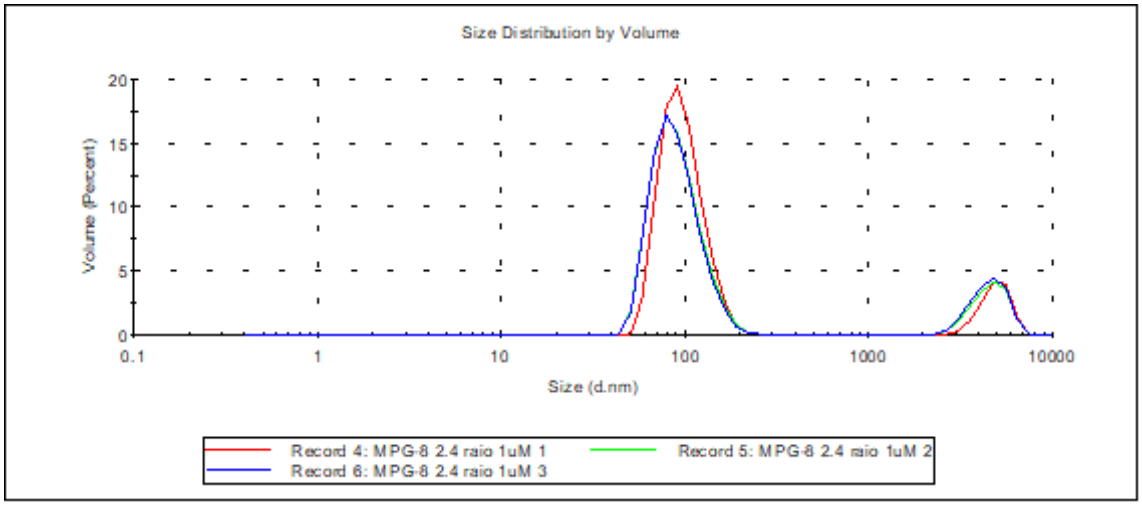

*Figure VI-7. DLS analysis of **MPG-8/FON1** NPs using 1µM **MPG-8** and 0.17µM **FON1**, 2.4 N/P ratio.*

VI.4. Crosslink evaluation and optimisation using the MPG-8/FON1 NPs

These NPs were evaluated for ICL formation by adding the complementary unmodified ODN, **ON1** (Table VI-2), and Ce6 as PS, both in an equimolar concentration to **FON1** (0.17 µM) as a 1:1 PS/duplex ratio was established as the optimal condition for ICL in chapter 3. The reaction mixture was then irradiated using red light and samples were taken at different times. In this case, only PAGE analysis was carried out since RP HPLC analysis proved troublesome, due to the presence of particles that resulted in system overpressures.

*Table VI-2. Duplex used during the ICL evaluation using peptide based NPs. **FON1** was complexed with the peptide and subsequently hybridised with the complementary strand **ON1**.*

Name	Sequence	Modification
FON1	5' - CTG ACG G**X**G TGC - 3'	X= 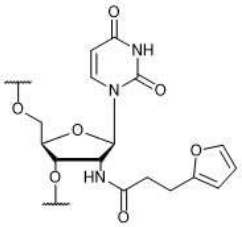
ON1	3' - GAC TGC CCC ACG - 5'	-

Unfortunately, no ICL formation was observed (figure VI-8) and it was hypothesized that **FON1** is not being released from the complex and therefore cannot recognise it complementary partner.

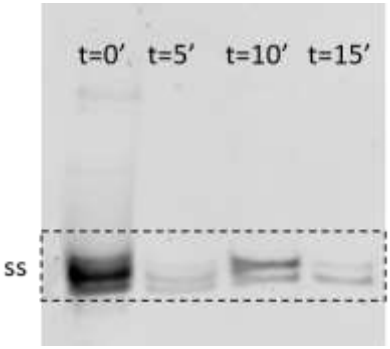

*Figure VI-8. No ICL formation was observed by PAGE analysis of the crosslink experiment using the **MPG-8/FON1** NPs ([duplex]= 0.17 μM, [**MPG-8**]= 1 μM) and Ce6 (0.17 μM). Visualized using GelRed™ (20% polyacrylamide, 1x TBE buffer).*

The effect of heparin on ICL formation was then evaluated, to attempt release of **FON1** from the peptide complex. To determine the necessary amount of heparin to induce the ODN release, the **MPG-8** NPs were analysed by DLS after applying different amounts of heparin, ranging from 2-200 eq. After addition of 10 eq, a new signal corresponding to a size of 5 nm appeared (figure VI-9a) and after addition of 100 eq this signal increased in intensity and the signal at around 100nm (corresponding to the NPs) was not observed anymore, being replaced by a signal at around 300 nm, indicating a change in the complex structure (figure VI-9b).

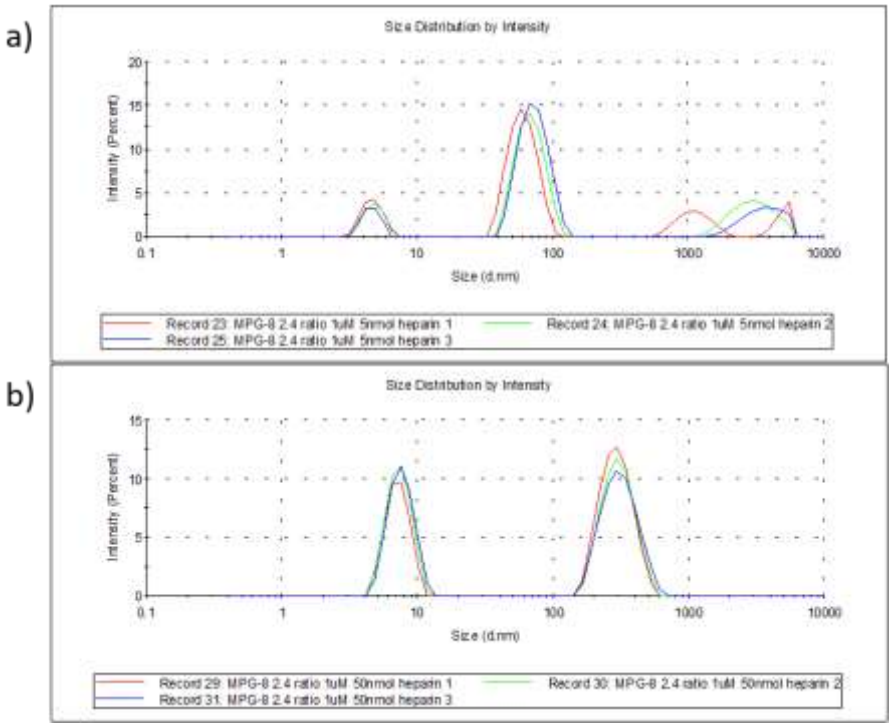

*Figure VI-9. DLS analysis of peptide/**FON1** NPs using 1μM **MPG-8** and 0.17μM **FON1**, 2.4 N/P ratio adding heparin a) 10 eq and b) 100 eq.*

Based on the DLS results, a new crosslink experiment using the **MPG-8**/**FON1** complex was designed. First, the NPs were formed by incubation as described in section VI.3, followed by addition of **ON1** and Ce6 in an equimolar concentration to **FON1**. After irradiation for 5 minutes, 100 eq heparin were added to assess whether competition of the anionic heparin facilitates FON1 release and irradiation proceeded for 5 minutes more.

As a reference, a crosslinking experiment was separately carried out using the **FON1**/**ON1** duplex and Ce6 using identical conditions ([duplex] = [Ce6] = 0.17 μM) as when using the peptide NPs but **MPG-8** peptide (1 μM) and heparin (100 eq) were only added after irradiation for 10 minutes. This experiment was also loaded during PAGE analysis to ensure correct assignment of the crosslink adduct band, since the presence of the peptide or heparin may influence its migration on the gel.

As can be observed in figure VI-10 heparin addition indeed seems to help the crosslink formation. However, irradiation after heparin addition does not increase the amount of ICL formed, suggesting that maybe **FON1** was partially consumed as $^1O_2$ was still generated in spite of **FON1** not being able to hybridise to **ON1**. For further experiments, heparin will be added before irradiation to maximise ICL formation.

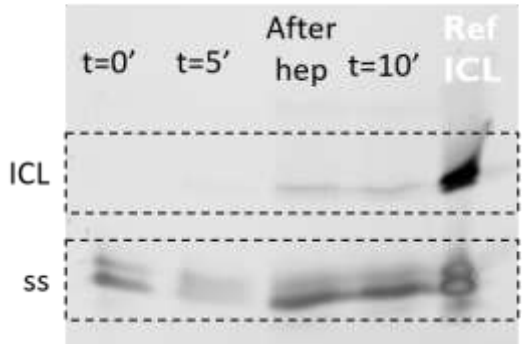

*Figure VI-10. PAGE analysis of ICL formation using the MPG-8/FON1 NPs ([duplex] = 0.17 μM, [**MPG-8**] = 1 μM) and Ce6 (0.17 μM), adding 100 eq heparin after 5 min irradiation. Reference ICL: [duplex] = [Ce6] = 0.17 μM, adding [**MPG-8**] = 1 μM and 100 eq heparin after the irradiation finishes. Visualized using GelRed™ (20% polyacrylamide, 1x TBE buffer).*

VI.5. Evaluation of Ce6 concentration for ICL formation

Another parameter that was optimised was the amount of Ce6 added. It was determined in chapter III that an equimolar ratio between the duplex and Ce6 was optimal to induce crosslink formation using this PS. During the crosslinking experiments carried out in this chapter, that ratio was therefore maintained but the concentration needed to be decreased more than 10 times (from 2 to 0.17 μM) in order to keep a 2.4 charge ratio between the **MPG-8** and **FON1** and a 1 μM concentration of **MPG-8**, for successful formation of NP of the desired size. However, the presence of the peptide and heparin might interfere with the $^1O_2$ generation by acting as quenchers of the excited state of Ce6 or even reacting with $^1O_2$, resulting in low yielding ICL. It is worth noticing that a lower Ce6 concentration itself does not seem to be an issue since the reference crosslink (section IV) was carried out at [Ce6]= 0.17 μM but without the presence of heparin or **MPG-8** during irradiation.

Using the conditions previously stablished, we set out to compare the ICL formation using 0.17 and 2 μM Ce6 concentration (in both experiments **MPG-8** concentration was still 1 μM and **FON1** 0.17 μM).

After incubation of the **MPG-8**/**FON1** NPs, addition of **ON1**, Ce6 and heparin was followed by irradiation (figure VI-11). PAGE evaluation of the samples taken a different times showed that indeed, an increased amount of Ce6 results in a higher yielding crosslinking (figure VI-12)

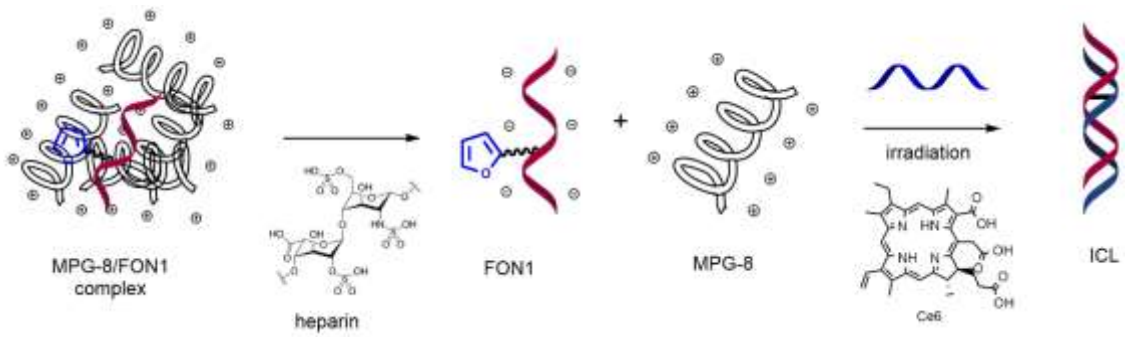

*Figure VI-11. Schematic representation of **FON1** release by heparin addition before irradiation.*

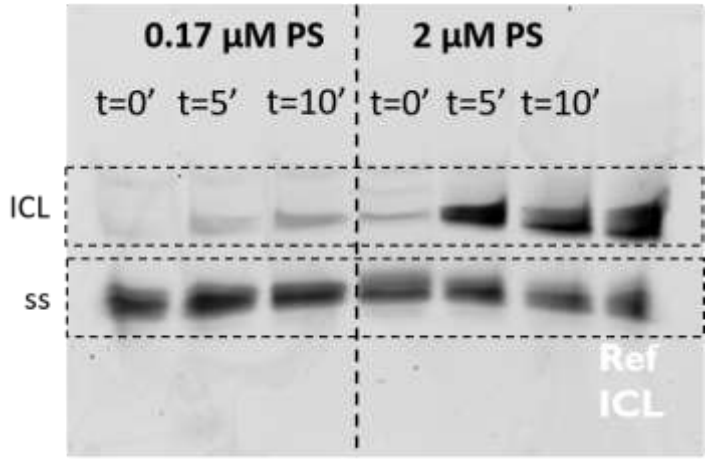

*Figure VI-12. PAGE analysis of ICL formation using the MPG-8/FON1 NPs ([duplex]= 0.17 µM, [**MPG-8**]= 1 µM, 100 eq heparin) and Ce6 at two different concentrations, 0.17 and 2 µM. Visualized using GelRed™ (20% polyacrylamide, 1x TBE buffer).*

Moreover, the need for the use of heparin to induce release was also assesed under this higher Ce6 concentration (figure VI-13). In agreement with previous experiments, the presence of heparin (100 eq) had a positive effect on the ICL formation.

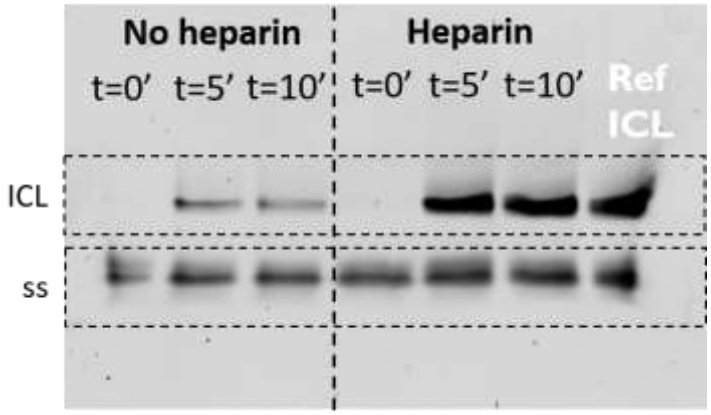

*Figure VI-13. PAGE analysis of ICL formation using the MPG-8/FON1 NPs ([duplex] = 0.17 µM, [**MPG-8**]= 1 µM) and Ce6 at 2 µM in the presence or absence of heparin. Visualized using GelRed™ (20% polyacrylamide, 1x TBE buffer).*

VI.6. Nanoparticle formation using Ce6MPG-8 peptide

Once the conditions for ICL formation using peptide based nanoparticles were optimised using unmodified **MPG-8**, we set out to characterise and evaluate the complexes made using **Ce6MPG-8** in combination with **FON1**, which results in a self-activating system (figure VI-14).

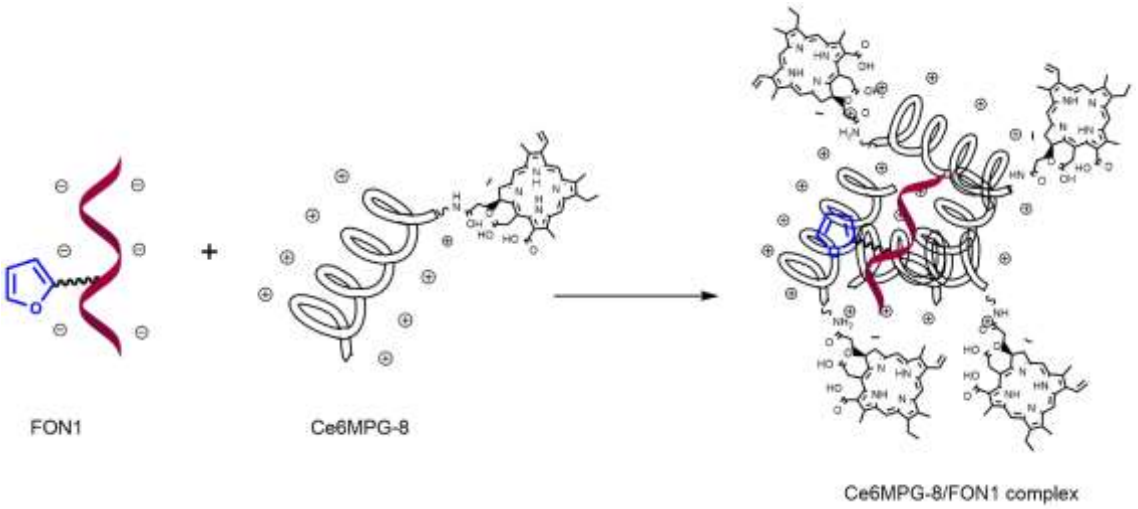

*Figure VI-14. Schematic representation of NP formation using **Ce6MPG-8** and **FON1**.*

The same incubation procedure as in section VI.3 was used, consisting of mixing **Ce6MPG-8** (1 μM) and **FON1** (0.17 μM) for 30 minutes at 37ºC, in this case keeping the solution in the darkness to avoid premature $^1O_2$ generation.

DLS analysis of the **Ce6MPG-8**/**FON1** NPs showed that in this case the NP size obtained is 130 nm (figure VI-15).

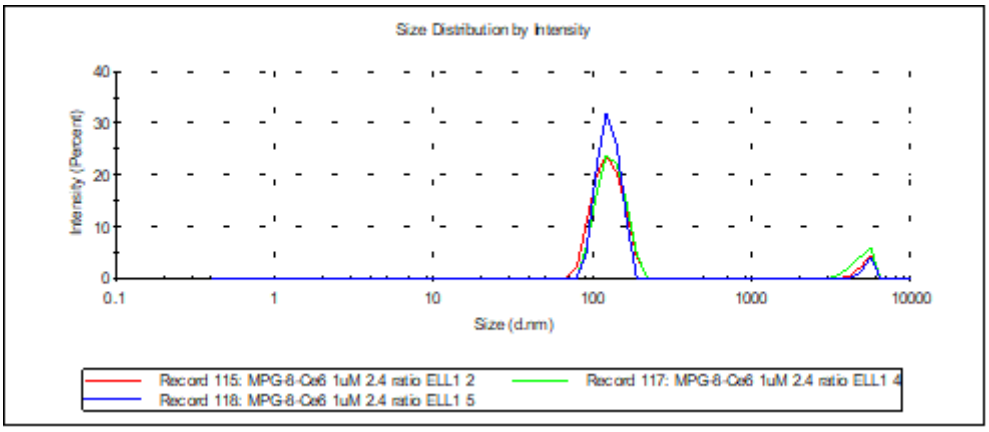

*Figure VI-15. DLS analysis of **Ce6MPG-8/FON1** NPs using 1μM **Ce6MPG-8** and 0.17μM **FON1**, 2.4 N/P ratio*

VI.7. ICL using self-activating nanoparticles

Ce6MPG-8/FON1 NPs were mixed with the complementary **ON1** and 100 eq of heparin. The reaction mixture was irradiated using red light for 10 min and samples were taken and analysed by PAGE, showing that ICL formation did occur without any external PS added (figure VI-16).

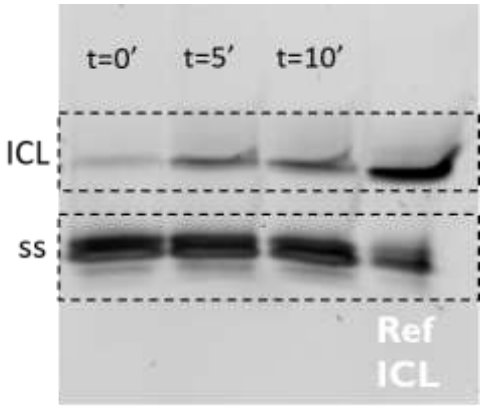

*Figure VI-16. PAGE analysis of ICL formation using **Ce6MPG-8/FON1** NPs ([duplex] = 0.17 μM, [**Ce6MPG-8**] = 1 μM) in the presence of heparin. Visualized using GelRed™ (20% polyacrylamide, 1x TBE buffer).*

Next, we set out to assess the influence of heparin on the ICL generation using the **Ce6MPG-8/FON1** complexes and also to establish a comparison between the use of the self-activating system and Ce6 externally added. For this purpose, four different crosslink experiments were carried out and loaded on the same gel, allowing a direct comparison. For all experiments, the peptide concentration was 1 μM and the duplex concentration was 0.17 μM.

For the first two experiments, Ce6 was used in solution at 1 and 2μM in the presence of heparin whereas for the third and fourth experiments, **Ce6MPG-8** was used and no external PS was added and heparin was only added in the third one (table in figure VI-17).

Only a slight difference in ICL formation can be observed between the experiments where 1 or 2 μM of Ce6 is used experiment. However, there is a substantial difference between the ICL formation when Ce6 is used in solution or attached to **MPG-8**, being lower in the latter. This result may be explained by a lower $^1O_2$ generation as it was previously observed that a lower Ce6 concentration had a dramatic effect on the crosslink formation. Unfortunately, in this case the PS concentration cannot be easily tuned as this would mean an increase in the peptide concentration as well, which would result in an increase in the NP size. Moreover, in the experiments using the unmodified **MPG-8** and Ce6 in solution, the PS was only added after incubation at 37ºC, to avoid any potential degradation. However, during the experiments using **Ce6MPG-8** this was not a possibility and it cannot be ruled out that Ce6 was damaged during

this process. A way to overcome this would be to use more stable PSs and/or a PS with higher $^1O_2$ quantum yield than Ce6.

Last, heparin addition showed to have a smaller influence on the ICL formation using the **Ce6MPG-8/FON1** complexes. The bigger size of these NPs seems to suggest that the presence of Ce6 results in bigger and maybe looser complexes that allow an easier recognition between **FON1** and **ON1** even without the presence of heparin.

	ICL 1	ICL 2	ICL 3	ICL4
[Peptide] (μM)	[MPG-8]=1	[MPG-8]=1	[Ce6MPG-8]=1	[Ce6MPG-8]=1
[Duplex] (μM)	0.17	0.17	0.17	0.17
[Ce6]	2	1	-	-
Heparin	100 eq	100 eq	100 eq	-

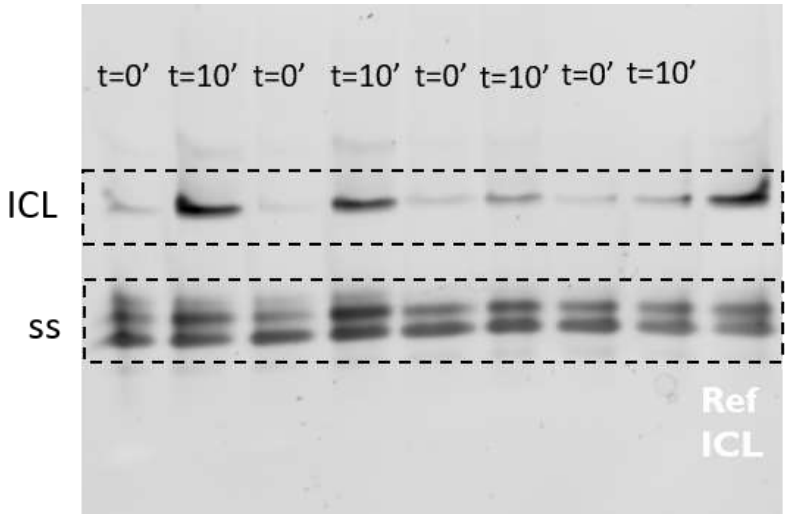

*Figure VI-17. PAGE analysis of ICL formation using **MPG-8/FON1** or **Ce6MPG-8/FON1** NPs under different conditions as presented in the table. Visualized using GelRed™ (20% polyacrylamide, 1x TBE buffer).*

VI.8. Conclusions

In this chapter, a new self-activating system based on the use of **MPG-8** peptide was designed and evaluated. Preliminary experiments where unmodified **MPG-8** was complexed with **FON1** and Ce6 was added in solution to induce ICL showed that crosslink formation is possible in the presence of a CPP as carrier, once conditions such as $^1O_2$ generation and furan ODN availability are optimised.

Next, self-activating NPs were formed and their crosslinking capacities were evaluated. **Ce6MPG-8** successfully complexed **FON1** and induces crosslink formation with the complementary strand, although to a lower extent than when Ce6 was added in solution, probably due to an insufficient $^1O_2$ generation and therefore the use of a different PS would be advantageous. Moreover, the need for heparin to allow ODN release and duplex formation seemed to be less acute in this case, maybe due a looser complex caused by the presence of Ce6 in the NPs.

VI.9. References

1. Stein CA, Cheng YC. Antisense oligonucleotides as therapeutic agents—is the bullet really magical. Science (80-). 1993;261(5124):1004–12.

2. Järver P, Langel Ü. The use of cell-penetrating peptides as a tool for gene regulation. Drug Discov Today. 2004;9(9):395–402.

3. Huang Y-W, Lee H-J, Tolliver LM, Aronstam RS. Delivery of nucleic acids and nanomaterials by cell-penetrating peptides: opportunities and challenges. Biomed Res Int. Hindawi Publishing Corporation; 2015;2015.

4. Trabulo S, Cardoso AL, Cardoso AMS, Morais CM, Jurado AS, de Lima MC. Cell-penetrating Peptides as Nucleic Acid Delivery Systems: From Biophysics to Biological Applications. Curr Pharm Des. 2013;19(16):2895–923.

5. Mäe M, Andaloussi S El, Lehto T, Langel Ü. Chemically modified cell-penetrating peptides for the delivery of nucleic acids. Expert Opin Drug Deliv. Taylor & Francis; 2009;6(11):1195–205.

6. Veldhoen S, Laufer SD, Restle T. Recent developments in peptide-based nucleic acid delivery. Int J Mol Sci. Molecular Diversity Preservation International; 2008;9(7):1276–320.

7. Gopal V. Bioinspired peptides as versatile nucleic acid delivery platforms. J Control Release. Elsevier; 2013;167(3):323–32.

8. Heitz F, Morris MC, Divita G. Twenty years of cell-penetrating peptides: from molecular mechanisms to therapeutics. Br J Pharmacol. 2009 Mar 20;157(2):195–206.

9. Zatsepin TS, Turner JJ, Oretskaya TS, Gait MJ. Conjugates of oligonucleotides and

analogues with cell penetrating peptides as gene silencing agents. Curr Pharm Des. Bentham Science Publishers; 2005;11(28):3639–54.

10. Margus H, Padari K, Pooga M. Cell-penetrating Peptides as Versatile Vehicles for Oligonucleotide Delivery. Mol Ther. Nature Publishing Group; 2012;20(3):525–33.

11. Juliano R, Alam MR, Dixit V, Kang H. Mechanisms and strategies for effective delivery of antisense and siRNA oligonucleotides. Nucleic Acids Res. Oxford Univ Press; 2008;36(12):4158–71.

12. Felgner PL, Gadek TR, Holm M, Roman R, Chan HW, Wenz M, et al. Lipofection: a highly efficient, lipid-mediated DNA-transfection procedure. Proc Natl Acad Sci U S A. 1987;84(21):7413–7.

13. Li W, Szoka FC. Lipid-based nanoparticles for nucleic acid delivery. Pharm Res. 2007;24(3):438–49.

14. Draghici B, Ilies M a. Synthetic Nucleic Acid Delivery Systems: Present and Perspectives. J Med Chem. 2015;150220140802004.

15. Morris MC, Vidal P, Chaloin L, Heotz F, Divita G. A new peptide vector for efficient delivery of oligonucleotide into nontransformed mammalian cells. Nucleic Acid Res. 1997;25(14):2730–6.

16. Simeoni F, Morris MC, Heitz F, Divita G. Insight into the mechanism of the peptide-based gene delivery system MPG: Implications for delivery of siRNA into mammalian cells. Nucleic Acids Res. 2003;31(11):2717–24.

17. Crombez L, Morris MC, Dufort S, Aldrian-Herrada G, Nguyen Q, Mc Master G, et al. Targeting cyclin B1 through peptide-based delivery of siRNA prevents tumour growth. Nucleic Acids Res. 2009;37(14):4559–69.

18. Veldhoen S, Laufer SD, Trampe A, Restle T. Cellular delivery of small interfering RNA by a non-covalently attached cell-penetrating peptide: Quantitative analysis of uptake and biological effect. Nucleic Acids Res. 2006;34(22):6561–73.

19. Morris MC, Depollier J, Mery J, Heitz F, Divita G. A peptide carrier for the delivery of biologically active proteins into mammalian cells. Nat Biotech. Nature Publishing Group; 2001 Dec;19(12):1173–6.

20. Morris MC, Chaloin L, Choob M, Archdeacon J, Heitz F, Divita G. Combination of a new

generation of PNAs with a peptide-based carrier enables efficient targeting of cell cycle progression. Gene Ther. 2004 Feb 12;11(9):757–64.

21. Morris MC, Gros E, Aldrian-Herrada G, Choob M, Archdeacon J, Heitz F, et al. A non-covalent peptide-based carrier for in vivo delivery of DNA mimics. Nucleic Acids Res. 2007;35(7).

22. Rittner K, Benavente A, Bompard-Sorlet A, Heitz F, Divita G, Brasseur R, et al. New Basic Membrane-Destabilizing Peptides for Plasmid-Based Gene Delivery in Vitro and in Vivo. Mol Ther. 2002 Feb;5(2):104–14.

23. Lehto T, Abes R, Oskolkov N, Suhorutšenko J, Copolovici D-M, Mäger I, et al. Delivery of nucleic acids with a stearylated (RxR)4 peptide using a non-covalent co-incubation strategy. J Control Release. 2010;141(1):42–51.

24. Mäe M, EL Andaloussi S, Lundin P, Oskolkov N, Johansson HJ, Guterstam P, et al. A stearylated CPP for delivery of splice correcting oligonucleotides using a non-covalent co-incubation strategy. J Control Release. 2009;134(3):221–7.

25. Lehto T, Simonson OE, Mäger I, Ezzat K, Sork H, Copolovici D-M, et al. A peptide-based vector for efficient gene transfer in vitro and in vivo. Mol Ther. Nature Publishing Group; 2011;19(8):1457–67.

26. Jones SW, Christison R, Bundell K, Voyce CJ, Brockbank S, Newham P, et al. Characterisation of cell-penetrating peptide-mediated peptide delivery. Br J Pharmacol. Wiley Online Library; 2005;145(8):1093–102.

27. Pooga M, Hällbrink M, Zorko M. Cell penetration by transportan. FASEB J. FASEB; 1998;12(1):67–77.

28. Soomets U, Lindgren M, Gallet X, Hällbrink M, Elmquist A, Balaspiri L, et al. Deletion analogues of transportan. Biochim Biophys Acta (BBA)-Biomembranes. Elsevier; 2000;1467(1):165–76.

29. Ezzat K, Andaloussi SEL, Zaghloul EM, Lehto T, Lindberg S, Moreno PMD, et al. PepFect 14, a novel cell-penetrating peptide for oligonucleotide delivery in solution and as solid formulation. Nucleic Acids Res. Oxford Univ Press; 2011;39(12):5284–98.

30. Andaloussi SEL, Lehto T, Mäger I, Rosenthal-Aizman K, Oprea II, Simonson OE, et al. Design of a peptide-based vector, PepFect6, for efficient delivery of siRNA in cell culture

and systemically in vivo. Nucleic Acids Res. Oxford Univ Press; 2011;39(9):3972–87.

31. Shigeno A, Sakamoto T, Yoshimura Y, Fujimoto K. Quick regulation of mRNA functions by a few seconds of photoirradiation. Org Biomol Chem. 2012;10(38):7820.

32. Rusnati M, Tulipano G, Spillmann D, Tanghetti E, Oreste P, Zoppetti G, et al. Multiple interactions of HIV-I Tat protein with size-defined heparin oligosaccharides. J Biol Chem. 1999;274(40):28198–205.

33. Tyagi M, Rusnati M, Presta M, Giacca M. Internalization of HIV-1 Tat Requires Cell Surface Heparan Sulfate Proteoglycans. J Biol Chem. 2001;276(5):3254–61.

34. Van Asbeck AH, Beyerle A, McNeill H, Bovee-Geurts PHM, Lindberg S, Verdurmen WPR, et al. Molecular parameters of siRNA-cell penetrating peptide nanocomplexes for efficient cellular delivery. ACS Nano. 2013;7(5):3797–807.

35. Schneider R, Tirand L, Frochot C, Vanderesse R, Thomas N, Gravier J, et al. Recent Improvements in the Use of Synthetic Peptides for a Selective Photodynamic Therapy. Anticancer Agents Med Chem. 2006 Sep 1;6(5):469–88.

36. Thomas N, Pernot M, Vanderesse R, Becuwe P, Kamarulzaman E, Da Silva D, et al. Photodynamic therapy targeting neuropilin-1: Interest of pseudopeptides with improved stability properties. Biochem Pharmacol. 2010;80(2):226–35.

37. Ke MR, Yeung SL, Fong WP, Ng DKP, Lo PC. A phthalocyanine-peptide conjugate with high in vitro photodynamic activity and enhanced in vivo tumor-retention property. Chem - A Eur J. 2012;18(14):4225–33.

38. Li F, Liu Q, Liang Z, Wang J, Pang M, Huang W, et al. Synthesis and biological evaluation of peptide-conjugated phthalocyanine photosensitizers with highly hydrophilic modifications. Org Biomol Chem. 2016;14(13):3409–22.

39. Bourré L, Giuntini F, Eggleston IM, Mosse C a, Macrobert AJ, Wilson M. Effective photoinactivation of Gram-positive and Gram-negative bacterial strains using an HIV-1 Tat peptide-porphyrin conjugate. Photochem Photobiol Sci. 2010;9(12):1613–20.

40. Berg K, Prasmickaite L, Selbo PK, Hellum M, Bonsted A, Høgset A. Photochemical internalization (PCI)--a novel technology for release of macromolecules from endocytic vesicles. Oftalmologia. Department of Biophysics, Institute for Cancer Research, Norwegian Radium Hospital, Montebello, N-0310 Oslo, Norway.

kristian.berg@labmed.uio.no; 2003;56(1):67–71.

41. Berg K, Folini M, Prasmickaite L, Selbo P, Bonsted A, Engesaeter B, et al. Photochemical Internalization: A New Tool for Drug Delivery. Curr Pharm Biotechnol. 2007 Dec 1;8(6):362–72.

42. Muthukrishnan N, Johnson G a., Erazo-Oliveras A, Pellois J-P. Synergy Between Cell-Penetrating Peptides and Singlet Oxygen Generators Leads to Efficient Photolysis of Membranes. Photochem Photobiol. 2013;89(3):625–30.

43. Wang JTW, Giuntini F, Eggleston IM, Bown SG, MacRobert AJ. Photochemical internalisation of a macromolecular protein toxin using a cell penetrating peptide-photosensitiser conjugate. J Control Release. Elsevier B.V.; 2012;157(2):305–13.

44. Palladino P, Stetsenko D a. New TFA-free cleavage and final deprotection in Fmoc solid-phase peptide synthesis: Dilute HCl in fluoro alcohol. Org Lett. 2012;14(11):6346–9.

45. Petros RA, DeSimone JM. Strategies in the design of nanoparticles for therapeutic applications. Nat Rev Drug Discov. Nature Publishing Group; 2010;9(8):615–27.

Chapter VII.

Conclusions and perspectives.

Many efforts have been devoted in the last decades to unravel the intricate puzzle that conforms all the roles that nucleic acids play in living beings. Not only do they define the genetic makeup of a given organism but they also participate in enzymatic processes and regulate gene expression. Therefore, the development of new tools that may serve for diagnosis or therapy based on those processes is of high interest.

It was previously stablished in the OBCR group that introduction of a furan moiety into an oligonucleotide could be easily achieved by automated synthesis resulting in a probe equipped with a masked reactive moiety that could induce the formation of a selective interstrand crosslink with a complementary sequence upon furan oxidation. Furan oxidation can be achieved using NBS or, in a more biocompatible fashion, singlet oxygen, and for the latter methylene blue and rose bengal were thoroughly studied.

The aim of the present study is to expand this methodology to the use of porphyrin based photosensitisers for singlet oxygen generation with the final aim to develop a method that can be applicable in a cellular context.

Three different porphyrin based photosensitisers were selected: the commercially available chlorin e6 (Ce6), a tripyridyl porphyrin (TriPyCOOH) and a zinc phthalocyanine decorated with tert-butyl groups (TT1).

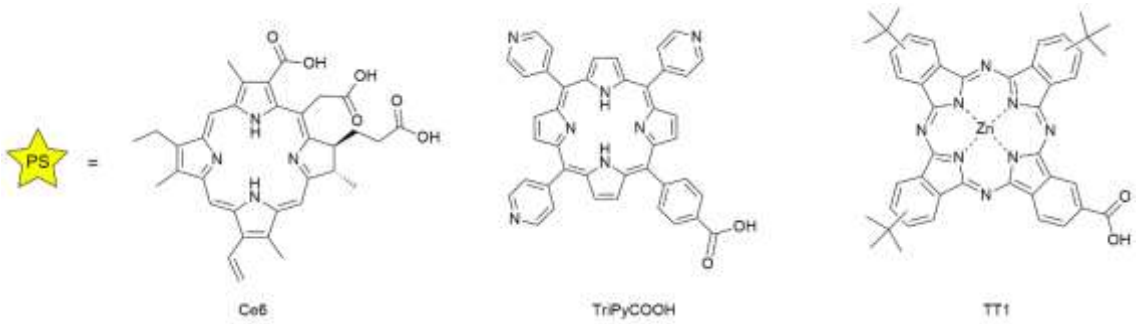

First, the ability of each photosensitiser to induce interstrand crosslink when they were added in solution was assessed. For this purpose, a furan modified oligonucleotide was hybridised with its complementary strand in the presence of the respective photosensitisers and, upon light

irradiation, the crosslink generation was evaluated. Careful optimisation of several factors was performed, including reaction time, photosensitiser concentration, ratio between the duplex and the photosensitiser and type of light. It was found that the use of Ce6 results in the most extensive crosslink generation (52% conversion) among the three photosensitisers when the optimal conditions were used. TriPyCOOH also allowed generating the crosslink adduct in good yields whereas TT1 was only able to do so to a low extent, due to the high insolubility of this compound in the aqueous conditions under which the reaction was carried out.

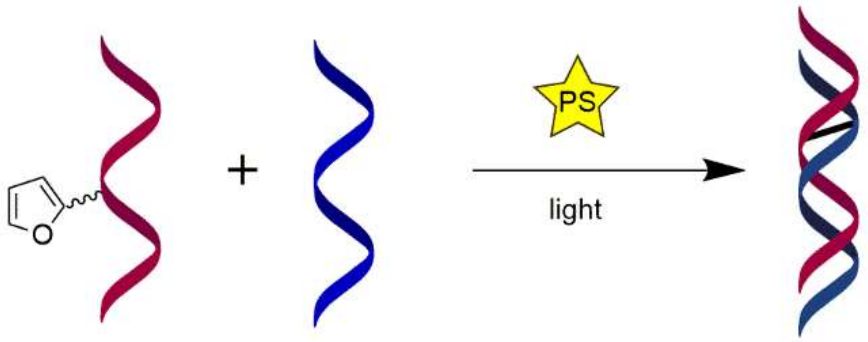

Next, it was hypothesised that conjugation of the photosensitisers to the complementary strand of the furan oligonucleotide would result in two important improvements: singlet oxygen generation in close proximity to the furan moiety and higher water solubility of the photosensitisers.

Different conjugation conditions were explored for each photosensitiser, based on activation of the carboxylic acid functionality in the dyes and subsequent addition of an amino modified oligonucleotide. TT1 conjugation was particularly challenging and the reaction had to be performed when the oligonucleotide was still attached to the solid support where it was synthesised, in order to avoid the used of aqueous conditions and concurrent solubility problems with TT1.

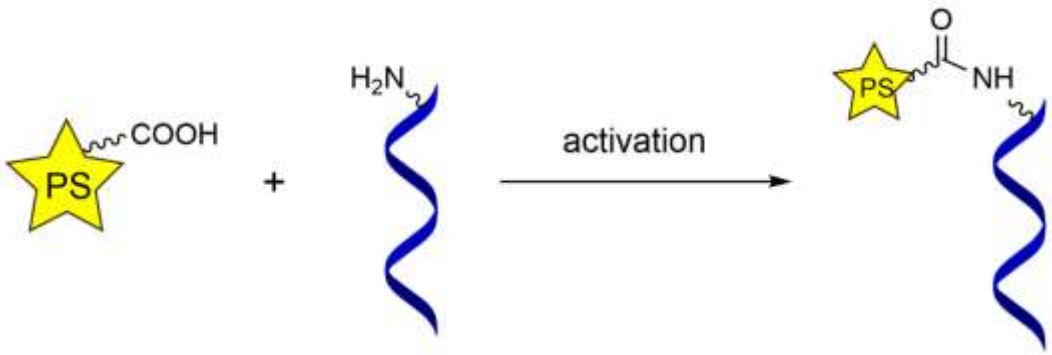

With the three conjugates in hands, they were hybridised to the furan containing oligonucleotides and the crosslink generation was evaluated. Again, the highest crosslink formation occurred when using the Ce6 conjugate, thanks to a sufficient singlet oxygen generation by this complex and a duplex stabilisation caused by the introduction of the chlorin. Surprisingly, the TriPyCOOH conjugated oligonucleotide was not able to induce a crosslinking presumably due to the large duplex stabilisation induced by the introduction of the porphyrin and a low singlet oxygen generation by the latter. The TT1 conjugated oligonucleotide showed a high singlet oxygen generation and allowed forming a crosslink but to a lower extent since the duplex was also destabilised due to the presence of the dye.

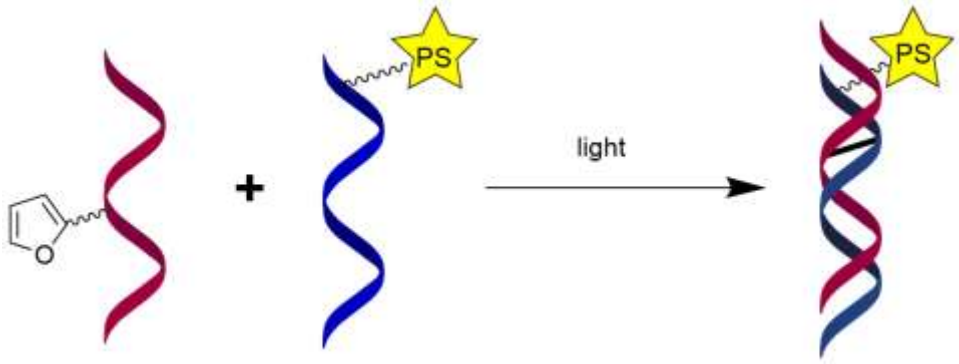

With the idea to allow crosslinking to target unmodified nucleic acid targets, the synthesis and evaluation of dual modified furan/photosensitiser probes was attempted. However, synthesis and handling of these self-activating probes was troublesome, probably due to premature singlet oxygen generation and inactivation of the probe, and when the crosslinking reaction was attempted it was never successful.

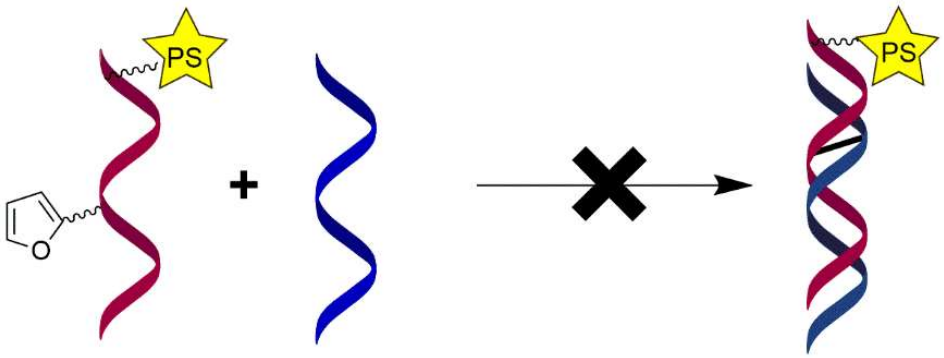

As an alternative, the use of a templated system was tested where the furan and the photosensitiser were placed in two different oligonucleotides, targeting a longer, unmodified strand, that brings both sequences in close proximity. While this approach had proven successful when using methylene blue or rose bengal modified probes, we here were not able to

demonstrate successful crosslinking. Time constraints that did not allow to investigate the system more in detail also because an alternative approach (*vide infra*) proved more successful.

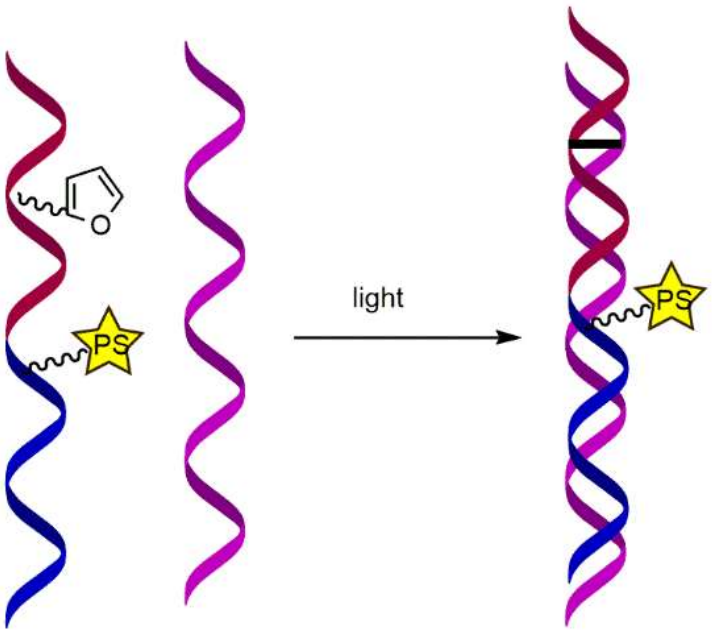

Indeed, as a further alternative, the use of a photosensitiser modified peptide carrier was explored. Nucleic acids are not able to gain access inside cells and the use of so-called cell penetrating peptides has been described to assist in the delivery of these compounds into cells for nucleic acid based therapies. More specifically, when using certain CPPs, supramolecular complexation between the positively charge peptide and the negatively charged oligonucleotide occurs spontaneously, resulting in the formation of nanoparticles.

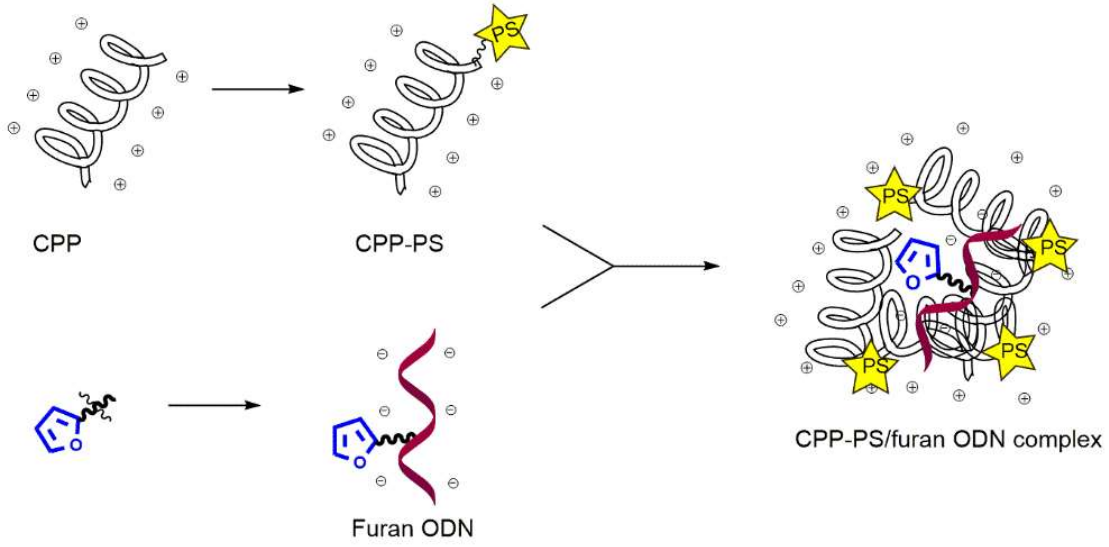

Here, the amphipathic 21 residue MPG-8 peptide was chosen for complexation with the furan oligonucleotide. Upon addition of the complementary unmodified strand and a sufficient amount of Ce6 as photosensitiser, crosslinking formation occurred, assisted by the presence of heparin to allow the release of the furan oligonucleotide when needed. Subsequently, the MPG-8 peptide was conjugated to Ce6 and complexation of this functionalised cell penetrating peptide with the furan oligonucleotide resulted in the formation of self-activating nanoparticles that were able to induce crosslink formation with an unmodified complementary oligonucleotide.

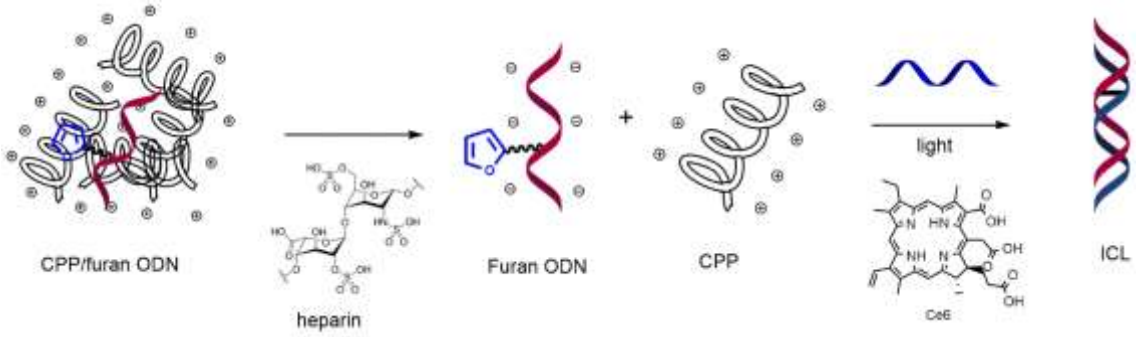

Perspectives

Since one of the applications of the furan technology could be its application for gene based therapy (antisense or antigene), the construction of the self-activating peptide nanoparticles opens the way to the use of the furan methodology in a cellular environment since it not only allows delivery but also protection of the oligonucleotides towards enzymatic degradation. Evaluation of alternative photosensitisers with higher singlet oxygen quantum yields might result in higher crosslinking yields.

Moreover, an unexplored possibility is the use of furan containing oligonucleotides for single stranded nucleic acid recognition for diagnosis and forensics. High-throughput analysis of nucleic acids sequences such as sequencing rely on hybridisation and there is a great potential for the use of the furan technology to improve the sensitivity of this techniques, especially in particularly challenging cases such as detection of single nucleotide polymorphisms.

Chapter VIII.

Nederlandse samenvatting.

Het ontrafelen van alle functies die nucleïnezuren vervullen vormde gedurende het laatste decennium een belangrijk onderwerp van onderzoek binnen vele onderzoeksgroepen wereldwijd. Niet alleen vormen nucleïnezuren de basis van het genetisch materiaal, bovendien nemen ze deel aan belangrijke enzymatische processen en genregulatie. Het ontwikkelen van nieuwe tools die kunnen dienen voor diagnose of therapie is daarom van groot belang in deze context.

Voorafgaandelijk onderzoek binnen OBCR toonde aan dat introductie van een furan eenheid in een oligonucleotide eenvoudig bewerkstelligd kan worden via automatische synthese resulterende in een probe die uitgerust is met een gemaskeerde reactieve entiteit. Deze is in staat is om, na furan oxidatie, crosslinking te veroorzaken met een complementaire sequentie. Furan-oxidatie kan bekomen worden door behandeling met NBS of op een meer biocompatibele wijze door het genereren van singlet zuurstof met behulp van Bengaals roze of methyleenblauw.

Het doel van huidige studie is het uitbreiden van deze methodologie naar het gebruik van porphyrine gebaseerde fotosensitizers voor singlet zuurstof generatie met het finale doel om een methode te ontwikkelen dit toepasbaar kan zijn in een cellulaire context.

Drie verschillende porphyrine gebaseerde fotosensitizers werden hiertoe geslecteerd: het commercieel beschikbaar chlorin e6 (Ce6), een tripyridyl porphyrine (TriPyCOOH) en een zink phthalocyanine gedecoreerd met tert-butyl groepen (TT1).

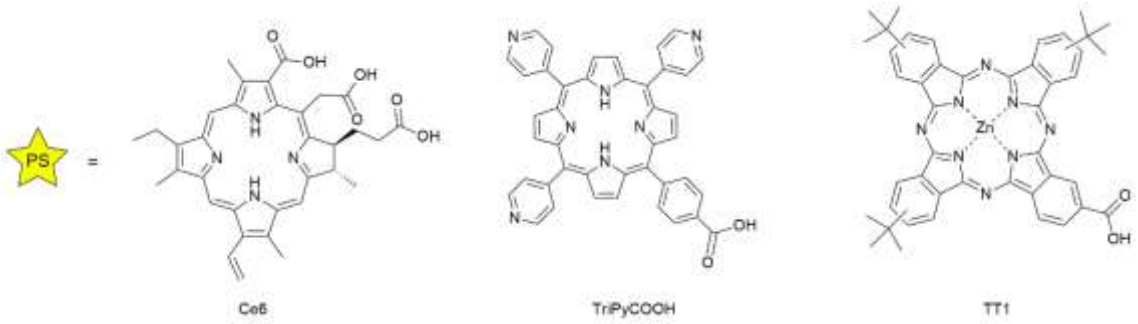

In eerste instantie werd de performantie van elke fotosensitizer getest door toevoegen in oplossing.

In tweede instantie werd nagegaan of conjugatie van de fotosensitizers aan het oligonucleotide complementair aan het furan-oligo verbetering kon brengen door het genereren van singlet zuurstof in de buurt van de furan eenheid en door een verhoogde oplosbaarheid van de fotosensitizers door conjugatie met de oligo's. Hiertoe dienden methoden ontwikkeld worden voor het conjugeren van de fotosensitizers aan de oligonucleotiden. Dit gebeurde door middel van activatie van een carbonzure functie op de fotosensitizers en reactie met een amino gemodificeerd oligo.

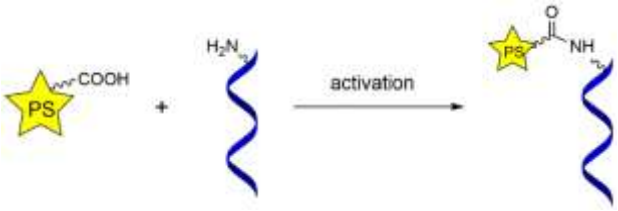

De hoogste crosslink performantie werd , zowel in oplossing als voor de geconjugeerde oligo's waargenomen voor het Ce6-conjugaat, mede door een voldoende singlet zuurstof generatie gecombineerd met een stabilisatie van de duplex door introductie van het chlorine.

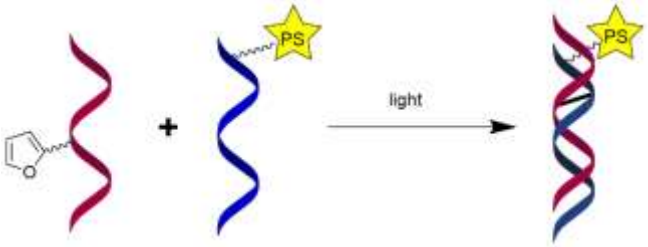

Met het idee om crosslinking te bewerkstelligen met een niet-gemodificeerd nucleïnezuurtarget, werden vervolgens dubbel gemodificeerde furan/fotosensitizer probes aangemaakt. Helaas bleek synthese en manipulatie van deze zelf-activerende probes geen sinecure mede door premature singelt zuurstof generatie en daarmee gepaard gaande inactivatie van de probes.

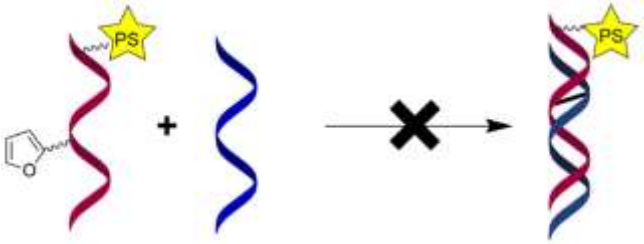

Als een volgend alternatief, werd het gebruik van een fotosensitizer-gemodificeerde peptidedrager geëxploreerd. Nucleïnezuren op zich kunnen niet opgenomen worden door cellen en het gebruik van zogenaamde celpenetrerende peptiden werd beschreven als een mogelijkheid om het afgeven van zulke verbindingen in cellen te bewerkstelligen in de context van nucleïnezuur gebaseerde therapieën. Meer bepaald worden bij het gebruik van bepaalde celpenetrerende peptide supramoleculaire complexen gevormd bestaande uit het positief geladen peptide en het negatief geladen oligo wat kan resulteren in de vorming van nanopartikels.

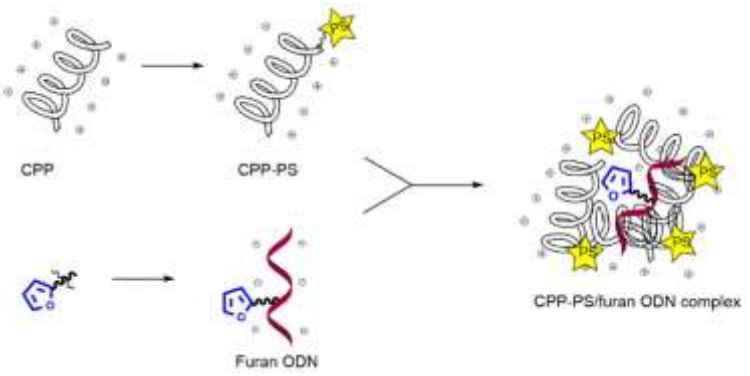

Het amfipatische 21-meer MPG-8 peptide werd gekozen voor complexatie met een furan oligo. Bij toevoeging van de complementaire streng en een voldoende hoeveelheid Ce6 als fotosensitizer, kon crosslinking waargenomen worden wanneer ook heparine werd toegevoegd om vrijstellen van het furan-oligo toe te laten. Vervolgens werd het MPG-8 peptide geconjugeerd met Ce6 en complexatie van dit gefunctionaliseerde celpenetrerende peptide met het furan oligo resulteerde in de vorming van zelfactiverende nanopartikles die in staat bleken te zijn crosslinkingvorming te induceren met een niet-gemodificeerde target nuceïnezuursequentie.

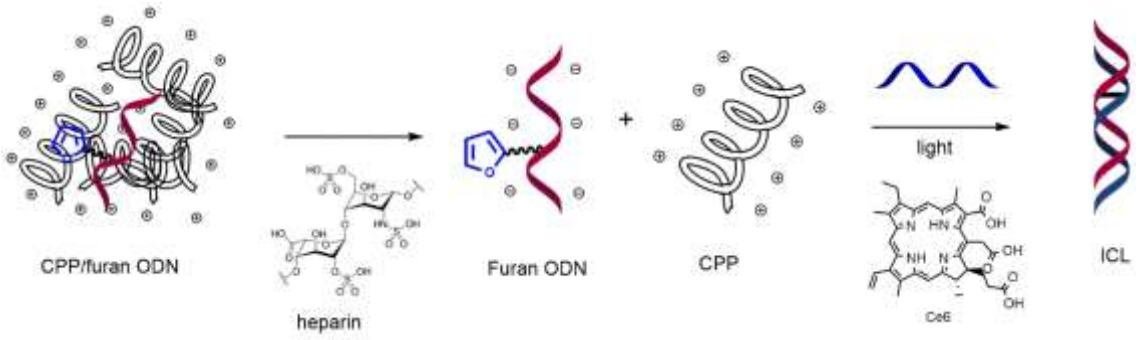

Perspectieven

De constructie van zelf-activerende peptide nanopartikels opent de weg naar het gebruik van furan methodologie in een cellulaire context aangezien dit niet alleen afgifte toelaat maar bovendien ook de oligonucleotiden beschermt tegen degradatie. Evaluatie van fotosensitizers met hogere singlet zuurstof quantum opbrengst zou kunnen resulteren in hogere crosslinkrendementen.

Chapter IX.

Resumen en español.

Muchos esfuerzos se han dedicado durante las últimas décadas a desvelar el intrincado puzle que conforman todos los papeles que juegan los ácidos nucleicos en los seres vivos. Los ácidos nucleicos no solo definen la constitución genética de un organismo sino que también participan en procesos enzimáticos y regulan la expresión genética. Por todo ello, existe un gran interés en el desarrollo de nuevas herramientas que puedan ser útiles en aplicaciones para diagnósticos o terapia basadas en estos procesos.

Previamente, se ha sido establecido en el grupo OBCR (Organic and Biomimetic Chemistry) que la introducción de un grupo furano en un oligonucleótido puede logarse de forma sencilla utilizando síntesis automática. Como resultado se obtiene una sonda equipada con un grupo funcional altamente reactivo que ha sido enmascarado y es capaz, una vez que el grupo furano ha sido oxidado, de producir un entrecruzamiento entre cadenas de forma selectiva con la secuencia complementaria. La oxidación del grupo furano se puede lograr o bien usando NBS o bien, de una forma más biocompatible, usando oxígeno singlete. Para la formación de este último, los compuestos azul de metileno y rosa de bengala han sido estudiados en detalle.

El objetivo de este estudio es expandir esta metodología al uso de fotosensibilizadores porfirínicos para la generación de oxígeno singlete con el objetivo final de desarrollar un método que se pueda aplicar en un contexto celular.

Para ello, se seleccionaron tres fotosensibilizadores distintos: la clorina e6 (comercial), una porfirínica tripiridínica (TriPyCOOH) y una ftalocianina de zinc decorada con grupos *tert*-butilo. (TT1).

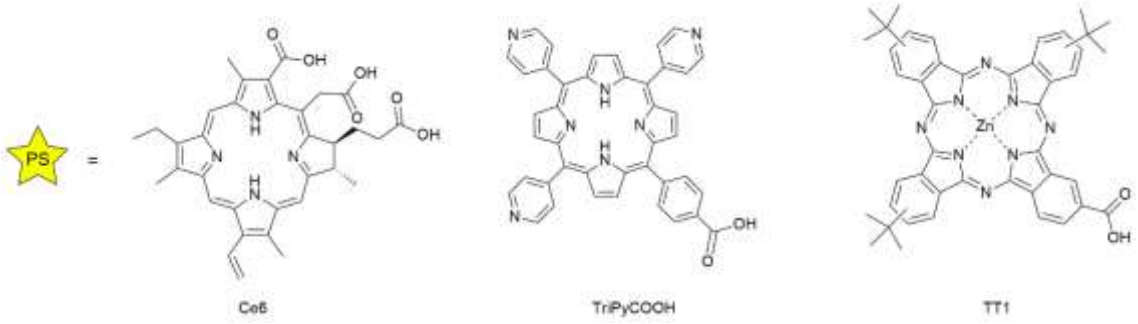

Primero, se evaluó la habilidad de cada fotosensibilizador para producir el entrecruzamiento entre cadenas cuando se añaden en solución. Para ello, un oligonucleótido modificado con un grupo furano fue hibridado con la cadena complementaia en presencia del respectivo fotosensibilizador para evaluar la generación del entrecruzamiento una vez se produce la irradiacción necesaria. Una cuidados optimización de varios factores se llevó a cabo, incluyendo el tiempo de reacción, la concentración de los fotosensibilizadores, el ratio entre el dúplex y el fotosensibilizador y el tipo de luz utilizada. Fue hallado que de los tres fotosensibilizadores, el uso de Ce6 produce los rendimientos de entrecruzamiento más altos (conversión del 52%) cuando las condiciones son óptimas. TT1 fue capaz de producir el entrecruzamiento solo a bajos rendimientos, debido a su insolubidad en condiciones acuosas que son necesarias para esta reacción.

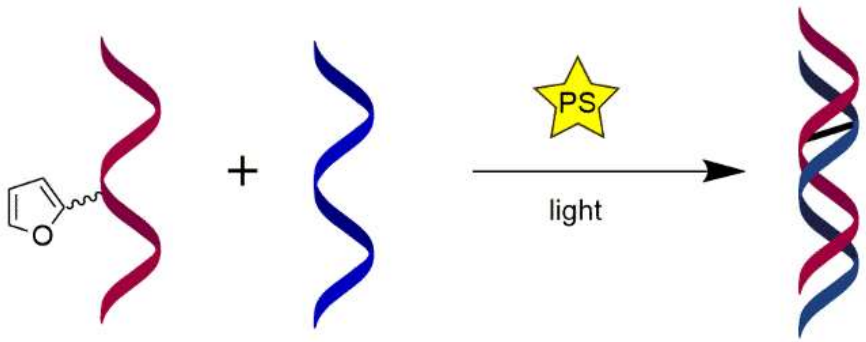

En el siguiente paso, se planteó la hipótesis de que al conjugar los fotosensibilizadores a la cadena complementaria al oligonucleótido que contiene el grupo furano resultaría en dos mejoras importantes: la generación de oxígeno singlete se produciría cerca del grupo furano y la solubilidad en agua de los fotosensibilizadores sería mayor.

Para conjugar cada fotosensibilizador se usó una estrategia de conjugación distinta, todas ellas basadas en la activación del ácido carboxílico en los fotosensibilizadores seguida por la adicción de un oligonucleótido que contiene un grupo amino. La conjugación de la TT1 fue particularmente problemática y esta reacción tuvo que llevarse a cabo con el oligonucleótido todavía en el soporte sólido donde se había sintetizado, para evitar el uso de condiciones acuosas y los problemas de solubilidad asociados.

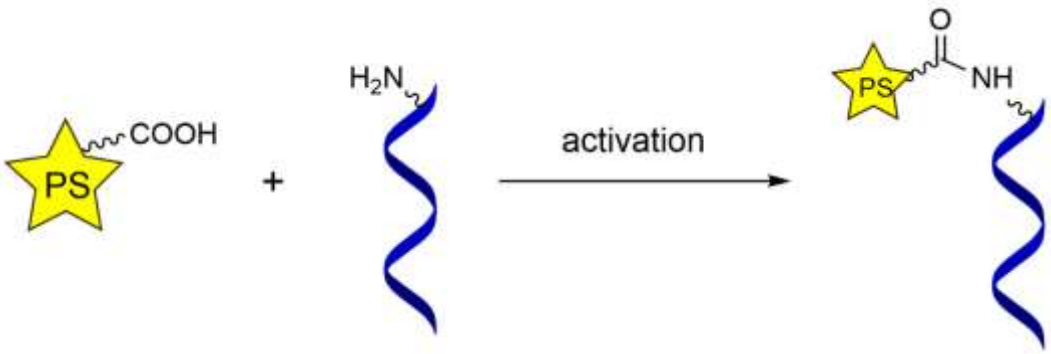

Una vez que los tres conjugados fueron sintetizados, se hibridaron al oligonucleótido que contiene el grupo furano y se evaluó la generación del entrecruzamiento. De nuevo, el entrecruzamiento que dio lugar a los rendimientos más altos fue en el que se usó el conjugado con Ce6, gracias una generación suficiente de oxígeno singlete y a una estabilización del dúplex que ocurre como consecuencia de introducir Ce6 en el oligonucleótido. Sorprendentemente, el uso del conjugado con TriPyCOOH no fue capaz de producir el entrecruzamiento, presuntamente debido la gran desestabilización que tiene lugar al introducir este fotosensibilizador y la pobre generación de oxígeno singlete. El conjugado con la TT1 mostró una alta generación de oxígeno singlete y fue capaz de producir el entrecruzamiento entre cadenas pero con rendimientos menores debido a una desestabilización del dúplex debido a la presencia del fotosensibilizador.

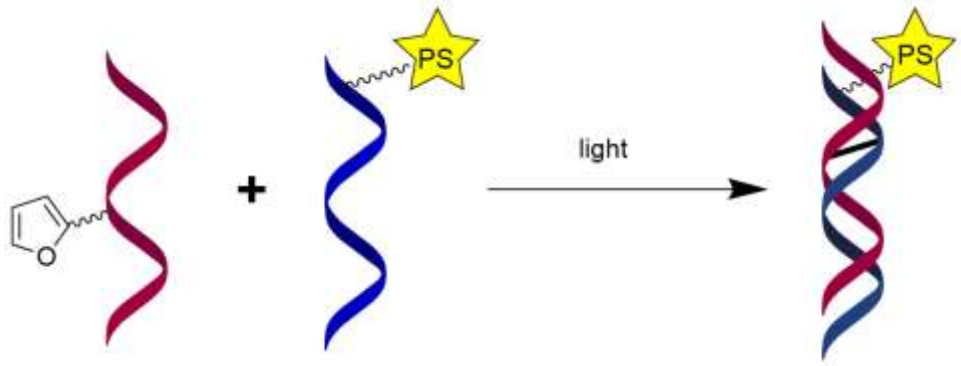

Con la idea de permitir el entrecruzamiento con una secuencia no modificada, se sintetizaron y evaluaron sondas doblemente modificadas con un grupo furano y un fotosensibilizador. Sin embargo, la síntesis y el manejo de estas sondas auto-activables fue problemática, probablemente debido a la generación prematura de oxígeno singlete y la consiguiente desactivación de las sondas, y cuando la reacción de entrecruzamiento se intentó llevar a cabo no tuvo éxito en ningún caso.

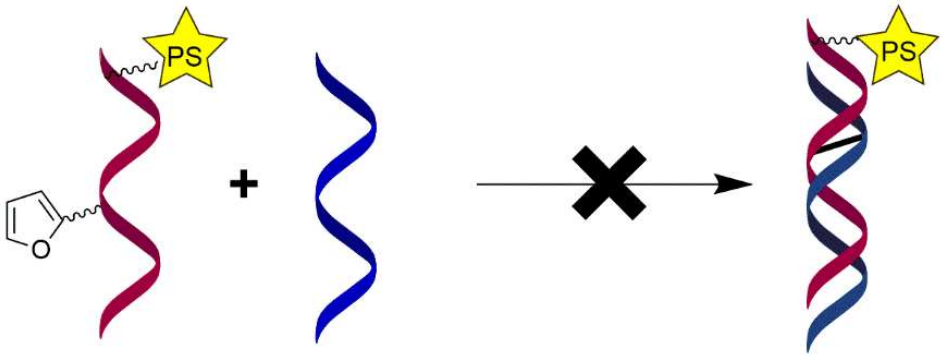

Como alternativa, se probó el uso de un sistema plantilla en el que el furano y el fotosensibilizador fueron introducidos en oligonucleótidos distintos y posteriormente hibridados a un oligonucleótido más largo sin modificaciones, que los mantiene próximos el uno al otro. Mientras que este enfoque tuvo éxito en un estudio anterior en el que se usaron sondas que contenían azul de metileno y rosa de bengala, en nuestro caso no pudimos demostrar la generación del entrecruzamiento. Debido a falta de tiempo, este enfoque no fue estudiado en más detalle ya que una tercera estrategia fue puesta en práctica (*vide infra*).

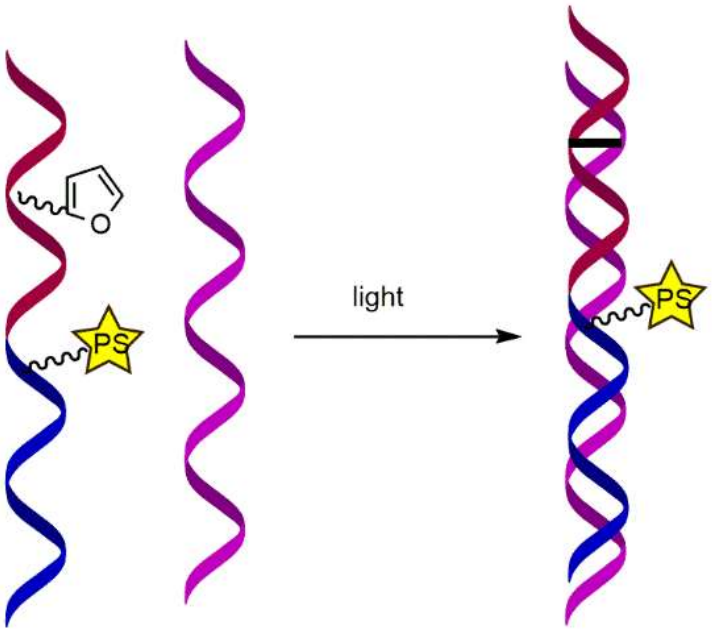

En esta nueva estrategia se estudió el uso de un péptido de penetración celular como transportador. Los ácido nucleicos no son capaces de ganar acceso a las células y se ha descrito el uso de estos péptidos para terapias basadas en el uso de ácidos nucleicos ya que son capaces de asistir en la internalización de los ácidos nucleicos. En concreto, algunos de estos péptidos son capaces de formar complejos supramoleculares entre los péptidos cargados positivamente

y los oligonucleótidos cargados negativamente, lo que resulta en la formación de nanopartículas.

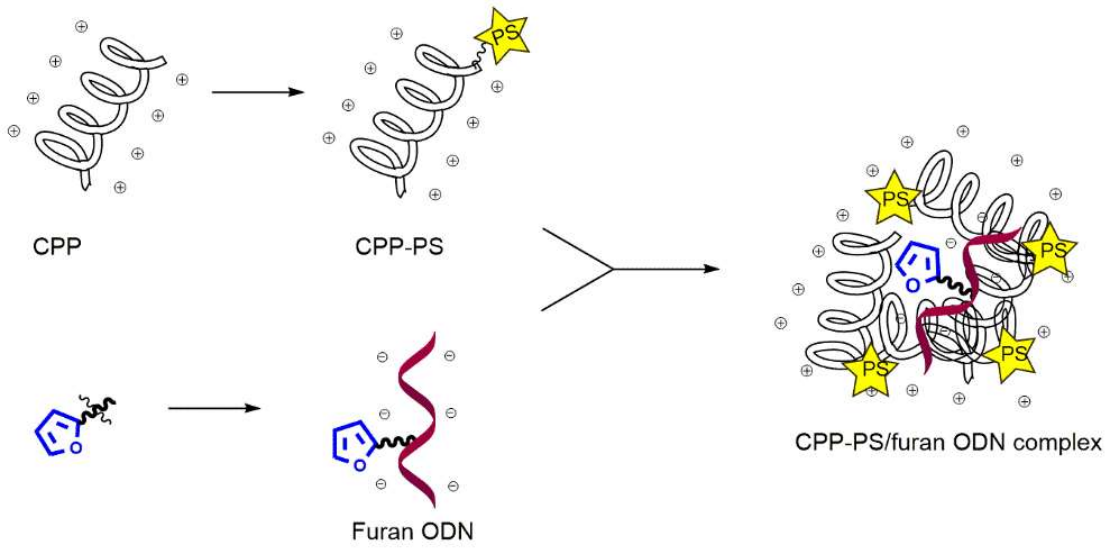

En este caso, el uso del péptido conocido como MPG-8, que contiene 21 aminoácidos, se eligió para la formación de complejos con el oligonucleótido que contienen el furano. Al añadir la cadena complementaria y una concentración suficiente de Ce6 como fotosensibilizador, se observó la formación del entrecruzamiento, usando heparina para facilitar la liberación del oligonucleótido cuando es necesario. Posteriormente, MPG-8 fue conjugado a Ce6 y la formación del correspondiente complejo con el oligonucleótido que contiene el furano resultó en la formación de nanopartículas auto-activables que fueron capaces de producir el entrecruzamiento con un oligonucleótido no modificado.

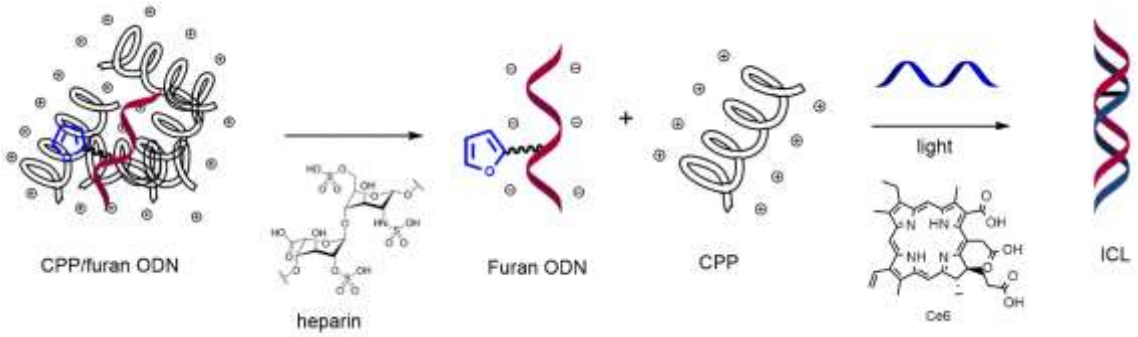

Perspectivas

Ya que una de las aplicaciones de esta tecnología basada en el grupo furano podría ser para terapia genética, la formación de nanopartículas auto-activables abre las puertas al uso de esta metodología en un contexto celular, ya que no solo permite internealizar oligonucleótido sino que también los protege contra la degradación enzimática. La evaluación de otros

fotosensibilizadores con rendimientos cuánticos mayores podría resultar en la producción de entrecruzamientos con mayores rendimientos.

Además, una posibilidad inexplorada es el uso de oligonucleótido que contiene el furano para el reconocimiento de ácidos nucleicos de cadena simpe para terapia y diagnóstico. Los análisis de alto rendimiento (high-throughput) de secuencias de ácidos nucleicos como por ejemplo el secuenciamiento están basados en la hibridación y el uso de la tecnología del furano tiene mucho potencial para mejorar la sensibilidad de estas técnicas, especialmente en casos problemáticos como la detección de polimorfismos de un único nucleótido.

Chapter X.

Materials and methods.

X.1. Small molecule materials and methods

All chemical reagents and solvents were purchased from Sigma Aldrich, Glen Research, Livchem Logistics and used without further purification. Photosensitisers were obtained via a collaboration between UGent and the University of Aveiro and the Autonomous University of Madrid in the context of an ITN.

X.1.1.Furan phosphoramidite

The furan building blocks for incorporation into the modified oligonucleotides was synthesised as previously described.(1,2)

X.1.2.Photosensitiser synthesis:

TriPyCOOH porphyrin (3) and TT1 phthalocyanine (4) were synthesised as previously described. Chlorin e6 (Ce6) was purchased from Livchem Logistics.

X.2. Oligonucleotide materials and methods

All chemical reagents and solvents were purchased from Sigma Aldrich, Glen Research, Livchem Logistics. Oligonucleotides were purchased from Eurogentec.

X.2.1.Oligonucleotides synthesis

Oligonucleotides were synthesized at 1 µmol scale on an ABI 394 DNA synthesizer. The sequences were synthesized on solid phase and the last nucleoside remained DMT-protected for later SEP-PAK purification, unless otherwise stated.

X.2.1.1. Synthesis of furan modified oligonucleotides

Synthesis (DMT-On) proceeded through an automated phosphoramidite coupling cycle and was interrupted for a manual incorporation of the furan modified phosphoramidites. This coupling involved an alternating application of a dry 0,05 M solution of the modified phosphoramidite in acetonitrile and a dry 0,1 M

dicyanoimidazole solution in acetonitrile, over 30 min. Then, and a mixture of Cap A (0.5 mL,) and Cap B (0.5 mL) was pushed over the column, after which it was again flushed with acetonitrile (1 mL) and automated synthesis was resumed.

X.2.1.2. Synthesis of on solid support amino modified oligonucleotides

The DMS(O)MT-amino modifier was installed on the synthesiser as an extra nucleobase. After incorporation at the 5' end of the growing ON, the amino group was deprotected on column by treatment with 5 mL TCA, 10 mL ACN, 5 mL 20% Et_2NH in ACN and 10 mL of ACN.

X.2.1.3. Synthesis of internally amino modified oligonucleotides

The trifluoroacetyl protected dT amino modifier was installed on the synthesiser as an extra nucleobase. After oligonucleotide synthesis, deprotection of the amino group occurs during the standard treatment with NH_4OH.

X.2.2.Oligonucleotide cleavage, deprotection and purification

The synthesized oligonucleotides were cleaved of the solid support by treatment with 1 mL of aqueous NH_4OH while shaking overnight at a temperature of 55°C.
Purification with concurrent DMT removal of the synthesized oligonucleotides was carried out using a Sep-Pak C18 cartridge obtained from Waters. After equilibrating the cartridge using ACN and a 5 mM solution of TEAA, the oligonucleotides were loaded and the following solutions were eluted: an aqueous solution of NH_4OH (2.5%), milliQ water, an aqueous solution of TFA (1.5%), milliQ water and finally 20% ACN in water to elute the desired oligonucleotide. The fractions were combined and analysed by RP HPLC and MALDI-TOF.

X.2.3.Oligonucleotide conjugation

Conjugation of the PS to the amino modified ODNs was performed by activating the carboxylic acid functionality on the dyes and subsequent addition of the amino ODN in buffer solution.

X.2.3.1. Conjugation to Ce6

DCC (64 eq) and NHS (64 eq) were added in DMF to chlorin e6 (1 mg, 64 eq) and the solution stirred for 1 h in the darkness under Ar atmosphere. Then, a 0.1 M aqueous solution of $NaHCO_3$ (30 µL, pH 8.3) and the amino modified

oligonucleotide (30 nmol) were added and the solution was stirred at room temperature for 18h in the darkness. Subsequently, 2x500 μL of mQ water were added and the resulting mixture centrifuged. The supernatant was collected, combined and lyophilised. The desired conjugate was obtained by purification via RP HPLC equipped with a Discovery BIO Wide Pore C5 column (linear gradient: 0-50% ACN in 15 min) and analysed by MALDI-TOF.

X.2.3.2. Conjugation to TriPyCOOH

TriPyCOOH was provided as the NHS ester (TriPyCOONHS). Conjugation with the amino modified oligonucleotides was carried out as follows: TriPyCOONHS (1 mg, 43 eq) was dissolved in DMSO (60 μL), then a 0.1 M aqueous solution of $NaHCO_3$ (30 μL, pH 8.3) and the amino modified oligonucleotide (30 nmol) were added and the solution stirred in the darkness at room temperature under Ar atmosphere for 18h. Subsequently, 2x500 μL of mQ water were added and the resulting mixture centrifuged. The supernatant was collected, combined and lyophilised. The desired conjugate was obtained by purification via RP HPLC equipped with a Discovery BIO Wide Pore C5 or an Aeris Wide Pore column (0-50% ACN in 15 min or 0-10% ACN in 15 min then 10-100% ACN in 15 min, respectively) and analysed by MALDI-TOF MS.

X.2.3.3. Conjugation to TT1

Conjugation using TT1 phthalocyanine was performed while the amino modified oligonucleotide was still attached to 1000 Å Control Pore Glass (CPG) as in the procedure followed by Kopecky et al.(5):

TT1 phthalocyanine (1 mg, 12 eq) was premixed with HBTU (10 eq) and DIPEA (6 μL) in DMF (30 μL) and added in 3 portions to the CPG (3 mg, aprox. 99 nmol of the oligonucleotide), every 1h. The mixture was shaken for 24h at 55º in the darkness. Subsequently, the mixture was washed with 3x500 μL DMF, 3x500 μL ACN and 3x500 μL Et_2O, then dried. Cleavage from the solid support was carried out adding 1mL of NH_4OH was added and the mixture shaken overnight at 55 ºC in the darkness. The crude was pre-purified using Sep-Pak C18 cartridge (Waters) and the fractions eluted with 50% ACN were collected, combined and lyophilized.

The residue was purified via RP HPLC equipped with a Discovery BIO Wide Pore C5 (linear gradient: 0-80% ACN in 15 min) and analysed by MALDI-TOF MS

X.2.4.Oligonucleotide analysis and characterisation

X.2.4.1. RP HPLC analysis

Oligonucleotides were analysed by RP-HPLC, using an Agilent 1200 system. The mobile phases consisted of A/acetonitrile and B/0,1 M TEAA buffer containing 5% acetonitrile. Furan and amino modified oligonucleotides were analysed using a Phenomenex Clarity 110 Å C18 column (250 x 4.6 mm, 5 µm), a Phenomenex Aeris Widepore column (150 x 4.6 mm, 3.6 µm) or a Waters XBridge 130 Å Oligonucleotide C18 column (2,5 µm, 4,6 mm X 50 mm) used at 50°C (linear method 0-20% ACN in 30 min).

The photosensitiser conjugated ODN were analysed and purified using RP HPLC equipped with a Discovery BIO Wide Pore C5 column (5 µm, 15 cm x 4,6 mm) and the mobile phases consisted of A/acetonitrile and B/0,1 M TEAA buffer containing 5% acetonitrile.

X.2.4.2. MALDI-TOF analysis

Masses of the oligonucleotides were determined by MALDI-TOF analysis on an ABI Voyager DE-STR MALDI-TOF. The oligonucleotide samples were mixed with a matrix consisting of 3-hydroxypicolinic acid (17 mg in 100 µL milliQ) and ammonium citrate (50 mg in 200 µL milliQ and 250 µL acetonitrile) present in a 9:1 ratio, in a 1:1 sample:matrix ratio. After mixing with the matrix, the samples were desalted by treatment with DOWEX beads. The samples were spotted on a MALDI plate, together with a commercial oligonucleotide sequence with a known mass (5'-GCA TCT CGT CAG-3'), purchased from Eurogentec, for calibration of the measurement.

X.2.4.3. UV analysis

Concentrations and UV-Vis spectrum (in the case of the photosensitiser conjugates) of the ODNs solutions were measured on the Trinean DropSense96 UV/VIS droplet reader, using 2 µL sample for each measurement. Each sample was measure in duplicate.

Melting temperatures of the duplexes were determined by recording their UV-Vis absorbance on a Varian Cary 300 Bio instrument equipped with a six-cell thermostatted cell holder. Melting curves were monitored at 260 nm with a heating

rate of 0.3 ºC/min. The buffer contained 100 mM NaCl and 10 mM phosphate buffer (pH 7). Oligonucleotide concentration was 1 µM for each strand. Melting temperatures were calculated from the first derivative of a tenth order polynomial function that fitted the data.

X.2.4.4. Singlet oxygen generation

2 µM of the PS conjugated ONs were dissolved in a 10 mM phosphate buffer (pH 7) containing 100 mM of NaCl. ABDA was added before irradiation (100µM) and samples were taken at 0, 0.5, 1, 2, 3, 4 and 5 min. Samples were measured using a Trinean DropSense96 UV/VIS droplet reader, using 2 µL samples for each measurement (each sampling was performed in duplicate).

X.3. Crosslinking experiments

X.3.1.Crosslinking using the photosensitisers in solution

Crosslinking reactions where the photosensitisers were externally added were carried out at 20 µM oligonucleotide concentration and also at 2 µM, for comparison with the crosslinking experiments where the photosensitiser conjugated oligonucleotides were used. The oligonucleotides were dissolved in a 10 mM phosphate buffer (pH 7) containing 100 mM of NaCl. The externally added photosensitisers were added just before starting the irradiation. Stock solutions of the photosensitiser were prepared in DMSO (1.96 mM for TriPyCOOH; 923.76 µM for TT1; 2.18 mM for Ce6), diluted 10x in water (DMSO for TT1) and added to the solution immediately before irradiation.

During the crosslinking reaction the temperature was kept constant at 25°C in an Eppendorf Thermomixer comfort with constant shaking at 950 rpm. Samples were irradiated using an Euromex fiber optic 100 W halogen light source Ek-1 equipped with a red filter when necessary and placed 1 cm above the sample. The spectrum when the red filter is placed was determined:

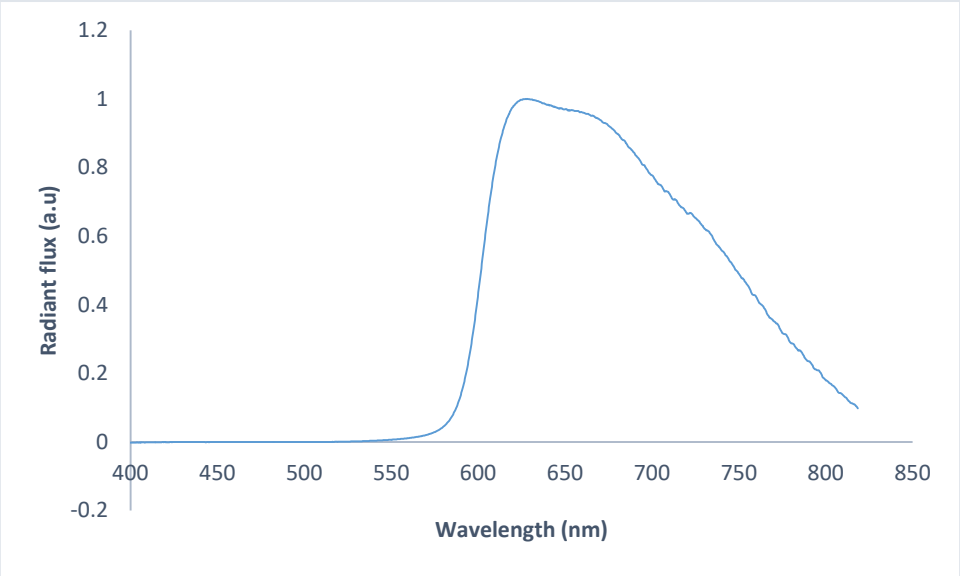

X.3.2.Crosslinking using the photosensitiser conjugated oligonucleotides

Crosslinking reactions using the photosensitiser conjugates were carried out under the same conditions as the crosslink experiments using the PSs in solution, but in this case no external photosensitiser was added.

X.3.3.Crosslinking using porphyrin containing nanoparticles

Crosslinking reactions using porphyrin containing NPs were carried out under the same conditions as the crosslink experiments using the PSs in solution, but before HPLC analysis of the samples, a filtration step using a PTFE filter was included to avoid obstruction of the equipment by the nanoparticles.

X.3.4.Crosslinking using peptide based nanoparticles

Previous to the crosslinking experiments, the peptide (1 μM) and the furan modified oligonucleotide (0.17 μM) were incubated together at 37ºC for 30 min in 10 mM phosphate buffer (pH 7) containing 100 mM of NaCl. After allowing the samples to cool down to 25 ºC, the complementary strand and the externally added Ce6 were added just before starting the irradiation. In the case that the Ce6 modified peptide is used, no external PS is added. In the relevant cases, heparin is also added before irradiation.

During the crosslinking reaction the temperature was kept constant at 25°C with constant shaking at 950 rpm and samples were taken for PAGE analysis. These samples

were lyophilised previous analysis, redissolved in 2 μL mQ and 18 μL formamide and kept for a few minutes in a sonic bath to ensure solubilisation of the ODNs.

X.3.5.Analysis of crosslinking experiments

Samples were taken at different times for RP HPLC and PAGE analysis. After the maximum crosslinking yield was obtained, prolonged irradiation resulted in degradation of the crosslinked species.

X.3.5.1. RP HPLC analysis

Crosslinking samples where the photosensitiser was externally added were analysed by RP-HPLC equipped with a XBridge C18 column. Crosslinking samples with the photosensitizer conjugated to the oligonucleotide were measured with the RP HPLC equipped with a Discovery Wide Pore C5 column. Crosslinking yields were determined by integration of the corresponding peaks in the HPLC chromatogram and by comparing the area of the peak of the crosslinked species with the peak of the limiting single oligonucleotide strand, both corrected for their extinction coefficient. The extinction coefficient of the duplex was calculated based on the method described by R. Owczarzy *et al.*(5).

X.3.5.2. PAGE analysis

Samples were analysed by denaturing gel electrophoresis. The gels were prepared by dissolving 4,2 g urea in 5 mL of 40% acrylamide:bisacrylamide (19:1) and 1 mL 10x TBE buffer. 100 μL of a 0,5 M solution of ammonium persulphate was added and the solution was diluted to 10 mL with milliQ water. After cooling the solution, N,N,N',N'- tetramethylethylenediamine was added and the resulting mixture was poured between glass plates and allowed to polymerize for one hour. The gels were subjected to a pre-run in the consort EV202 at a voltage power of 225V during half an hour. After mixing the samples with formamide in 9:1 formamide:sample ratio , they were loaded on the gel. During a run of approximately one hour, the temperature was kept at 25°C with a Julabo F12. The gels were stained with GelRed™ or GelGreen™ Nucleic acid gel stain (VWR) and photographed using an Autochemi imaging system.

X.4. Peptide materials and methods.

X.4.1.Synthesis of MPG-8

MPG-8 was synthesised by Jos Van de Begin following a modified version of the protocol previously reported (6–8). The synthesis was carried out on solid phase using Cysteamine 4-methoxytrityl resin on an automated peptide synthesizer (SYRO Multiple Peptide Synthesizer equipped with a vortexing unit (Multisyntech, Witten, Germany). The peptide was synthesised using a standard Fmoc-*t*Bu strategy.

X.4.1.1. Cleavage, deprotection and purification

MPG-8 deprotection was carried out using a mixture 94:2.5:2.5:1 of TFA/H_2O/ EDT/TIS, allowing to react for 4 hours to ensure deprotection of the Arg residue. After this time, the solution was collected, the resin was washed with TFA and the two fractions combined and dried under a nitrogen flow. Pre-purification of the peptide was carried out by precipitation using cold MTBE, twice. The remaining pellet was dried under nitrogen and redissolved in 1:1 ACN/mQ.

MPG-8 was purified by RP HPLC equipped with a Luna C18 column, linear gradient of 0-100% ACN in 15 minutes), lyophilised and redissolved in mQ for mass analysis.

X.4.1.2. MS analysis

The peptide was successfully identified by LC-MS analysis by an Agilent 1100 Series instrument equipped with a Phenomenex Kinetex C18 100 Å column (150 x 4.6 mm, 5 μm at 35 °C) with an ES-MSD type VL mass detector (quadrupole ion trap mass spectrometer) using a flow rate of 1.5 ml/min (eluent: 0.1% HCOOH in H_2O and CH_3CN).

X.4.2.Ce6 conjugation to MPG-8

A mixture of Ce6 (3.6 mg, 2.50 eq), HBTU (2.4 eq) and DIPEA (5 eq) in 300 μL DMF were added to MPG-8 (5.8 mg, 2.40 μmol) still attached to the resin. The reaction mixture was allowed to react overnight under argon atmosphere in the darkness. Next, the resin was sequentially washed using 500 μL of 3xDMF, 3 MeOH and 3x Et_2O.

X.4.2.1. Cleavage, deprotection and purification of Ce6MPG-8

Ce6MPG-8 was deprotected using a mixture of 0.1M HCl in HFIP (HCl in HFIP/EDT/TIS 96.5:2.5:1), allowing to react for 4 hours in the darkness under argon atmosphere.

After this time, the solution was collected, the resin was washed with HFIP and the two fractions combined and dried under a nitrogen flow. Pre-purification of the peptide was carried out by precipitation using cold MTBE twice. The remaining pellet was dried under nitrogen and redissolved in 1:1 ACN/mQ.

Ce6MPG-8 was purified by RP HPLC equipped with a Luna C18 column, linear gradient of 0-100% ACN in 25 minutes) and the three obtained fractions were lyophilised and redissolved in mQ for mass analysis.

X.4.2.2. MS analysis

LC-MS analysis of Ce6MPG-8 was unsuccessfully attempted but the correct mass could be found by MALDI-TOF in all fractions. The first obtained fraction was used for the following experiments for showing a higher purity.

X.4.3.Size determination of the peptide/ODN nanoparticles.

The peptide (1 μM) and the furan modified oligonucleotide (0.17 μM) were incubated together at 37ºC for 30 min in 10 mM phosphate buffer (pH 7) containing 100 mM of NaCl to allow nanoparticle formation.

The size of this nanoparticles was assessed by dynamic light scattering (DLS) using a Malvern Zetasizer Nano Series running DTS software and operating a 4 mW He-Ne laser at 633 nm. Detection was performed at an angle of 173°.

X.5. Experimental data

X.5.1.Experimental data for Chapter III

X.5.1.1. Characterisation of synthesised ODNs

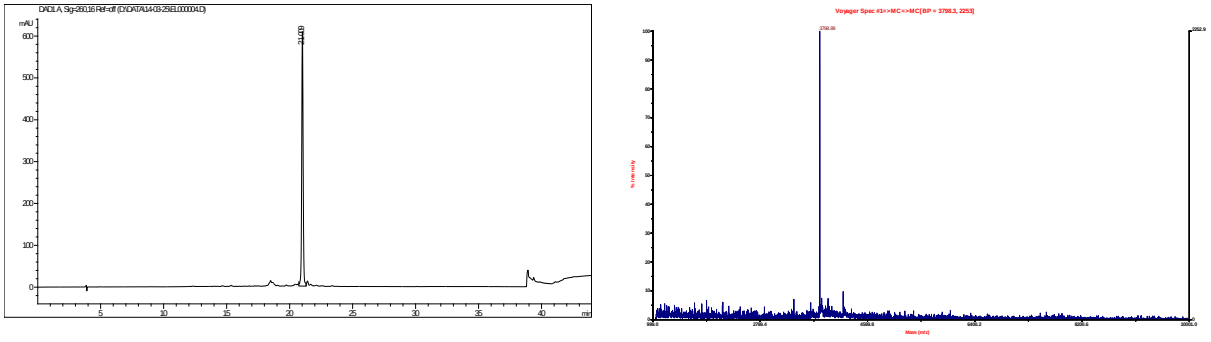

Figure 1. Left: HPLC chromatogram of FON1. Right: MALDI-TOF MS analysis. Expected mass: 3799 Da. Observed mass: 3799 Da

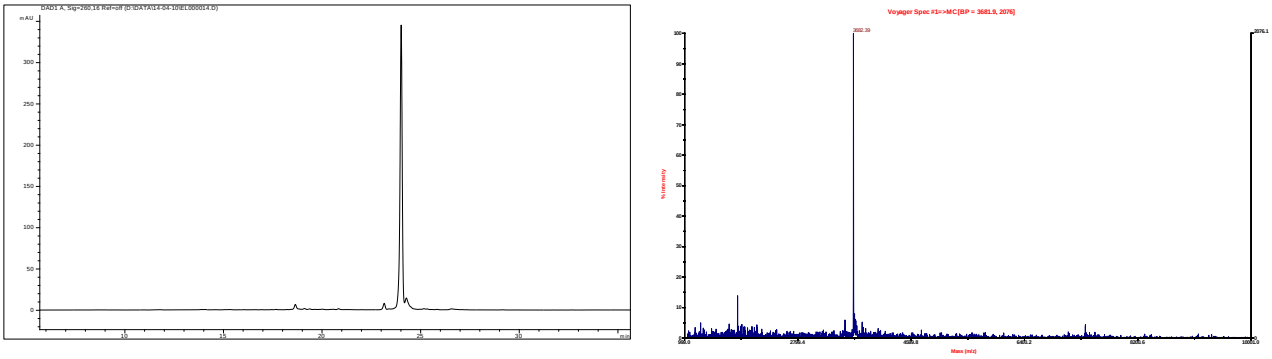

Figure 2. Left: HPLC chromatogram of FON2. Right: MALDI-TOF MS analysis. Expected mass: 3682 Da. Observed mass: 3682 Da

X.5.1.2. ICL experiments using Ce6 in solution

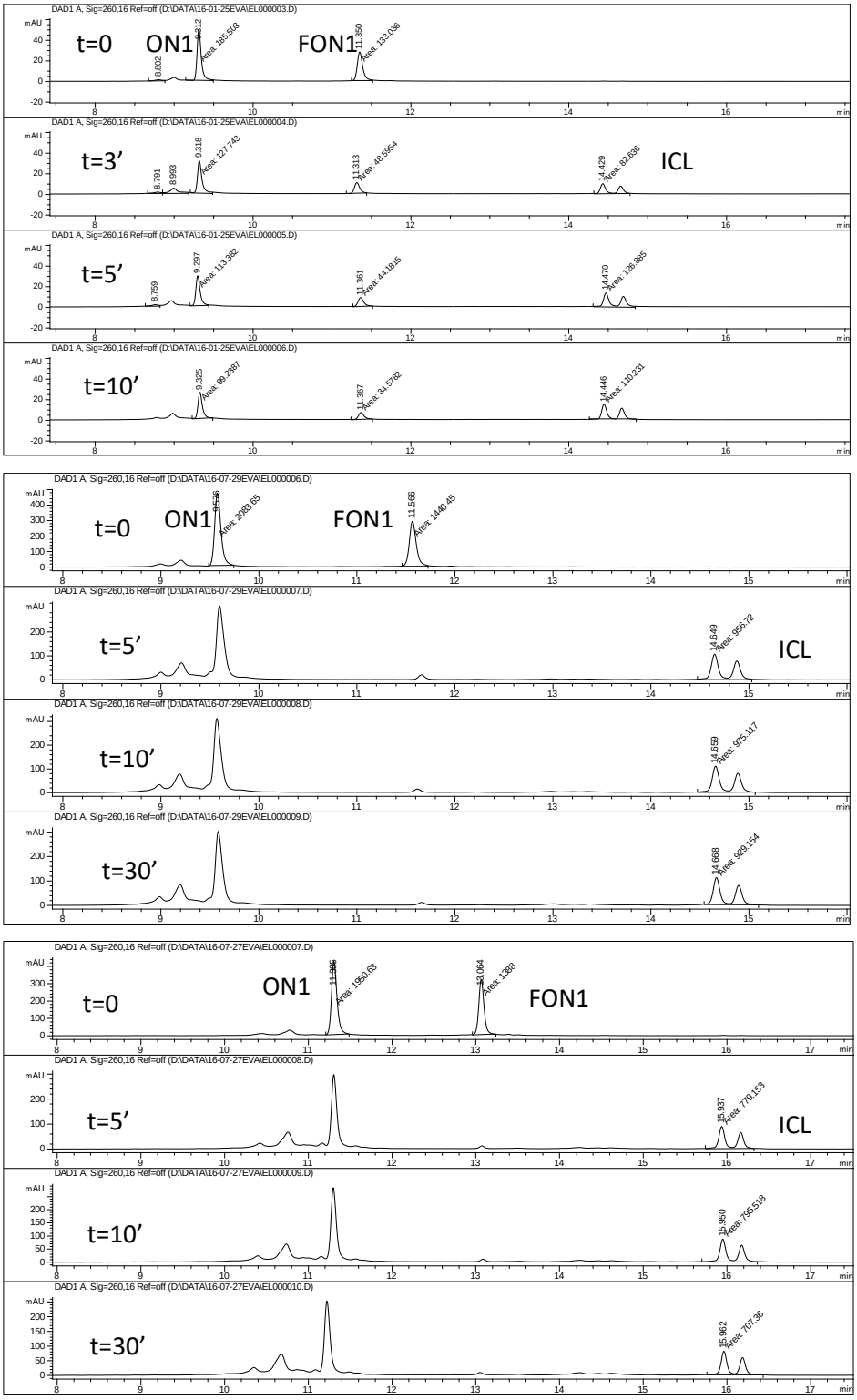

Figure 3. HPLC traces of crosslinking experiments using Ce6 (1% DMSO). Top: [duplex] = 2 μM, [Ce6] = 2 μM; middle: [duplex] = 20 μM, [Ce6] = 5 μM; bottom: [duplex] = 20 μM, [Ce6] = 10 μM

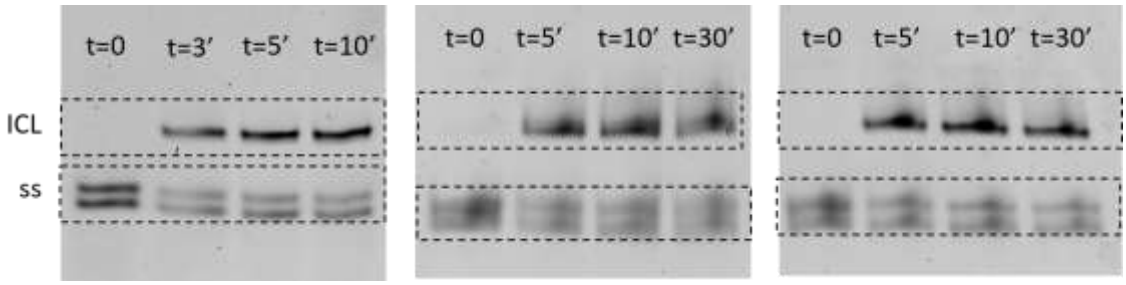

Figure 4. PAGE analysis of crosslinking experiments using Ce6 (1% DMSO). Left: [duplex] = 2 μM, [Ce6] = 2 μM; middle: [duplex] = 20 μM, [Ce6] = 5 μM; right: [duplex] = 20 μM, [Ce6] = 10 μM

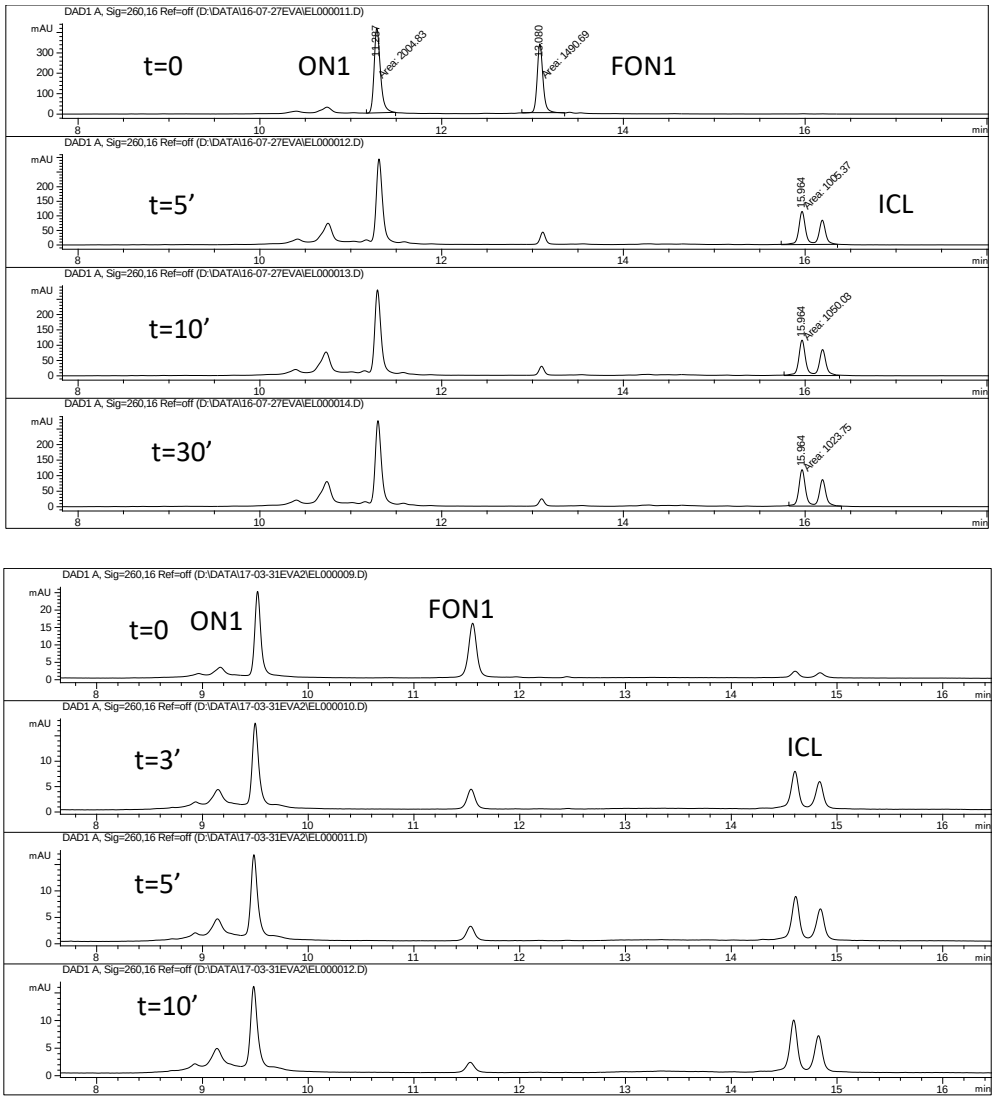

Figure 5. HPLC traces of crosslinking experiments using Ce6 at different DMSO percentage. Top: [duplex] = 20 μM, [Ce6] = 5 μM, no DMSO; bottom: [duplex] = 2 μM, [Ce6] = 2 μM, 20% DMSO

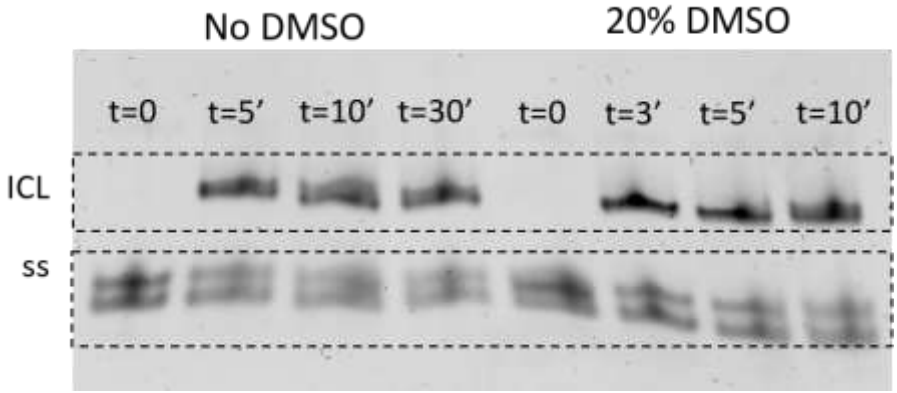

Figure 6. PAGE analysis of crosslinking experiments using Ce6 at different DMSO percentage. Left: [duplex] = 20 μM, [Ce6] = 5 μM, no DMSO; right: [duplex] = 2 μM, [Ce6] = 2 μM, 20% DMSO

X.5.1.3. ICL experiments using TriPyCOOH in solution

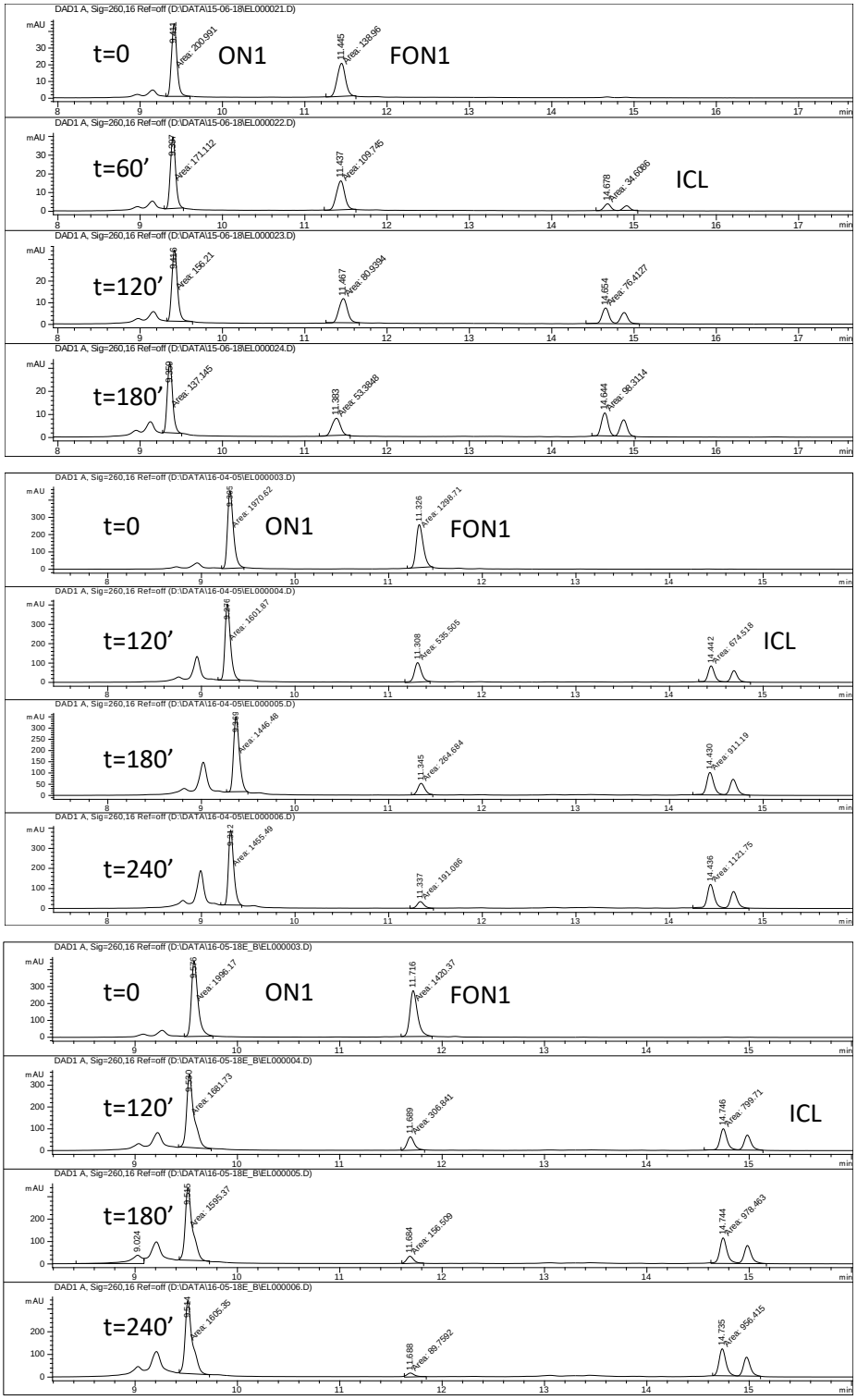

Figure 7. HPLC traces of crosslinking experiments using TriPyCOOH. Top: [duplex] = 2 μM, [TriPyCOOH] = 2 μM; middle: [duplex] = 20 μM, [TriPyCOOH] = 5 μM; bottom: [duplex] = 20 μM, [TriPyCOOH] = 10 μM

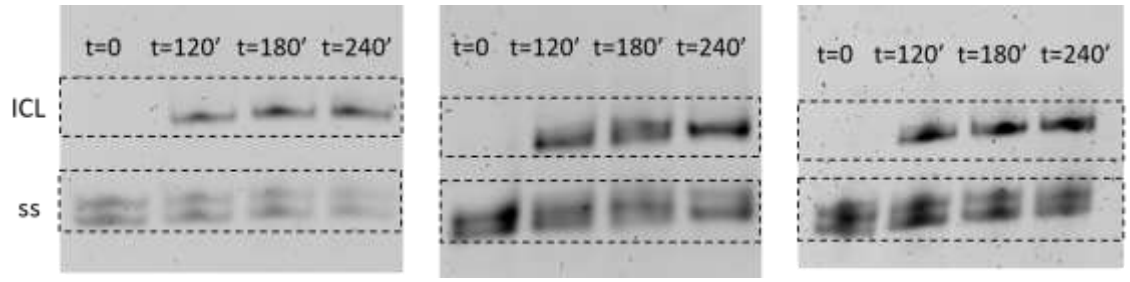

Figure 8. PAGE analysis of crosslinking experiments using TriPyCOOH. Left: [duplex] = 2 μM, [TriPyCOOH] = 2 μM; middle: [duplex] = 20 μM, [TriPyCOOH] = 5 μM; right: [duplex] = 20 μM, [TriPyCOOH] = 10 μM

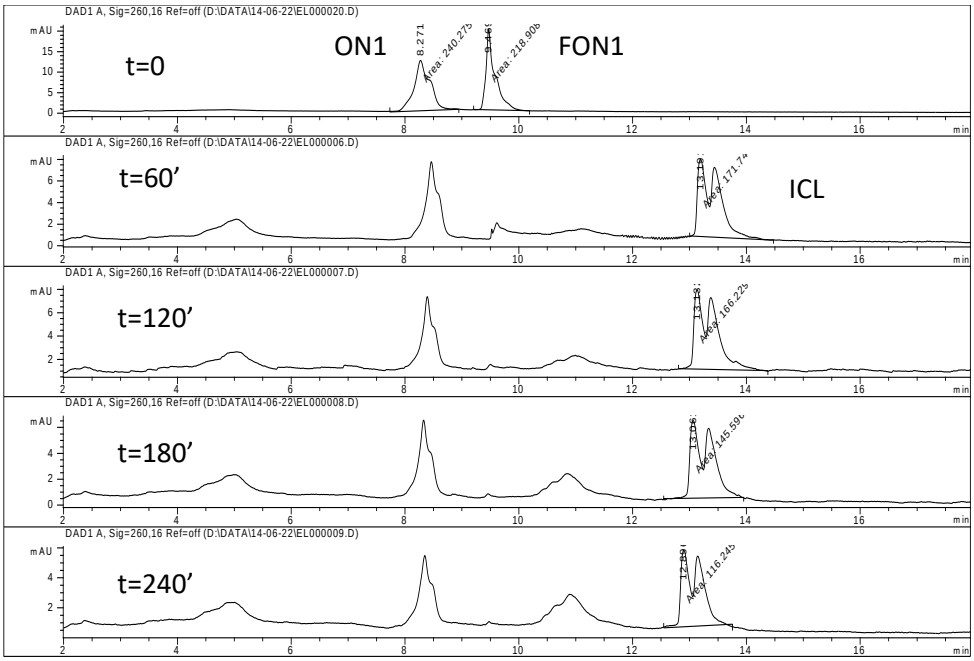

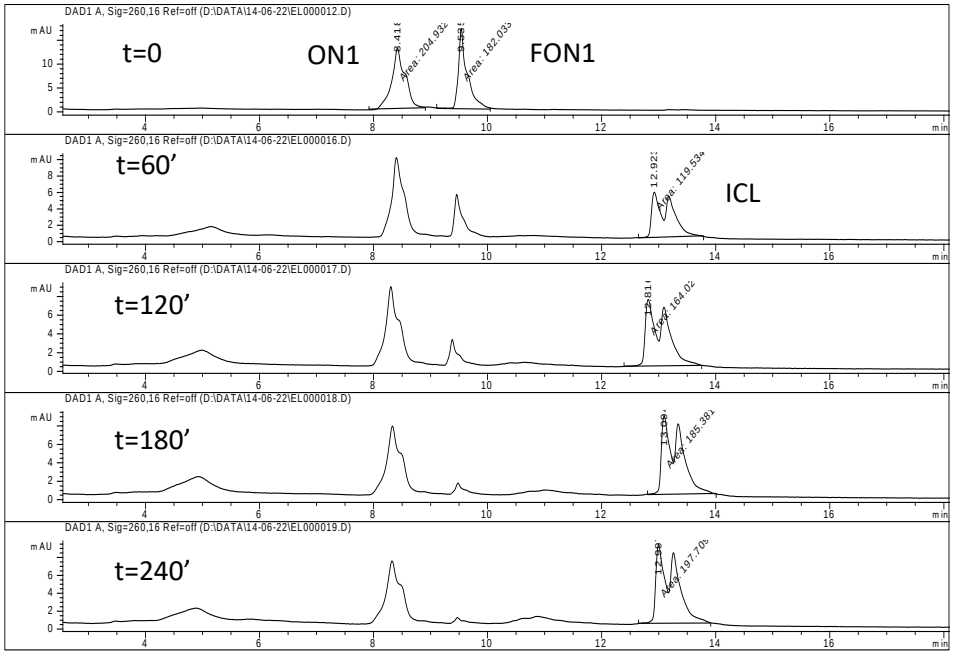

Figure 9. HPLC traces of crosslinking experiments using [duplex] = 20 μM, [TriPyCOOH] = 5 μM. Top: white light; bottom: red light.

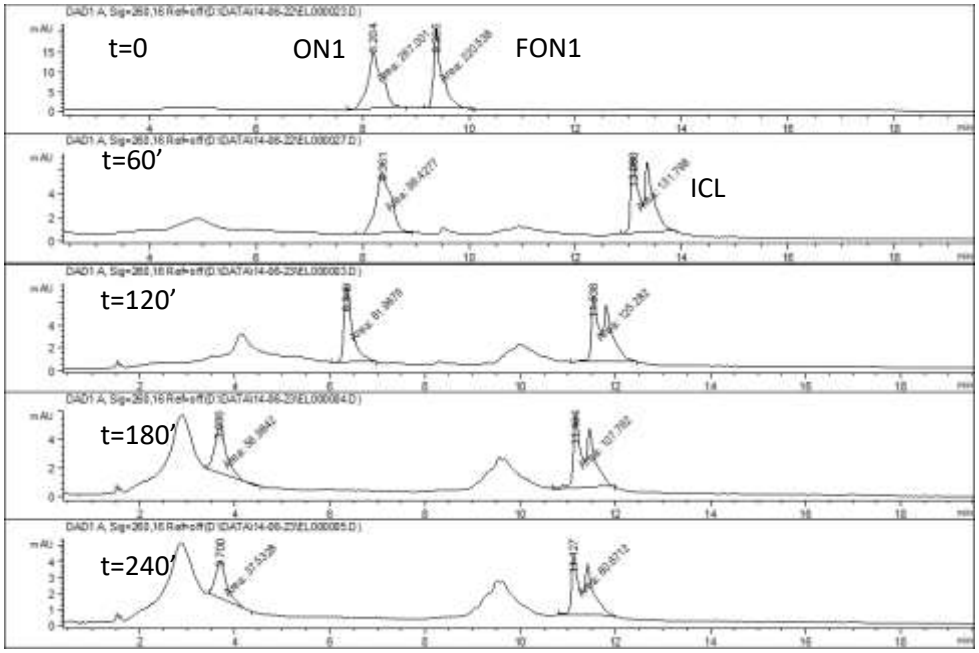

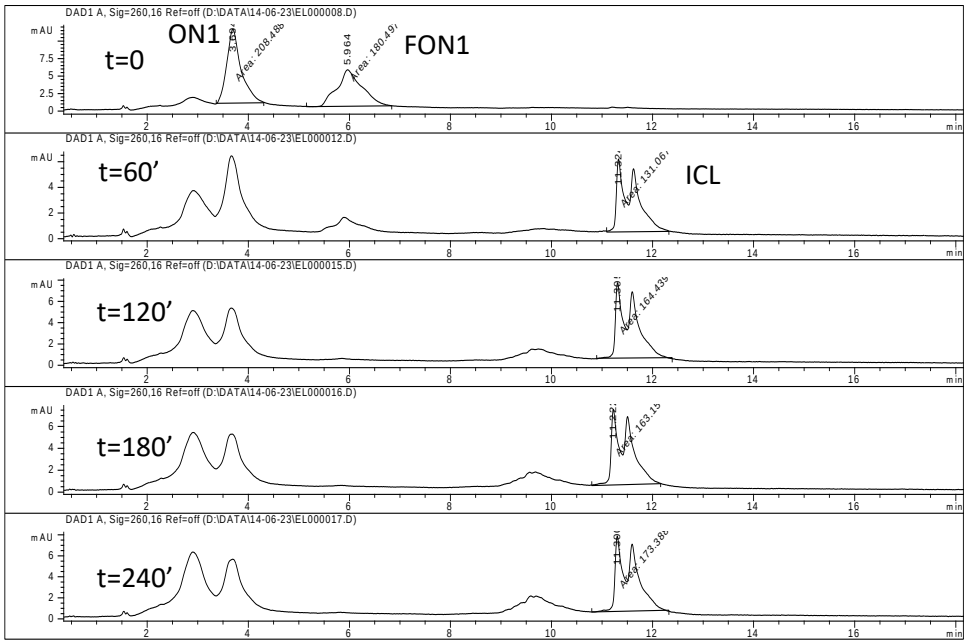

Figure 10. HPLC traces of crosslinking experiments using [duplex] = 20 μM, [TriPyCOOH] = 10 μM. Top: white light; bottom: red light

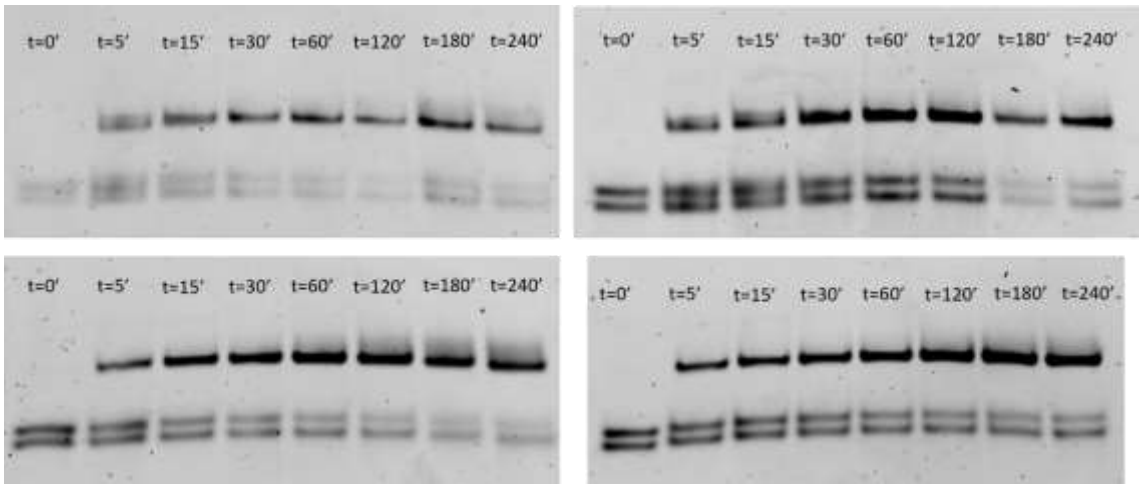

Figure 11. PAGE analysis of red and white evaluation crosslinking experiments. Top left: [duplex] = 20 μM, [TriPyCOOH] = 5 μM, white light; top right: [duplex] = 20 μM, [TriPyCOOH] = 5 μM, red light; bottom left: [duplex] = 20 μM, [TriPyCOOH] = 10 μM, white light; bottom right: [duplex] = 20 μM, [TriPyCOOH] = 10 μM, red light.

X.5.1.4. ICL experiments using TT1 in solution

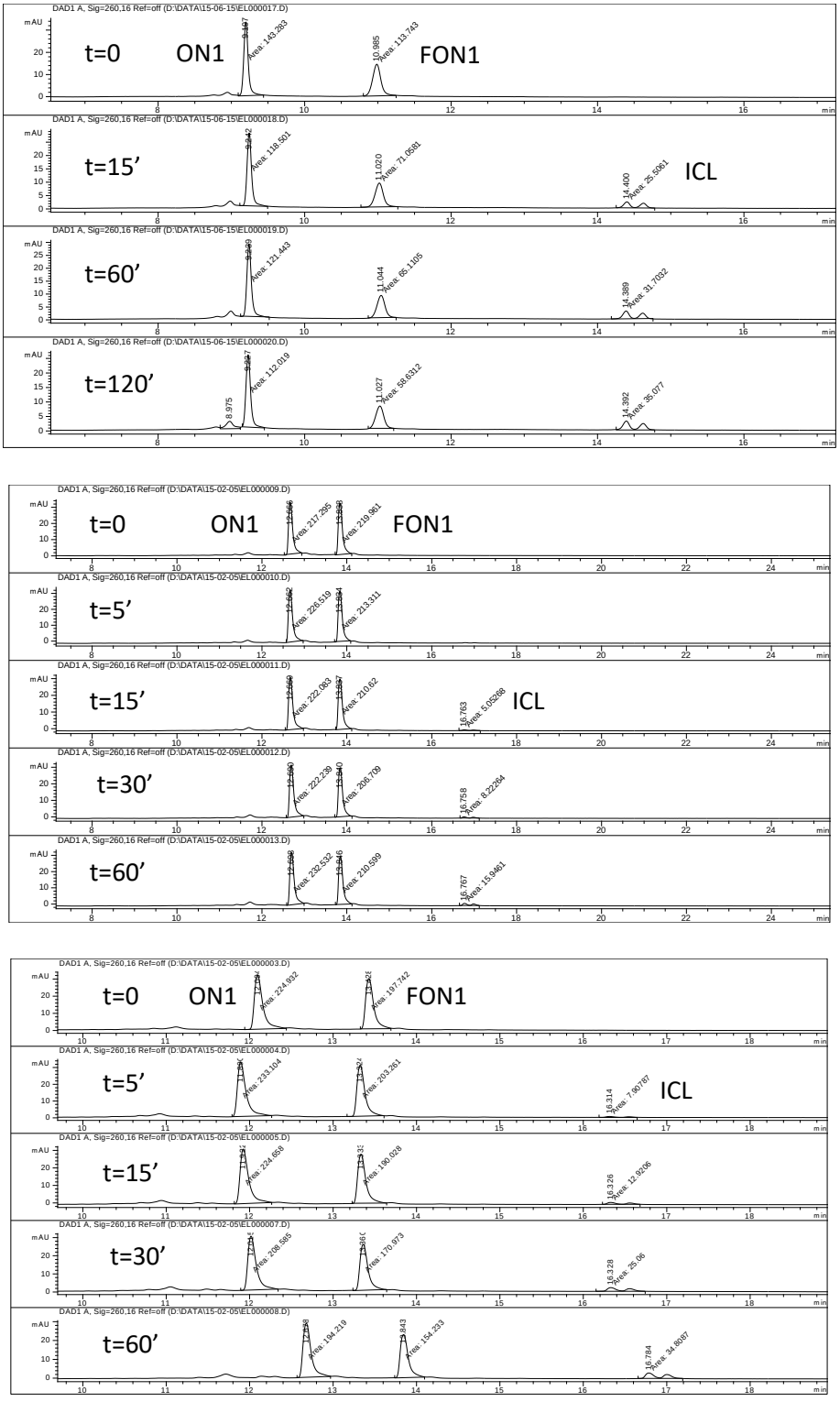

Figure 12. HPLC traces of crosslinking experiments using TT1. Top: [duplex] = 2 μM, [TT1] = 2 μM; middle: [duplex] = 20 μM, [TT1] = 5 μM; bottom: [duplex] = 20 μM, [TT1] = 10 μM

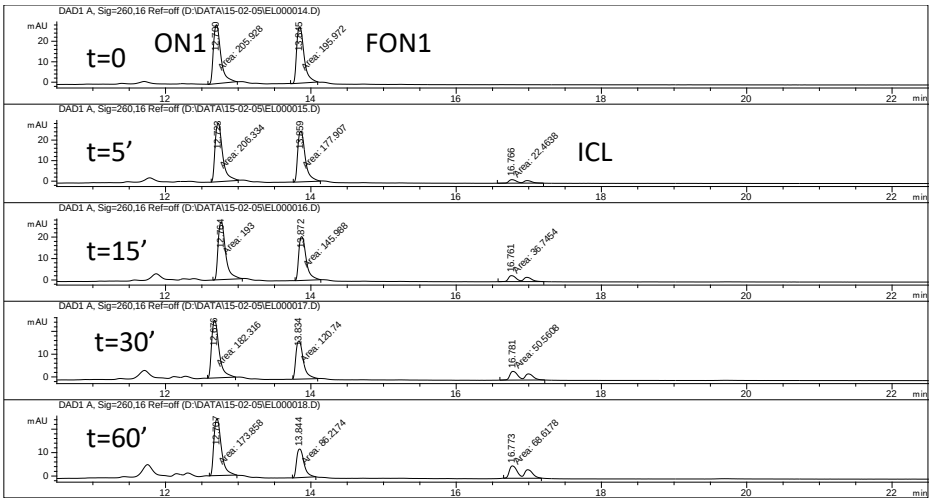

Figure 13. HPLC traces of crosslinking experiments using TT1. [duplex] = 20 μM, [TT1] = 20 μM.

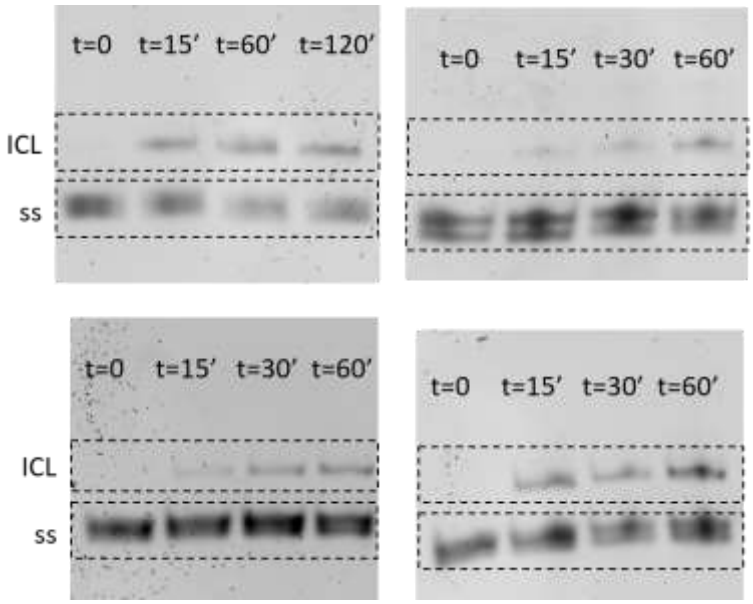

Figure 14. PAGE analysis using TT1. Top left: [duplex] = 2 μM, [TT1] = 2 μM; top right: [duplex] = 20 μM, [TT1] = 5 μM; bottom left: [duplex] = 20 μM, [TT1] = 10 μM; bottom right: [duplex] = 20 μM, [TT1] = 20 μM

X.5.1.5. ICL experiements using a non-nucleobase furan building block.

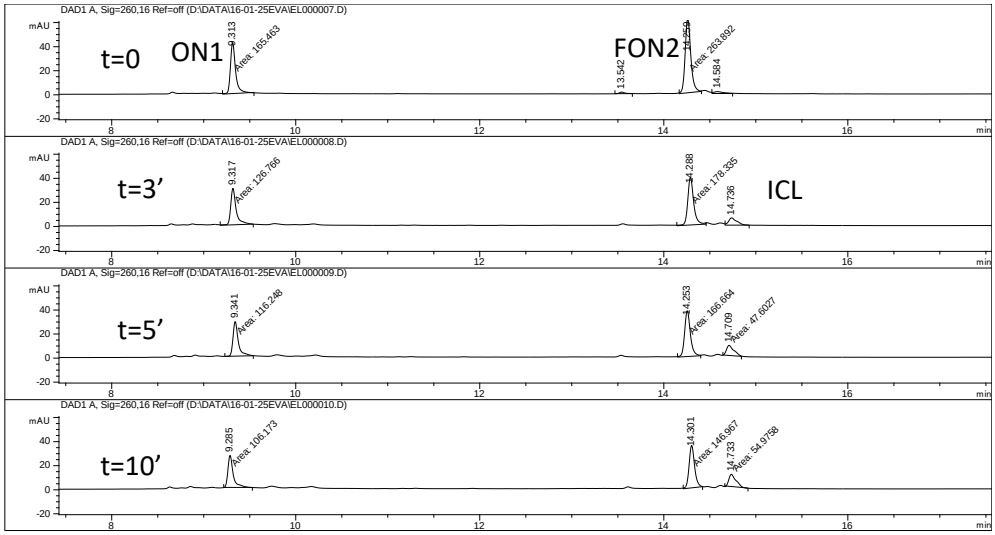

Figure 15. HPLC traces of crosslinking experiments using Ce6 and FON2/ON1 duplex. [duplex] = 2 μM, [Ce6] = 2 μM;

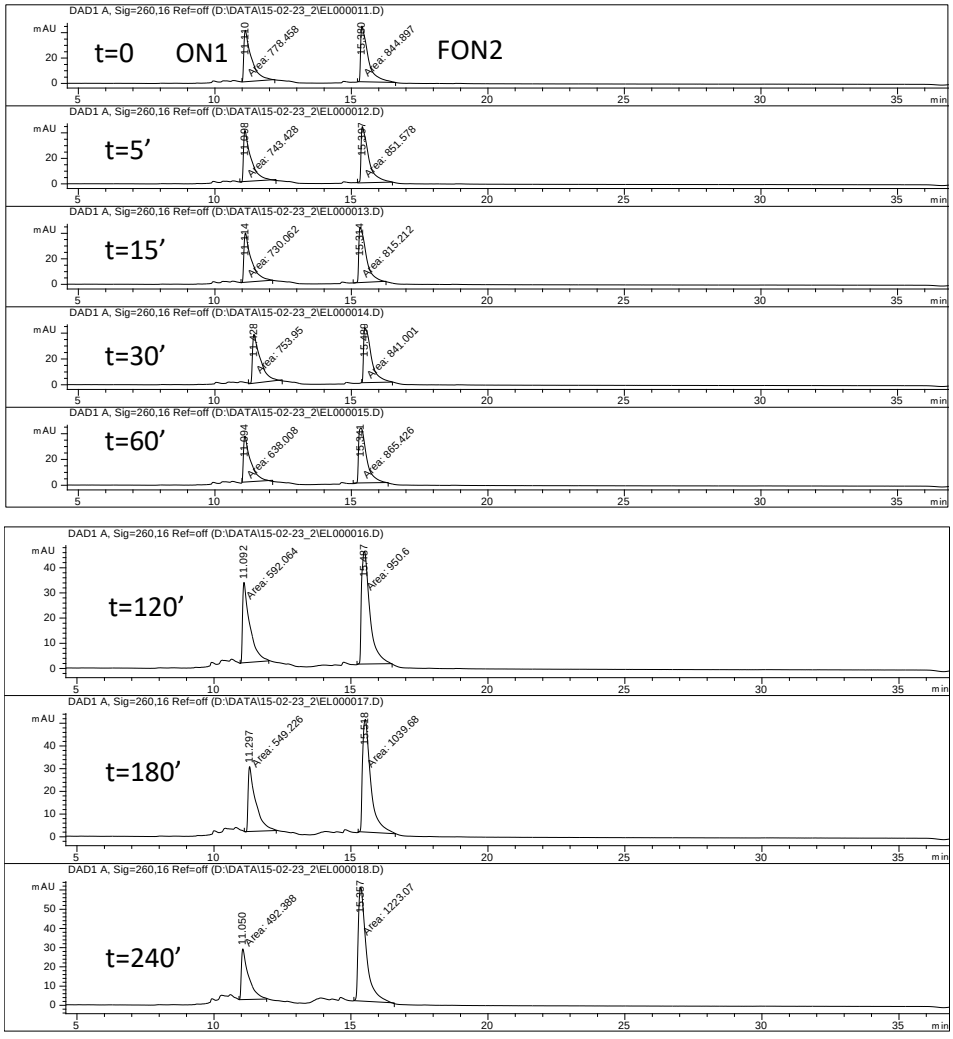

Figure 16. HPLC traces of crosslinking experiments using TriPyCOOH and FON2/ON1 duplex. [duplex] = 20 μM, [TriPyCOOH] = 5 μM.

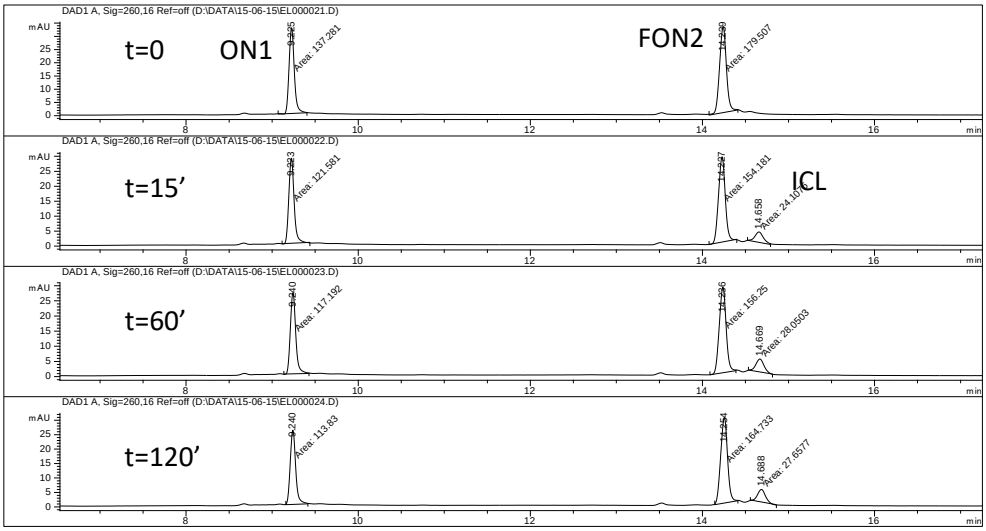

Figure 17. HPLC traces of crosslinking experiments using TT1 and FON2/ON1 duplex. [duplex] = 2 μM, [TT1] = 2 μM.

X.5.2.Experimental data for chapter IV

X.5.2.1. Characterisation of the synthesised ODNs

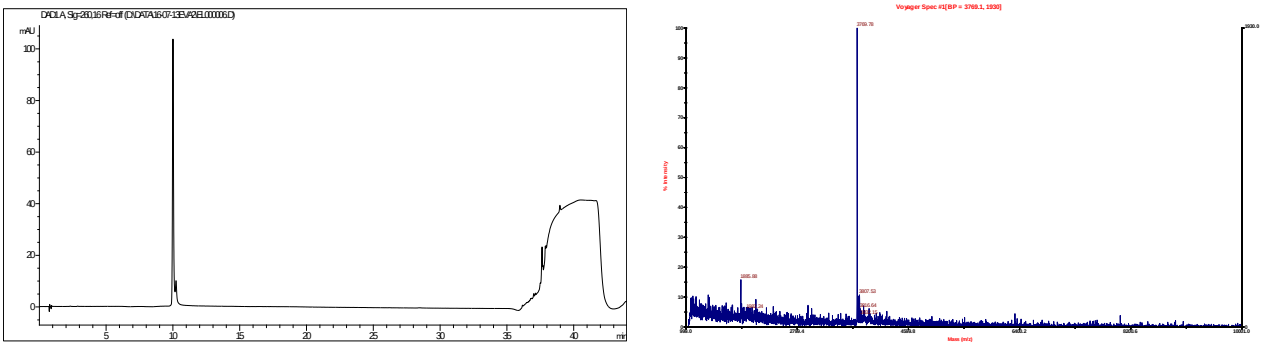

Figure 18. Left: HPLC chromatogram of ON2. Right: MALDI-TOF MS analysis. Expected mass: 3769 Da. Observed mass: 3770 Da

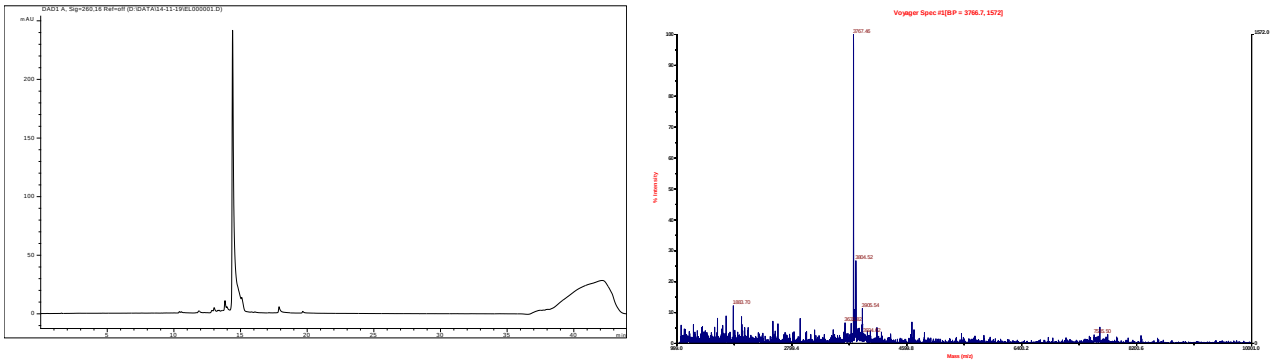

Figure 19. Left: HPLC chromatogram of ON4. Right: MALDI-TOF MS analysis. Expected mass: 3765 Da. Observed mass: 3767 Da

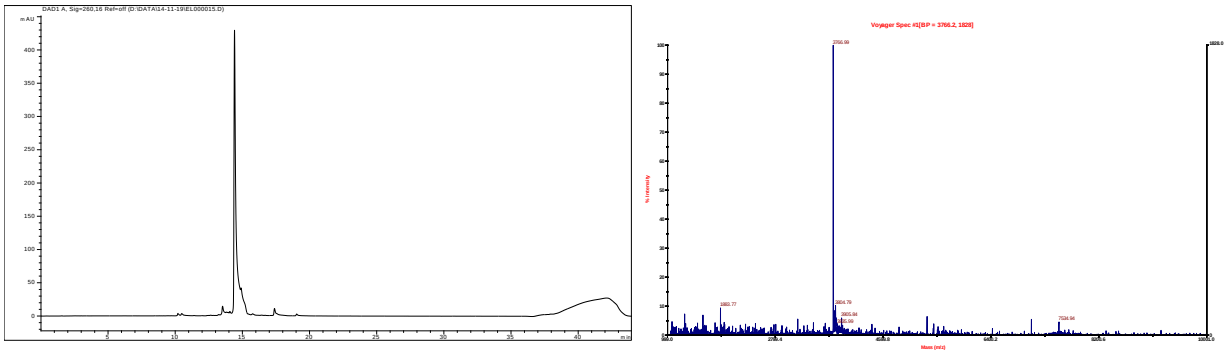

Figure 20. Left: HPLC chromatogram of ON5. Right: MALDI-TOF MS analysis. Expected mass: 3765 Da. Observed mass: 3767 Da

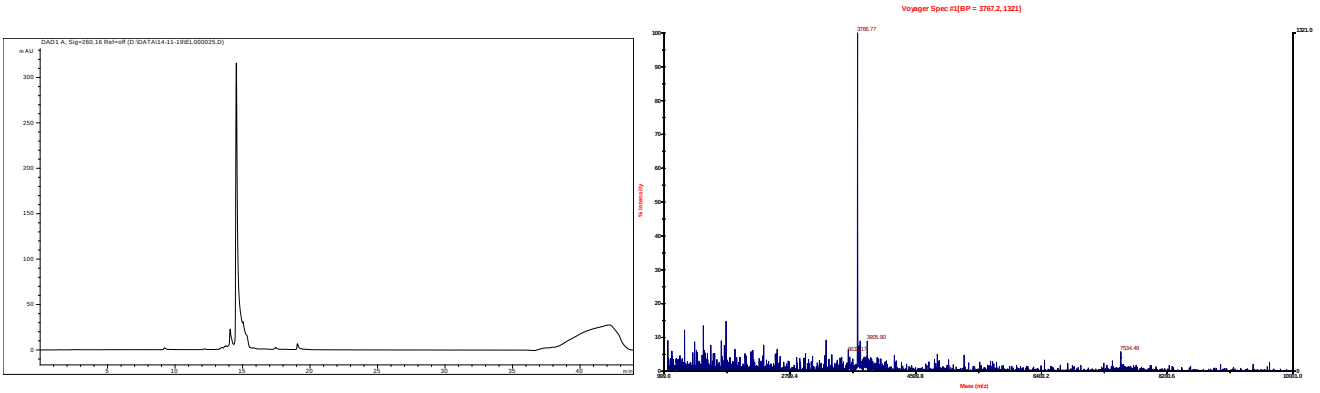

Figure 21. Left: HPLC chromatogram of ON6. Right: MALDI-TOF MS analysis. Expected mass: 3765 Da. Observed mass: 3767 Da

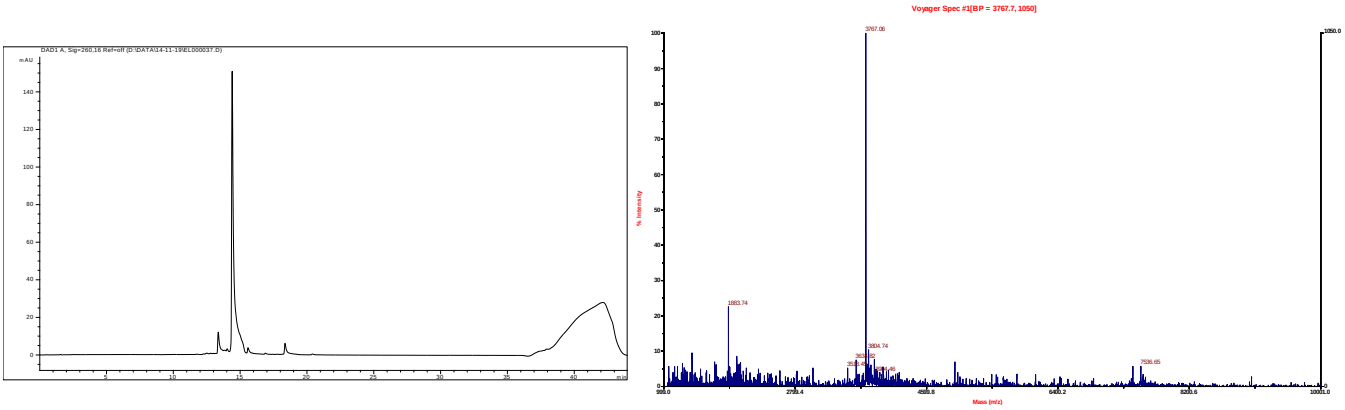

Figure 22. Left: HPLC chromatogram of ON7. Right: MALDI-TOF MS analysis. Expected mass: 3765 Da. Observed mass: 3767 Da

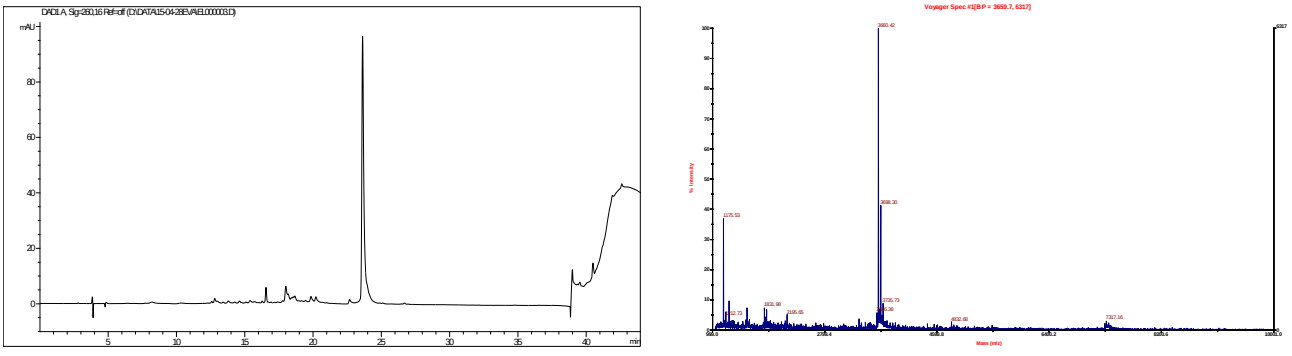

Figure 23. Left: HPLC chromatogram of FON3. Right: MALDI-TOF MS analysis. Expected mass: 3659 Da. Observed mass: 3660 Da

X.5.2.2. Characterisation of the photosensitiser conjugates

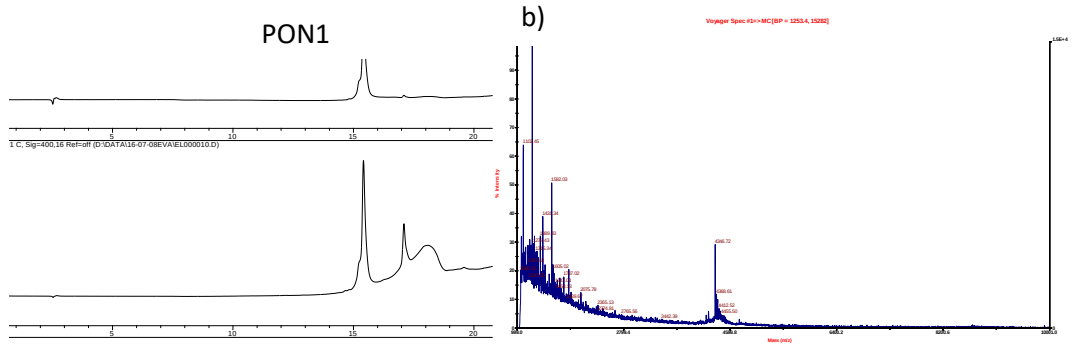

Figure 24. a) HPLC chromatograms of purified PON1 at 260 and 400 nm using a Discovery BIO Wide Pore C5 column. b) MALDI-TOF analysis. Observed mass: 4347 Da. Expected mass: 4347 Da

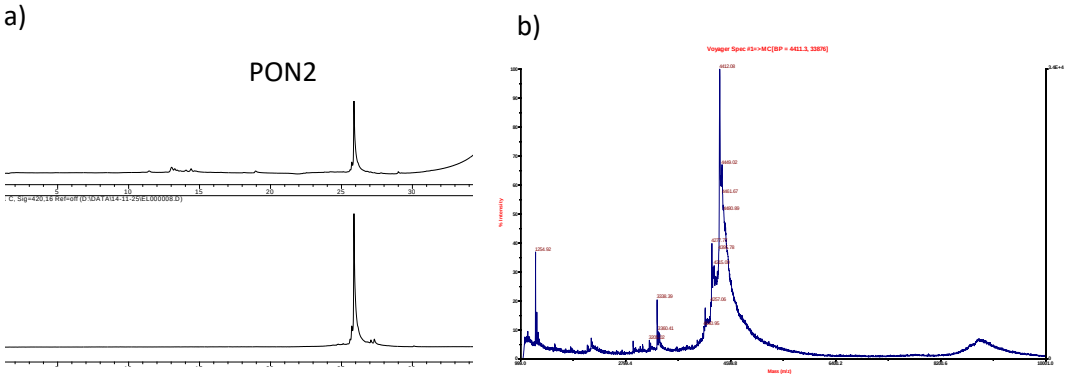

Figure 25. a) HPLC chromatograms of purified PON2 at 260 and 420 nm analysed using an Aeris Wide Pore column. b) MALDI-TOF analysis. Observed mass: 4412 Da. Expected mass: 4412 Da

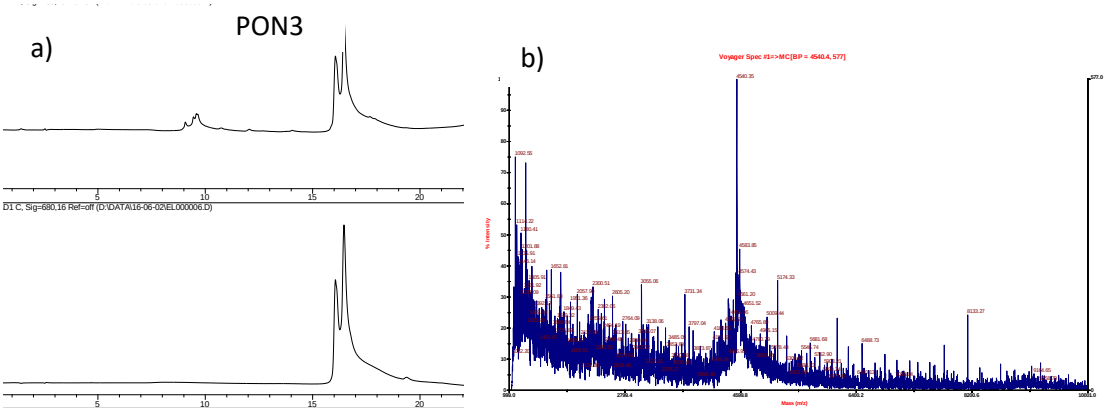

Figure 26. a) HPLC chromatograms of purified PON3 at 260 and 680 nm analysed using a Discovery BIO Wide Pore C5 column. Double signal is appearing due to the fact that TT1 is used as a regioisomeric mixture. b) MALDI-TOF analysis. Observed mass: 4540 Da. Expected mass: 4539 Da.

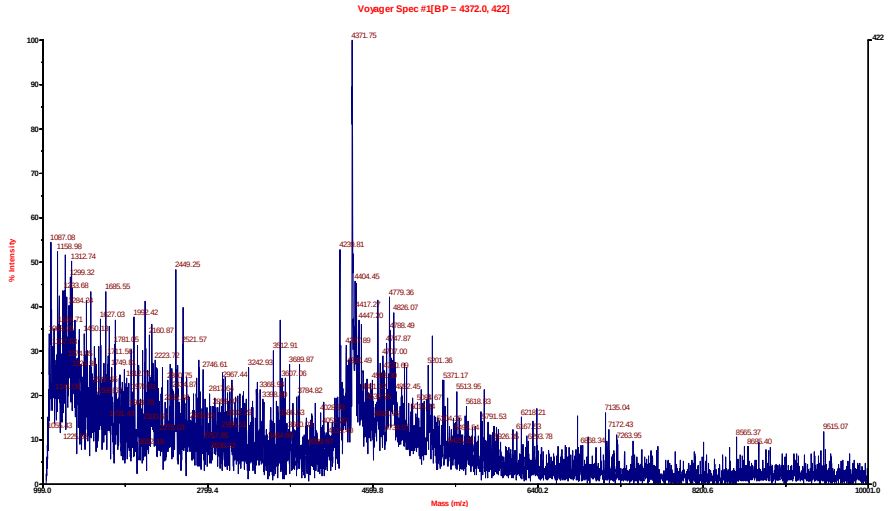

Figure 27. PON4 MALDI-TOF MS analysis. Expected mass: 4370 Da. Observed mass: 4372 Da

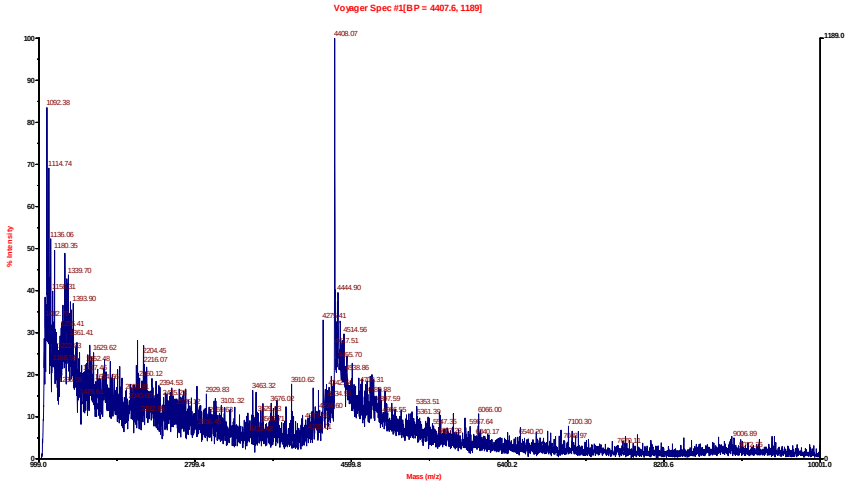

Figure 28. PON5 MALDI-TOF MS analysis. Expected mass: 4408 Da. Observed mass: 4408 Da

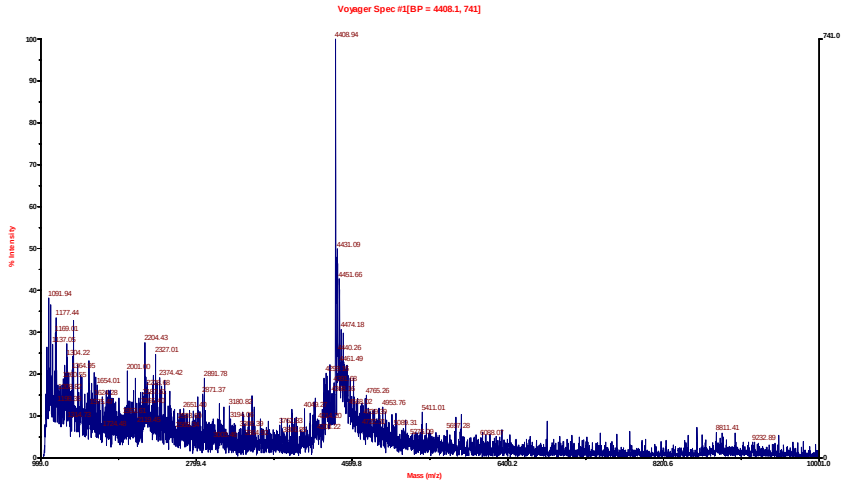

Figure 29. PON6 MALDI-TOF MS analysis. Expected mass: 4408 Da. Observed mass: 4409 Da

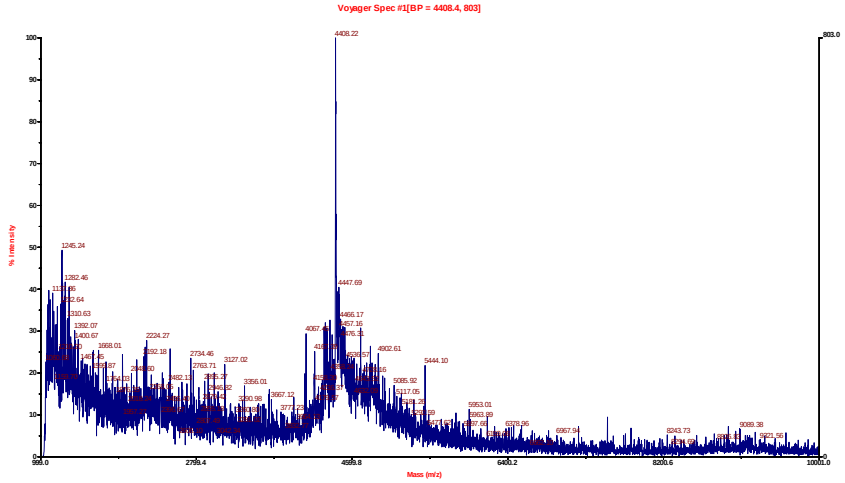

Figure 30. PON7 MALDI-TOF MS analysis. Expected mass: 4408 Da. Observed mass: 4408 Da

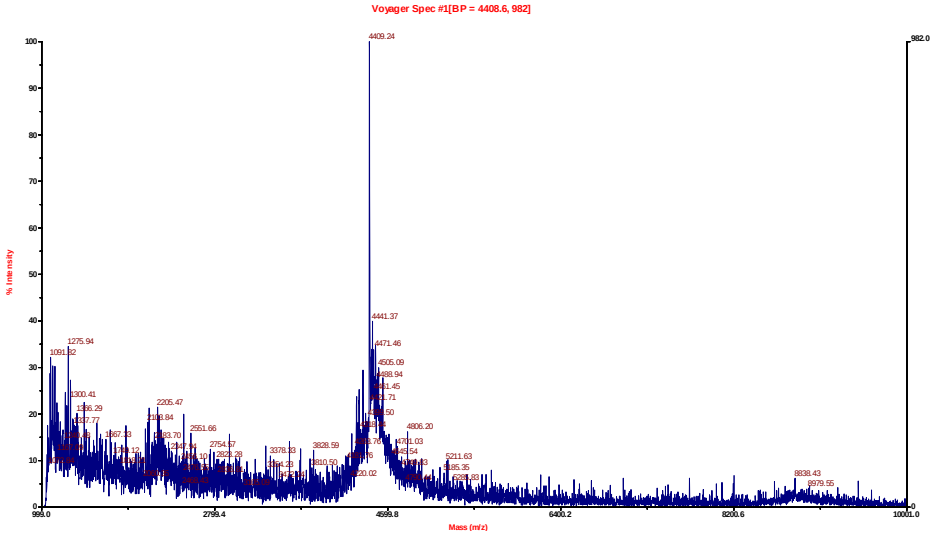

Figure 31. PON8 MALDI-TOF MS analysis. Expected mass: 4408 Da. Observed mass: 4409 Da

X.5.2.3. ICL experiments using photosensitiser conjugates and FON1

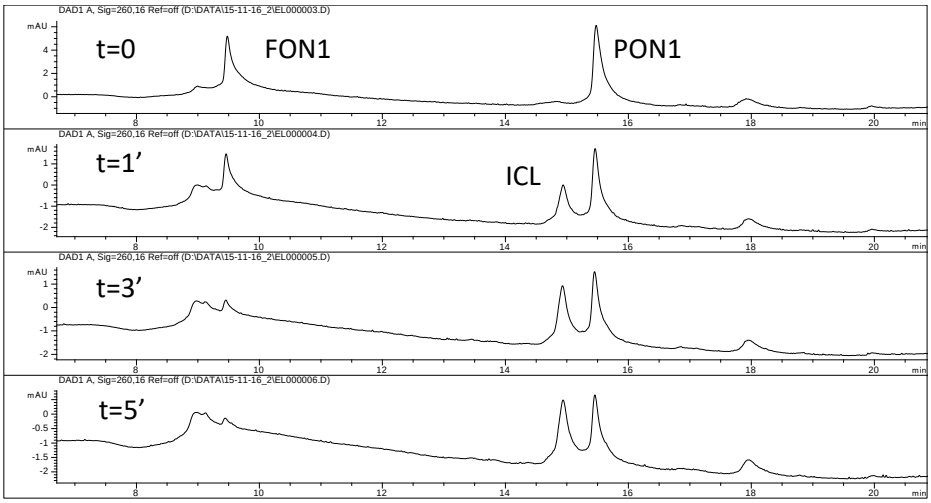

Figure 32. HPLC traces at 260 nm of ICL experiments using PON1/FON1 at 2 μM concentration.

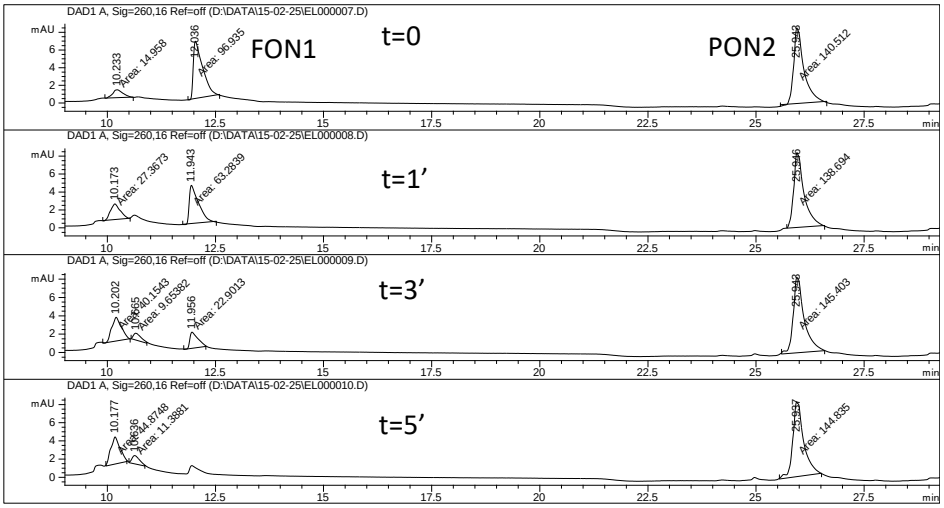

Figure 33. HPLC traces at 260 nm of ICL experiments using PON2/FON1 at 2 μM concentration.

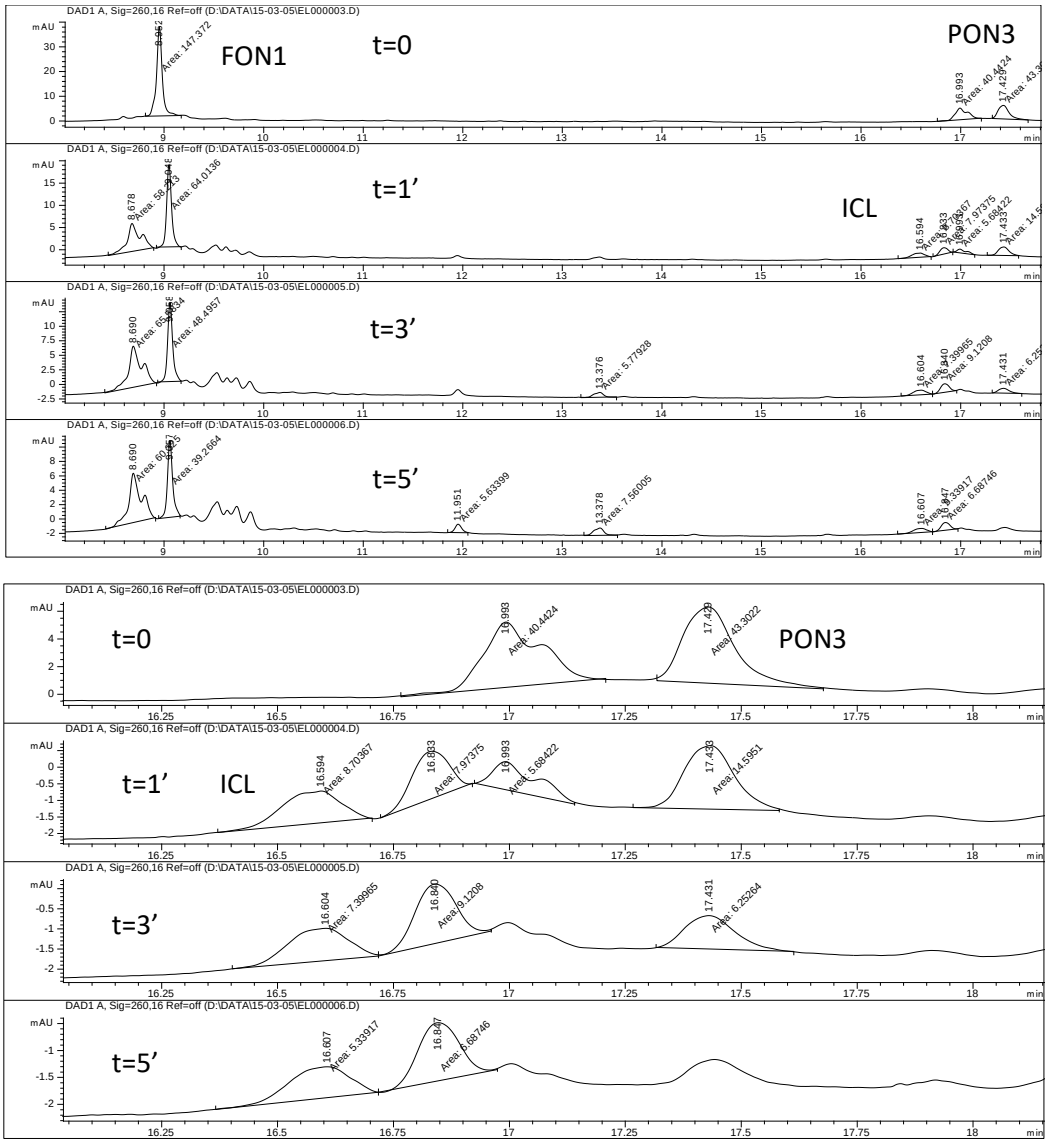

Figure 34. Top: HPLC traces at 260 nm of ICL experiments using PON3/FON1 at 2 μM concentration. Bottom: zoom in of the region where the crosslinked adduct appears.

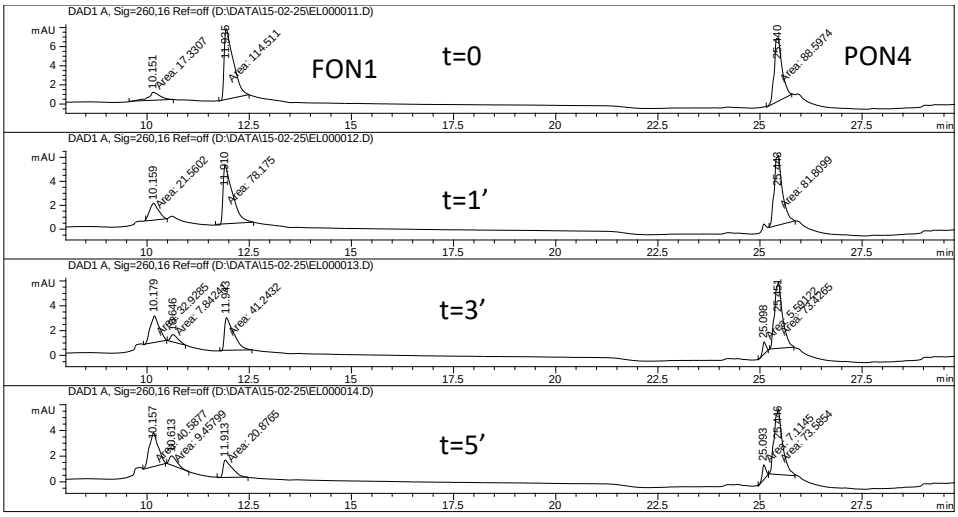

Figure 35. HPLC traces at 260 nm of ICL experiments using PON4/FON1 at 2 μM concentration.

X.5.2.4. ICL experiments at lower temperature

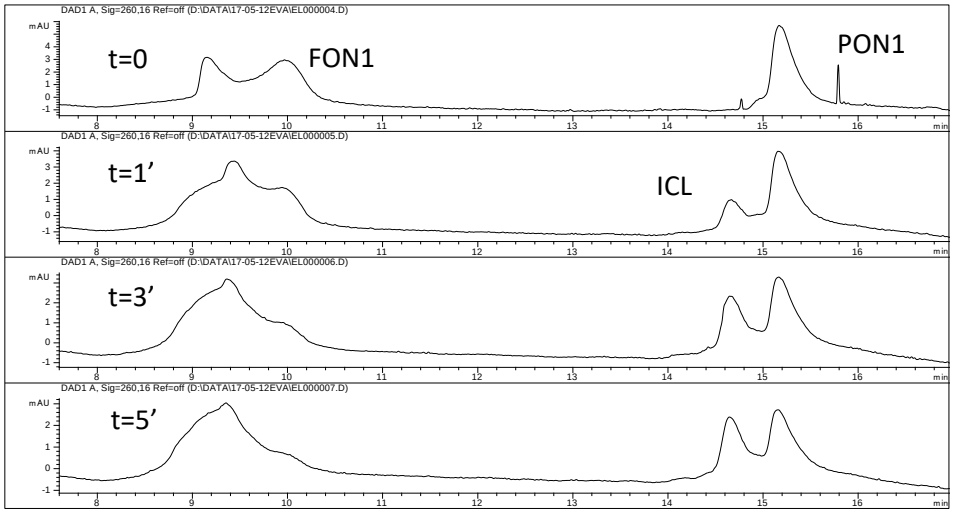

Figure 36. HPLC traces at 260 nm of ICL experiments using PON1/FON1 at 2 μM concentration at 10ºC.

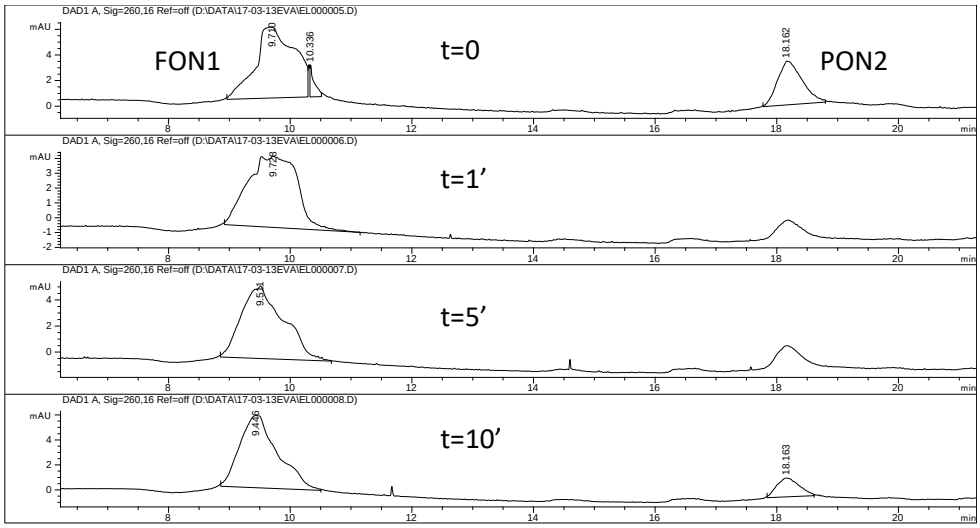

Figure 37. HPLC traces at 260 nm of ICL experiments using PON2/FON1 at 2 μM concentration at 10ºC.

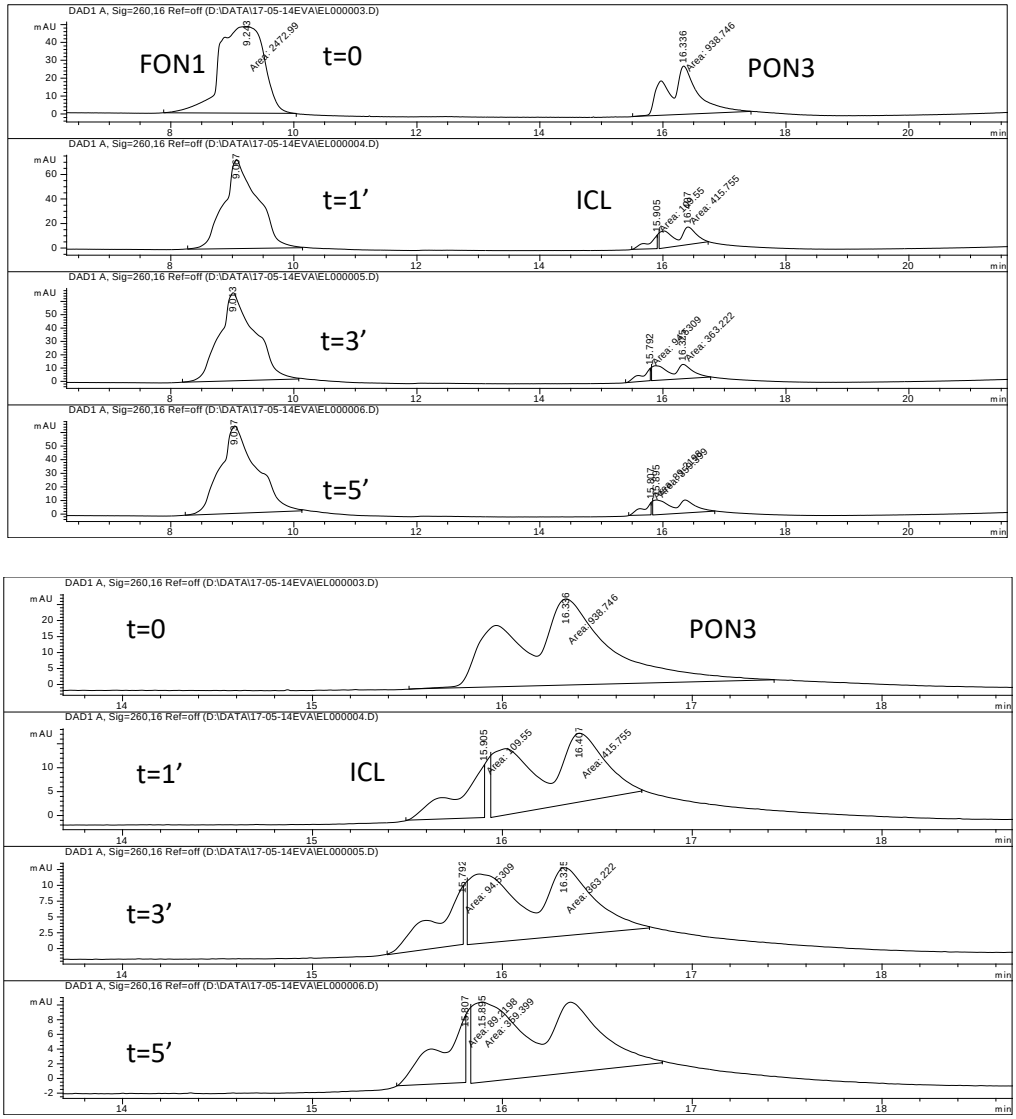

Figure 38. Top: HPLC traces at 260 nm of ICL experiments using PON3/FON1 at 2 μM concentration at 10ºC. Bottom: zoom in of the region where the crosslinked adduct appears.

X.5.2.5. ICL experiments using a non-nucleobase furan building block

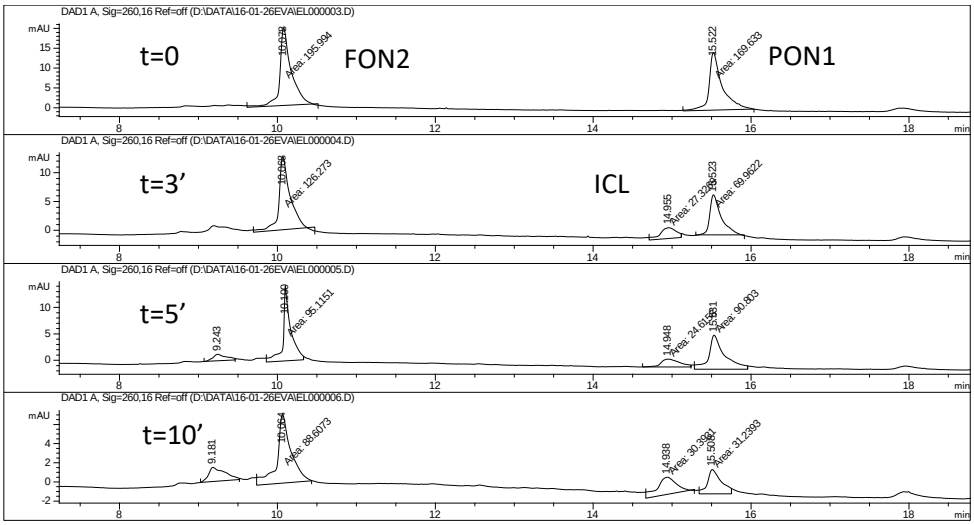

Figure 39. HPLC traces at 260 nm of ICL experiments using PON1/FON2 at 2 μM concentration.

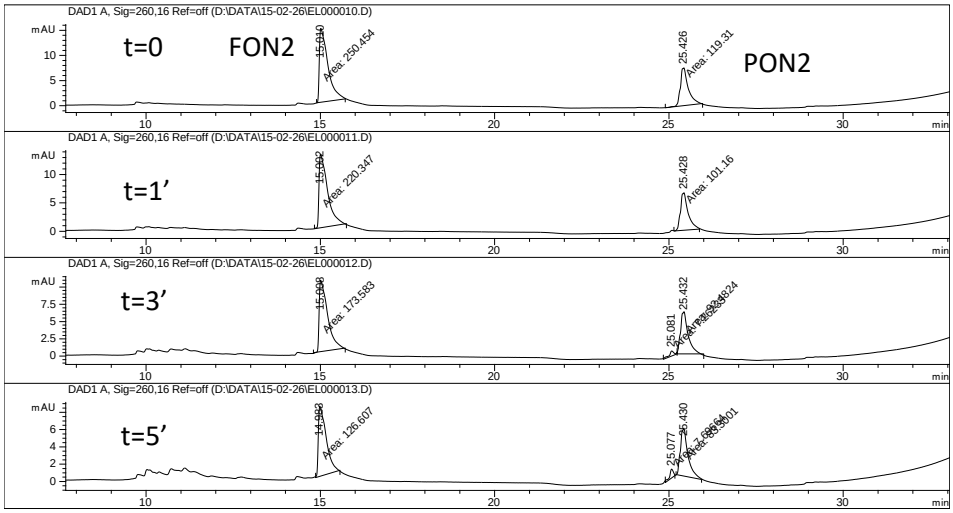

Figure 40. HPLC traces at 260 nm of ICL experiments using PON2/FON2 at 2 μM concentration.

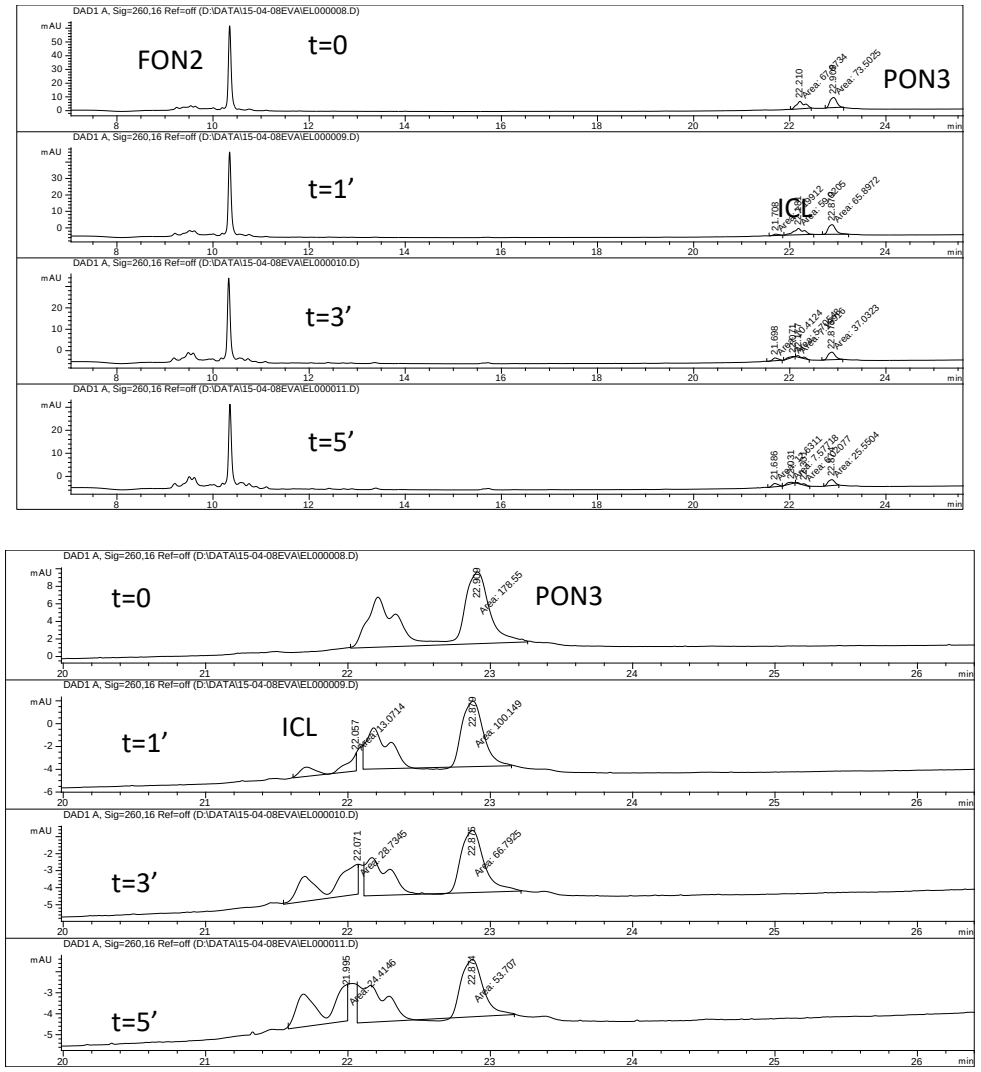

Figure 41. Top: HPLC traces at 260 nm of ICL experiments using PON3/FON2 at 2 μM concentration. Bottom: zoom in of the region where the crosslinked adduct appears.

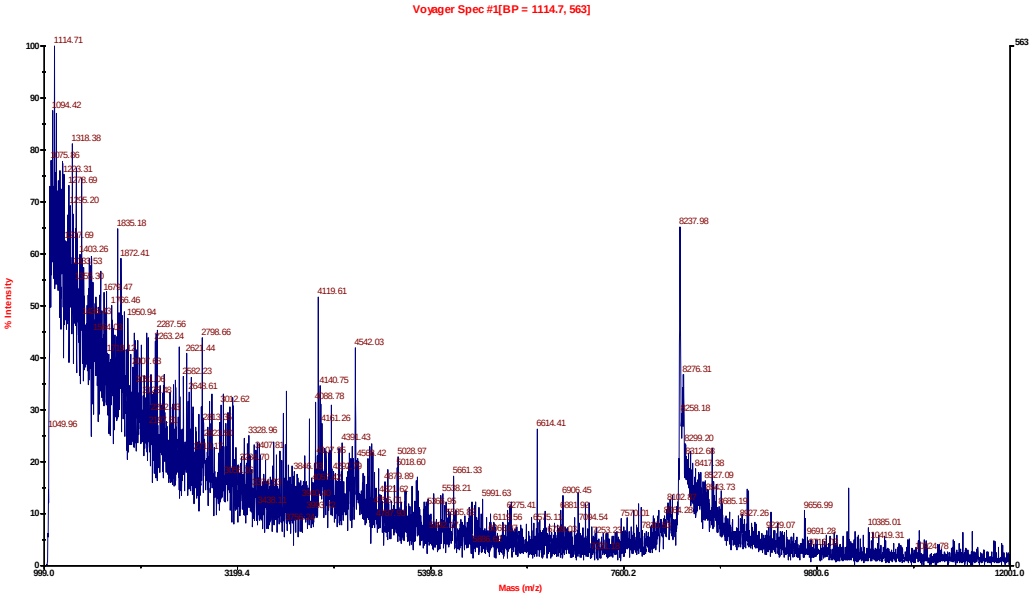

Figure 42. MALDI-TOF analysis of PON3/FON2 crosslinked adduct. Expected mass: 8237 Da; observed mass: 8238 Da

X.5.2.6. Distance evaluation ICL experiments

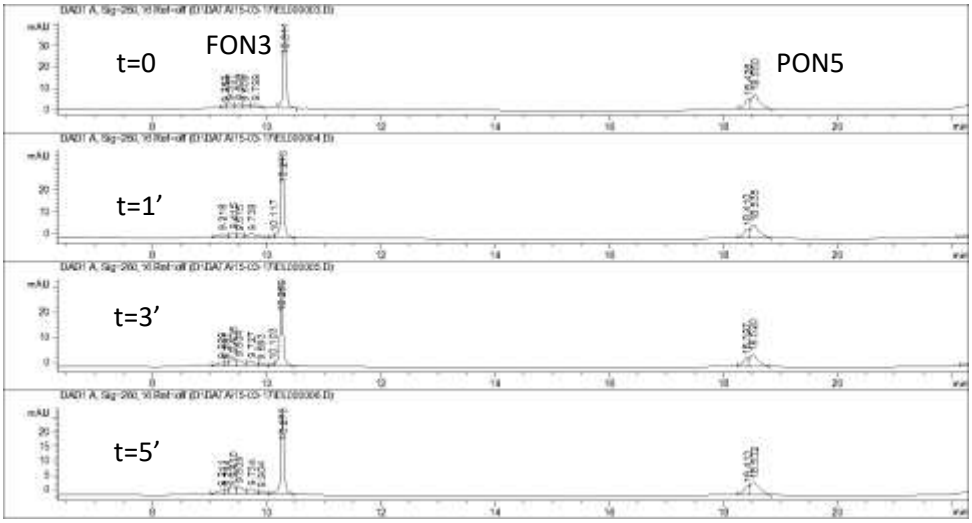

Figure 43. HPLC traces at 260 nm of ICL experiments using PON5/FON3 at 2 μM concentration.

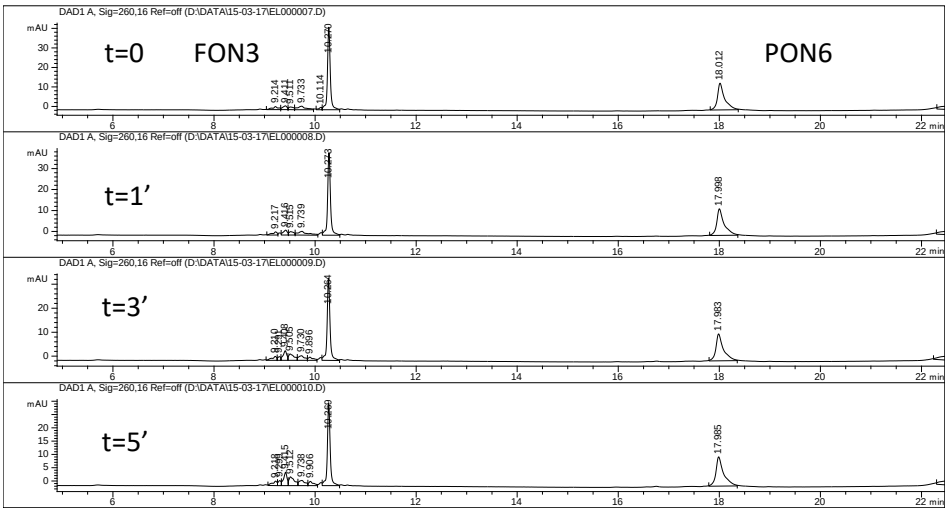

Figure 44. HPLC traces at 260 nm of ICL experiments using PON6/FON3 at 2 μM concentration.

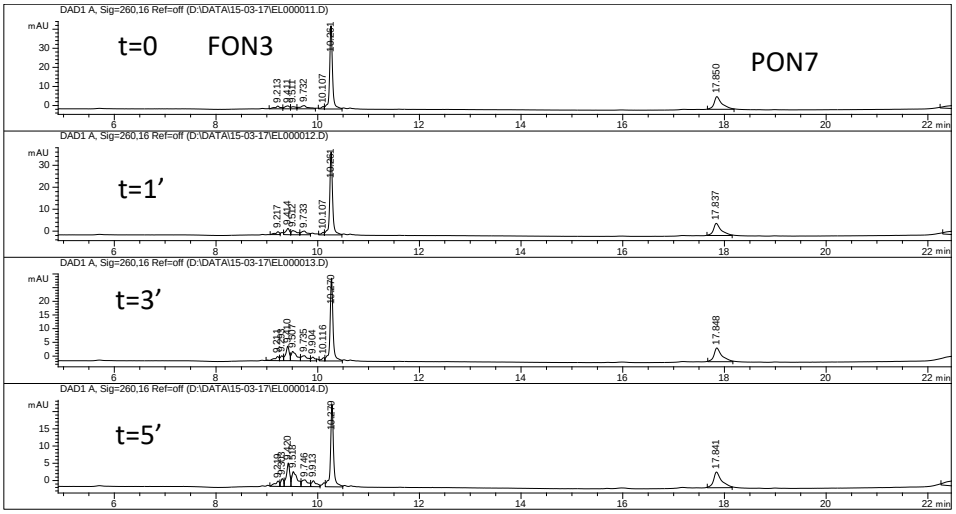

Figure 45. HPLC traces at 260 nm of ICL experiments using PON7/FON3 at 2 μM concentration.

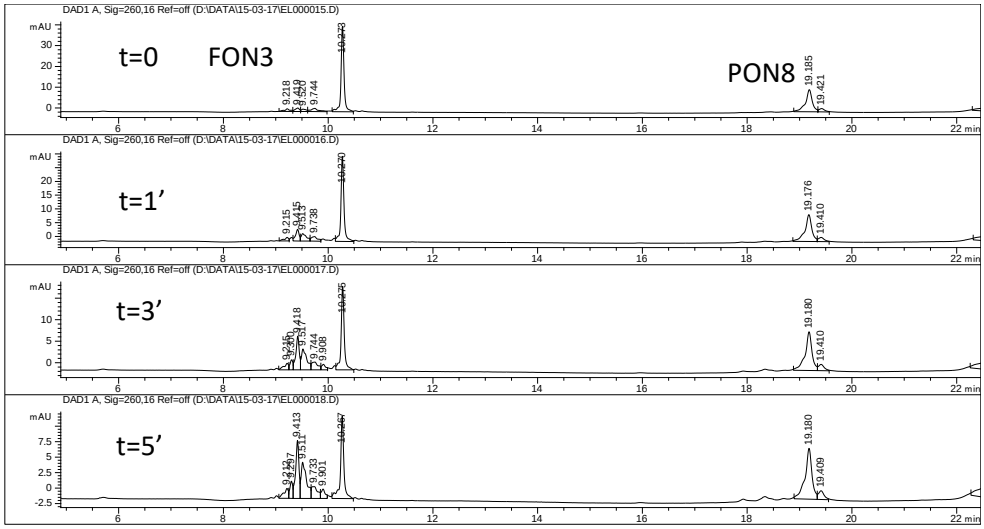

Figure 46. HPLC traces at 260 nm of ICL experiments using PON8/FON3 at 2 μM concentration.

X.5.3.Experimental data for chapter V

X.5.3.1. Characterisation of the synthesised ODNs

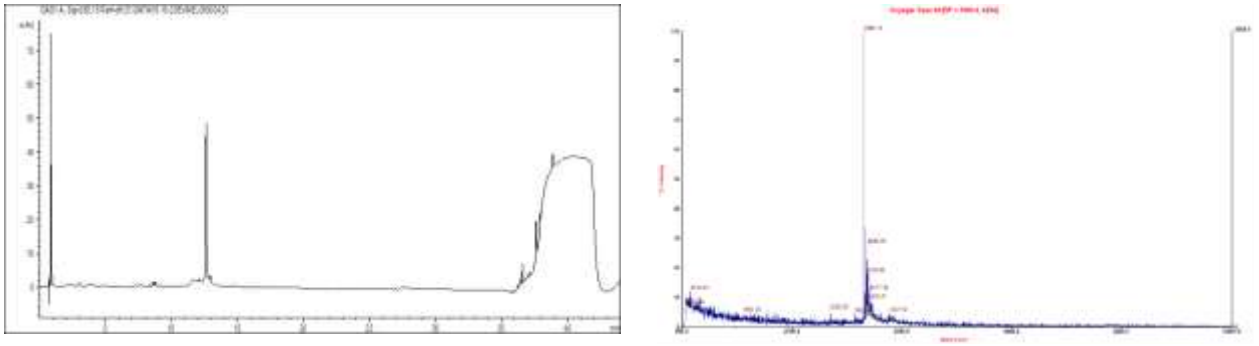

Figure 48. HPLC chromatogram of FON4 after preliminary Seppak purification. Right: MALDI-TOF MS analysis. Expected mass: 3979 Da. Observed mass: 3980 Da

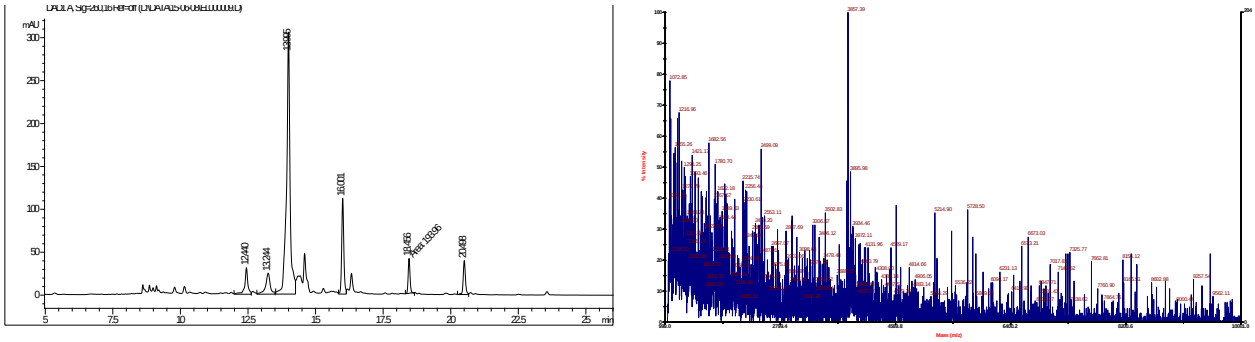

Figure 47. Left: HPLC chromatogram of FON5 after preliminary Seppak purification. Right: MALDI-TOF MS analysis. Expected mass: 3765 Da. Observed mass: 3767 Da

X.5.3.2. Characterisation of the photosensitiser conjugates

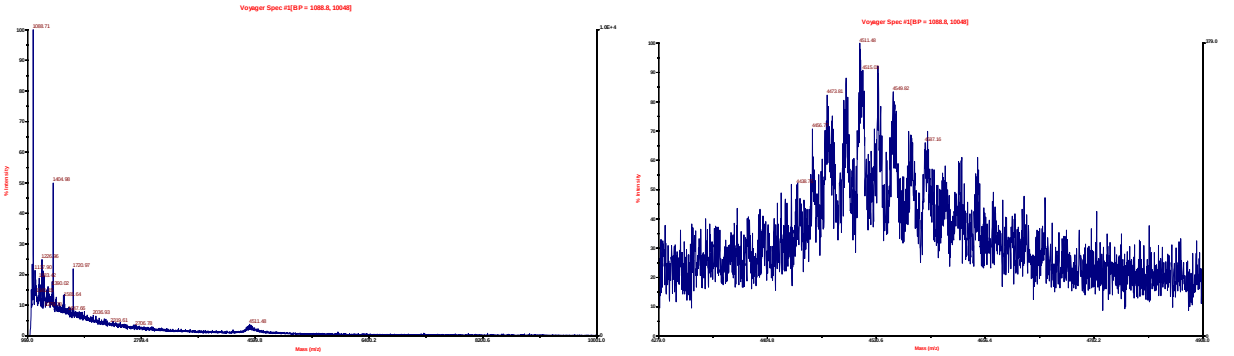

Figure 49. MALDI-TOF analysis of the conjugation between FON5 and Ce6. The expected mass (4439 Da) could not be observed. Right: zoom in of the broad signal.

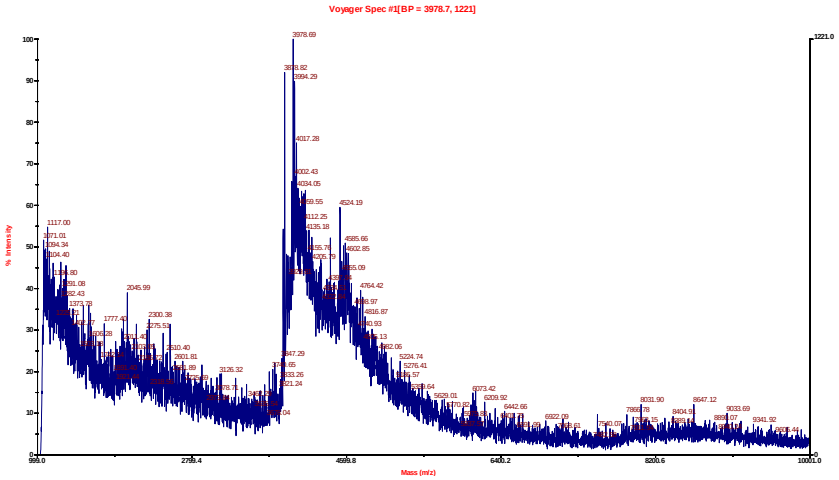

Figure 50. MALDI-TOF analysis of the conjugation between FON5 and TriPyCOOH. The expected mass (4504 Da) could not be observed.

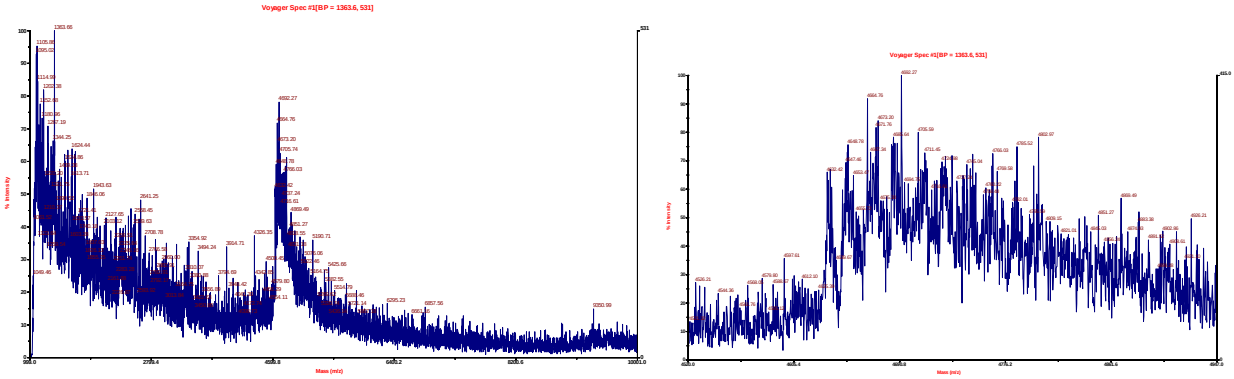

Figure 51. MALDI-TOF analysis of the conjugation between FON5 and TT1. The expected mass (4631 Da) could be observed within the boar signal. Right: zoom in of the broad signal.

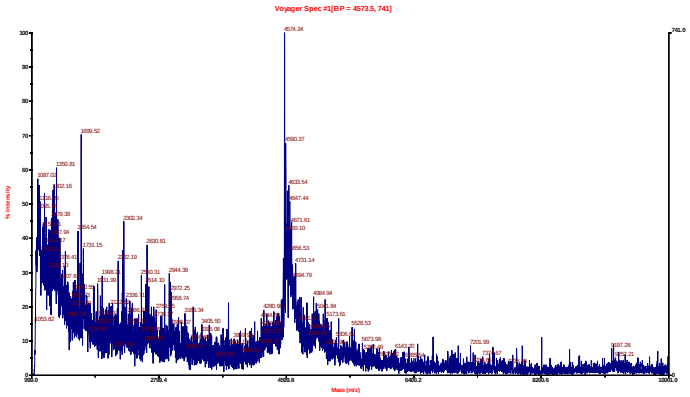

Figure 52. MALDI-TOF analysis of the conjugation between FON4 and Ce6. The observed mass (4574 Da) corresponds to the oxidised probe (non-oxidised expected =4556 Da)

X.5.3.3. ICL experiments using Ce6 self-activating probe

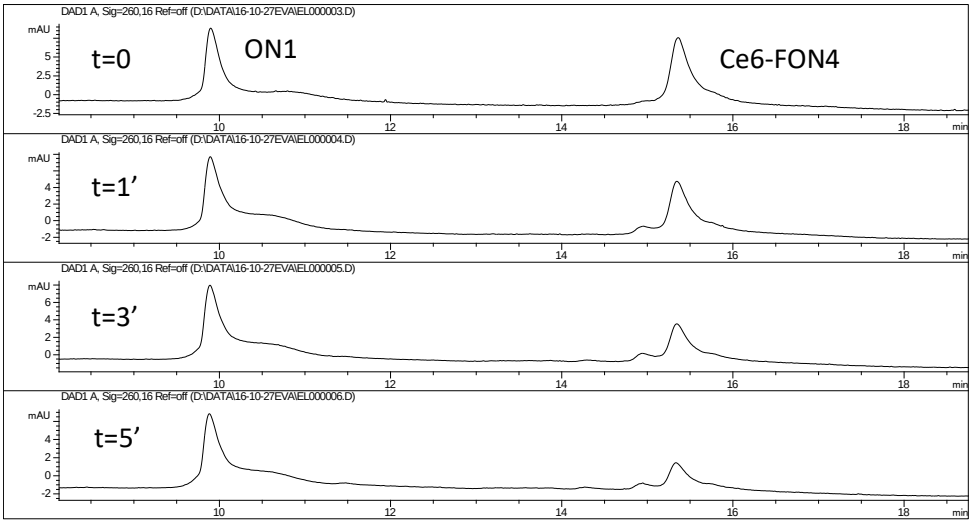

Figure 53. HPLC traces at 260 nm of ICL experiments using Ce6-FON4/ON1 at 2 μM concentration.

X.5.3.4. ICL experiment using TT1 self-activating probe

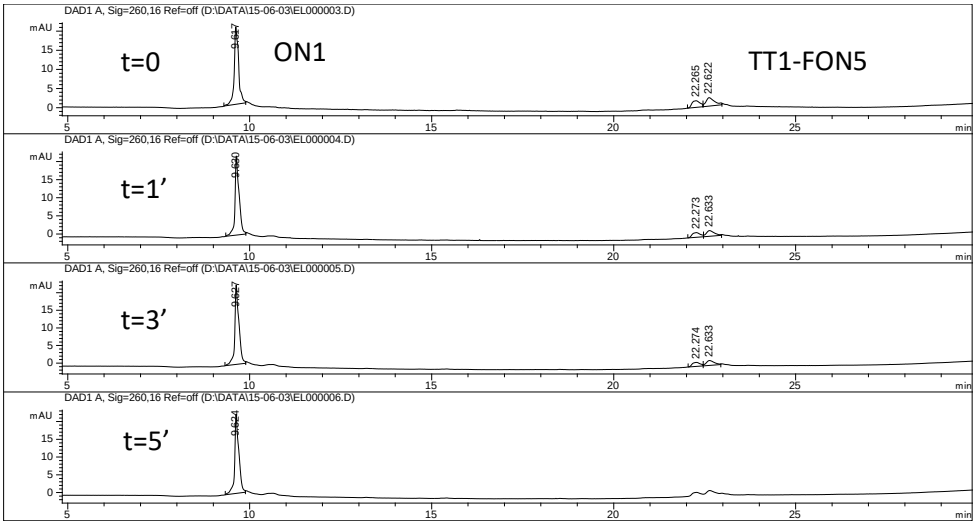

Figure 54. HPLC traces at 260 nm of ICL experiments using TT1-FON5/ON1 at 2 μM concentration.

X.5.3.5. ICL experiments using the templated system

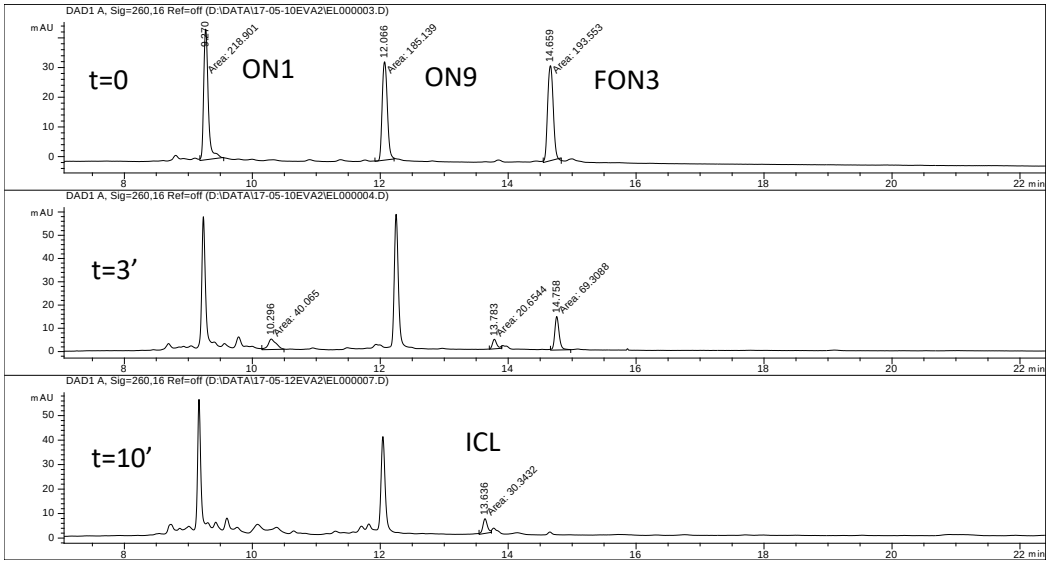

Figure 55. HPLC traces of ICL experiments using the templated ON1/ON9/FON3 at 200 nM concentration and Ce6 at 20 μM concentration.

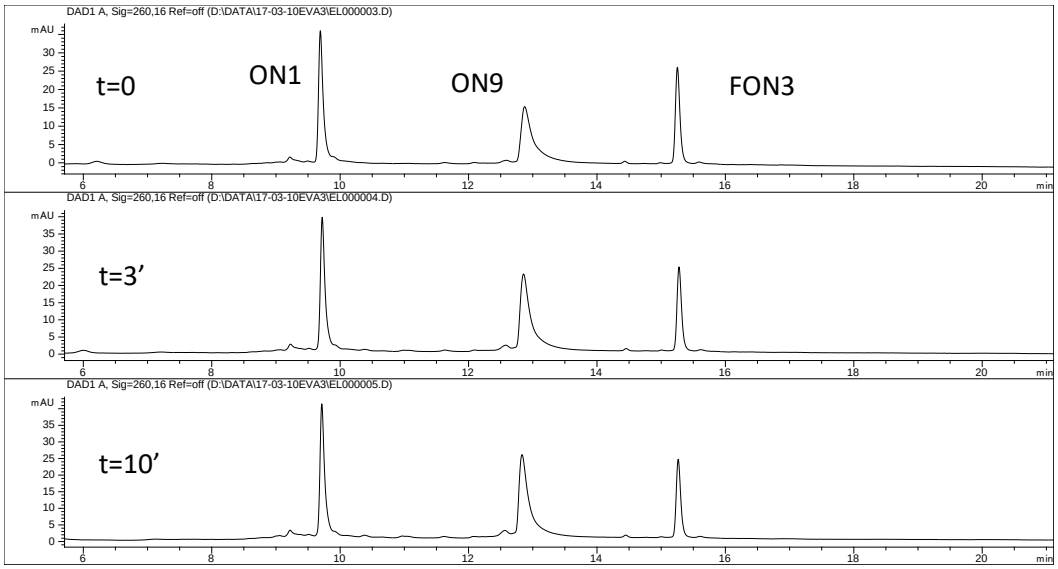

Figure 56. HPLC traces of ICL experiments using the templated ON1/ON9/FON3 at 200 nM concentration and Ce6 at 200 nM concentration.

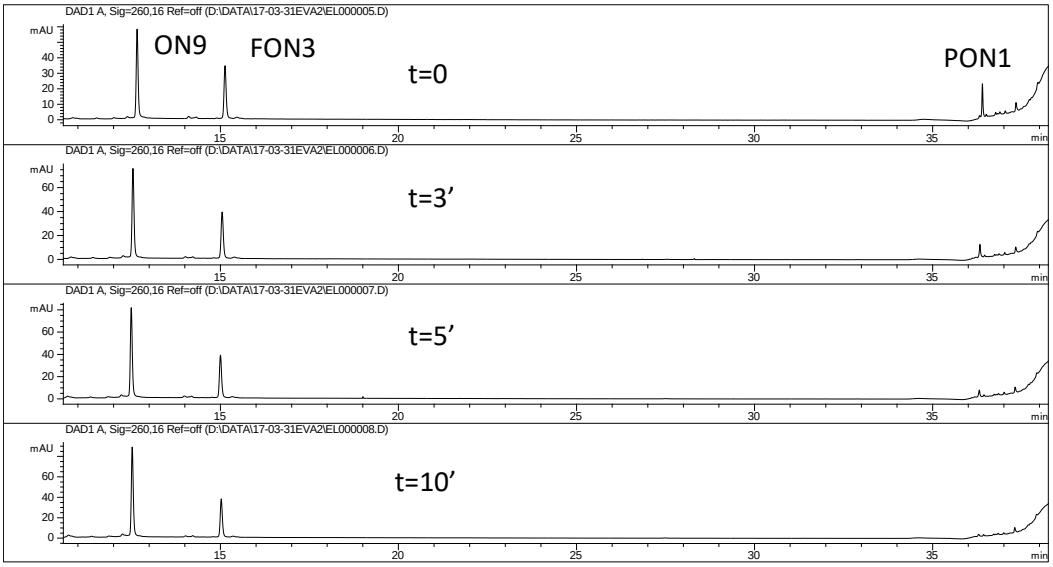

Figure 57. PLC traces of ICL experiments using the PON1/ON9/FON3 templated system at 200 nM concentration.

X.5.4.Experimental data for chapter VI

X.5.4.1. Characterisation of the synthesised peptide

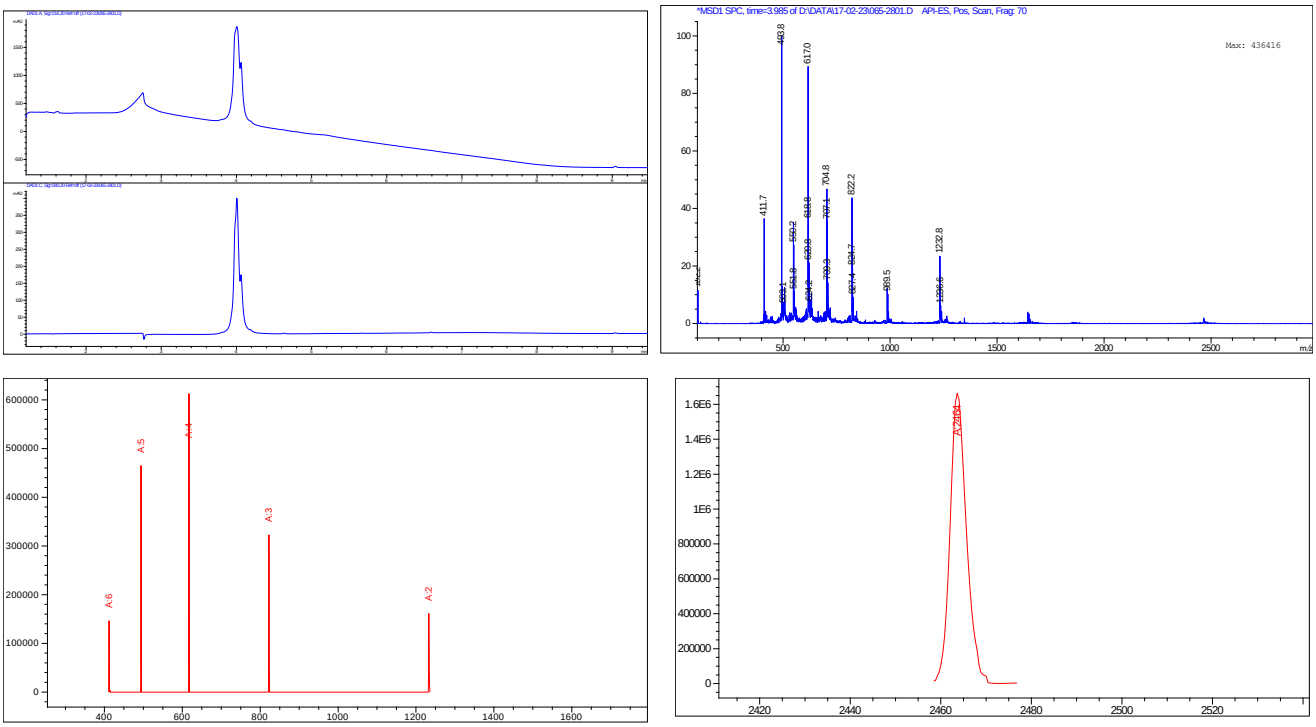

Figure 58. LC-MS analysis of MPG-8 peptide. Expected mass: 2463.3 Da. Observed mass: 2464 Da. Top left: RP HPLC chromatogram; top right: ESI-MS spectrum; bottom left: trace of multiply charged ions of MPG-8; bottom right: deconvoluted mass of MPG-8.

X.5.4.2. Characterisation of the synthesised peptide conjugate

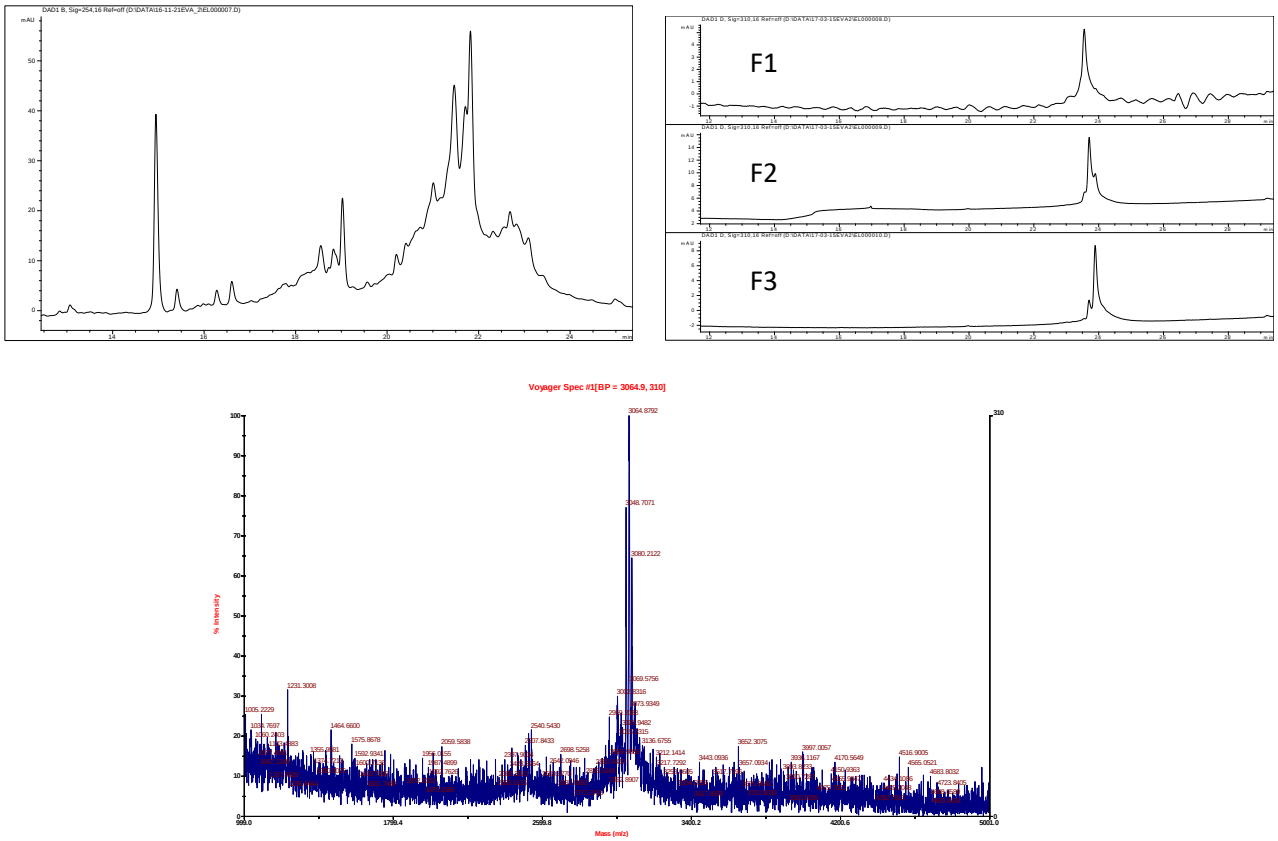

Figure 59. Top left: RP HPLC analysis of Ce6MPG-8, before purification; top right: RP HPLC analysis of Ce6MPG-8 after purification, where three fractions were separated; bottom: MALDI-TOF analysis of Ce6MPG-8 (F1), expected mass: 3042 Da, observed mass: 3049 Da.

X.6. References

1. Op de Beeck M, Madder A. Unprecedented C-selective interstrand cross-linking through in situ oxidation of furan-modified oligodeoxynucleotides. J Am Chem Soc. 2011 Feb 2;133(4):796–807.

2. Stevens K, Claeys DD, Catak S, Figaroli S, Hocek M, Tromp JM, et al. Furan-oxidation-triggered inducible DNA cross-linking: acyclic versus cyclic furan-containing building blocks--on the benefit of restoring the cyclic sugar backbone. Chemistry. 2011 Jun 14;17(25):6940–53.

3. Tomé JPC, Neves MGPMS, Tomé AC, Cavaleiro J a S, Soncin M, Magaraggia M, et al. Synthesis and antibacterial activity of new poly-S-lysine-porphyrin conjugates. J Med Chem. 2004 Dec 16;47(26):6649–52.

4. Cid J-J, Yum J-H, Jang S-R, Nazeeruddin MK, Martínez-Ferrero E, Palomares E, et al. Molecular Cosensitization for Efficient Panchromatic Dye-Sensitized Solar Cells. Angew Chemie. 2007 Nov 12;119(44):8510–4.

5. Tataurov A V., You Y, Owczarzy R. Predicting ultraviolet spectrum of single stranded and double stranded deoxyribonucleic acids. Biophys Chem. 2008;133(1–3):66–70.

6. Morris MC, Vidal P, Chaloin L, Heotz F, Divita G. A new peptide vector for efficient delivery of oligonucleotide into nontransformed mammalian cells. Nucleic Acid Res. 1997;25(14):2730–6.

7. Simeoni F, Morris MC, Heitz F, Divita G. Insight into the mechanism of the peptide-based gene delivery system MPG: Implications for delivery of siRNA into mammalian cells. Nucleic Acids Res. 2003;31(11):2717–24.

8. Crombez L, Morris MC, Dufort S, Aldrian-Herrada G, Nguyen Q, Mc Master G, et al. Targeting cyclin B1 through peptide-based delivery of siRNA prevents tumour growth. Nucleic Acids Res. 2009;37(14):4559–69.